

Fachbereich Geowissenschaften der
Universität Bremen

**Pore water profiles and early diagenetic signals in marine
sediments as indicators for (paleo-)environmental and
depositional conditions**

Dissertation zur Erlangung des akademischen
Doktorgrades der Naturwissenschaften
(Dr. rer. nat.)

vorgelegt von
Susann Henkel

Bremen, April 2011

Gutachter: 1. PD Dr. habil. Sabine Kasten

2. Prof. Dr. Gert J. de Lange

*Die Neugier steht immer an erster Stelle eines Problems,
das gelöst werden will.*

Galileo Galilei

Preface

This study was conducted in the framework of the International Graduate College “*Proxies in Earth History*” (EUROPROX) funded by the Deutsche Forschungsgemeinschaft (DFG). Part of the research was performed within project SD3: “*Slope architecture and evolution of sedimentary regimes*” at the DFG Research Center/Cluster of Excellence “The Ocean in the Earth System” (MARUM). Financial support was also provided by the Helmholtz Association (Alfred Wegener Institute for Polar and Marine Research, Bremerhaven, Germany). The present work is submitted as dissertation and was supervised by PD Dr. habil. Sabine Kasten (AWI) and Prof. Dr. Gert J. de Lange (Utrecht University, The Netherlands).

The dissertation comprises a brief introduction into marine pore water geochemistry and early diagenetic processes (in particular barium and phosphorus redistribution) in sediments as well as the motivation for this study (Chapter 1). The main part of the thesis includes four research articles. Three of the manuscripts (Chapters 2-4) are submitted or under revision for publication in international journals and the 4th edition of the Springer series “Submarine Mass-Movements and Their Consequences”. One article is in preparation for submission (Chapter 5). The abstract of a manuscript in preparation to which I contributed as co-author is included as Chapter 6. The main findings of the thesis are summarized in Chapter 7. In this last part, open questions that are to be part of further research are given.

The first article (Chapter 2) is based on samples and data collected during research cruises P317/2 with RV *Poseidon* in September 2004 and M72/1 with RV *Meteor* in February 2007 to the Black Sea. My contribution to this article consists of scanning electron microscopic analyses, which were performed in close cooperation with Dr. Christine Franke and Dr. Eric Robin, geochemical modeling in cooperation with Dr. Kerstin Nöthen, and authorship. Part of the data presented in this manuscript was produced in the frame of the unpublished Master thesis of Kara Bogus. Methane and isotopic data was kindly provided by Dr. Richard Seifert and Dr. Martin Blumenberg. Prof. Dr. Gert J. de Lange, Dr. André Bahr, Dr. Thomas Pape, and Dr. Christian März were involved in the data discussion and writing and were therefore added to the list of authors. Chapters 3-5 contain data collected during and after RV *Meteor* cruise M78/3 (May-July 2009) along the continental margin off Uruguay and Argentina. My own contribution to these manuscripts involves sampling, pore water analyses, performance of sequential phosphorus extractions, transport and reaction modeling, and authorship. All of the co-authors contributed data and were involved in the data discussion. I performed extensive biomarker and element analyses in the frame of the study outlined in Chapter 6 and took part in the data discussion and writing of the respective manuscript.

Table of contents

Thesis summary	1
Kurzfassung	4
Chapter 1: Introduction and motivation	8
1.1 (Bio-)geochemical processes in marine sediments	9
1.2 Barium cycling in marine sediments underlying anoxic waters	11
1.3 Identification and dating of recent mass-transport events by pore water geochemistry and modeling	12
1.4 Phosphorus cycling in marine sediments	13
References	15
Chapter 2: Diagenetic barium cycling in Black Sea sediments – A case study for anoxic marine environments	21
Abstract	22
2.1 Introduction	23
2.2 Geological and geochemical setting of the study area	24
2.3 Materials and methods	26
2.3.1 Sampling procedure	26
2.3.2 Pore water analyses	27
2.3.3 Solid phase analyses	28
2.3.4 Geochemical model	29
2.4 Results and discussion	32
2.4.1 Sediment composition and core stratigraphy	32
2.4.2 Sedimentation rates	35
2.4.3 Depth of the sulfate-methane transition zone	35
2.4.4 Diagenetic barium redistribution	37
2.4.5 Numerical modeling of the SMTZ migration	39
2.5 Conclusions	46
References	48
Chapter 3: An interdisciplinary investigation of a recent submarine mass-transport deposit at the continental margin off Uruguay	58
Abstract	58

3.1 Introduction	59
3.2 Setting	61
3.3 Material and methods	63
3.3.1 Geophysical mapping	63
3.3.2 Sampling	63
3.3.3 Geotechnical and sedimentological analyses	64
3.3.4 Pore water analyses	64
3.3.5 Dating of sediment	64
3.3.6 Modeling of sulfate profile development	65
3.3.7 Limit Equilibrium slope stability analysis	66
3.4 Results	67
3.4.1 Geotechnical and sedimentological data	67
3.4.2 Geochemical data	69
3.5 Discussion	71
3.5.1 Non-steady state pore water conditions at site GeoB 13804	71
3.5.2 Earthquakes as possible trigger for the slope failure?	76
3.6 Conclusions	79
References	80

Chapter 4: Pore water geochemistry as a tool for identifying and dating recent mass-transport deposits _____ **86**

Abstract	86
4.1 Introduction	87
4.2 Study area	88
4.3 Material and methods	88
4.4 Results and discussion	90
Pore water profiles at potential MTD sites	92
Geochemical transport/reaction modeling	93
4.5 Conclusions	94
References	95

Chapter 5: Diagenetic phosphorus cycling in surface and subseafloor sediments at the continental margin off Uruguay and Argentina _____ **98**

Abstract	98
5.1 Introduction	99
5.2 Study sites	100
5.3 Material and methods	104
5.3.1 Sampling	104

5.3.2 Analyses	105
5.4 Results	109
5.4.1 Pore water geochemistry	109
5.4.2 Sediment composition	112
5.5 Discussion	117
5.5.1 Bulk sediment and sulfate-methane transition zone	117
5.5.2 Phosphate fluxes into the bottom water	120
5.5.3 Organic phosphorus	121
5.5.4 Inorganic phosphorus	123
5.6 Summary and Conclusions	126
References	127
Chapter 6: Perturbations of the sulfur, iron, and phosphorus cycles during Cretaceous oceanic anoxic events (Abstract)	135
References	136
Chapter 7: Conclusions and outlook	137
Danksagung	140

Thesis summary

Unraveling present-day environmental changes and their link to the biogeochemical cycling of elements, primary productivity, and climate requires identifying the driving forces behind such changes in the past. Marine sediments store information about past environmental and depositional conditions. They consist of particles that are formed in the ocean or derived from the continents and may thus record the conditions in the water column and/or the terrestrial input into the ocean for thousands or millions of years. Diagenetic overprinting of the sediments in different redox zones may alter or even wipe out these primary signals. However, authigenic mineral enrichments and pore water profiles can shed light on the geochemical conditions in the sediment and ultimately on the factors the redox zonation is determined by (sedimentation rate, the upward flux of methane, bioirrigation etc.).

The present study focuses on the diagenetic cycling of barium (Ba) and phosphorus (P) in sediments of the Black Sea and the continental margin off Uruguay and Argentina. Furthermore, the value of pore water profile shapes for assessing the occurrence and timing of recent mass-transport deposits (MTDs) at the northwestern rim of the Argentine Basin is investigated.

In the open ocean, barite (BaSO_4) typically forms in the water column during the decay and settling of organic matter. Barium can therefore be used as a proxy for primary productivity and was as such frequently applied for Cretaceous Oceanic Anoxic Event (OAE) successions - sediments that deposited during widespread oxygen depletion in the water column. The present-day Black Sea shows a stratified, mainly anoxic water column and therefore is considered as modern analog to ocean basins during the OAEs. Pore water profiles and the sediment composition at two sites in the northwestern Black Sea indicate an intense redistribution of Ba at the sulfate-methane transition zone (SMTZ) and the precipitation of authigenic barite at ~1.5-2 m depth. Below the SMTZ, barite is dissolved due to undersaturation. The primary (possibly biogenic) Ba signal is completely erased in deeper sediments below the SMTZ, which is evidence for the limitation of Ba as productivity proxy in settings that are characterized by a shallow SMTZ. The enhanced preservation of organic material due to anoxia in the water column leads to high organic matter concentrations in the sediment and fuels the generation of methane. High diffusive upward fluxes of methane, in turn, result in a shallow SMTZ and a low preservation of barite. Barite particles in the Black Sea surface sediment show shapes that differ from typical biogenic or marine barite. Over-saturation of the bottom water with respect to barite possibly leads to an additional flux of particulate Ba into the sediment. Furthermore, barite precipitation in anoxic waters likely is

diminished by the enhanced preservation of organic matter. Thus, even if the Ba-signal would record water column processes, it could not directly be linked to primary productivity.

The Black Sea, a freshwater lake during the Pleistocene, was flooded with seawater in the Holocene. Consequently, it was subject to drastic salinity changes during the past ~9 kyrs. In response to increasing salinity and sulfate concentrations in the bottom water, the SMTZ migrated downward to its present depth at ~2 m in the study area. Since barite enrichments are preserved in sulfate-bearing sediments, relict authigenic enrichments of this mineral were assumed to trace the downward movement of the SMTZ. However, transport and reaction modeling considering sedimentation rate, diffusion of sulfate into the sediment, a constant diffusive methane flux from deep sediments, and anaerobic oxidation of methane as a sink for both species revealed that the sediments that were potentially affected by diagenetic barite formation during the downward movement of the SMTZ are at present located below the SMTZ. Thus, they were subject to BaSO₄ dissolution and the Ba signal does not provide information with respect to this drastic salinity increase anymore.

Sediment cores and pore water profiles of sites at the continental margin off Uruguay and Argentina were examined in order to identify deposits that show transient pore water conditions as a result of recent mass movements. Whereas a linear decrease of sulfate with sediment depth usually relates to steady state pore water conditions, kink- and concave-shaped sulfate profiles may be indicative for submarine landslides. Previous studies on this subject mostly lacked sediment echosounder surveys and/or clear sedimentological evidence for the coupling of non-linear sulfate profiles to mass movements. Furthermore, it remained unclear, how profiles disturbed by mass movements can be discriminated from those related to any other perturbing processes, such as advection or sudden increases of the upward flux of methane. The integration of sediment echosounder, sedimentological, geotechnical, and pore water data from several sites at the continental margin was carried out for the first time in this study. The data reveal that in this very dynamic depositional setting, non-steady state pore water profiles are often, but not exclusively related to mass movements. At sites where mass movement events likely caused the observed non-linearity of the pore water profiles, the diffusive re-equilibration of the sulfate profile was simulated applying a transport and reaction model. In this way, the ages of the MTDs were estimated. At one site, the geochemical simulation revealed an age of the MTD of less than 30 years, which suggested a coupling to a weak earthquake that hit the region in 1988. Limit Equilibrium slope stability analysis revealed that the 1988 earthquake was indeed a likely trigger for slope failure in the investigated area.

Sediments at continental margin settings, such as the area off Uruguay and Argentina, receive high inputs of P either adsorbed onto Fe (oxyhydr)oxides, incorporated into organic matter, fish debris or associated with terrigenous material. Previous studies by other authors showed that during early diagenesis, P is not only released into the pore water close to the sediment surface but also at and above the SMTZ. Diagenetic precipitation of apatite and vivianite was suggested to represent a major and irrevocable sink for pore water phosphate. We investigated pore water, the bulk sediment composition, and P and Fe fractions at three stations at the continental slope off Uruguay and Argentina and observed that even below the SMTZ, phosphate is liberated into the pore water. We relate this phosphate release in deep sediments to the reduction of deeply buried Fe (oxyhydr)oxides that passed the SMTZ rapidly and without severe alteration due to extremely high sedimentation rates during the Pleistocene. The process of this deep iron reduction is not yet understood, but apparently it has a major impact on the P cycling at the investigated sites. The formation of authigenic apatite likely plays a role in the investigated sediment intervals. However, with the extraction method applied, we were not able to distinguish between biogenic and authigenic apatite. The pore water profiles reveal that vivianite precipitation does not represent a major sink for dissolved phosphate and iron.

Besides the sedimentation rates, the retention potential of the sediment determines the shape of the phosphate profiles. Highest dissolved phosphate concentrations of up to 450 μM are found at a site with high carbonate concentrations in the sediment. The carbonate dilutes the portion of reactive Fe particles and thus diminishes the retention potential of the sediment with respect to phosphate. A third important factor for the redistribution of P (and Fe) in continental margin settings is the extent of the sulfidic zone or rather the time a respective sediment horizon is exposed to sulfidic conditions. A stable SMTZ with a broad sulfidic zone results in a very effective transformation of Fe (oxyhydr)oxides into Fe sulfides and thus prevents the Fe (oxyhydr)oxide reduction within the methanic zone.

Compared to nutrient cycling and benthic processes, there has been little research to element redistributions in deeper sediments. This thesis contributes to a better understanding of post-depositional alterations of Ba and P records and to more reliable interpretations of respective fossil records.

Kurzfassung

Um heutige Umweltveränderungen und Ihre Auswirkungen auf die biogeochemischen Stoffkreisläufe, die Primärproduktion und das Klima zu erfassen, ist es nötig, die Steuerungsfaktoren solcher Veränderungen in der Vergangenheit zu kennen. Marine Sedimente liefern Informationen über Umwelt- und Ablagerungsbedingungen in der Vergangenheit. Da Sedimente aus im Ozean gebildeten sowie terrigenen Partikeln bestehen, können sie die Bedingungen in der Wassersäule und den Eintrag von Material vom Kontinent über Tausende oder Millionen von Jahren aufzeichnen. Diagenetische Überprägung der Sedimente in verschiedenen Redoxzonen kann dazu führen, dass diese primären Signale verändert oder komplett gelöscht werden. Authigene Mineralanreicherungen sowie Porenwasserprofile geben jedoch Aufschluss über aktuelle und vergangene geochemische Bedingungen im Sediment und lassen damit Rückschlüsse auf die Faktoren zu, durch die die Redoxzonierung und die Lösung und Fällung von Mineralphasen bestimmt werden (Sedimentationsrate, diffusiver Fluss von Methan, Bioirrigation etc.).

Die vorliegende Arbeit beschäftigt sich mit der diagenetischen Überprägung von Barium (Ba) und Phosphor (P) in Sedimenten des Schwarzen Meers sowie des Kontinentalhangs vor Uruguay und Argentinien. Weiterhin wird die Nutzbarkeit von Porenwasserprofilen für das Identifizieren und Datieren junger Rutschungen am nordwestlichen Rand des Argentinienbeckens untersucht.

Im offenen Ozean wird Baryt (BaSO_4) während des Abbaus und Absinkens von organischem Material gebildet. Barium in der Festphase wird daher als Proxy-Parameter für Primärproduktion genutzt und wurde als solcher auch für kreidezeitliche Abfolgen Ozeanischer Anoxischer Ereignisse (OAEs) - Phasen weitreichender Sauerstoffarmut im Ozean - verwendet. Das heutige Schwarze Meer wird durch seine stratifizierte und überwiegend anoxische Wassersäule als ein Analogon zu Meeresbecken während der OAEs betrachtet. Porenwasserprofile und die Sedimentzusammensetzung wurden an zwei Stationen im nordwestlichen Schwarzen Meer untersucht. Diese Stationen zeigen eine starke Umverteilung von Ba an der Sulfat-Methan Übergangszone (SMTZ) und eine Fällung von authigenem Baryt in 1,5-2 m Tiefe. Unterhalb der SMTZ wird Baryt infolge von Untersättigung gelöst. Das primäre (möglicherweise biogene) Ba-Signal in tieferen Sedimenten unter der SMTZ wurde vollständig „ausgelöscht“, was die begrenzte Nutzbarkeit von Ba als Produktivitätsproxy in Sedimenten mit flacher SMTZ belegt. Die gute Erhaltung von organischem Material durch anoxische Bedingungen in der Wassersäule führt zu hohen Organik-Gehalten im Sediment, was wiederum die Methanbildung erhöht. Hohe aufwärtsgerichtete diffusive

Flüsse von Methan sorgen für eine flache SMTZ und eine geringere Erhaltung von Baryt. Baryte im Oberflächensediment des Schwarzen Meeres zeigen für biogene oder marine Baryte untypische Formen. Möglicherweise führt die Übersättigung des Bodenwassers in Bezug auf Baryt zu einem zusätzlichen partikulären Ba-Fluss in das Sediment. Zudem wirkt sich vermutlich die bessere Erhaltung von organischem Material in der anoxischen Wassersäule vermindern auf die Barytfällung aus. Daher ließe das Ba-Signal, selbst wenn es ausschließlich auf Prozesse in der Wassersäule zurückzuführen wäre, nicht direkt auf die Primärproduktion schließen.

Das Schwarze Meer war im Pleistozän ein See und wurde erst im Holozän mit Meerwasser geflutet. In den vergangenen ~9 ka hat das Schwarze Meer dadurch eine drastische Salinitätsänderung erfahren. Infolge der ansteigenden Salinität und Sulfat-Konzentrationen im Bodenwasser wanderte die SMTZ tiefer in das Sediment. Im Arbeitsgebiet befindet sich die SMTZ heute in etwa 2 m Tiefe. Da Barytanreicherungen in der Sulfat-Zone erhalten bleiben, bestand die Möglichkeit, dass reliktsche Baryt-Fronten das Hinunterwandern der SMTZ nachzeichnen. Eine Transport- und Reaktionsmodellierung unter Berücksichtigung der Sedimentationsrate, der Diffusion von Sulfat in das Sediment, eines konstanten Methanflusses aus dem tiefen Sediment und anaerober Methanoxidation als Senke für Sulfat und Methan ergab jedoch, dass die Horizonte, die möglicherweise von diagenetischer Barytfällung während des Wanderns der SMTZ in tiefere Sedimente betroffen waren, heute unterhalb der SMTZ liegen. Dementsprechend wurde Baryt inzwischen gelöst und das Ba-Signal erlaubt keine Rückschlüsse mehr auf den drastischen Salinitätsanstieg im Zuge der Flutung des Schwarzen Meeres.

Vor dem Hintergrund, die Rekonstruktion der Sedimentationsgeschichte an Kontinentalhängen zu verbessern, wurde am Kontinentalhang vor Uruguay und Argentinien die Nutzung instationärer Porenwasserprofile für das Erkennen rezenter Massenumlagerungen untersucht. Eine lineare Abnahme der Sulfatkonzentration mit der Sedimenttiefe wird generell mit einem Gleichgewichtszustand des Porenwassersystems in Verbindung gebracht. Kink-förmige und konkave Sulfatprofile hingegen können durch submarine Hangrutschungen entstehen. Frühere Arbeiten zu diesem Thema beinhalteten jedoch keine Sedimentechlot-Daten und/oder klare sedimentologische Beweise für den Zusammenhang zwischen nicht-linearen Sulfatprofilen und Massenumlagerungsprozessen. Außerdem ist bisher unklar, wie durch Massenumlagerungen nicht-lineare Profile von solchen zu unterscheiden sind, die durch andere Prozesse wie z.B. Advektion oder ein plötzliches Ansteigen des aufwärtsgerichteten Methanflusses beeinflusst sind. Das Zusammenführen von Sedimentechlot-, sedimentologischen, geotechnischen und Porenwasser-Daten wird zum ersten Mal für mehrere Stationen am Kontinentalhang vor Uruguay und Argentinien

gezeigt. Die Ergebnisse belegen, dass instationäre Porenwasser-Profile in diesem sehr dynamischen Ablagerungsraum oftmals, aber nicht ausschließlich auf Massenumlagerungen zurückzuführen sind. Für Stationen, an denen nicht-lineare Sulfatprofile auf Massenumlagerungen zurückgehen, wurde mit einem Transport- und Reaktionsmodell der diffusive Ausgleich des Sulfatprofils simuliert. Auf diese Art konnte das Alter der Massenumlagerung abgeschätzt werden. An einer Station ergab dieser geochemische Modellansatz ein Alter der Massenablagerung von weniger als 30 Jahren, was einen Zusammenhang mit einem schwachen Erdbeben in der Region im Jahr 1988 vermuten lässt. Hangstabilitätsanalysen ergaben, dass die Stärke des Erdbebens von 1988 tatsächlich Rutschungen im Arbeitsgebiet verursacht haben könnte.

Große Mengen von P werden in Sedimente an Kontinentalhängen, wie dem vor Uruguay und Argentinien, eingetragen. Phosphor ist adsorbiert an Eisenoxide/-hydroxide oder assoziiert mit organischem Material, Bio-Apatit oder der terrigenen Fraktion. Arbeiten anderer Autoren haben gezeigt, dass Phosphor durch Diagenese nicht nur im Oberflächensediment, sondern auch an und über der SMTZ in das Porenwasser freigesetzt wird. Die diagenetische Bildung von Apatit und Vivianit wurde als wichtige und endgültige Senke für gelöstes Phosphat betrachtet. Wir untersuchten die Zusammensetzung des Sediments, Bindungsformen von P und Fe in der Festphase und Porenwasser an drei Stationen am Kontinentalhang vor Uruguay und Argentinien. Die Daten zeigen eine Phosphatfreisetzung in das Porenwasser unterhalb der SMTZ. Wir führen diese auf die Reduktion von Eisenoxiden/-hydroxiden zurück, die durch extrem hohe Sedimentationsraten im Pleistozän schnell und ohne starke Alteration unter die SMTZ „vergraben“ wurden. Der Prozess dieser tiefen Eisenreduktion ist bisher noch nicht verstanden, hat aber offenbar große Auswirkungen auf den P-Kreislauf in den untersuchten Sedimenten. Wahrscheinlich spielt auch die Bildung von authigenem Apatit eine Rolle für die untersuchten Intervalle. Mit der angewandten Extraktionsmethode konnten wir jedoch die biogene Fraktion nicht von der authigenen Apatitphase unterscheiden. Die Porenwasserprofile weisen darauf hin, dass Vivianit keine signifikante Senke für gelöstes Phosphat und Eisen darstellt.

Neben den Sedimentationsraten bestimmt vor allem das Rückhaltungspotential des Sediments das Phosphatprofile. Die höchsten Konzentrationen an gelöstem Phosphat (bis 450 μM) wurden an der Station mit den höchsten Karbonatgehalten gemessen. Das Karbonat setzt den relativen Anteil an Eisenoxide/-hydroxiden im Sediment herab und mindert somit das Potential, Phosphat durch Adsorption zurückzuhalten. Ebenfalls entscheidend für die Umverteilung von P (und Fe) ist das Ausmaß der sulfidischen Zone im Sediment bzw. die Verweilzeit einer bestimmten Sedimentlage unter sulfidischen Bedingungen. Eine gleichbleibende Tiefe der SMTZ und eine breite Zone von Sulfid im

Porenwasser führen zu einer effektiven Umbildung von Eisenoxiden/-hydroxiden zu Eisensulfiden und verhindern somit die Reduktion von Eisenoxiden/-hydroxiden in tieferen Sedimentschichten.

Im Vergleich zu Nährstoffkreisläufen und benthischen Prozessen gibt es wenige Arbeiten zur Elementumverteilung in tiefen Sedimenten. Diese Arbeit erweitert unser Prozessverständnis in Bezug auf die Diagenese von Ba- und P-Phasen im Sediment und soll zu einer besseren Interpretation entsprechender fossiler Profile führen.

Chapter 1: Introduction and motivation

Since the first global marine research expedition of the H.M.S. *Challenger* from 1872 to 1876, mankind explores the ocean, marine biodiversity, and seafloor structures and sediments. It has mainly been scientific curiosity and the interest in understanding the Earth's structure, processes, and evolution that facilitated this first scientific cruise (Corfield, 2003). Ever since then, our knowledge about the marine environment has increased substantially and it became clear that not only large-scale structures (e.g., oceanic ridges and deep-sea trenches) host valuable information about the Earth's past, but that even the tiniest and most inconspicuous particles can be used for paleo-environmental reconstructions.

Marine sediment records represent excellent archives for tracking past changes in climate and depositional conditions and numerous geochemical proxies (measurable parameters that provide quantitative information about these changes) were developed during the last decades. Most of the current research questions in the field of Marine Geology focus on climate, water column parameter, and productivity reconstructions. Therefore, proxies are usually based on particles that either formed in the water column or were transported into the ocean from the continents. Numerous biomarker and stable isotope proxies (e.g., TEX₈₆, U^K₃₇, $\delta^{18}\text{O}_{\text{carb}}$) are for example used for the determination of sea surface temperatures. Furthermore, there are elements that trace the input of terrigenous material (Al, Ti) and allow reconstructing the primary productivity (e.g., Ba). However, sediments do not exclusively comprise primary/initial signals. Substantial chemical alteration may occur during and after burial (syn- and post-depositionally). Therefore, every proxy - organic and inorganic - has its limitation and care is required particularly when sediments have been diagenetically overprinted for a long time. Since early diagenetic processes practically start at the day of settling, it can be expected that most of the sediment records are to some extent affected by degradation of organic carbon, bioturbation, mineral dissolution, and/or precipitation of authigenic minerals. Although authigenic minerals usually represent only a minor fraction of the bulk sediment, the overprint may significantly change the distribution of elements that are used for paleoproductivity reconstructions (Ca, Ba; e.g., Torres et al., 1996; Moore et al., 2004; Paytan et al., 2004). Furthermore, early diagenetic processes may alter magnetic characteristics that are used as stratigraphic tools or for provenance studies (e.g., Roberts et al., 1999, Riedinger et al., 2005, Rowan et al., 2009) and physical properties of the sediment, such as porosity and permeability (Moore, 1989). Ignoring *in situ* geochemical processes might therefore lead to misinterpretations and wrong conclusions. Multi-proxy approaches reduce the risk of misinterpretation, but the application of a proxy always requires knowledge

about the processes potentially affecting its preservation. It is the purpose of this study to investigate the diagenetic cycling of specific elements (Ba and P) in modern marine settings and to decipher the processes that might also have affected paleo-records, which are used for climate and productivity reconstructions.

Besides the negative effect of diagenesis to erase and change initial signals, diagenetic enrichments and pore water profiles can provide valuable information about sub-recent environmental changes. The state of the pore water system (i.e., the shape of profiles of dissolved pore water species) depends on the ambient and depositional conditions, in particular on sedimentation rate, temperature, salinity, the upward flux of methane, advection, and the accumulation of organic carbon. It is a major aim of this study to elucidate the applicability of pore water geochemistry and authigenic mineral enrichments (e.g., of barite, BaSO_4) in order to track sub-recent migrations of the sulfate-methane transition zone (see Chapter 1.1) in response to changes in depositional and environmental conditions.

The following part of the introduction gives an overview of early diagenetic processes in marine sediments. Subsequently, the background and scope of the three major topics addressed in this dissertation will be outlined.

1.1 (Bio-)geochemical processes in marine sediments

Froelich et al. (1979) and Berner (1981) identified distinct redox zones in marine sediments that are defined by the availability of oxidants needed for the microbial degradation of organic compounds. From the surface to the deeper sediment, the succession of oxidants comprises dissolved oxygen (O_2), manganese-oxides, nitrate (NO_3^-), iron-(oxyhydr)oxides, and sulfate (SO_4^{2-}) (Fig. 1). The final step of organic matter decay is the fermentation of methane (CH_4). The sequence of oxidants is determined by the yield of free energy gained by the microorganisms that are involved in the respective reaction. Pore water profiles of the reactants (O_2 , NO_3^- , SO_4^{2-}) and products (Mn^{2+} , NH_4^+ , Fe^{2+} , HS^- , alkalinity) can therefore be used to assess the present depths of reaction fronts at which mineral dissolution/precipitation occurs (e.g., Schulz et al., 1994, Kasten et al., 2003). It should be noted that iron (oxyhydr)oxide reduction and sulfate reduction may occur simultaneously and that the sequence of these organic matter degradation steps can even be reversed depending on the types of Fe(III) minerals that are present in the sediment (Postma and Jakobsen, 1996).

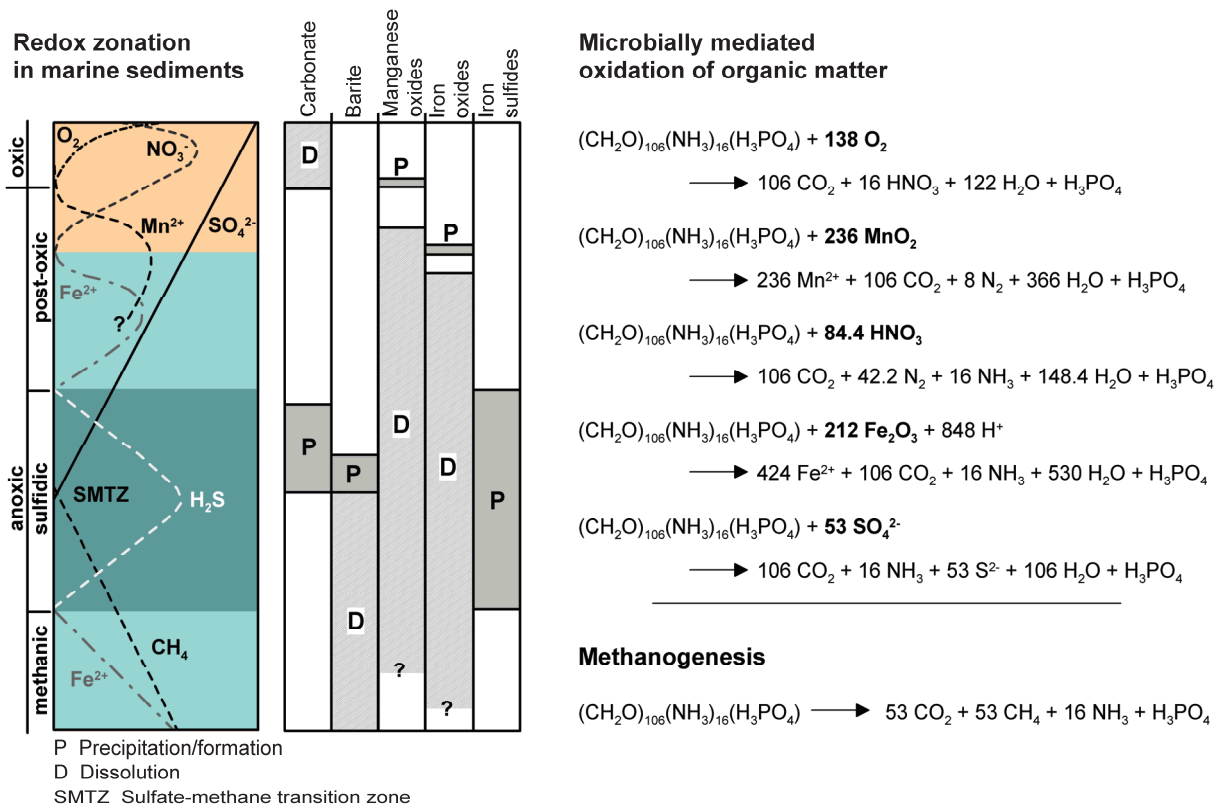


Fig. 1: Schematic graph showing the succession of redox zones in marine sediments and the zones of dissolution and authigenic formation of selected minerals, modified after Kasten et al. (2003). The classification of the redox zones (oxic, post-oxic etc.) is presented according to Berner (1981). The respective reactions of organic matter degradation according to Froelich (1979) and Schulz (2000) are shown on the right side.

The interval at which SO_4^{2-} and CH_4 coexist is referred to as sulfate-methane transition zone (SMTZ; Fig. 1). Pore water systems are classified into steady state and non-steady state systems (Froelich et al., 1979). The term “steady state” expresses a balance between the fluxes of oxidants and reductants (e.g., SO_4^{2-} and CH_4) and results in the precipitation of authigenic minerals at distinct depths relative to the sediment surface (Froelich et al., 1979; Pruyssers et al., 1993). In sediments where SO_4^{2-} reduction is mainly controlled by the diffusive upward flux of methane, steady state conditions are indicated by a linear decrease of SO_4^{2-} concentrations from ~28 mM at the sediment/water interface (e.g., Goldhaber, 2005) to complete or near depletion at the SMTZ, where SO_4^{2-} and CH_4 are used in a 1:1 stoichiometry (Barnes and Goldberg, 1976; Borowski et al., 1996). The SMTZ is the depth at which anaerobic oxidation of methane (AOM) by sulfate occurs. This reaction is mediated by archaea and SO_4^{2-} -reducing bacteria (Hinrichs et al., 1999; Boetius et al., 2000). Hydrogen sulfide (HS^-) and hydrogen carbonate (HCO_3^-) are released during AOM and favor the precipitation of sulfide minerals and carbonate. In general, the classification into steady state and non-steady state pore water systems is practicable for the geochemical assessment of a study site. However, it should be noted that the differentiation between the two states hosts some imprecision, because it ultimately depends on the time scale that is taken into

consideration: seasonal migrations of reaction fronts can for example only be resolved when the sampling resolution is high enough. This issue has to be kept in mind especially for Chapter 2, where an increase in bottom water salinity during the flooding of the Black Sea is considered to have led to a downward migration of the SMTZ over hundreds to thousands of years. This downward migration implies non-steady state conditions in the respective time interval. Yet, due to the slowness of the salinity increase and the downward movement of the SMTZ, the SO_4^{2-} profile appeared linear (see discussion, Chapter 2.4.5 and Fig. 8). Furthermore, steady state conditions require constant sedimentation rates and therefore are unlikely in natural systems (Pruysers et al., 1993; Schulz, 2006).

1.2 Barium cycling in marine sediments underlying anoxic waters

The extent of post-depositional alteration is hard to assess for fossil sediment for which pore water data are not available. This is for example the case for Cretaceous black shales, which accumulated during the Oceanic Anoxic Events (OAEs). These sediments are rich in organic carbon and are of particular interest for studies on climate-ocean interactions. The OAE sediments show millennial-scale changes in paleoproductivity and the redox state of ocean basins (e.g., Kolonic et al., 2005; Kuhnt et al., 2005; März et al., 2008b). A prerequisite for identifying authigenic mineral enrichments in paleo-records is to understand the *in situ* processes in modern sediments, where pore water data are accessible. The Black Sea is a perfect site to study processes that might also have occurred during the OAEs. It shows anoxia in large parts of its water column (Özsoy and Ünlüata, 1997) as it is also suggested for periods during the OAEs (e.g., Kolonic et al., 2005; Kuhnt et al., 2005).

The first topic of this study is the cycling of barium (Ba) in Black Sea sediments. Marine Ba, also referred to as non-lithogenic or excess Ba (Ba_{xs}), has been established as productivity proxy since 1958, when the “relationship between the present productivity of the surface layer of the ocean and the recent rate of accumulation of barium on the ocean floor below” was observed for the first time (Goldberg and Arrhenius, 1958). In surface waters, Ba is incorporated in organic matter, carbonate, and in celestite (SrSO_4) skeletons of acantharians (Dehairs et al., 1980; Collier, 1984; Jacquet et al., 2008). In the deeper water column, however, particulate Ba is predominantly associated with barite (BaSO_4) (e.g., Dehairs et al., 1990). Although the exact formation process in the water column is still under debate (e.g., Bishop, 1988; Bertram and Cowen, 1997; Ganeshram et al., 2003; Bernstein and Byrne, 2004), it is evident that barite precipitates during the decay of organic matter and that increases in Ba_{xs} accumulation in the open ocean thus relate to enhanced primary

productivity (e.g., Dehairs et al., 1992; Dymond and Collier, 1996). The advantage of using the Ba-proxy for paleoproductivity reconstructions instead of the more conventional proxy total organic carbon (TOC) is, that BaSO₄ is highly refractory (Paytan and Kastner, 1996). Marine barite was successfully used as productivity proxy in oxic ocean basins (e.g., Dehairs et al., 1980; Gingele and Dahmke, 1994; Jacquet et al., 2007), but was also applied to reconstruct paleoproductivity during Cretaceous OAEs (Turgeon and Brumsack, 2006, Drzewiecki and Simo, 1997, Kuypers et al. 2002, Båk, 2007, and Jiménez Berrocoso et al., 2008). It is, however, highly questionable whether the formation of barite in anoxic oceanic basins is similar to the precipitation process under oxic conditions. Furthermore, sediments underlying anoxic waters usually show high amounts of preserved total organic carbon (TOC) and a shallow depth of the SMTZ. Thus, barite may reach SO₄²⁻-depleted conditions at shallow sediment depth, where it is dissolved (Fig. 1; e.g., von Breymann, 1992; Torres et al., 1996). The aim of Chapter 2 is to clarify, whether the sedimentary Ba record in the Black Sea (and similar ancient settings) is to be interpreted as biogenic signal and can thus be used to trace paleoproductivity or whether Ba is diagenetically redistributed and rather reflects the current (and/or relict) depth(s) of the SMTZ. In the frame of this study, sediments and pore waters of two sites (501 and 1686 m water depth) in the northwestern Black Sea were examined using geochemical and microscopic methods. During the Holocene flooding of the Black Sea, salinity in the bottom water increased and shifted the SMTZ downwards. Since barite is preserved when the SMTZ moves downward (Dickens, 2001), authigenic barite enrichments in the uppermost meters of the Black Sea sediment column possibly represent relicts of past SMTZ positions. In Chapter 2, this link between diagenetic BaSO₄ enrichments and (non-)steady state conditions in Black Sea sediments will be investigated and discussed in detail. Horizons affected by the SMTZ were identified by application of a transport and reaction model.

1.3 Identification and dating of recent mass-transport events by pore water geochemistry and modeling

As stated before, the concentration gradients of chemical species in the interstitial water host valuable information about depositional conditions. The factors controlling the shape of sulfate profiles include sudden variations in the upward CH₄ flux and/or drastic changes in sedimentation rates, bioirrigation, and the burial of organic matter (e.g., Borowski, 1999; Fossing et al., 2000; Kasten et al., 2003; Riedinger et al., 2005). The first study that showed the effect of submarine landslides on a pore water system was published by De Lange (1983). The data presented in this study suggested that slide masses might cause kink-

shaped pore water profiles by maintaining their initial sediment succession and thus carrying their original pore water signature downslope to the place of deposition. The transfer of a sediment block that maintains its initial gradients of pore water species may lead to a disequilibrium of the pore water system at the site of deposition (Zabel and Schulz, 2001; Hensen et al., 2003). According to these studies, a recent mass-transport deposit (MTD) can, ideally, be identified by a kink-shaped SO_4^{2-} profile. Over time, the profile re-equilibrates due to molecular diffusion of the pore water constituents and shows a concave and finally a linear shape. Simulation of the diffusive re-equilibration and fitting of the model results to observed non-linear profiles can thus be applied for estimating the ages of recent mass movements (Zabel and Schulz, 2001; Hensen et al., 2003). These findings offer chances to improve the identification and dating of recent (ages of max. several thousands of years) landslide deposits. The studies of Zabel and Schulz (2001) and Hensen et al. (2003) include data of two sites in the Zaire/Congo deep-sea fan and three sites at the continental margin off Uruguay and Argentina. However, seismo-acoustic profiles that would explicitly prove the link between non-steady state conditions and mass movements were only presented for one of these sites. Moreover, it remained unclear how non-linear profiles caused by mass movements can be distinguished from those caused by any other of the aforementioned processes. Chapters 3 and 4 aim at expanding the previous approaches by investigating specifically such sites that show indications for mass movements by sediment echosounder data. The continental slope off Uruguay and Argentina is an appropriate setting for such a study, because the area is characterized by very dynamic depositional conditions and a widespread occurrence of MTDs is known from extensive geological mapping (Lonardi and Ewing, 1971; Klaus and Ledbetter, 1988; Krastel et al., in press). In Chapters 3 and 4 we integrate sediment echosounder data with geochemical, sedimentological, and geotechnical investigations to discriminate non-steady state pore water systems caused by recent submarine landslides from those controlled by other processes. Transient pore water profiles are linked to inhomogeneities/discontinuities in the investigated cores. Chapter 4 particularly addresses the landslide-community and aims to demonstrate the possibilities that arise from combining classical landslide-related disciplines with pore water geochemical investigations and transport and reaction modeling.

1.4 Phosphorus cycling in marine sediments

Phosphorus (P) is an essential nutrient for every living organism. Thus, primary productivity and consequently carbon sequestration and the development of the climate are coupled to the P budget of the ocean (Froelich et al., 1982; Van Cappellen and Ingall, 1996). Diagenetic

processes, particularly the remineralization of organic matter and the dissolution of iron (oxyhydr)oxides, control the release of phosphorus from marine sediments. Furthermore, the dissolution of fish debris/biogenic apatite (hydroxyapatite) may contribute significantly to benthic phosphate fluxes (e.g., Schenau and De Lange, 2001). The close connection between P and iron (Fe) is attributed to the strong affinity of dissolved phosphate (HPO_4^{2-}) to adsorb onto Fe (oxyhydr)oxide particles (e.g., Krom and Berner, 1981; Froelich, 1988; Anschutz et al., 1998). Several previous studies have emphasized the special role of near-shore environments/continental margins and deep-sea fans for the cycling of P (Slomp et al., 1996; Burns, 1997; Ruttenberg and Goñi, 1997; Anschutz et al., 1998; März et al., 2008a). The sediments in these areas usually receive large amounts of organic matter either due to direct fluvial input or as a consequence of high primary productivity caused by the availability of nutrients. Additionally, particulate matter in rivers is rich in Fe (oxyhydr)oxides (Poulton and Raiswell, 2002), which increases the burial efficiency of P in front of large rivers (Ruttenberg and Berner, 1993) and contributes to the authigenic formation of thermodynamically stable carbonate fluorapatite (CFA; Slomp et al., 1996).

In comparison to the benthic P-cycling, relatively little is known about the diagenetic P redistribution in deeper sediments (in the sulfidic and methanic zone; Fig. 1). It has been demonstrated by Schulz et al. (1994), Burns (1997), and März et al. (2008a) that sediments from the Amazon and the Zambezi deep-sea fan show a liberation of P at the SMTZ and a drastic decrease of dissolved phosphate concentrations below the SMTZ. The authors attributed this drawdown to the formation of authigenic vivianite ($\text{Fe}_3(\text{PO}_4)_2 \times 8(\text{H}_2\text{O})$) and concluded that due to the diagenetic processes including P mobilization at the SMTZ, the sedimentary P record may be altered significantly. In the 4th manuscript (Chapter 5) geochemical pore water profiles, the composition of bulk sediment, and results of sequential P and Fe extractions of sediments from off Uruguay and Argentina are presented in order to identify the depths of P release into the pore water and post-depositional P mineral formation. Furthermore, we aim at deciphering the depositional processes that ultimately determine the overprint of the P record particularly below the SMTZ.

References

- Anschutz, P., Zhong, S., Sundby, B., Mucci, A., and Gobeil, C., 1998, Burial efficiency of phosphorus and the geochemistry of iron in continental margin sediments: *Limnology and Oceanography*, v. 43, p. 53-64.
- Bąk, K., 2007, Organic-rich and manganese sedimentation during the Cenomanian-Turonian boundary event in the Outer Carpathian basins; a new record from the Skole Nappe, Poland: *Palaeogeography, Palaeoclimatology, Palaeoecology*, v. 256, p. 21-46.
- Barnes, R.O. and Goldberg, E.D., 1976, Methane production and consumption in anoxic marine sediments: *Geology*, v. 4, p. 297-300.
- Berner, R.A., 1981, A new geochemical classification of sedimentary environments: *Journal of Sedimentary Petrology*, v. 51, p. 359-365.
- Bernstein, R.E. and Byrne, R.H., 2004, Acantharions and marine barite: *Marine Chemistry*, v. 86, p. 45-50.
- Bertram, M.A. and Cowen, J.P., 1997, Morphological and compositional evidence for biotic precipitation of marine barite: *Journal of Marine Research*, v. 55, p. 577-593.
- Bishop, J.K.B., 1988, The barite-opal-organic carbon association in oceanic particulate matter: *Nature*, v. 332, p. 341-343.
- Boetius, A., Ravensschlag, K., Schubert, C.J., Rickert, D., Widdel, F., Gieseke, A., Amann, R., Jørgensen, B.B., Witte, U., and Pfannkuche, O., 2000, A marine microbial consortium apparently mediating anaerobic oxidation of methane: *Nature*, v. 407, p. 623-626.
- Borowski, W.S., Paull, C.K., and Ussler, W., 1996, Marine pore-water sulfate profiles indicate in situ methane flux from underlying gas hydrate: *Geology*, v. 24, p. 655-658.
- , 1999, Global and local variations of interstitial sulfate gradients in deep-water, continental margin sediments: Sensitivity to underlying methane and gas hydrates: *Marine Geology*, v. 159, p. 131-154.
- Burns, S.J., 1997, Early diagenesis in Amazon Fan sediments, *in* Flood, R.D., Piper, D.J.W., Klaus, A., and Peterson, L.C., eds., *Proceedings of the Ocean Drilling program, Scientific Results, Volume 155*: College Station, TX.
- Collier, R. and Edmond, J., 1984, The trace-element geochemistry of marine biogenic particulate matter: *Progress in Oceanography*, v. 13, p. 113-199.
- Corfield, R.M., 2003, *The Silent Landscape: The Scientific Voyage of HMS Challenger*, Joseph Henry Press, 304 p.
- De Lange, G.J., 1983, Geochemical evidence of a massive slide in the southern Norwegian Sea: *Nature*, v. 305, p. 420-422.

- Dehairs, F., Baeyens, W., and Goeyens, L., 1992, Accumulation of suspended barite at mesopelagic depths and export production in the Southern Ocean: *Science*, v. 258, p. 1332-1335.
- Dehairs, F., Chesselet, R., and Jedwab, J., 1980, Discrete suspended particles of barite and the barium cycle in the open ocean: *Earth and Planetary Science Letters*, v. 49, p. 528-550.
- Dehairs, F., Goeyens, L., Stroobants, N., Bernard, P., Goyet, C., Poisson, A., and Chesselet, R., 1990, On suspended barite and the oxygen minimum in the Southern Ocean: *Global Biogeochemical Cycles*, v. 4, p. 85-102.
- Dickens, G.R., 2001, Sulfate profiles and barium fronts in sediment on the Blake Ridge: present and past methane fluxes through a large gas hydrate reservoir: *Geochimica et Cosmochimica Acta*, v. 65, p. 529-543.
- Drzewiecki, P.A. and Simo, J.A.T., 1997, Carbonate platform drowning and oceanic anoxic events on a mid-Cretaceous carbonate platform, south-central Pyrenees, Spain: *Journal of Sedimentary Research*, v. 67, p. 698-714.
- Dymond, J. and Collier, R., 1996, Particulate barium fluxes and their relationships to biological productivity: *Deep Sea Research Part II: Topical Studies in Oceanography*, v. 43, p. 1283-1308.
- Fossing, H., Ferdelman, T.G., and Berg, P., 2000, Sulfate reduction and methane oxidation in continental margin sediments influenced by irrigation (South-East Atlantic off Namibia): *Geochimica et Cosmochimica Acta*, v. 64, p. 897-910.
- Froelich, P.N., 1988, Kinetic control of dissolved phosphate in natural rivers and estuaries - a primer on the phosphate buffer mechanism: *Limnology and Oceanography*, v. 33, p. 649-668.
- Froelich, P.N., Bender, M.L., Luedtke, N.A., Heath, G.R., and Devries, T., 1982, The marine phosphorus cycle: *American Journal of Science*, v. 282, p. 474-511.
- Froelich, P.N., Klinkhammer, G.P., Bender, M.L., Luedtke, N.A., Heath, G.R., Cullen, D., Dauphin, P., Hammond, D., Hartman, B., and Maynard, V., 1979, Early oxidation of organic matter in pelagic sediments of the eastern equatorial Atlantic: suboxic diagenesis: *Geochimica et Cosmochimica Acta*, v. 43, p. 1075-1090.
- Ganeshram, R.S., Francois, R., Commeau, J., and Brown-Leger, S.L., 2003, An experimental investigation of barite formation in seawater: *Geochimica et Cosmochimica Acta*, v. 67, p. 2599-2605.
- Gingele, F.X. and Dahmke, A., 1994, Discrete barite particles and barium as tracers of paleoproductivity in South Atlantic sediments: *Paleoceanography*, v. 9, p. 151-168.
- Goldberg, E.D. and Arrhenius, G.O.S., 1958, Chemistry of Pacific pelagic sediments: *Geochimica et Cosmochimica Acta*, v. 13, p. 153-212.

- Goldhaber, M.B., 2005, Forms of sulfur in marine sediments, *in* Holland, H.D., and Turekian, K.K., eds., *Sediments, diagenesis, and sedimentary rocks, Volume 7: Treatise on Geochemistry*: Oxford, Elsevier, p. 257-282.
- Hensen, C., Zabel, M., Pfeifer, K., Schwenk, T., Kasten, S., Riedinger, N., Schulz, H.D., and Boetius, A., 2003, Control of sulfate pore-water profiles by sedimentary events and the significance of anaerobic oxidation of methane for the burial of sulfur in marine sediments: *Geochimica et Cosmochimica Acta*, v. 67, p. 2631-2647.
- Hinrichs, K.-U., Hayes, J.M., Sylva, S.P., Brewer, P.G., and DeLong, E.F., 1999, Methane-consuming archaeobacteria in marine sediments: *Nature*, v. 398, p. 802-805.
- Jacquet, S.H.M., Dehairs, F., Savoye, N., Obernosterer, I., Christaki, U., Monnin, C., and Cardinal, D., 2008, Mesopelagic organic carbon remineralization in the Kerguelen Plateau region tracked by biogenic particulate Ba: *Deep Sea Research Part II: Topical Studies in Oceanography*, v. 55, p. 868-879.
- Jacquet, S.H.M., Henjes, J., Dehairs, F., Worobiec, A., Savoye, N., and Cardinal, D., 2007, Particulate Ba-barite and acantharians in the Southern Ocean during the European Iron Fertilization Experiment (EIFEX): *Journal of Geophysical Research*, v. 112.
- Jiménez Berrocoso, Á., MacLeod, K.G., Calvert, S.E., and Elorza, J., 2008, Bottom water anoxia, inoceramid colonization, and benthopelagic coupling during black shale deposition on Demerara Rise (Late Cretaceous western tropical North Atlantic): *Paleoceanography*, v. 23.
- Kasten, S., Zabel, M., Heuer, V., and Hensen, C., 2003, Processes and signals of nonsteady-state diagenesis in deep-sea sediments and their pore waters, *in* Wefer, G., Mulitza, S., and Ratmeyer, V., eds., *The South Atlantic in the Late Quaternary: Reconstruction of Mass Budget and Current Systems*: Berlin, Heidelberg, New York, Springer, p. 431-459.
- Klaus, A. and Ledbetter, M.T., 1988, Deep-sea sedimentary processes in the Argentine Basin revealed by high-resolution seismic records (3.5 kHz echograms): *Deep Sea Research Part I. Oceanographic Research Papers*, v. 35, p. 899-917.
- Kolonic, S., Wagner, T., Forster, A., Sinninghe Damsté, J.S., Walsworth-Bell, B., Erba, E., Turgeon, S., Brumsack, H.-J., Chellai, E.I., Tsikos, H., Kuhnt, W., and Kuypers, M.M.M., 2005, Black shale deposition on the northwest African Shelf during the Cenomanian/Turonian oceanic anoxic event: Climate coupling and global organic carbon burial: *Paleoceanography*, v. 20, PA 1006.
- Krastel, S., Wefer, G., Antobreh, A.A., Freudenthal, T., Hanebuth, T.J.J., Preu, B., Schwenk, T., Strasser, M., Violante, R., Winkelmann, D., and M78/3 shipboard scientific crew, *in* press, Sediment dynamics and geohazards off Uruguay and the de la Plata River region (Northern-Argentina): *Geo-Marine Letters*.

- Krom, M.D. and Berner, R.A., 1981, The diagenesis of phosphorus in a nearshore marine sediment: *Geochimica et Cosmochimica Acta*, v. 45, p. 207-216.
- Kuhnt, W., Luderer, F., Nederbragt, S., Thurow, J., and Wagner, T., 2005, Orbital-scale record of the late Cenomanian-Turonian oceanic anoxic event (OAE-2) in the Tarfaya Basin (Morocco): *International Journal of Earth Sciences*, v. 94, p. 147-159.
- Kuypers, M.M.M., Pancost, R.D., Nijenhuis, I.A., and Sinninghe Damsté, J.S., 2002, Enhanced productivity led to increased organic carbon burial in the euxinic North Atlantic basin during the late Cenomanian oceanic anoxic event: *Paleoceanography*, v. 17, p. 1051.
- Lonardi, A.G. and Ewing, M., 1971, Sediment transport and distribution in the Argentine Basin. 6. Exploration and study of the Argentine basin: *Physics and Chemistry of the Earth*, v. 8, p. 253-263.
- März, C., Hoffmann, J., Bleil, U., de Lange, G.J., and Kasten, S., 2008a, Diagenetic changes of magnetic and geochemical signals by anaerobic methane oxidation in sediments of the Zambezi deep-sea fan (SW Indian Ocean): *Marine Geology*, v. 255, p. 118-130.
- März, C., Poulton, S.W., Beckmann, B., Küster, K., Wagner, T., and Kasten, S., 2008b, Redox sensitivity of P cycling during marine black shale formation: Dynamics of sulfidic and anoxic, non-sulfidic bottom waters: *Geochimica et Cosmochimica Acta*, v. 72, p. 3703-3717.
- Moore, C.H., 1989, *Carbonate Diagenesis and Porosity*: Amsterdam, Elsevier, 350 p.
- Moore, T.S., Murray, R.W., Kurtz, A.C., and Schrag, D.P., 2004, Anaerobic methane oxidation and the formation of dolomite: *Earth and Planetary Science Letters*, v. 229, p. 141-154.
- Özsoy, E. and Ünlüata, Ü., 1997, Oceanography of the Black Sea: A review of some recent results: *Earth-Science Reviews*, v. 42, p. 231-272.
- Paytan, A. and Kastner, M., 1996, Benthic Ba fluxes in the central Equatorial Pacific, implications for the oceanic Ba cycle: *Earth and Planetary Science Letters*, v. 142, p. 439-450.
- Paytan, A., Martínez-Ruiz, F., Eagle, M., Ivy, A., and Wankel, S.D., 2004, Using sulfur isotopes to elucidate the origin of barite associated with high organic matter accumulation events in marine sediments, *in* Amend, J.P., Edwards, K.J., and Lyons, T.W., eds., *Sulfur biogeochemistry - Past and Present*: Boulder (Colorado), Geological Society of America, p. 151-160.
- Postma, D. and Jakobsen, R., 1996, Redox zonation: Equilibrium constraints on the Fe(III)/SO₄-reduction interface: *Geochimica et Cosmochimica Acta*, v. 60, p. 3169-3175.

- Poulton, S.W. and Raiswell, R., 2002, The low-temperature geochemical cycle of iron: From continental fluxes to marine sediment deposition: *American Journal of Science*, v. 302, p. 774-805.
- Pruyters, P.A., de Lange, G.J., Middelburg, J.J., and Hydes, D.J., 1993, The diagenetic formation of metal-rich layers in sapropel-containing sediments in the eastern Mediterranean: *Geochimica et Cosmochimica Acta*, v. 57, p. 527-536.
- Riedinger, N., Pfeifer, K., Kasten, S., Garming, J.F.L., Vogt, C., and Hensen, C., 2005, Diagenetic alteration of magnetic signals by anaerobic oxidation of methane related to a change in sedimentation rate: *Geochimica et Cosmochimica Acta*, v. 69, p. 4117-4126.
- Roberts, A.P., Stoner, J.S., and Richter, C., 1999, Diagenetic magnetic enhancement of sapropels from the eastern Mediterranean Sea: *Marine Geology*, v. 153, p. 103-116.
- Rowan, C.J., Roberts, A.P., and Broadbent, T., 2009, Reductive diagenesis, magnetite dissolution, greigite growth and paleomagnetic smoothing in marine sediments: A new view: *Earth and Planetary Science Letters*, v. 277, p. 223-235.
- Ruttenberg, K.C. and Berner, R.A., 1993, Authigenic apatite formation and burial in sediments from non-upwelling, continental-margin environments: *Geochimica et Cosmochimica Acta*, v. 57, p. 991-1007.
- Ruttenberg, K.C. and Goñi, M.A., 1997, Depth trends in phosphorus distribution and C:N:P ratios of organic matter in Amazon Fan sediments: Indices of organic matter source and burial history, *in* Flood, R.D., Piper, D.J.W., Klaus, A., and Peterson, L.C., eds., *Proceedings of the Ocean Drilling Program, Scientific Results, Volume 155*: College Station, TX.
- Schenau, S.J. and De Lange, G.J., 2001, Phosphorus regeneration vs. burial in sediments of the Arabian Sea: *Marine Chemistry*, v. 75, p. 201-217.
- Schulz, H.D., 2000, Redox measurements in marine sediments, *in* Schüring, J., Schulz, H.D., Fischer, W.R., Böttcher, J., and Duijnisveld, W.H.M., eds., *Redox – Fundamentals, Processes and Applications*: Heidelberg, Heidelberg, New York, Springer, p. 235-246.
- , 2006, Quantification of early diagenesis: dissolved constituents in pore water and signals in the solid phase, *in* Schulz, H.D., and Zabel, M., eds., *Marine Geochemistry*: Berlin, Springer, p. 73-124.
- Schulz, H.D., Dahmke, A., Schinzel, U., Wallmann, K., and Zabel, M., 1994, Early diagenetic processes, fluxes, and reaction rates in sediments of the South Atlantic: *Geochimica et Cosmochimica Acta*, v. 58, p. 2041-2060.
- Slomp, C.P., Epping, E.H.C., Helder, W., and Van Raaphorst, W., 1996, A key role for iron-bound phosphorus in authigenic apatite formation in North Atlantic continental platform sediments: *Journal of Marine Research*, v. 54, p. 1179-1205.

- Torres, M.E., Brumsack, H.-J., Bohrmann, G., and Emeis, K.C., 1996, Barite fronts in continental margin sediments: a new look at barium remobilization in the zone of sulfate reduction and formation of heavy barites in diagenetic fronts: *Chemical Geology*, v. 127, p. 125-139.
- Turgeon, S. and Brumsack, H.-J., 2006, Anoxic vs dysoxic events reflected in sediment geochemistry during the Cenomanian-Turonian Boundary Event (Cretaceous) in the Umbria-Marche Basin of central Italy: *Chemical Geology*, v. 234, p. 321-339.
- Van Cappellen, P. and Ingall, E.D., 1996, Redox stabilization of the atmosphere and oceans by phosphorus-limited marine productivity: *Science*, v. 271, p. 493-496.
- von Breymann, M.T., Brumsack, H.-J., and Emeis, K.C., 1992, Depositional and diagenetic behavior of barium in the Japan Sea, *in* Pisciotta, L., Ingle, J.C., von Breymann, M.T., and J., B., eds., *Proceedings of the Ocean Drilling Program, Scientific Results, Volume 128*, p. 651-665.
- Zabel, M. and Schulz, H.D., 2001, Importance of submarine landslides for non-steady state conditions in pore water systems - lower Zaire (Congo) deep-sea fan: *Marine Geology*, v. 176, p. 87-99.

Chapter 2: Diagenetic barium cycling in Black Sea sediments – A case study for anoxic marine environments

Susann Henkel¹, Kerstin Nöthen¹, Christine Franke², Kara Bogus³, Eric Robin⁴, André Bahr⁵, Martin Blumenberg⁶, Thomas Pape⁷, Richard Seifert⁸, Christian März⁹, Gert J. de Lange¹⁰, and Sabine Kasten¹

¹Alfred Wegener Institute for Polar and Marine Research, Am Handelshafen 12, 27570 Bremerhaven, Germany.

²Centre des Géosciences, Mines ParisTech, 35, rue Saint Honoré, 77305 Fontainebleau Cedex, France.

³Department of Geosciences, University of Bremen, Klagenfurter Str., 28359 Bremen, Germany.

⁴Laboratoire des Sciences du Climat et de l'Environnement, (CEA/CNRS/UVSQ), Avenue de la Terrasse, Bâtiment 12, 91198 Gif-sur-Yvette Cedex, France.

⁵Institute of Geoscience, Goethe-University Frankfurt, Altenhöferallee 1, 60438 Frankfurt am Main, Germany.

⁶Geoscience Center, Geobiology Group, Georg-August-University Göttingen, Goldschmidtstr. 3, 37077 Göttingen, Germany.

⁷MARUM – Center for Marine Environmental Sciences and Department of Geosciences, University of Bremen, Klagenfurter Str., P.O. Box 330440, D-28334 Bremen, Germany.

⁸Institute of Biogeochemistry and Marine Chemistry, University of Hamburg, Bundesstr. 55, 20146 Hamburg, Germany.

⁹School of Civil Engineering and Geosciences (CEG), Newcastle University, Newcastle upon Tyne, NE1 7RU, United Kingdom.

¹⁰ Department of Earth Sciences - Geochemistry, Utrecht University, P.O. Box 80.021, 3508 TA Utrecht, The Netherlands.

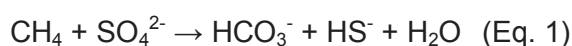
Manuscript under revision for publication in *Geochimica et Cosmochimica Acta*

Abstract

High-resolution sedimentary records of major and minor elements (Al, Ba, Ca, Sr, Ti) and total organic carbon (TOC) as well as pore water profiles (SO_4^{2-} , CH_4 , Ca^{2+} , Ba^{2+} , Mg^{2+} , alkalinity) were obtained for two gravity cores (755 and 214) retrieved from the northwestern Black Sea in 501 and 1686 m water depth, respectively. The records were examined in order to gain insight into the cycling of Ba in anoxic marine sediments that are characterized by a shallow sulfate-methane transition zone (SMTZ). Bulk and excess Ba (the non-detrital fraction, Ba_{xs}) records are presented in combination with pore water data. The Ba records are strongly overprinted by diagenetic barite (BaSO_4) precipitation and remobilization; authigenic Ba enrichments were found in both cores at and slightly above the current SMTZ. Transport reaction modeling was applied to simulate the downward migration of the SMTZ in response to the increase in bottom water SO_4^{2-} concentrations after the Holocene seawater intrusion into the Black Sea at ~9.3 kyrs BP. Based on this approach we could identify those intervals of the sediment column that were potentially affected by past diagenetic Ba redistribution. Depending on the evolution of the salinity increase in the bottom water, steady state SMTZ depths may have been reached between 3.8 and 7.5 kyrs after the first flooding of the Black Sea. At site 214, the organic-rich Unit II (sapropel) is located below the SMTZ favoring microbial methanogenesis. An increase in the formation rate of microbial CH_4 , as evidenced by trends in $\delta^{13}\text{C}$ values of CH_4 , may have initiated an upward migration of the SMTZ in the recent past. We emphasize that apart from being controlled by the presence/absence of SO_4^{2-} , diagenetic BaSO_4 dissolution and precipitation are indirectly controlled by anoxia enhancing TOC preservation and stimulating higher rates of (microbial) methanogenesis. Elevated CH_4 formation rates shift the SMTZ closer to the sediment surface and provoke diagenetic barite redistribution at shallow depth. The Ba_{xs} records of Black Sea sediments differ significantly from those known for the Mediterranean Sea. In the latter, barite-Ba appears to be a good tracer for initial productivity and TOC fluxes. In the Black Sea, in contrast, the intensely overprinted Ba and Ba_{xs} record hardly allows drawing conclusions with respect to primary productivity. These findings have implications for other modern and ancient anoxic basins, e.g., sections covering the Oceanic Anoxic Events for which the Ba-proxy is frequently used. Our study also demonstrates the limitations concerning the use of Ba_{xs} as a tracer for SMTZ migrations in the Black Sea: due to high sedimentation rates, any diagenetic barite enrichments are buried below the shallow SMTZ within a relatively short period. If at all, “relict” barite fronts would therefore be preserved only for a few thousands of years.

2.1 Introduction

Biogenic barite (BaSO_4) and non-terrigenous barium (excess Ba; Ba_{xs}) are frequently used to reconstruct marine primary productivity because the flux and accumulation of biogenic barite in open ocean settings relates to the flux of total organic carbon (e.g., Goldberg and Arrhenius, 1958; Chow and Goldberg, 1960; Dymond et al., 1992; François et al., 1995; Dymond and Collier, 1996; Paytan and Griffith, 2007). Barite is highly refractory under oxic conditions. However, early diagenetic barite redistribution in sulfate (SO_4^{2-})-depleted depths limits this proxy's application (e.g., von Breyman et al., 1992; Torres et al., 1996). The sulfate-methane transition zone (SMTZ) develops as a result of anaerobic oxidation of methane (AOM), as expressed by the net equation:



(e.g., Barnes and Goldberg, 1976; Reeburgh, 1976). This reaction was shown to be mediated by SO_4^{2-} -reducing bacteria and methane (CH_4)-consuming archaea (Hoehler et al., 1994; Hinrichs et al., 1999; Boetius et al., 2000).

The depth of the SMTZ is determined by the upward flux of CH_4 and/or other hydrocarbons, the sedimentation rate, and the SO_4^{2-} concentration at the sediment-water interface (e.g., Borowski et al., 1996; Dickens, 2001; Riedinger et al., 2005; Arndt et al., 2006). Any change in these parameters leads to a migration of the SMTZ relative to the sediment surface and thus to a transient/non-steady state situation in the pore water system (Kasten et al., 2003). Under SO_4^{2-} -depleted conditions, BaSO_4 is subject to dissolution (Eq. 2), leading to enhanced levels of dissolved barium (Ba^{2+}) in the pore water:



Dissolved Ba^{2+} diffuses upward reprecipitates as authigenic barite at the transition to the SO_4^{2-} -bearing zone (Brumsack, 1986; van Os et al., 1991; von Breyman et al., 1992; Torres et al., 1996; Dickens, 2001; Kasten et al., 2003; Riedinger et al., 2006; Snyder et al., 2007). Authigenic barite fronts/enrichments are preserved when the SMTZ moves downward and can therefore potentially be used to trace such shifts (Dickens, 2001). Prominent barite enrichments distributed over several hundreds of meters have been identified for example above deeply buried black shales at the Demerara Rise (Ocean Drilling Program Leg 207) (Arndt et al., 2006; Arndt et al., 2009). They were shown to trace the downward movement of

the SMTZ in response to changing sedimentation rates, increasing SO_4^{2-} concentrations, and a decrease in methanogenesis within the black shale over time.

In the Black Sea, water column SO_4^{2-} concentrations have varied considerably since the last glacial period when the freshwater lake turned into a brackish/marine environment (e.g., Ross and Degens, 1974; Jørgensen et al., 2004). The increasing salinity (SO_4^{2-} concentration) caused a downward movement of the SMTZ and thereby affected the biogeochemical processes in the sediment as well as the position of the authigenic Ba-front. Given the present shallow position of the SMTZ at around 2-4 m below seafloor (mbsf) at Black Sea non-seep sites (Jørgensen et al., 2001; Neretin et al., 2004; Knab et al., 2009), it may be anticipated that the distinct geochemical changes in bottom and pore waters are reflected by relict (preserved) diagenetic barite enrichments within the uppermost meters of the sediment column.

Up to now, only a few datasets on bulk Ba concentration have been published for Black Sea sediments (Brumsack, 1989; Calvert, 1990; Lüschen, 2004) – all of them lacking pore water data. With this study, we aim to assess the formation and redistribution mechanisms of solid Ba in anoxic ocean basins. We compile pore water and solid phase data from two sites in the Black Sea. In order to identify the sediment intervals potentially affected by a post-depositional overprint of solid phase Ba, we applied the numerical transport and reaction model CoTRem (Adler et al., 2001; Wenzhöfer et al., 2001) and simulated the movement of the SMTZ in response to increasing SO_4^{2-} concentrations at the sediment/water interface after the Holocene flooding of the Black Sea with seawater.

2.2 Geological and geochemical setting of the study area

The Black Sea has a surface area of 423,000 km² and a maximum water depth of 2200 m (Ross and Degens, 1974). The sill depth of the Bosphorus Strait, the only connection to the Mediterranean Sea, is shallow (at present 35 m below sea level) causing a high sensitivity of the Black Sea to sea level changes. After the last glacial period, the Black Sea was flooded by saline waters from the Mediterranean Sea and evolved from an oxygenated freshwater lake to a well-stratified marine basin with anoxic conditions below ca. 150 m water depth (Degens and Ross, 1972; Ross and Degens, 1974; Hay et al., 1991; Jones and Gagnon, 1994). Saline waters ($T > 8.5^\circ\text{C}$, salinity $> 21\text{‰}$) originating from the Mediterranean Sea are forming the deep water mass (Özsoy and Ünlüata, 1997).

The environmental and geochemical/redox variations are well-documented in the sedimentary record: From the late Pleistocene to Holocene, the typical Black Sea sedimentary succession comprises three major units: Unit III (older than about 7500 yrs BP) consists of lacustrine deposits formed below a well-oxygenated water column; Unit II (about 7500–3500 yrs BP) is a marine sapropel with total organic carbon (TOC) contents of 1-20 wt%, reflecting a permanently stratified, mainly anoxic water column; Unit I (0 – about 3500 yrs BP) is represented by finely laminated calcareous ooze with 1-10 wt% TOC that deposited after invasion of coccolithophores into the Black Sea (Ross and Degens, 1974; Hay et al., 1991; Arthur et al., 1994; Arthur and Dean, 1998; Pape et al., 2010). Sedimentation rates between 5 and 33 cm kyr⁻¹ are reported for the Units I and II in the northwestern Black Sea (Bahr et al., 2005).

The timing and evolution of the Holocene seawater intrusion into the Black Sea still is a matter of debate (e.g., Ross et al., 1970; Degens and Ross, 1972; Deuser, 1972; Ross and Degens, 1974; Ryan et al., 1997; Ballard et al., 2000; Major et al., 2002; Bahr et al., 2008; Soulet et al., 2010). Most recent studies on Sr/Ca ratios, stable oxygen, and strontium isotopes of carbonate shells indicate that the seawater intrusion started around 9.5 - 9.3 kyrs BP (Bahr et al., 2006; Major et al., 2006; Bahr et al., 2008). Based on $\delta^{18}\text{O}$ data on ostracod valves Bahr et al. (2008) estimated that the equilibrium of the Black Sea and the global sea level was reached ~100 yrs after the first seawater intrusion. Simulations of trace metal cycling, however, suggest a progressive/slow increase in salinity in the Black Sea after the seawater intrusion (Lüschen, 2004). Studies on salinity changes in the course of the seawater intrusion are rare and often limited to changes in the biotic assemblages reflecting the conditions in the oxic shallow/surface water (e.g., Wall and Dale, 1974; Ryan et al., 1997; Marret et al., 2009). There is, however, a study on $\delta^{18}\text{O}$ pore water profiles in Black Sea sediment indicating that modern hydrologic conditions might not have been reached until ~2 kyrs BP and that the increase in salinity accordingly took ~7 kyrs (Soulet et al., 2010). Besides the post-glacial establishment of anoxia, the Black Sea water column is characterized by its exceptionally high dissolved Ba²⁺ concentrations. In the deep water, where the concentrations amount to ~450 nM, oversaturation is reached with respect to pure barite by at least a factor of two (Falkner et al., 1993).

2.3 Materials and methods

2.3.1 Sampling procedure

The two gravity cores 755 and 214 investigated in this study were retrieved from the northwestern Black Sea continental margin during RV *Poseidon* cruise P317/2 (September 2004) and RV *Meteor* cruise M72/1 (February 2007), respectively (Fig. 2). Core 755 (44°44.13' N, 32°01.70' E; 574 cm length) was recovered from 501 m and core 214 (44°24.10' N; 32°51.27' E; 412 cm length) from 1686 m water depth.

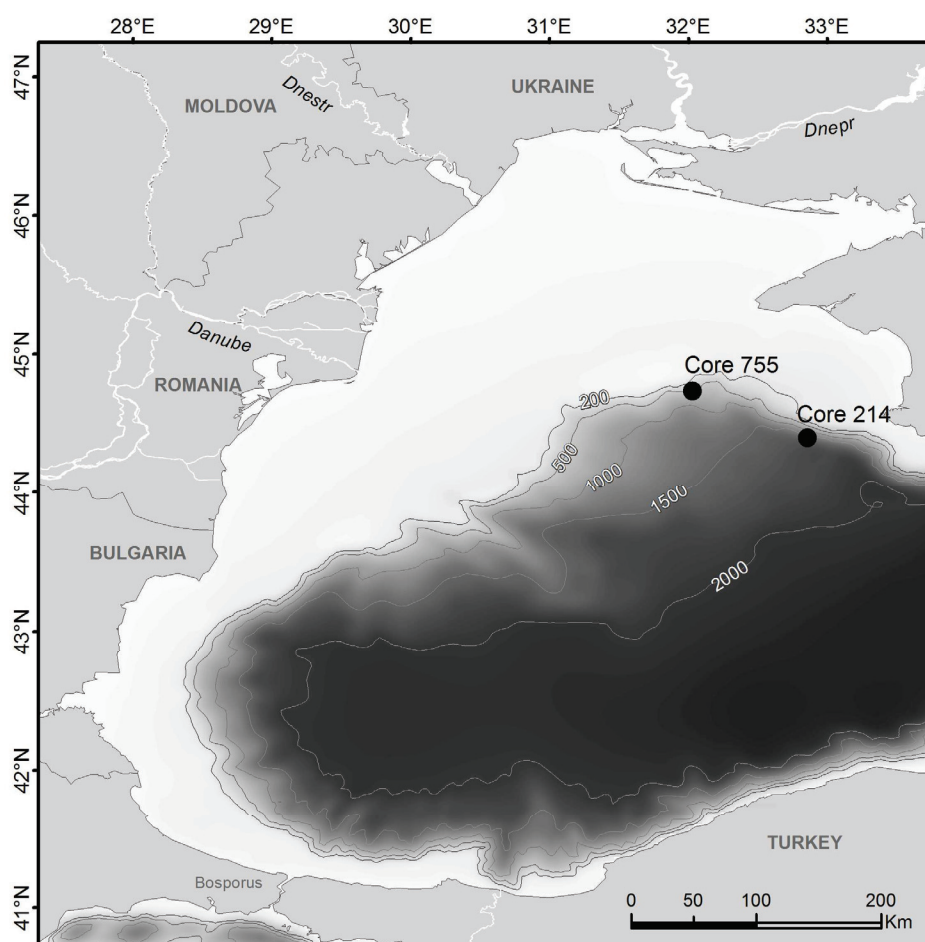


Fig. 2: Map and bathymetry (m) of the western Black Sea showing the positions of gravity cores 214 and 755.

Immediately after recovery, the cores were cut into 1m-segments. For CH₄ analysis, samples were taken following the method described by Schulz (2006). While segmenting the core, 5 ml of sediment were sampled from the lower end of each segment using syringes with cut tips. The sediment was transferred into headspace vials that contained a saturated NaCl-solution. The vials were closed gas-tight, shaken, and stored at 4°C until analysis. Additional

sampling for CH₄ was carried out through small openings cut into the core liner in 25 cm depth intervals. Pore water samples from core 755 were obtained by use of the squeezer method in an argon-flooded glove box (Reeburgh, 1967; Schlüter, 1990; De Lange, 1992) while for core 214 the rhizon technique (pore size 0.1 µm) was applied (Seeberg-Elverfeldt et al., 2005). Subsamples were taken for alkalinity (only for core 755), Fe²⁺, hydrogen sulfide (fixed as ZnS), SO₄²⁻, and cation analysis. All pore water samples as well as the cores were stored at 4°C.

Solid phase samples were taken in 2 cm intervals using plastic syringes with cut tips (core 755) or a ceramic knife (core 214). The sediment samples were freeze-dried and homogenized before analysis.

2.3.2 Pore water analyses

Alkalinity was determined aboard by titration with HCl following the procedure by Grasshoff (1983). Methane concentrations were measured aboard either using a *Thermo Trace* gas chromatograph pulse-discharge detector (GC-PDD) as previously described by Blumenberg et al. (2007) (core 755), or applying a *Carlo Erba* gas chromatograph equipped with a flame ionization detector (GC-FID; direct injection) as described by Seifert et al. (1999) (core 214). The values were corrected for a sediment porosity of 0.8. The CH₄ concentrations reported here, as with all conventional sampling devices, are affected by degassing during and after core retrieval due to pressure loss (e.g., Dickens et al., 1997) and therefore represent minimum values. Site 214 lies within the methane hydrate stability field, located below ~720 m water depth in the Black Sea (Bohrmann et al., 2003; Naudts et al., 2006; Pape et al., 2010). Remarkable degassing features in the sediment, probably due to gas hydrate destabilization induced by pressure release, were observed in this core at about 260 cmbsf. Stable carbon isotope signatures of CH₄ in core 214 were analyzed at the University of Hamburg as described by Seifert et al. (2006).

Sulfide, sulfate, and cation analyses were performed at the University of Bremen and at the Alfred Wegener Institute for Polar and Marine Research (AWI). Hydrogen sulfide was analyzed photometrically using the methylene blue method after Cline (1969). Sulfate concentrations were measured using ion chromatography. Aliquots of 1:40 (core 214) and 1:20 (core 755) diluted samples were injected into an ion chromatograph (*Metrohm IC Net 2.3*) with a *Metrosep A Supp 5* anion column. The consistency of the measurement was checked by analyzing replicates of a sulfate standard and standard seawater (International Association for the Physical Sciences of the Ocean) after every 15th sample. In core 214, SO₄²⁻ was detected below the SMTZ (at 155-275 cmbsf). These data need to be considered

with caution because they are possibly affected by HS⁻ oxidation during storage. Inductively coupled plasma optical emission spectrometry (ICP-OES; *Perkin Elmer Optima 3300*) was applied to measure the cation concentrations (Ba²⁺, Ca²⁺, Mg²⁺) in the pore water samples.

The computer program PHREEQC 2.15 (Parkhurst and Appelo, 1999) was used to calculate the saturation index for BaSO₄: $SI = \log(IAP/K_{sp})$, where *IAP* denotes the Ion Activity Product and *K_{sp}* the solubility product constant of barite ($\log K_{sp} = -10.28$ at a temperature of 8.5°C). The *SI* was converted into the saturation state ($\Omega = IAP/K_{sp}$) indicating super-saturation at $\Omega > 1$.

2.3.3 Solid phase analyses

Major and minor elements

About 50 mg of dry bulk sediment were dissolved in a microwave system (*MLS ETHOS 1600* and *MEGA II* for core 755, *CEM MARS* for core 214) using a concentrated acid mixture of HNO₃, HCl, and HF (3:2:2 for core 755, 6:4:1 for core 214). After full evaporation of the solution, the residue was redissolved in a HNO₃ solution. For core 755, the standard reference sediment USGS-MAG1 (Gladney and Roelandts, 1988) and the two in-house marine sediment standards MAX and CAMAX (Gleiß, 2005) were processed every 10 samples to check the accuracy of the digestion and the analytical procedure. For core 214, the standard reference material SRM2702 (National Institute of Standards & Technology) was used. Elements present in the digestion solution of core 755 were measured by ICP-OES (*Perkin-Elmer Optima 3300*) at the University of Bremen. The recoveries were 101.0 ± 2.8% for Al, 99.0 ± 3.8% for Ba, 102.4 ± 4.2% for Ca, 98.5 ± 4.3% for Sr, and 103.9 ± 3.7% for Ti. The multi-element analyses of core 214 were performed at the AWI using an ICP sector field mass spectrometer (ICP-MS, *Thermo Finnigan MAT Element 2* with an *Apex-Q* nebulizer). Rhodium was added to the samples as an internal standard. For all elements, the analytical precision was better than 3%. The error with respect to the certified concentrations of elements in the standard material was less than 5%. Excess barium was calculated following the approach of Dymond et al. (1992):

$$Ba_{xs} = Ba_{total} - (Al \times Ba/Al_{detritus}) \quad (\text{Eq. 3})$$

We used the lowest Ba/Al mass ratio determined for the two cores (0.004) for the detrital fraction (Ba/Al_{detritus}). This ratio is at the lower end of values that are typical for crustal rocks (Taylor, 1964; Rösler and Lange, 1972). It fits, however, very well to the global average ratio

proposed by Reitz et al. (2004) (0.0037) and the ratio in Danube River sediment (0.005) (Yiğiterhan and Murray, 2008). According to Panin and Jipa (2002), the Danube River is the main source of suspended material discharged into the northwestern Black Sea. However, it needs to be pointed out that the calculation of Ba_{xs} using a single Ba/Al mass ratio harbors some difficulties if the ratio in detrital material changed over time.

Total organic carbon

Total organic carbon (TOC) concentrations in samples from both cores were determined with a Leco CS-200 combustion analyzer at the University of Bremen. Before combustion, the sediment was decalcified with 12.5% HCl, washed twice, and dried on a heating plate. The TOC concentrations of core 214 were published by Blumenberg et al. (2009).

Shapes of barite particles

Grains of heavy minerals were examined for selected depths in core 214 (0-2 cmbsf, 64-66 cmbsf, 94-96 cmbsf, 120-122 cmbsf, and 150-152 cmbsf) at the Laboratoire des Sciences du Climat et de l'Environnement (LSCE). About 250 μg of the pulverized bulk sediment were dispersed in ethanol by use of ultrasonification and subsequently filtered onto nuclepore filters (0.2 μm pore size). The filters were fixed onto sample stubs and coated with a thin layer of carbon before being introduced into a scanning electron microscope (SEM) sample chamber. The SEM (type JEOL JSM 840) was coupled to an energy dispersive spectrometer (EDS) and an automated particle counting and classification system. The first image was processed at 500x magnification from the backscattered electron (BSE) beam. After conversion into a binary image, a threshold that allows for the detection of heavy minerals such as barite (BaSO_4), rutile (TiO_2), and pyrite (FeS_2) was adjusted. The mineralogy of each particle was identified with an X-ray spectrum (15 kV, 3 s). In this way, up to 3400 grains per sample were classified automatically. Pictures of selected barites visualized in the secondary electron (SE) mode were used to classify the grains according to their shapes. The procedure was described in detail by Robin et al. (2003).

2.3.4 Geochemical model

The migration of the SMTZ caused by the increase in water column SO_4^{2-} concentrations in the course of the Holocene Black Sea flooding was simulated with CoTReM, a modular, numerical, transient transport and reaction model based on the operator splitting approach. A detailed description of the software is given by Adler et al. (2001) and Wenzhöfer et al.

(2001). The sites investigated in this study are unaffected by gas seepage and advective fluid flow. Transport processes at the study sites are therefore dominated by molecular diffusion and can be adequately simulated by this one-dimensional model. CoTRem was already successfully applied by Hensen et al. (2003) and Riedinger et al. (2005) to simulate the SMTZ movement as a consequence of changing sedimentation rates and upward CH₄ fluxes. The respective model set-ups were similar to the one used in this study.

A vertical model length of 13 m, subdivided into cells of 5 cm thickness, was chosen. This length allows displaying potential changes of the SMTZ depth whilst inhibiting excessive computing times. The time-step to fulfill numerical stability was set to 1×10^{-1} yrs. Analogous to Hensen et al. (2003) and Riedinger et al. (2005) we used a constant porosity and applied the value 0.8 corresponding to averaged values given in the literature (Keller, 1974; Jørgensen et al., 2001; Weber et al., 2001; Jørgensen et al., 2004). Transport mechanisms were molecular diffusion (D_s) for all solutes in the pore water and sediment accumulation for solutes and solid phase. It should be noted that neither BaSO₄ precipitation/dissolution nor Ba²⁺ diffusion towards the SMTZ were simulated, as our goal was confined to gaining information about the sediment depths, which have potentially experienced SMTZ-related diagenesis. Any simulation of BaSO₄ precipitation and dissolution in this setting would require too many assumptions on the model constraints, for instance regarding adsorption/desorption processes as well as the original Ba²⁺ concentration in the limnic/brackish early Holocene Black Sea. Since we only considered the development of the SO₄²⁻ profile, we did not include adsorption and desorption processes in our model. The only reaction considered is AOM (Eq. 1).

The SMTZ migration after the initial flooding of the Black Sea was simulated using a constant CH₄ concentration at the lower model boundary. According to Borowski et al. (1996) and Niewöhner et al. (1998), sulfate reduction at sites with constant sulfate gradients is dominated by AOM. The CH₄ concentration applied at 13 mbsf (63 mM) was therefore adjusted to induce an upward CH₄ flux that corresponds to the current downward-directed SO₄²⁻ flux at site 755, where a current steady state of the pore water system seems reasonable (see discussion). In fact, this approach harbors some shortcomings, because the past upward diffusive CH₄ flux cannot be well constrained and might have changed over time. Since we were not able to reconstruct the past CH₄ flux (e.g., at 9.3 kyrs BP), we decided to keep it constant and to simulate the downward migration of the SMTZ as controlled by changing SO₄²⁻ concentrations in the bottom water.

Tab. 1: Parameters and boundary conditions used in the CoTReM simulations.

Basic parameters for CoTReM			
Model length [m]	13		
Cell discretisation [cm]	5		
Time step SMTZ simulation [yr]	0.1		
Time step Mg ²⁺ simulation [yr]	1		
Porosity ϕ	0.8		
Temperature of interstitial water [°C]	8.5		
Boundary conditions			
	lacustrine	marine	
	Unit III	Unit II	Unit I
Sedimentation rate [cm kyr ⁻¹]			
core 755	22	29	29
core 214	8	35	23
Upper boundary			
Mg ²⁺ [mM]	0.126 ^a	≤ 34 ^b	
SO ₄ ²⁻ [mM]	0	≤ 16 ^b	
CH ₄ [mM]	0	0	
Lower boundary			
SO ₄ ²⁻ [mM]	0	0	
CH ₄ [mM]	63 ^c	63 ^c	
Diffusion coefficients ^d	D ₀	D _{sed}	
SO ₄ ²⁻ [cm ² yr ⁻¹]	216.0	149.4	
CH ₄ [cm ² yr ⁻¹]	347.8	240.5	
Mg ²⁺ [cm ² yr ⁻¹]	146.8	101.5	

^a From Kenison Falkner et al. (1991) for Lake Baikal.

^b Different model runs concerning the concentration increase in the bottom water after first intrusion of seawater (see Fig. 6 and text).

^c Methane concentration at 13 mbsf adjusted to recent SO₄²⁻ gradient following the approach of Borowski et al. (1996) and Niewöhner et al. (1998).

^d Diffusion coefficient in free solution (D₀) calculated for a temperature of 8.5°C and corrected for tortuosity (θ) after Boudreau (1997); D_{sed} = D₀/ θ^2 , while $\theta^2 = 1 - \ln(\phi^2)$.

The reaction-specific change in concentration at a specific sediment depth ($\Delta C_{s,d}$) was calculated as follows:

$$\Delta C_{s,d} = R_{s,d} \times dt_{num} \times SC_{s,d}$$

where $R_{s,d}$ [in mol l⁻¹ yr⁻¹] is the reaction rate, dt_{num} is the time step used in the model run, and $SC_{s,d}$ is a stoichiometric factor. If the concentrations decreased, the rates were automatically reduced to the available amount of reactants in each cell to avoid negative concentrations (2nd order kinetics, for details see Hensen et al., 2003; Riedinger et al., 2005). Diffusion coefficients were corrected for tortuosity (Boudreau, 1997) using a temperature of 8.5°C for deep water. The effect of the salinity differences on the diffusion coefficients was disregarded as they were found to amount to only 0-8% (Li and Gregory, 1974).

The upper boundary conditions are defined by the bottom water concentrations of the chemical species. Organoclastic sulfate reduction (SR) was not taken into account during the simulation. Jørgensen et al. (2001) observed that due to the short diffusion paths at the top of the sediment column, organoclastic SR in the uppermost centimeter leads to a SO₄²⁻ concentration decrease of only 1/200 if compared to a similar SR rate at 200 cmbsf. The impact of organoclastic SR on the SO₄²⁻ concentration at the sediment top does therefore not compromise the reliability of our model. The lower model boundary is defined as an open boundary for the solutes except for CH₄, which means that the gradient of the last two cells is extrapolated to allow diffusion across the boundary. A compilation of the input parameters for all simulation runs is given in Table 1.

2.4 Results and discussion

2.4.1 Sediment composition and core stratigraphy

For core 755, a linear extrapolation of SO₄²⁻ data to the sediment-water interface suggests the upper 35 cm were not recovered (Fig. 3d). The sampled interval appears unaffected by turbidites or slumps and contains all three lithological units. The Unit III/II boundary (~7500 yrs BP) is marked by the onset of a gradual upward increase in TOC concentrations starting at 215 cmbsf (Fig. 3a). The maximum TOC concentration of 8.6 wt% is reached at 192 cmbsf. At 202 cmbsf, solid phase Ca and Sr show pronounced peaks (140.8 g kg⁻¹ and 1.85 g kg⁻¹, compared to background values of about 60 g kg⁻¹ and 0.2 g kg⁻¹, respectively) indicating the characteristic aragonite layer, which is located in the lower Unit II (Ross and Degens, 1974; Jones and Gagnon, 1994; Morse et al., 2007). The sharp increase in Ca contents from 39.3 g kg⁻¹ at 100 cmbsf to 87.4 g kg⁻¹ at 98 cmbsf marks the Unit II/I boundary.

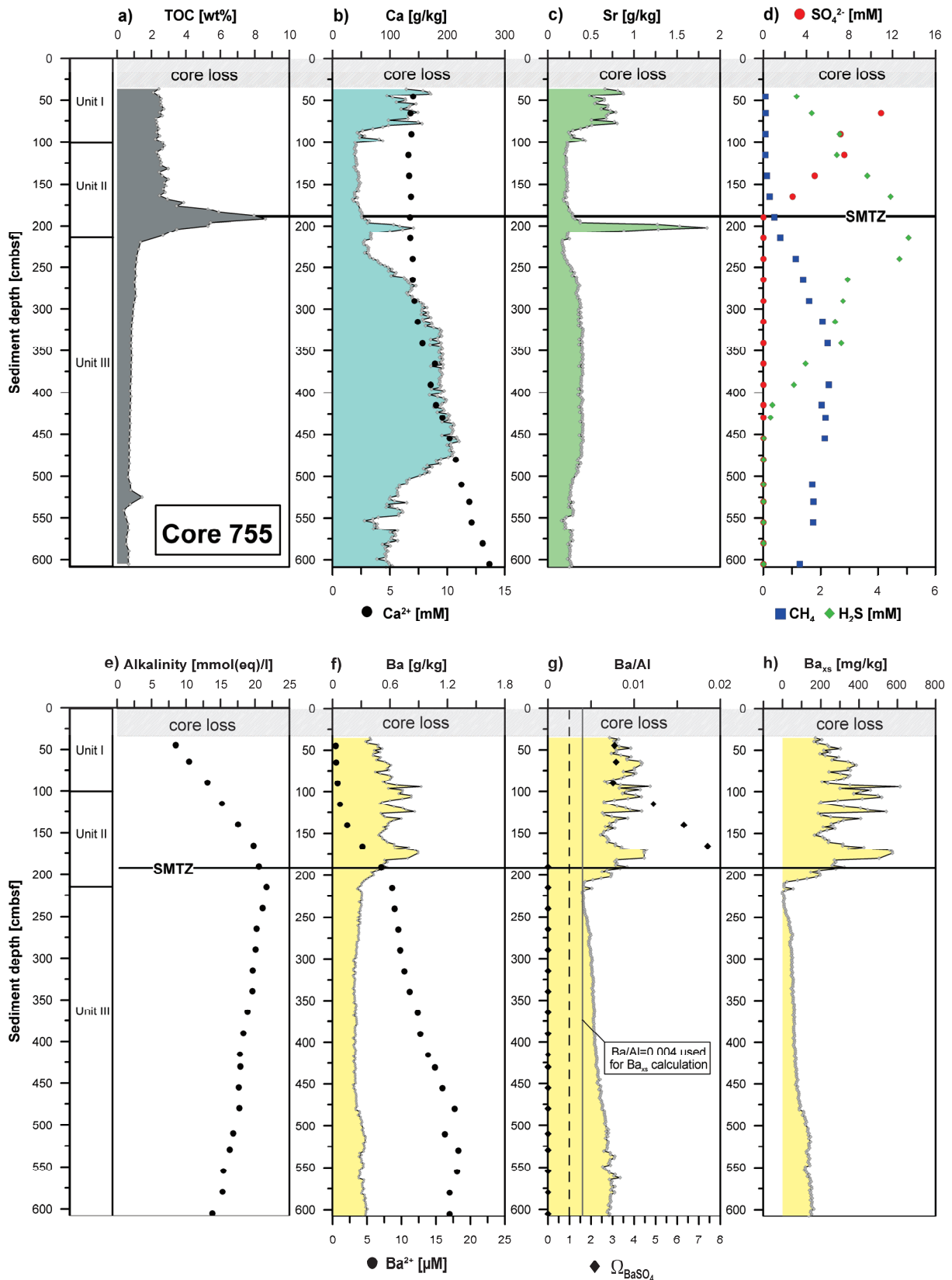


Fig. 3: Geochemical pore water and solid phase data of gravity core 755 (a-h). The horizontal black line indicates the position of the SMTZ. Note: The uppermost ca. 35 cm of core 755 were lost during core retrieval (see text). The vertical dashed line in g) at $\Omega_{\text{BaSO}_4}=1$ indicates saturation with respect to BaSO_4 .

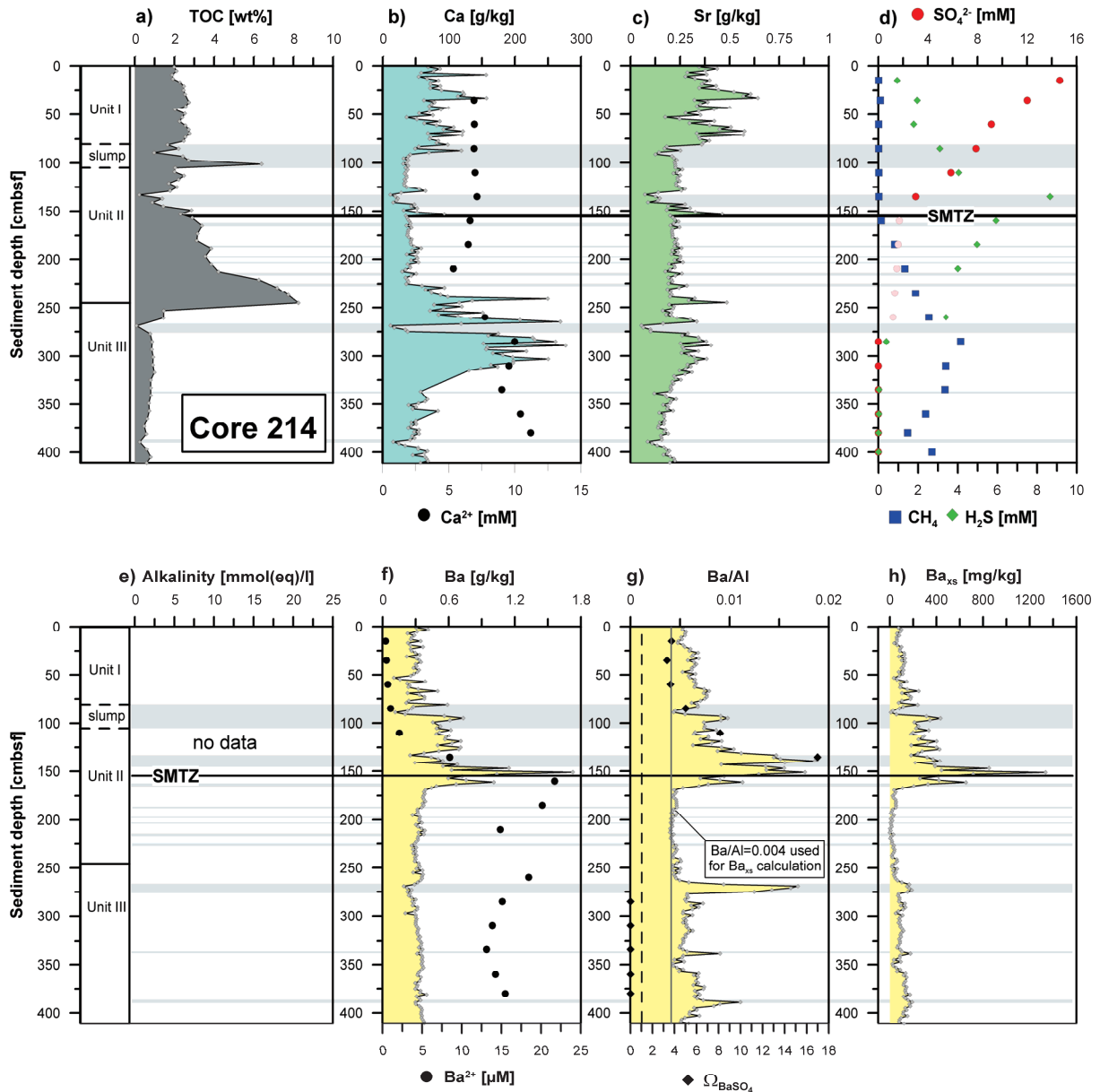


Fig. 4: Pore water and solid phase data of gravity core 214 (a-h). The light gray shaded horizontal bars indicate disturbed sediment layers (slump or turbidites). The light red dots in the SO_4^{2-} profile indicate the values potentially affected by sulfide oxidation during sample storage. The saturation state with respect to barite (g) is not shown for this core interval (150-175 cmbsf) because of the questionable SO_4^{2-} values. The vertical dashed line at $\Omega_{\text{BaSO}_4}=1$ indicates saturation with respect to BaSO_4 .

The stratigraphy for core 214 (Fig. 4a-h) was established by Blumenberg et al. (2009). The Unit III/II boundary is located at 245 cmbsf. A slump deposit between 80 and 105 cmbsf prevented the precise identification of the Unit II/I boundary. However, the sediment below the slump deposit is identified as the sapropelic Unit II, whereas the material above the slump belongs to Unit I. At 133-145.5 cmbsf a turbiditic sequence is present. Further below, several thin turbidites appear as light gray clayey intervals (161.5-165 cmbsf, 187-188.5 cmbsf, 197-199 cmbsf, 202-203.5 cmbsf, 214-217 cmbsf, and 225.5-228.5 cmbsf). Three additional coarse-grained turbidites are identified at 268-276 cmbsf, 337-339 cmbsf,

and 387-390 cmbsf. Most of the turbidites are reflected by higher Ba/Al ratios than the rest of the core (>0.009 compared to ~ 0.005 ; Fig. 4g) and fairly low Ca and TOC concentrations. We suggest a dilution of the latter components by lithogenic Si.

2.4.2 Sedimentation rates

The averaged sedimentation rates calculated for site 755 are 29 cm kyr^{-1} for Units I and II. The respective values for core 214 (assuming that no erosion took place in relation with the slump or the turbidites) are 23 cm kyr^{-1} (Unit I) and 35 cm kyr^{-1} (Unit II). The sedimentation rates for Unit III were calculated only for the section that reflects the transition from limnic to marine conditions according to Major et al. (2002). It has been shown by Bahr et al. (2005) that this transition interval is characterized by fairly low Ca contents and high sedimentary Ti/Ca ratios, which reflect a dominance of detrital components over carbonate precipitation. In the cores investigated (Ti/Ca not shown), the intervals 215-255 cmbsf (core 755) and 245-260 cmbsf (core 214) represent this change from limnic to brackish/marine conditions. In core 214, its determination was difficult due to several turbidites within the respective section. The approximated average sedimentation rates for the transition interval are 22 cm kyr^{-1} for core 755 and 8 cm kyr^{-1} for core 214. These results are in accordance with the findings of Bahr et al. (2005), who observed similar thicknesses of Units I and II in five cores (western Black Sea) over a transect from 465 m to almost 2000 m water depth, but large variations in the thicknesses of Unit III.

2.4.3 Depth of the sulfate-methane transition zone

The pore water profiles of SO_4^{2-} , CH_4 , H_2S , alkalinity, and Ca^{2+} of cores 755 and 214 are illustrated in Figures 3 and 4. For both sites, the depth profiles indicate a current SMTZ position within Unit II (at about 190 cmbsf for core 755 and at 150-155 cmbsf for core 214). Core 755 shows an extended zone (~ 140 -180 cmbsf) in which CH_4 and SO_4^{2-} coexist. A similar tailing of the CH_4 profile was also described from other sites in the Black Sea (Reeburgh et al., 1991; Jørgensen et al., 2001; Knab et al., 2009) and was explained by inefficient AOM, for which the reasons remain speculative.

At site 214, the sapropel of Unit II is completely located below the SMTZ (Figs. 4 and 5) favoring *in situ* methanogenesis as the ultimate step in the microbial degradation of organic

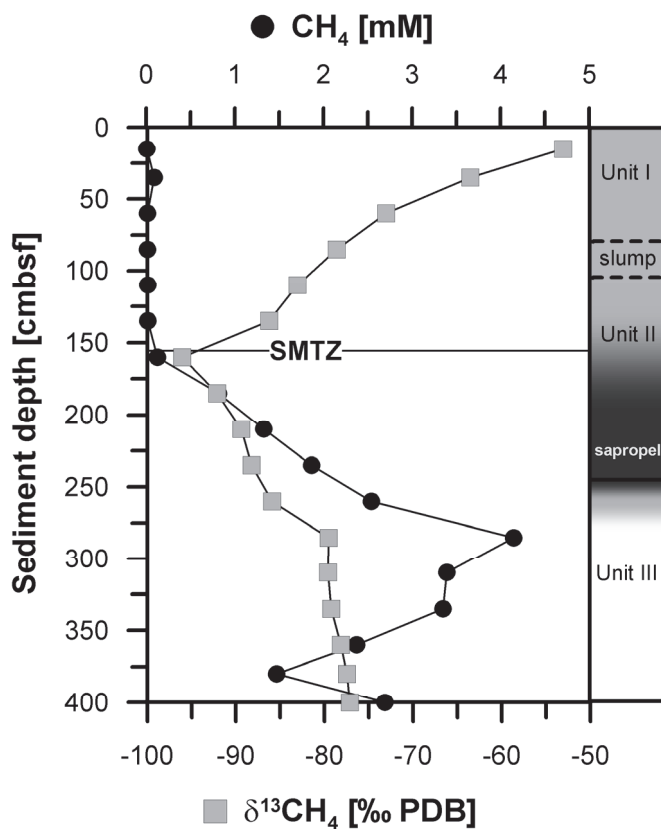


Fig. 5: $\delta^{13}\text{C}$ -values of methane of core 214. Strong ^{13}C -depletions within the lower Unit II suggest microbial *de novo* formation of CH_4 .

matter (OM) (e.g., Martens and Klump, 1984). Strong ^{13}C -depletion (about -78‰) indicate a microbial origin of the upward diffusing CH_4 . The shift to even more negative values at the transition into Unit II suggests an additional CH_4 source within the sapropel (Fig. 5). The lightest $\delta^{13}\text{C}_{\text{CH}_4}$ values (-95‰) are found directly at the SMTZ. Strongly negative values possibly result from successive carbon cycling at this biogeochemical reaction zone. Borowski et al. (1997) proposed that the repeated reaction from CH_4 to CO_2 (by AOM) and back to CH_4 (CO_2 reduction) leads to a progressive ^{13}C depletion and extremely negative $\delta^{13}\text{C}$ values at the top of the methanogenic zone. However, *in situ* CH_4 production in the upper layers of

Black Sea sediments was proven by Krüger et al. (2005), Knab et al. (2009), and Pape et al. (2010). The remaining CH_4 , which diffuses upward from the SMTZ, however, becomes relatively ^{13}C -enriched due to the preferential $^{12}\text{CH}_4$ consumption during AOM (e.g., Whiticar, 1999; Pohlman et al., 2009).

The H_2S profiles at both locations (Fig. 3d and 4d) are consistent with the inferred SMTZ depths. During AOM, both HCO_3^- and H_2S are liberated into the interstitial water (see Eq. 1), increasing the alkalinity (Fig. 3e). The H_2S profiles at both sites indicate an upward diffusive flux towards and across the sediment/water interface and a downward flux into the limnic deposits of Unit III. Sulfide concentrations were below detection limit at 480 cmbsf (core 755) and at 360 cmbsf (core 214). According to Jørgensen et al. (2004), Neretin et al. (2004), and Knab et al. (2009) the depletion of H_2S within Unit III is attributed to the formation of iron sulfides upon reaction with upward diffusing Fe^{2+} that is released from the limnic deposits.

2.4.4 Diagenetic barium redistribution

The EDS spectra of the Ba-containing particles in the five selected samples revealed that BaSO₄ is the dominant Ba-containing heavy mineral above the SMTZ (Tab. 2). The only other Ba-mineral detected was gorceixite (BaAl₃(PO₄)(PO₃OH)(OH)₆). Nevertheless, the heavy minerals do not account for the complete Ba concentrations. Silicates and carbonates were not detected by SEM/EDS. Excess barium was therefore calculated to correct for Ba associated with detrital minerals.

Tab. 2: Average equivalent diameters for all Ba-containing heavy minerals identified for core 214 by SEM/EDS. Barium-containing grains larger than 6 µm were not detected in any of the samples.

Depth [cmbsf]	Grains analysed	Heavy Ba-minerals	Average Equivalent Diameter (AED)							Sum of grains
			0.2-0.5 µm	0.5-1 µm	1-2 µm	2-3 µm	3-4 µm	4-5 µm	5-6 µm	
0-2	3400	BaSO ₄	0	55	51	7	3	2	0	118
		other Ba-containing	0	0	2	0	0	0	0	2
64-66	2119	BaSO ₄	0	55	57	5	1	1	0	119
		other Ba-containing	0	1	0	0	0	0	0	1
94-96	1459	BaSO ₄	0	86	79	6	3	1	0	175
		other Ba-containing	0	1	1	0	1	0	0	3
120-122	1256	BaSO ₄	0	26	30	9	2	0	1	68
		other Ba-containing	0	0	1	0	1	0	0	2
150-152	957	BaSO ₄	0	35	49	3	1	0	0	88
		other Ba-containing	0	0	0	0	0	0	0	0

At site 755, dissolved Ba²⁺ concentrations range between 0.5 µM at the core top and 18.0 µM in the lower core section (Fig. 3f). For site 214, Ba²⁺ concentrations between 0.4 µM and 21.7 µM (160 cmbsf) were determined (Fig. 4f). The Ba²⁺ profile of core 755 suggests two sources for Ba²⁺: the first one is situated directly below the SMTZ at ~200 cmbsf (~Unit II/III boundary), which indicates dissolution of a Ba-containing mineral, supposedly barite; the second source is located at about 500 cmbsf, within the limnic deposits (Unit III). For site 214, the Ba²⁺ profile indicates BaSO₄ dissolution at ~170 cmbsf (Unit II). At ~325 cmbsf in the limnic Unit III there is a sink for Ba²⁺, which we cannot specify further. Towards the bottom of core 214, Ba²⁺ concentrations increase again. We suggest that a deep relict BaSO₄ front buried far below the SMTZ cannot represent a potential Ba²⁺ source for any of the sites. Compared to the rest of the Unit III sediments at location 755, the sedimentary Ba concentrations are not elevated at ~500 cmbsf (depth of Ba²⁺ source) and at site 214, a pronounced barite enrichment below the cored depth would be necessary to at least partly

“survive” the absence of SO_4^{2-} for hundreds or even thousands of years. If SO_4^{2-} has at some point penetrated these depths (>400 cmbsf) in the past, the system was not in a steady state, which makes the formation of such a distinct barite enrichment improbable. More likely, the Ba^{2+} release far below the SMTZ at both sites is related to desorption processes. Hanor and Chan (1977) showed that Ba^{2+} becomes desorbed from suspended clays in rivers as soon as mixing with seawater occurs. The same process was inferred for Baltic Sea sediments. There, formation of authigenic barite micronodules seemed to be related to liberation of adsorbed Ba^{2+} from underlying freshwater sediments due to percolation by saline water (Suess, 1982; Böttcher and Lepland, 2000). The increase in Ca^{2+} concentrations towards the bottom of the cores probably also reflects salinity changes rather than carbonate dissolution, because with respect to exchangeable cations “clay minerals deposited in a freshwater environment are predominantly in the Ca-form, whereas those in the marine environment are mostly in the Na, Mg, K form” (De Lange, 1983). Although some Ba generally may be related to carbonates (e.g., Dymond et al., 1992), the attribution of carbonate dissolution to an increase in Ba^{2+} is thus considered to be low.

For core 755, a sink for Ba^{2+} resulting from authigenic barite precipitation is indicated by tailing of the profile between 190 and 100 cmbsf. The PHREEQC calculations suggest supersaturation with respect to BaSO_4 for the whole SO_4^{2-} -bearing zone (Fig. 3g). The Ba_{xs} peak located between 150 and 210 cmbsf (Fig. 3h) is relatively broad. It comprises concentrations of up to 600 mg kg^{-1} and is, due to its position, interpreted to represent the actively forming diagenetic barite front. According to the BaSO_4 saturation state, the lowermost part of the Ba-enrichment (190-210 cmbsf) is presently subject to dissolution. The imprint on the pore water profile resulting from Ba^{2+} release directly below the SMTZ is, however, not as pronounced as at site 214 (upward Ba^{2+} flux from SMTZ: $0.0096 \mu\text{mol cm}^{-2} \text{ yr}^{-1}$ (core 755) compared to $0.0246 \mu\text{mol cm}^{-2} \text{ yr}^{-1}$ (core 214)), which might result from slower dissolution rates. At site 755, continuous but slow BaSO_4 dissolution obviously occurs in line with sediment accumulation and is not fuelled by an upward migration of the SMTZ burying “relict” Ba enrichments into the SO_4^{2-} -depleted zone. The Ba_{xs} profile at site 214 shows a distinct maximum of $>1300 \text{ mg kg}^{-1}$ at 151 cmbsf, slightly above the SMTZ. A second Ba_{xs} peak ($>700 \text{ mg kg}^{-1}$) appears at 161 cmbsf. This lower Ba enrichment coincides partly with a sandy turbidite deposit (161-165 cmbsf). However, since the Ba enrichment extends to the sediment above the sandy turbidite, it must have formed after its deposition and likely is a product of authigenic BaSO_4 precipitation. This lower Ba_{xs} enrichment coincides with maximum Ba^{2+} concentrations. Therefore, we suggest that it currently is subject to dissolution (similar to ODP Site 994; Snyder et al., 2007). Accordingly, the total Ba and Ba_{xs} concentrations at this depth might have been higher in the past, depending on how long

dissolution has already been active. Due to the short distance between the peaks at 161 and 151 cm, it is not clear whether these two maxima are the relicts of a broader Ba_{xs} enrichment or whether they reflect a slight recent shift of the SMTZ due to changes in the CH_4 flux from below. As shown for site 214, a slight shift of the SMTZ due to archaeal *in situ* methanogenesis in Unit II (Fig. 5) is possible while the rate of deeper methanogenesis might have remained constant. The tailing of Ba^{2+} between 130 and 75 cmbsf as well as the values for the saturation state ranging between 3 and 17 above the SMTZ (Fig. 4f,g), indicate a broad zone of $BaSO_4$ precipitation.

2.4.5 Numerical modeling of the SMTZ migration

Three scenarios regarding the timing and rapidity of the adjustment of hydrochemical conditions in the deep Black Sea were used for all of the CoTRem simulations (Fig. 6, Tab. 1): A) catastrophic flooding leading to present-day bottom water conditions directly after the connection to the Mediterranean Sea (based on findings of Ryan et al., 1997), B) progressive flooding and moderate adjustment to present-day conditions until 1.2 kyrs after the first seawater intrusion, and C) progressive seawater inflow and slow adjustment to present-day conditions until 2 kyrs BP (based on the results of Soulet et al., 2010).

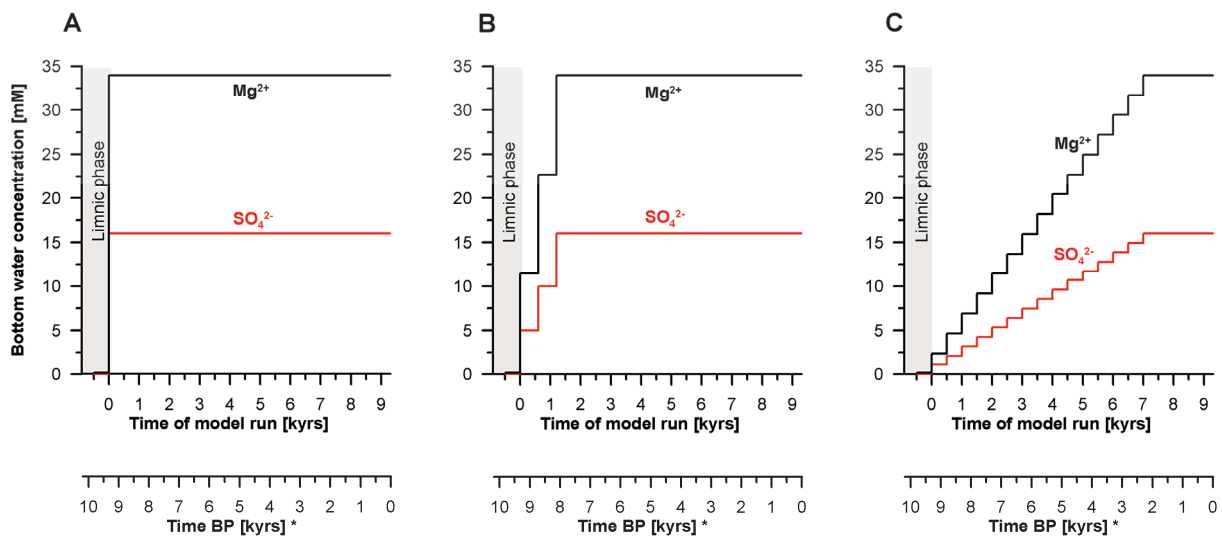


Fig. 6: Scenarios A, B, and C used for CoTRem simulations. A: Abrupt increase of SO_4^{2-} and Mg^{2+} in the bottom water immediately after first seawater intrusion. B: Gradual increase of SO_4^{2-} and Mg^{2+} until 1.2 kyrs after the first seawater intrusion. C: Slow increase of concentrations in the bottom water until 7 kyrs after first seawater intrusion.

Dissolved magnesium is considered as a conservative element following the approach of De Lange et al. (1983). Dolomite ($\text{CaMg}(\text{CO}_3)_2$) precipitation can be excluded due to opposing trends of Ca^{2+} and Mg^{2+} (Figs. 3b, 7). In order to assess which scenario for the salinity increase in bottom water (A-C) fits best to the data set, we simulated the development of the Mg^{2+} profile at site 755. An initial Mg^{2+} concentration of $126 \mu\text{M}$, determined for a freshwater environment (Falkner et al., 1991), was used for Black Sea deep water prior to the marine intrusion. Given that the first seawater intrusion occurred at ~ 9.3 kyrs BP, as inferred from Bahr et al. (2008), the measured Mg^{2+} concentrations in the pore water of core 755 fit best to the simulated profile of scenario C (slow increase in Mg^{2+} bottom water concentrations; Fig. 7). Scenarios A and B would lead to higher present-day Mg^{2+} concentrations in the interstitial water than those measured.

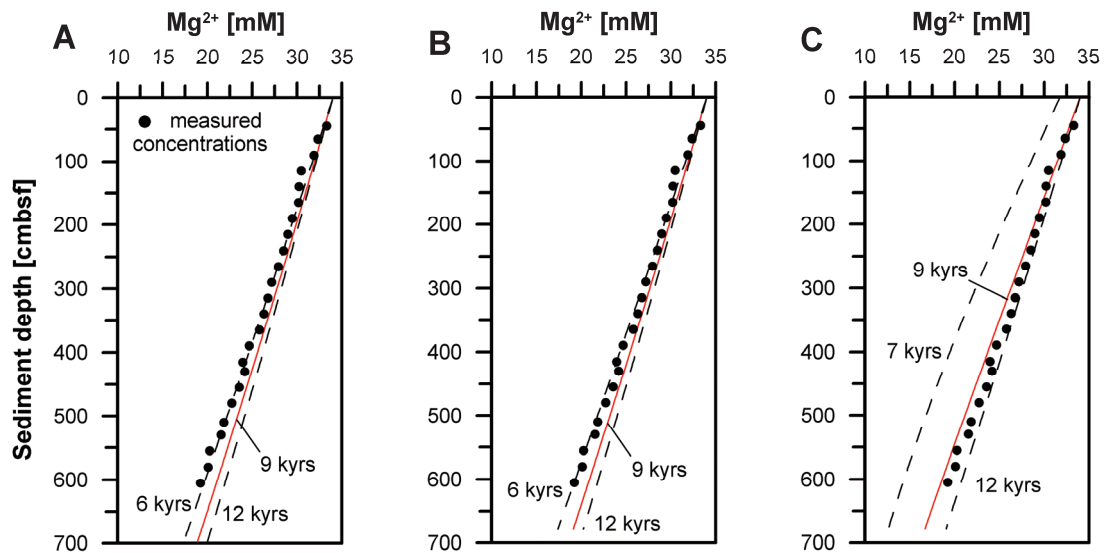


Fig. 7: Modeled pore water profile of the conservative element Mg^{2+} in comparison to measured concentrations at site 755. (Scenarios A, B, and C according to Fig. 6.) The modern upper boundary for Mg^{2+} (34 mM) was inferred from the extended trendline of the gravity core data.

Subsequently, the shift of the SMTZ during Black Sea flooding was simulated according to scenarios A-C Mg^{2+} described above, of which scenario C seems to be the most reasonable based on Mg^{2+} modeling results. Since we did not observe any clear sedimentological evidence for present and past non-steady state conditions at site 755, we infer a constant SMTZ depth since the adjustment to present-day SO_4^{2-} concentrations in the deep water. While in scenarios A and B, such a constant SMTZ depth is reached ~ 3.8 kyrs (i.e. 5.5 kyrs BP) after the first seawater inflow (Fig. 8a), in scenario C this “steady state” is not reached until 7.5 kyrs (i.e. 1.8 kyrs BP) after the marine intrusion. Higher SO_4^{2-} concentrations in the bottom water or a lower CH_4 flux in the sediment at $t=0$ (beginning of seawater intrusion) would accelerate the downward SMTZ migration accordingly.

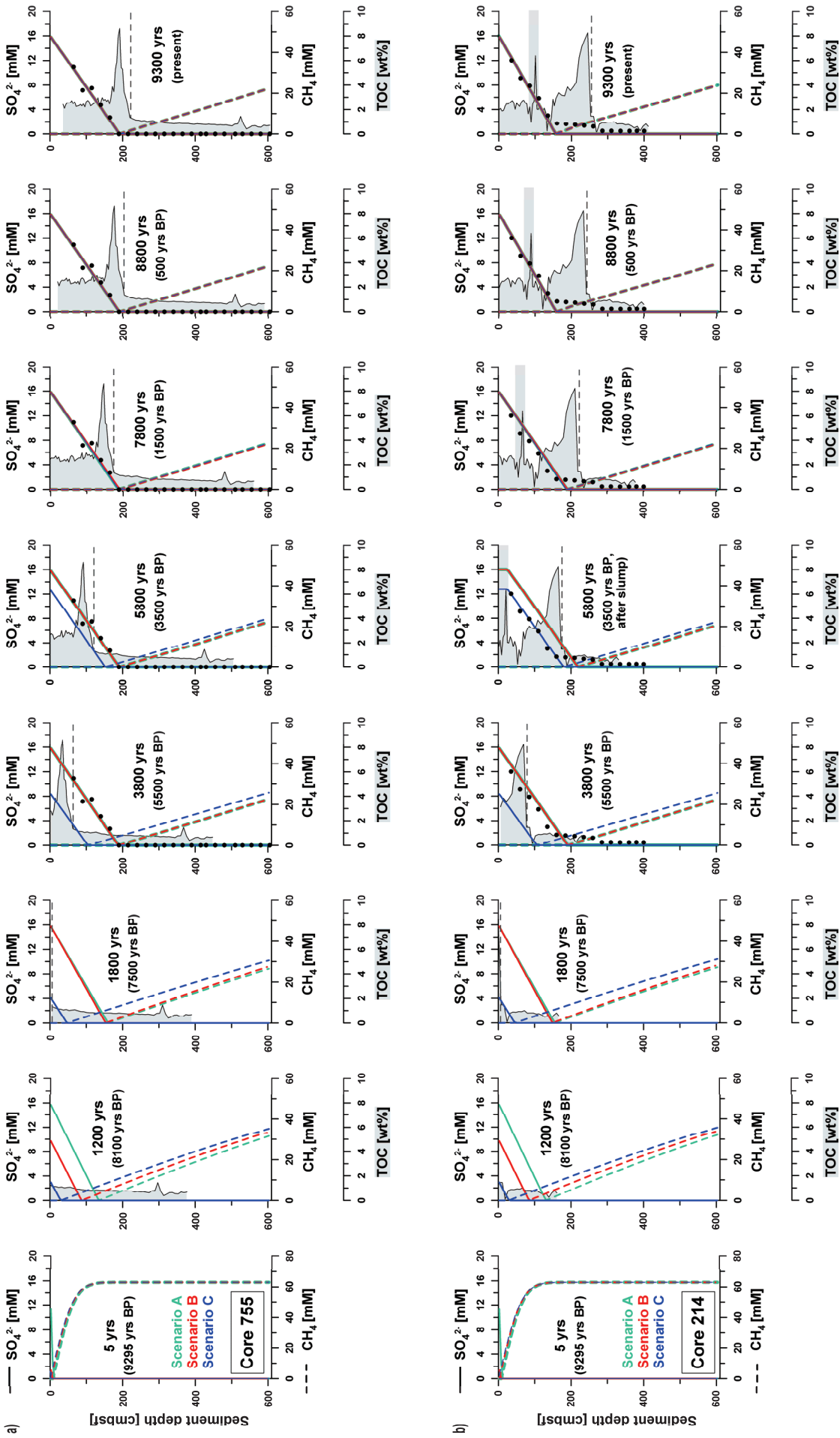


Fig. 8: Results of the CoReM simulation concerning the migration of the SMTZ at sites 755 (a) and 214 (b) since the Holocene spilling of Mediterranean seawater. The dashed black lines indicate the Unit II/III boundary. Black dots show the measured SO_4^{2-} concentrations. The gray horizontal bar in the diagrams for core 214 marks the slump deposit. Please note that the displayed depth (6 m) does not represent the complete model length and that the CH_4 concentration at 13 m depth remained constant.

If we assume a constant sedimentation rate of 29 cm kyr⁻¹ for Unit I at site 755 and a stable sediment depth of the SMTZ for the last couple of thousand years (which was not necessarily the case), the lowermost Unit II sediments were placed/shifted below the SMTZ less than 1 kyrs BP. It is usually expected that the initial barite content of limnic deposits (here Unit III) is low, because low SO₄²⁻ concentrations and the presence of humic substances prevent precipitation in freshwater systems (Smith et al., 2004). However, Ba²⁺ is nowadays liberated from the limnic deposits and it is likely that the process responsible has already been active during the past. Thus, authigenic barite precipitation at both sites must have started immediately within Unit III sediments when the interstitial freshwater containing deep-sourced Ba²⁺ got in contact with SO₄²⁻ ions that diffused downward from the more saline bottom water. The contribution of biogenic barite to the overall Ba redistribution started a couple of thousand years later, when marine sediments were buried into the SO₄²⁻-depleted zone (site 755: <1 kyrs BP, site 214: 1.5-2.0 kyrs BP).

As mentioned above, at site 214 a slight offset between the main Ba_{xs} peak at 151 cmbsf and the relict Ba_{xs} peak at 161 cmbsf might possibly be explained by an increased CH₄ flux due to *in situ* CH₄ production. Although it is somewhat speculative since we do not know the original extent of what we interpret as relict barite front nor the exact *in situ* CH₄ production rate, we provide a possible scenario for how the SO₄²⁻ gradient might have developed over time using similar boundary conditions like at site 755 (scenarios A-C). The only parameters adapted for these calculations, are the sedimentation rates including the slump deposition (Tab. 1) and the *in situ* CH₄ production beginning at the moment the sapropel was shifted below the SMTZ. Like at site 755, the diffusion of SO₄²⁻ ions at site 214 is always faster than sediment accumulation (Fig. 8b). The deepest sediments that have potentially been penetrated by the SMTZ after the reconnection of the Black Sea with the Mediterranean Sea are nowadays found at ~400 cmbsf at site 755 and at the base of core 214 (Fig. 8a,b, scenarios A and B), respectively. At site 214, the slump at ~3.5 kyrs BP caused a transient “downward kink” shape of the SO₄²⁻ profile followed by an upward shift of the SMTZ. This upward migration lasted for about 1 kyrs until the profile was equilibrated with respect to the bottom water SO₄²⁻ concentrations (Fig. 8b). Beginning at 7.8 kyrs after the first seawater intrusion (TOC-peak starts to be buried below the SMTZ), we considered a CH₄ source in our model at the depth of the sapropel (3 to 7 cells at 5 cm thickness supplying 0.1 mmol CH₄ dm⁻³_(aq) yr⁻¹ each). After every step of 200 yrs, the simulation was interrupted for adapting the CH₄-source to the new position of the SMTZ and the sapropel. Applying much higher or lower rates would lead to a shallower or deeper SMTZ, respectively. However, the CH₄ production rate used here should not be over-interpreted because of the aforementioned poor constraints.

Based on the fact that our study sites are not affected by CH₄ seepage and upward advection of hydrocarbon-charged fluids, sudden upward “methane pulses” seem unlikely. Long-term shifts of the SMTZ by several tens of centimeters cannot be excluded unambiguously, but they also cannot be proven since we do not find any clear relict barite fronts neither above nor below the current SMTZ except the one at 161 cmbsf at site 214. We suggest that after adjustment to the current SO₄²⁻ bottom water concentration, the SMTZ depth has not undergone significant variations and that, according to the present Ba²⁺ profiles, the sections 0-100 cmbsf (core 755) and 0-75 cmbsf (core 214) are not or not significantly affected by barite dissolution and precipitation. Due to the lack of a correlation between Ba_{xs} and TOC we were not able to determine the relative amounts of biogenic and diagenetic barite within the main Ba_{xs}-fronts. Therefore, flux calculations to estimate the time necessary to build up the BaSO₄ enrichment at the stable SMTZ (with respect to the sediment surface) as they were applied for example by Riedinger et al. (2006) would lead to questionable results. This is particularly the case for core 755, where Ba_{xs} varies considerably and unrelated to the TOC contents also within the diagenetically “unaffected” section. It seems somewhat odd that the Ba_{xs} concentration at the sediment top at site 755 (501 m water depth) is higher than at site 214 (1686 m water depth), because biogenic barite abundance usually increases with water depth (e.g., von Breyman et al., 1992). Further research is necessary to resolve the barite formation processes in the Black Sea water column.

2.4.6 Uncoupling of Ba and TOC and implications for the use of Ba in anoxic ocean basins

In the cores investigated in this study, TOC and Ba_{xs} are - as expected - completely uncoupled below the SO₄²⁻-zone. At site 214, a correlation is also absent within the SO₄²⁻-bearing zone (Fig. 9b), whereas at site 755 at least part of the Ba_{xs} maximum at 160-180 cmbsf coincides with the TOC peak (175-210 cmbsf). Since both sedimentary TOC and Ba_{xs} are usually controlled by marine productivity and preservation, a correlation between the two parameters has often been found for sediment trap samples and for sediment unaffected by severe post-depositional OM oxidation or diagenetic BaSO₄ redistribution (e.g., Dymond et al., 1992; François et al., 1995; Dymond and Collier, 1996; Martínez-Ruiz et al., 2000). The (de)coupling of Ba and TOC was extensively studied in the Mediterranean Sea: Sapropels which partly or completely underwent organic matter burn-down due to post-depositional oxidation are still recognizable by their enrichments in sedimentary Ba (e.g., van Santvoort et al., 1996; van Santvoort et al., 1997; De Lange et al., 2008). In the Black Sea sediment, the decoupling of both parameters (Fig. 9a,b) has other reasons: 1) the Ba_{xs} signal

has been overprinted extensively by early diagenetic redistribution of Ba (see also Brumsack, 2006) and 2) TOC burial in anoxic basins is not only driven by productivity, but also by enhanced preservation (e.g., Arthur and Dean, 1998; Zonneveld et al., 2010). Since biogenic barite formation is associated with OM degradation in the water column (e.g., Chow and Goldberg, 1960; Bishop, 1988; Bernstein et al., 1992; Ganeshram et al., 2003), the inhibition of OM decay may additionally limit the rate of biogenic barite formation. The establishment of an initial correlation between TOC and Ba_{xs} during accumulation of the marine units is therefore more than questionable. Indeed, the lack of an initial close relationship between TOC and total Ba in the water column was previously shown by Falkner et al. (1993).

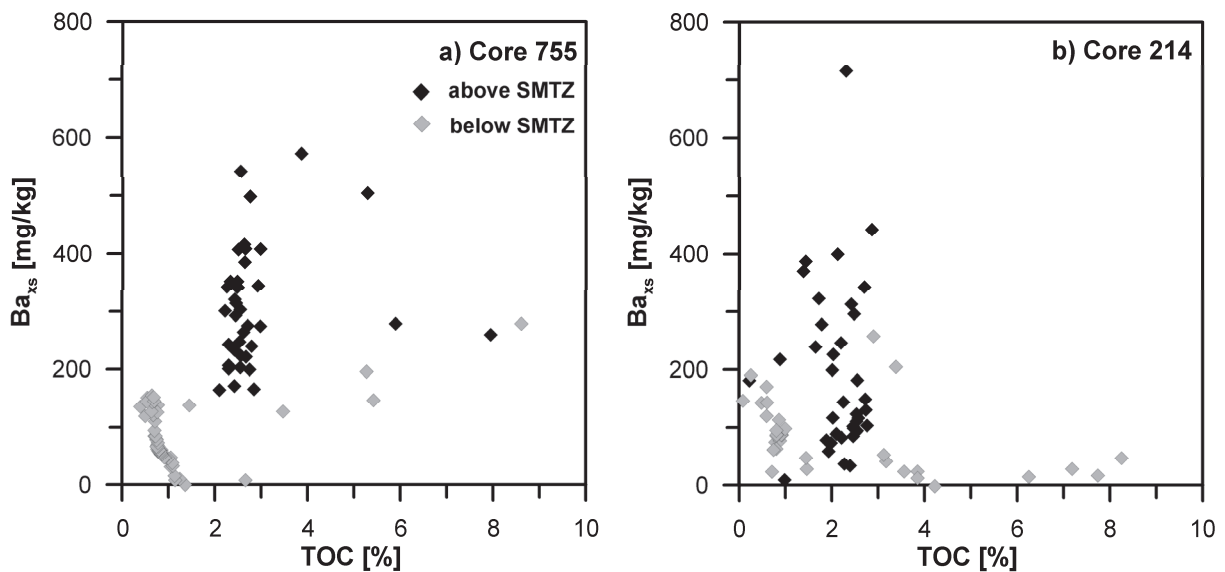


Fig. 9: TOC vs. Ba_{xs} in the gravity cores 755 and 214. A correlation between these parameters is not discernible above as well as below the SMTZ.

Authigenic and biogenic barite can usually be distinguished by their crystal morphology and size (Torres et al., 1996; Paytan et al., 2002; Paytan and Griffith, 2007). In the surface sediment and at 120-122 cmbsf (site 214), biogenic barite particles (ellipsoidal shape) were identified (Fig. 10a,b). However, at the same depths and at 150-152 cmbsf, also irregular shaped barites were detected (Fig. 10c-f). A differentiation of biogenic and diagenetic barites based on grain sizes (Tab. 2) was not possible for the investigated sediment. Since they occur in the surface sediment where Ba redistribution is unlikely, the barite crystals with irregular shape seem not (or not exclusively) to originate from diagenetic precipitation. It must thus be considered that 1) irregular shaped barite is supplied from allochthonous sources, that 2) the shape of biogenic barite formed in an anoxic water column differs from that in oxic ocean basins or that 3) $BaSO_4$ precipitation partly occurs unrelated to marine productivity, possibly from deep water being oversaturated with respect to barite, as suggested by Falkner et al. (1993).

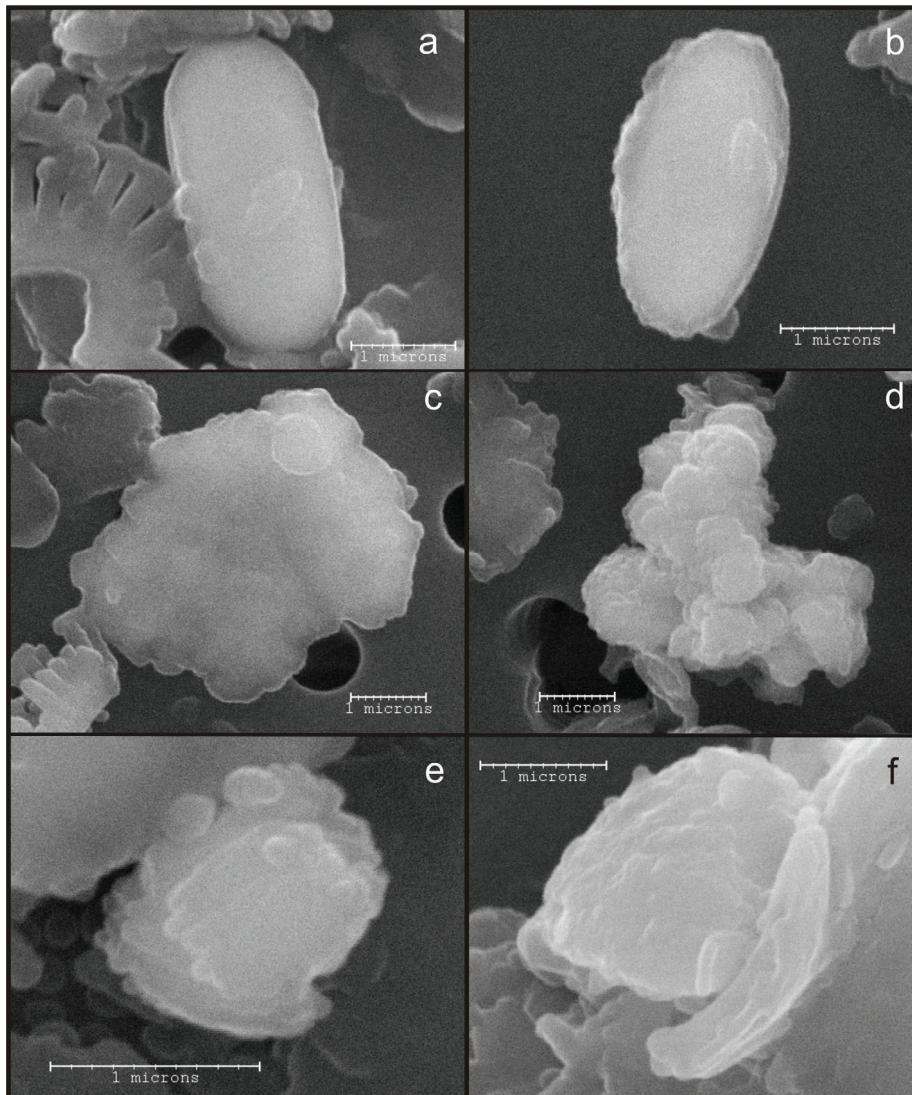


Fig. 10: Biogenic barite in samples core 214, 0-2 cmbsf (a) and 120-122 cmbsf (b). Irregular barite crystals in samples 0-2 cmbsf (c), 120-122 cmbsf (d), and 150-152 cmbsf (e and f).

Yet, there are numerous studies of anoxic ocean basins, in particular covering the Oceanic Anoxic Events (OAEs), for which sedimentary Ba was used as a productivity indicator assuming that the causal relation between Ba and TOC is similar to that in oxic ocean basins: Calvert (1990) presented solid phase Ba data of two gravity cores from the central and eastern Black Sea. The Ba/Al peaks found in Unit I of the sedimentary records coincided with TOC maxima. In the sapropel section, the correlation was less pronounced. Based on this Ba record, Calvert (1990) argued for an increase in nutrient availability in the Black Sea during the formation of the sapropel. Turgeon and Brumsack (2006) examined data of the Furlo section in Italy (Cenomanian/Turonian OAE 2) and stated that the overall high Ba contents in the sediments suggest a high paleoproductivity in that area. The authors also discuss the possibility of early diagenesis, but interpret the Ba concentrations as primary productivity signal based on the dominance of small (tens of microns) barite crystals. At that

time, diagenetic barites were assumed to form “large (20-700 μm), flat, tabular-shaped crystals” (Paytan et al., 2002). The present study, however, shows that the size of the barite crystals is not necessarily indicative for their origin, especially not in anoxic ocean basins. Similar, possibly misleading interpretations of Ba-records covering the OAE2 were presented by Drzewiecki and Simo (1997) (Sopeira section in Spain), Kuypers et al. (2002) (proto-North Atlantic), Bąk (2007) (Splawa section of the Skole Nappe, Poland), and Jiménez Berrocoso et al. (2008) (Demerara Rise). Scopelliti et al. (2004) considered Ba_{xs} as an indicator for productivity for OAE deposits in Sicily and anticipated Ba_{xs} -enrichments in the Bonarelli Level equivalent reflecting high productivities. However, the unexpected fairly low Ba_{xs} concentrations were attributed to a low degree of barite saturation in the oxygen-deficient bottom water Scopelliti et al. (2004). The present study as well as previous ones (e.g., Falkner et al., 1993; Dean et al., 1997) clearly demonstrate that oxygen-depletion alone does not lead to a BaSO_4 undersaturation and that it is rather the absence of SO_4^{2-} that controls its dissolution in marine settings.

2.5 Conclusions

Two gravity cores from the northwestern Black Sea have been investigated in order to assess the cycling of Ba and to unravel the Ba-TOC relationship in sediments of anoxic ocean basins. Numerical simulations of pore water Mg^{2+} suggest a slow (lasting several thousands of years) increase in bottom water salinity after the first intrusion of Mediterranean seawater into the Black Sea. Since the first seawater intrusion, at the sites investigated the SMTZ penetrated the limnic deposits of Unit III over thousands of years. The base of the marine sediments at site 755 and 214 was buried below the SMTZ for the first time only ~1-2 kyrs BP. Diagenetic Ba_{xs} enrichments were found at both locations at and slightly above the current SMTZ. At site 214, where due to higher sedimentation rates, the marine sapropel (Unit II) is nowadays buried below the SO_4^{2-} -zone, Ba_{xs} was completely remobilized from this horizon. The burial of the TOC-rich section below the SMTZ might have fuelled the microbial CH_4 formation and possibly induced a slight upward shift of the SMTZ, as indicated by a relict Ba_{xs} front ~10 cm below the current SO_4^{2-} - CH_4 counter-diffusion boundary. In the Black Sea and comparable settings, *in situ* methanogenesis at shallow depth might exert a strong control on biogeochemical processes and on the overprint of primary sedimentary Ba signals. Accordingly, water column redox conditions indirectly affect the cycling of Ba in the sediment by favoring TOC preservation and *in situ* CH_4 production. The investigated Black Sea records provide evidence for a lack of correlation for Ba_{xs} and TOC not only below the SMTZ, but also in sections that are unaffected by diagenetic barite redistribution. Within the SO_4^{2-} zone, this is probably due to processes taking place in the water column, such as

barite precipitation from oversaturated deep water, lateral transport of Ba-containing minerals or biogenic barite formation controlled by TOC preservation rather than only by productivity. The patterns of sedimentary Ba_{xs} and TOC in our samples differ from those in the Mediterranean Sea, where oxidized sapropels are identified by productivity-related Ba enrichments. In the Black Sea, it is the OM that remains comparatively unaffected after burial, while Ba_{xs} is remobilized diagenetically at the shallow SMTZ. The remaining questions with regard to the water column processes as well as to the low preservation of the original Ba-signal within the sediment give reason for extreme care in reconstructing paleoproductivity based on Ba_{xs} records in modern and ancient depositional settings resembling the modern Black Sea.

Acknowledgments. We thank the captains, staff members, and scientific parties of cruises P317/2 of RV *Poseidon* and M72/1 of RV *Meteor* for their excellent work and collaboration and the University of Hamburg and the Deutsche Forschungsgesellschaft (DFG) for financial support. We are indebted to Brit Kockisch for the TOC measurements as well as to Silvana Pape for technical assistance. Matthew Jones is highly acknowledged for element analyses on core 755. Birte Oppermann is thanked for support with onboard measurements of CH_4 and Ralf Lendt for support with isotope analyses. We thank David Fischer (MARUM), Tim Haarmann (University of Bremen), and Ludmila Baumann (AWI) for sample preparation and laboratory support. We are indebted to Martyn Drury and Tilly Bouten for their help with SEM analyses at Utrecht University. Two anonymous reviewers, Glen Snyder, and Robert C. Aller are greatly acknowledged for detailed and constructive comments on an earlier version of the manuscript. Sandra Arndt and Gerald R. Dickens are thanked for comments and helpful suggestions. This study was conducted in the frame of the International Graduate College EUROPROX "Proxies in Earth History" funded by the DFG. We acknowledge further financial support from the Helmholtz Association. All data are available in the geological database Pangaea (<http://www.pangaea.de>).

References

- Adler, M., Hensen, C., Wenzhöfer, F., Pfeifer, K., and Schulz, H.D., 2001, Modeling of calcite dissolution by oxic respiration in supralysoclineal deep-sea sediments: *Marine Geology*, v. 177, p. 167-189.
- Arndt, S., Brumsack, H.-J., and Wirtz, K.W., 2006, Cretaceous black shales as active bioreactors: A biogeochemical model for the deep biosphere encountered during ODP Leg 207 (Demerara Rise): *Geochimica et Cosmochimica Acta*, v. 70, p. 408-425.
- Arndt, S., Hetzel, A., and Brumsack, H.-J., 2009, Evolution of organic matter degradation in Cretaceous black shales inferred from authigenic barite: A reaction-transport model: *Geochimica et Cosmochimica Acta*, v. 73, p. 2000-2022.
- Arthur, M.A. and Dean, W.E., 1998, Organic-matter production and preservation and evolution of anoxia in the Holocene Black Sea: *Paleoceanography*, v. 13, p. 395-411.
- Arthur, M.A., Dean, W.E., Neff, E.D., Hay, B.J., King, J., and Jones, G.A., 1994, Varve calibrated records of carbonate and organic carbon accumulation over the last 2000 years in the Black Sea: *Global Biogeochemical Cycles*, v. 8, p. 195-217.
- Bahr, A., Arz, H.W., Lamy, F., and Wefer, G., 2006, Late glacial to Holocene paleoenvironmental evolution of the Black Sea, reconstructed with stable oxygen isotope records obtained on ostracod shells: *Earth and Planetary Science Letters*, v. 241, p. 863-875.
- Bahr, A., Lamy, F., Arz, H., Kuhlmann, H., and Wefer, G., 2005, Late glacial to Holocene climate and sedimentation history in the NW Black Sea: *Marine Geology*, v. 214, p. 309-322.
- Bahr, A., Lamy, F., Arz, H., Major, C., Kwicien, O., and Wefer, G., 2008, Abrupt changes of temperature and water chemistry in the late Pleistocene and early Holocene Black Sea: *Geochemistry, Geophysics, Geosystems (G3)*, v. 9.
- Bąk, K., 2007, Organic-rich and manganese sedimentation during the Cenomanian-Turonian boundary event in the Outer Carpathian basins; a new record from the Skole Nappe, Poland: *Palaeogeography, Palaeoclimatology, Palaeoecology*, v. 256, p. 21-46.
- Ballard, R.D., Coleman, D.F., and Rosenberg, G.D., 2000, Further evidence of abrupt Holocene drowning of the Black Sea shelf: *Marine Geology*, v. 170, p. 253-261.
- Barnes, R.O. and Goldberg, E.D., 1976, Methane production and consumption in anoxic marine sediments: *Geology*, v. 4, p. 297-300.
- Bernstein, R.E., Byrne, R.H., Betzer, P.R., and Greco, A.M., 1992, Morphologies and transformations of celestite in seawater: The role of acantharians in strontium and barium geochemistry: *Geochimica et Cosmochimica Acta*, v. 56, p. 3273-3279.

- Bishop, J.K.B., 1988, The barite-opal-organic carbon association in oceanic particulate matter: *Nature*, v. 332, p. 341-343.
- Blumenberg, M., Seifert, R., Kasten, S., Bahlmann, E., and Michaelis, W., 2009, Euphotic zone bacterioplankton sources major sedimentary bacteriohopanepolyols in the Holocene Black Sea: *Geochimica et Cosmochimica Acta*, v. 73, p. 750-766.
- Blumenberg, M., Seifert, R., and Michaelis, W., 2007, Aerobic methanotrophy in the oxic-anoxic transition zone of the Black Sea water column: *Organic Geochemistry*, v. 38, p. 84-91.
- Boetius, A., Ravensschlag, K., Schubert, C.J., Rickert, D., Widdel, F., Gieseke, A., Amann, R., Jørgensen, B.B., Witte, U., and Pfannkuche, O., 2000, A marine microbial consortium apparently mediating anaerobic oxidation of methane: *Nature*, v. 407, p. 623-626.
- Bohrmann, G., Ivanov, M., Foucher, J.-P., Spiess, V., Bialas, J., Greinert, J., Weinrebe, W., Abegg, F., Aloisi, G., Artemov, Y., Blinova, V., Drews, M., Heidersdorf, F., Krabbenhöft, A., Klauke, I., Krastel, S., Leder, T., Polikarpov, I., Saburova, M., Schmale, O., Seifert, R., Volkonskaya, A., and Zillmer, M., 2003, Mud volcanoes and gas hydrates in the Black Sea: new data from Dvurechenskii and Odessa mud volcanoes: *Geo-Marine Letters*, v. 23, p. 239-249.
- Borowski, W.S., Paull, C.K., and Ussler, W., 1996, Marine pore-water sulfate profiles indicate in situ methane flux from underlying gas hydrate: *Geology*, v. 24, p. 655-658.
- Borowski, W.S., Paull, C.K., and Ussler, W., 1997, Carbon cycling within the upper methanogenic zone of continental rise sediments; an example from the methane-rich sediments overlying the Blake Ridge gas hydrate deposits: *Marine Chemistry*, v. 57, p. 299-311.
- Böttcher, M.E. and Lepland, A., 2000, Biogeochemistry of sulfur in a sediment core from the west-central Baltic Sea: evidence from stable isotopes and pyrite textures: *Journal of Marine Systems*, v. 25, p. 299-312.
- Boudreau, B.P., 1997, Diagenetic models and their implementation: modeling transport and reactions in aquatic sediments: Berlin, Heidelberg, New York, Springer, 414 p.
- Brumsack, H.-J., 2006, The trace metal content of recent organic carbon-rich sediments: Implications for Cretaceous black shale formation: *Palaeogeography, Palaeoclimatology, Palaeoecology*, v. 232, p. 344-361.
- Brumsack, H.-J., 1986, The inorganic geochemistry of Cretaceous black shales (DSDP Leg 41) in comparison to modern upwelling sediments from the Gulf of California, *in* Summerhayes, C.P. and Shackleton, N.J., eds., *North Atlantic Palaeoceanography*, Geological Society Special Publication, p. 447-462.
- , 1989, Geochemistry of recent TOC-rich sediments from the Gulf of California and the Black Sea: *Geologische Rundschau*, v. 78, p. 851-882.

- Calvert, S.E., 1990, Geochemistry and origin of the Holocene sapropel in the Black Sea, *in* Ittekkot, V., Kempe, S., Michaelis, W., and Spitz, A., eds., *Facets of Modern Biogeochemistry*: Berlin, Springer, p. 328-358.
- Chow, T.J. and Goldberg, E.D., 1960, On the marine geochemistry of barium: *Geochimica et Cosmochimica Acta*, v. 20, p. 192-198.
- Cline, J.D., 1969, Spectrophotometric determination of hydrogen sulfide in natural waters: *Limnology and Oceanography*, v. 14, p. 454-458.
- De Lange, G.J., 1983, Geochemical evidence of a massive slide in the southern Norwegian Sea: *Nature*, v. 305, p. 420-422.
- , 1992, Shipboard routine and pressure-filtration system for pore-water extraction from suboxic sediments: *Marine Geology*, v. 109, p. 77-81.
- De Lange, G.J., Thomson, J., Reitz, A., Slomp, C.P., Speranza Principato, M., Erba, E., and Corselli, C., 2008, Synchronous basin-wide formation and redox-controlled preservation of a Mediterranean sapropel: *Nature Geoscience*, v. 1, p. 606-610.
- Dean, W.E., Gardner, J.V., and Piper, D.Z., 1997, Inorganic geochemical indicators of glacial-interglacial changes in productivity and anoxia on the California continental margin: *Geochimica et Cosmochimica Acta*, v. 61, p. 4507-4518.
- Degens, E.T. and Ross, D.A., 1972, Chronology of the Black Sea over the last 25,000 years: *Chemical Geology*, v. 10, p. 1-16.
- Deuser, W.G., 1972, Late-Pleistocene and Holocene history of the Black Sea as indicated by stable isotope studies: *Journal of Geophysical Research*, v. 77, p. 1071-1077.
- Dickens, G.R., 2001, Sulfate profiles and barium fronts in sediment on the Blake Ridge: present and past methane fluxes through a large gas hydrate reservoir: *Geochimica et Cosmochimica Acta*, v. 65, p. 529-543.
- Dickens, G.R., Paull, C.K., and Wallace, P.J., 1997, Direct measurement of in situ methane quantities in a large gas-hydrate reservoir: *Nature*, v. 385, p. 426-428.
- Drzewiecki, P.A. and Simo, J.A.T., 1997, Carbonate platform drowning and oceanic anoxic events on a mid-Cretaceous carbonate platform, south-central Pyrenees, Spain: *Journal of Sedimentary Research*, v. 67, p. 698-714.
- Dymond, J. and Collier, R., 1996, Particulate barium fluxes and their relationships to biological productivity: *Deep Sea Research Part II: Topical Studies in Oceanography*, v. 43, p. 1283-1308.
- Dymond, J., Suess, E., and Lyle, M., 1992, Barium in deep-sea sediment: a geochemical proxy for paleoproductivity: *Paleoceanography*, v. 7, p. 163-181.
- Falkner, K.K., Klinkhammer, G.P., Bowers, T.S., Todd, J.F., Lewis, B.L., Landing, W.M., and Edmond, J.M., 1993, The behavior of barium in anoxic marine waters: *Geochimica et Cosmochimica Acta*, v. 57, p. 537-554.

- Falkner, K.K., Measures, C.I., Herbelin, S.E., and Edmond, J.M., 1991, The major and minor element geochemistry of Lake Baikal: *Limnology and Oceanography*, v. 36, p. 413-423.
- François, R., Honjo, S., Manganini, S.J., and Ravizza, G.E., 1995, Biogenic barium fluxes to the deep sea: Implications for paleoproductivity reconstruction: *Global Biogeochemical Cycles*, v. 9, p. 289-303.
- Ganeshram, R.S., François, R., Commeau, J., and Brown-Leger, S.L., 2003, An experimental investigation of barite formation in seawater: *Geochimica et Cosmochimica Acta*, v. 67, p. 2599-2605.
- Gladney, E.S. and Roelandts, I., 1988, 1987 Compilation of elemental concentration data for USGS, BHVO-1, MAG-1, QLO-1, RGM-1, SCo-1, SDC-1, SGR-1 and STM-1: *Geostandards Newsletter*, v. 12, p. 253-262.
- Gleiß, R., 2005, Herstellung und Dokumentation eines Laborstandards für Marine Sedimente [Diploma thesis]: Bremen, University of Bremen.
- Goldberg, E.D. and Arrhenius, G.O.S., 1958, Chemistry of Pacific pelagic sediments: *Geochimica et Cosmochimica Acta*, v. 13, p. 153-212.
- Grasshoff, K., Kremling, K., and Ehrhardt, M., 1983, *Methods of seawater analysis*: Weinheim, NY, Wiley-VCH, 600 p.
- Hanor, J.S. and Chan, L.-H., 1977, Non-conservative behavior of barium during mixing of Mississippi River and Gulf of Mexico waters: *Earth and Planetary Science Letters*, v. 37, p. 242-250.
- Hay, B.J., Arthur, M.A., Dean, W.E., Neff, E.D., and Honjo, S., 1991, Sediment deposition in the Late Holocene abyssal Black Sea with climatic and chronological implications: *Deep Sea Research Part II*, v. 38 (Suppl.), p. 1237-1254.
- Hensen, C., Zabel, M., Pfeifer, K., Schwenk, T., Kasten, S., Riedinger, N., Schulz, H.D., and Boetius, A., 2003, Control of sulfate pore-water profiles by sedimentary events and the significance of anaerobic oxidation of methane for the burial of sulfur in marine sediments: *Geochimica et Cosmochimica Acta*, v. 67, p. 2631-2647.
- Hinrichs, K.-U., Hayes, J.M., Sylva, S.P., Brewer, P.G., and DeLong, E.F., 1999, Methane-consuming archaeobacteria in marine sediments: *Nature*, v. 398, p. 802-805.
- Hoehler, T.M., Alperin, M.J., Albert, D.B., and Martens, C.S., 1994, Field and laboratory studies of methane oxidation in an anoxic marine sediment: Evidence for a methanogen-sulfate reducer consortium: *Global Biogeochemical Cycles*, v. 8, p. 451-463.
- Jiménez Berrocoso, A., MacLeod, K.G., Calvert, S.E., and Elorza, J., 2008, Bottom water anoxia, inoceramid colonization, and benthopelagic coupling during black shale

- deposition on Demerara Rise (Late Cretaceous western tropical North Atlantic): *Paleoceanography*, v. 23, PA3212.
- Jones, G.A. and Gagnon, A.R., 1994, Radiocarbon chronology of Black Sea sediments: *Deep Sea Research Part I: Oceanographic Research Papers*, v. 41, p. 531-557.
- Jørgensen, B.B., Böttcher, M.E., Lüschen, H., Neretin, L.N., and Volkov, I.I., 2004, Anaerobic methane oxidation and a deep H₂S sink generate isotopically heavy sulfides in Black Sea sediments: *Geochimica et Cosmochimica Acta*, v. 68, p. 2095-2118.
- Jørgensen, B.B., Weber, A., and Zopfi, J., 2001, Sulfate reduction and anaerobic methane oxidation in Black Sea sediments: *Deep Sea Research Part I: Oceanographic Research Papers*, v. 48, p. 2097-2120.
- Kasten, S., Zabel, M., Heuer, V., and Hensen, C., 2003, Processes and signals of nonsteady-state diagenesis in deep-sea sediments and their pore waters, *in* Wefer, G., Mulitza, S., and Ratmeyer, V., eds., *The South Atlantic in the Late Quaternary: Reconstruction of Mass Budget and Current Systems*: Berlin, Heidelberg, New York, Springer, p. 431-459.
- Keller, G.H., 1974, Mass physical properties of some western Black Sea sediments, *in* Ross, D.A., and Degens, E.T., eds., *The Black Sea - Geology, Chemistry, and Biology*, Volume 20: Tulsa, American Association of Petroleum Geologists, p. 332-337.
- Knab, N.J., Cragg, B.A., Hornibrook, E.R.C., Holmkvist, L., Pancost, R.D., Borowski, C., Parkes, R.J., and Jørgensen, B.B., 2009, Regulation of anaerobic methane oxidation in sediments of the Black Sea: *Biogeosciences*, v. 6, p. 1505-1518.
- Krüger, M., Treude, T., Wolters, H., Nauhaus, K., and Boetius, A., 2005, Microbial methane turnover in different marine habitats: *Palaeogeography, Palaeoclimatology, Palaeoecology*, v. 227, p. 6-17.
- Kuypers, M.M.M., Pancost, R.D., Nijenhuis, I.A., and Sinninghe Damsté, J.S., 2002, Enhanced productivity led to increased organic carbon burial in the euxinic North Atlantic basin during the late Cenomanian oceanic anoxic event: *Paleoceanography*, v. 17, 1051.
- Li, Y.-H. and Gregory, S., 1974, Diffusion of ions in sea water and in deep-sea sediments: *Geochimica et Cosmochimica Acta*, v. 38, p. 703-714.
- Lüschen, H., 2004, Vergleichende anorganisch-geochemische Untersuchungen an phanerozoischen C_{org}-reichen Sedimenten: Ein Beitrag zur Charakterisierung ihrer Fazies [Dissertation thesis]: Oldenburg, Carl von Ossietzky Universität.
- Major, C.O., Goldstein, S.L., Ryan, W.B.F., Lericolais, G., Piotrowski, A.M., and Hajdas, I., 2006, The co-evolution of Black Sea level and composition through the last deglaciation and its paleoclimatic significance: *Quaternary Science Reviews*, v. 25, p. 2031-2047.

- Major, C.O., Ryan, W., Lericolais, G., and Hajdas, I., 2002, Constraints on Black Sea outflow to the Sea of Marmara during the last glacial-interglacial transition: *Marine Geology*, v. 190, p. 19-34.
- Marret, F., Mudie, P., Aksu, A., and Hiscott, R.N., 2009, A Holocene dinocyst record of a two-step transformation of the Neoeuxinian brackish water lake into the Black Sea: *Quaternary International*, v. 197, p. 72-86.
- Martens, C.S. and Klump, J.V., 1984, Biogeochemical cycling in an organic-rich coastal marine basin 4. An organic carbon budget for sediments dominated by sulfate reduction and methanogenesis: *Geochimica et Cosmochimica Acta*, v. 48, p. 1987-2004.
- Martínez-Ruiz, F., Kastner, M., Paytan, A., Ortega-Huertas, M., and Bernasconi, S.M., 2000, Geochemical evidence for enhanced productivity during S1 sapropel deposition in the eastern Mediterranean: *Paleoceanography*, v. 15, p. 200-209.
- Morse, J.W., Arvidson, R.S., and Lüttge, A., 2007, Calcium carbonate formation and dissolution: *Chemical Reviews*, v. 107, p. 342-381.
- Naudts, L., Greinert, J., Artemov, Y., Staelens, P., Poort, J., Van Rensbergen, P., and De Batist, M., 2006, Geological and morphological setting of 2778 methane seeps in the Dnepr paleo-delta, northwestern Black Sea: *Marine Geology*, v. 227, p. 177-199.
- Neretin, L.N., Böttcher, M.E., Jørgensen, B.B., Volkov, I.I., Lüschen, H., and Hilgenfeldt, K., 2004, Pyritization processes and greigite formation in the advancing sulfidization front in the upper Pleistocene sediments of the Black Sea: *Geochimica et Cosmochimica Acta*, v. 68, p. 2081-2093.
- Niewöhner, C., Hensen, C., Kasten, S., Zabel, M., and Schulz, H.D., 1998, Deep sulfate reduction completely mediated by anaerobic methane oxidation in sediments of the upwelling area off Namibia: *Geochimica et Cosmochimica Acta*, v. 62, p. 455-464.
- Özsoy, E. and Ünlüata, Ü., 1997, Oceanography of the Black Sea: A review of some recent results: *Earth-Science Reviews*, v. 42, p. 231-272.
- Panin, N. and Jipa, D., 2002, Danube River sediment input and its interaction with the northwestern Black Sea: *Estuarine, Coastal and Shelf Science*, v. 54, p. 551-562.
- Pape, T., Bahr, A., Rethemeyer, J., Kessler, J.D., Sahling, H., Hinrichs, K.U., Klapp, S.A., Reeburgh, W.S., and Bohrmann, G., 2010, Molecular and isotopic partitioning of low-molecular-weight hydrocarbons during migration and gas hydrate precipitation in deposits of a high-flux seepage site: *Chemical Geology*, v. 269, p. 350-363.
- Parkhurst, D.L. and Appelo, C.A.J., 1999, User's guide to PHREEQC (Version 2.0) - A computer program for speciation, batch-reaction, one-dimensional transport, and inverse geochemical calculations, Water-Resources Investigations Report 99-4259, U.S. Geol. Surv., p. 312.

- Paytan, A. and Griffith, E.M., 2007, Marine barite: Recorder of variations in ocean export productivity: *Deep Sea Research Part II: Topical Studies in Oceanography*, v. 54, p. 687-705.
- Paytan, A., Mearon, S., Cobb, K., and Kastner, M., 2002, Origin of marine barite deposits: Sr and S isotope characterization: *Geology*, v. 30, p. 747-750.
- Pohlman, J.W., Bauer, J.E., Canuel, E.A., Grabowski, K.S., Knies, D.L., Mitchell, C.S., Whiticar, M.J., and Coffin, R.B., 2009, Methane sources in gas hydrate-bearing cold seeps: evidence from radiocarbon and stable isotopes: *Marine Chemistry*, v. 115, p. 102-109.
- Reeburgh, W.S., 1967, An improved interstitial water sampler: *Limnology and Oceanography*, v. 12, p. 163-165.
- , 1976, Methane consumption in Cariaco Trench waters and sediments: *Earth and Planetary Science Letters*, v. 28, p. 337-344.
- Reeburgh, W.S., Ward, B.B., Whalen, S.C., Sandbeck, K.A., Kilpatrick, K.A., and Kerkhof, L.J., 1991, Black Sea methane geochemistry: *Deep Sea Research*, v. 38 (Suppl. 2), p. 1189-1210.
- Reitz, A., Pfeifer, K., De Lange, G.J., and Klump, J., 2004, Biogenic barium and the detrital Ba/Al ratio: a comparison of their direct and indirect determination: *Marine Geology*, v. 204, p. 289-300.
- Riedinger, N., Kasten, S., Gröger, J., Franke, C., and Pfeifer, K., 2006, Active and buried authigenic barite fronts in sediments from the Eastern Cape Basin: *Earth and Planetary Science Letters*, v. 241, p. 876-887.
- Riedinger, N., Pfeifer, K., Kasten, S., Garming, J.F.L., Vogt, C., and Hensen, C., 2005, Diagenetic alteration of magnetic signals by anaerobic oxidation of methane related to a change in sedimentation rate: *Geochimica et Cosmochimica Acta*, v. 69, p. 4117-4126.
- Robin, E., Rabouille, C., Martinez, G., Lefevre, I., Reyss, J.L., van Beek, P., and Jeandel, C., 2003, Direct barite determination using SEM/EDS-ACC system: implication for constraining barium carriers and barite preservation in marine sediments: *Marine Chemistry*, v. 82, p. 289-306.
- Rösler, H.J. and Lange, H., 1972, *Geochemical Tables*: New York, Elsevier.
- Ross, D.A. and Degens, E.T., 1974, Recent sediments in the Black Sea, *in* Ross, D.A. and Degens, E.T., eds., *The Black Sea - Geology, Chemistry, and Biology*, Volume 20: Tulsa, American Association of Petroleum Geologists, p. 183-199.
- Ross, D.A., Degens, E.T., and MacIlvaine, J., 1970, Black Sea: recent sedimentary history: *Science*, v. 170, p. 163-165.

- Ryan, W.B.F., Pitman, W.C., Major, C.O., Shimkus, K., Moskalenko, V., Jones, G.A., Dimitrov, P., Gorür, N., Saking, M., and Yüce, H., 1997, An abrupt drowning of the Black Sea shelf: *Marine Geology*, v. 138, p. 119-126.
- Schlüter, M., 1990, Zur Frühdiagenese von organischem Kohlenstoff und Opal in Sedimenten des südlichen und östlichen Weddellmeeres: geochemische Analyse und Modellierung Berichte zur Polarforschung: Bremerhaven, p. 156.
- Schulz, H.D., 2006, Quantification of early diagenesis: dissolved constituents in pore water and signals in the solid phase, *in* Schulz, H.D. and Zabel, M., eds., *Marine Geochemistry*: Berlin, Springer, p. 73-124.
- Scopelliti, G., Bellanca, A., Coccioni, R., Luciani, V., Neri, R., Baudin, F., Chiari, M., and Marcucci, M., 2004, High-resolution geochemical and biotic records of the Tethyan 'Bonarelli Level' (OAE2, latest Cenomanian) from the Calabianca-Guidaloca composite section, northwestern Sicily, Italy: *Palaeogeography, Palaeoclimatology, Palaeoecology*, v. 208, p. 293-317.
- Seeberg-Elverfeldt, J., Schlüter, M., Feseker, T., and Kölling, M., 2005, Rhizon sampling of porewaters near the sediment-water interface of aquatic systems: *Limnology and Oceanography: Methods*, v. 3, p. 361-371.
- Seifert, R., Delling, N., Richnow, H.H., Kempe, S., Hefter, J., and Michaelis, W., 1999, Ethylene and methane in the upper water column of the subtropical Atlantic: *Biogeochemistry*, v. 44, p. 73-91.
- Seifert, R., Nauhaus, K., Blumenberg, M., Krüger, M., and Michaelis, W., 2006, Methane dynamics in a microbial community of the Black Sea traced by stable carbon isotopes *in vitro*: *Organic Geochemistry*, v. 37, p. 1411-1419.
- Smith, E., Hamilton-Taylor, J., Davison, W., Fullwood, N.J., and McGrath, M., 2004, The effect of humic substances on barite precipitation-dissolution behaviour in natural and synthetic lake waters: *Chemical Geology*, v. 207, p. 81-89.
- Snyder, G.T., Dickens, G.R., and Castellini, D.G., 2007, Labile barite contents and dissolved barium concentrations on Blake Ridge: New perspectives on barium cycling above gas hydrate systems: *Journal of Geochemical Exploration*, v. 95, p. 48-65.
- Soulet, G., Delaygue, G., Vallet-Coulomb, C., Böttcher, M.E., Sonzogni, C., Lericolais, G., and Bard, E., 2010, Glacial hydrologic conditions in the Black Sea reconstructed using geochemical pore water profiles: *Earth and Planetary Science Letters*, v. 296, p. 57-66.
- Suess, E., 1982, Authigenic barite in varved clays: result of marine transgression over freshwater deposits and associated changes in interstitial water chemistry, *in* Fanning, K.A. and Manheim, F.T., eds., *The dynamic environment of the ocean floor*: Lexington, Massachusetts, Toronto, Lexington Books, p. 502.

- Taylor, S.R., 1964, Abundance of chemical elements in the continental crust: a new table: *Geochimica et Cosmochimica Acta*, v. 28, p. 1273-1285.
- Torres, M.E., Brumsack, H.-J., Bohrmann, G., and Emeis, K.C., 1996, Barite fronts in continental margin sediments: a new look at barium remobilization in the zone of sulfate reduction and formation of heavy barites in diagenetic fronts: *Chemical Geology*, v. 127, p. 125-139.
- Turgeon, S. and Brumsack, H.-J., 2006, Anoxic vs dysoxic events reflected in sediment geochemistry during the Cenomanian-Turonian Boundary Event (Cretaceous) in the Umbria-Marche Basin of central Italy: *Chemical Geology*, v. 234, p. 321-339.
- van Os, B.J.H., Middelburg, J.J., and De Lange, G.J., 1991, Possible diagenetic mobilization of barium in sapropelic sediment from the eastern Mediterranean: *Marine Geology*, v. 100, p. 125-136.
- van Santvoort, P.J.M., De Lange, G.J., Langereis, C.G., Dekkers, M.J., and Paterne, M., 1997, Geochemical and paleomagnetic evidence for the occurrence of "missing" sapropels in eastern Mediterranean sediments: *Paleoceanography*, v. 12, p. 773-786.
- van Santvoort, P.J.M., De Lange, G.J., Thomson, J., Cussen, H., Wilson, T.R.S., Krom, M.D., and Ströhle, K., 1996, Active post-depositional oxidation of the most recent sapropel (S1) in sediments of the eastern Mediterranean Sea: *Geochimica et Cosmochimica Acta*, v. 60, p. 4007-4024.
- von Breyman, M.T., Emeis, K.-C., and Suess, E., 1992, Water depth and diagenetic constraints on the use of barium as a palaeoproductivity indicator, *in* Summerhayes, C.P., Prell, W.L., and Emeis, K.C., eds., *Upwelling Systems: Evolution since the Early Miocene*, Volume 64, Geological Society Special Publication, p. 273-284.
- Wall, D. and Dale, B., 1974, Dinoflagellates in the late Quaternary deep-water sediments of the Black Sea, *in* Degens, E.T. and Ross, D.A., eds., *The Black Sea – Geology, Chemistry and Biology*, Volume 20: Tulsa, American Association of Petroleum Geologists, p. 364-380.
- Weber, A., Riess, W., Wenzhoefer, F., and Jørgensen, B.B., 2001, Sulfate reduction in Black Sea sediments: in situ and laboratory radiotracer measurements from the shelf to 2000 m depth: *Deep Sea Research Part I: Oceanographic Research Papers*, v. 48, p. 2073-2096.
- Wenzhöfer, F., Adler, M., Kohls, O., Hensen, C., Strotmann, B., Boehme, S., and Schulz, H.D., 2001, Calcite dissolution driven by benthic mineralization in the deep-sea: in situ measurements of Ca^{2+} , pH, pCO_2 and O_2 : *Geochimica et Cosmochimica Acta*, v. 65, p. 2677-2690.
- Whiticar, M.J., 1999, Carbon and hydrogen isotope systematics of bacterial formation and oxidation of methane: *Chemical Geology*, v. 161, p. 291-314.

- Yiğiterhan, O. and Murray, J.W., 2008, Trace metal composition of particulate matter of the Danube River and Turkish rivers draining into the Black Sea: *Marine Chemistry*, v. 111, p. 63-76.
- Zonneveld, K.A.F., Versteegh, G.J.M., Kasten, S., Eglinton, T.I., Emeis, K.C., Huguet, C., Koch, B.P., De Lange, G.J., de Leeuw, J.W., Middelburg, J.J., Mollenhauer, G., Prahl, F.G., Rethemeyer, J., and Wakeham, S.G., 2010, Selective preservation of organic matter in marine environments; processes and impact on the sedimentary record: *Biogeosciences*, v. 7, p. 483-511.

Chapter 3: An interdisciplinary investigation of a recent submarine mass-transport deposit at the continental margin off Uruguay

Susann Henkel¹, Michael Strasser², Tilmann Schwenk³, Till J.J. Hanebuth², Johannes Hüsener⁴, Gail L. Arnold⁵, Daniel Winkelmann⁶, Michael Formolo⁷, Juan Tomasini⁸, Sebastian Krastel⁶, and Sabine Kasten¹

¹Alfred Wegener Institute for Polar and Marine Research, Am Handelshafen 12, 27570, Bremerhaven, Germany

²Center for Marine Environmental Sciences (MARUM), Leobener Str., 28359, Bremen, Germany

³Center for Marine Environmental Sciences (MARUM) and Faculty of Geosciences, University of Bremen, Klagenfurter Str., 28359, Bremen, Germany

⁴Faculty of Geosciences, University of Bremen, Klagenfurter Str., 28359, Bremen, Germany

⁵Max Planck Institute for Marine Microbiology, Biogeochemistry Department, Celsiusstr. 1, 28359 Bremen, Germany

⁶Leibniz Institute of Marine Sciences (IFM-GEOMAR), Wischhofstr. 1-3, 24148 Kiel, Germany

⁷Department of Geosciences, The University of Tulsa, 800 South Tucker Drive, Tulsa, OK, 74104, USA

⁸Administración Nacional de Combustibles Alcohol y Portland (ANCAP), Paysandú s/n esq. Avenida del Libertador, Montevideo, 11100, Uruguay

Manuscript submitted to *Geochemistry, Geophysics, Geosystems*

Abstract

Assessing the frequency and extent of mass movement at continental margins is crucial to evaluate risks for offshore constructions and coastal areas. A multidisciplinary approach including geophysical, sedimentological, geotechnical, and geochemical methods was applied to investigate a mass-transport deposit (MTD) off Uruguay, on top of which no surficial hemipelagic drape was detected based on echosounder data. Non-steady state pore water conditions are evidenced by a distinct gradient change of the sulfate (SO_4^{2-}) profile at

2.8 m depth. A sharp sedimentological contact at 2.43 m coincides with an abrupt downward increase in shear strength from ~10 to >20 kPa. This boundary is interpreted as a paleosurface that has recently been overthrust by a sediment package. The MTD supposedly originated from an upslope position and carried its initial pore water signature downward. The kink in the SO_4^{2-} profile ~35 cm below the contact indicates that bioirrigation affected the paleosurface before deposition of the MTD. Based on modeling of the diffusive re-equilibration of SO_4^{2-} the age of the MTD is estimated to be <30 years. The mass movement was possibly related to an earthquake in 1988 (~70 km southwest of the core location). Probabilistic slope stability back-analysis of the observed structure reveals that slope failure initiation required additional ground accelerations and that the earthquake was a reasonable trigger if additional weakening processes (e.g., excess pore pressure) preconditioned the slope. Our study reveals the necessity of multidisciplinary approaches to accurately recognize and date recent slope failures in complex settings such as the continental margin off Uruguay.

3.1 Introduction

Increasing numbers of offshore constructions including undersea cables, pipelines, and oil rigs require detailed hazard assessments with regard to submarine mass movement. Reasons for slope failure are multifold and include slope oversteepening, earthquake loading, internal wave activity, rapid sediment accumulation and associated under-consolidation, gas charging, gas-hydrate dissociation, seepage, glacial and hydro isostasy, and volcanic island growth (Locat and Lee, 2002). Gaining reliable data about frequency, causes, and consequences of submarine mass movement in a specific region is often challenging. Hydro-acoustic mapping can reveal the presence of slump and slide deposits, but does not allow complete determination of the internal structures of mass-transport deposits (MTDs) due to its limited horizontal and vertical resolution. Sedimentological analyses of sediment cores overcome most of these limitations but accurate dating of the slide event, identification of the original trigger mechanism, as well as the differentiation between *in situ* and transported coherent sediment blocks still represent major challenges. In the case of very young (tens to hundreds of years old) MTDs, pore water geochemistry can help to recognize the remobilized/transported character of sediment blocks (De Lange, 1983; Zabel and Schulz, 2001; Hensen et al., 2003). One of the most important pore water parameters in this regard is the sulfate (SO_4^{2-}) concentration. In marine, “undisturbed” environments the SO_4^{2-} and alkalinity pore water profiles are shaped predominantly by the upward methane (CH_4) flux, SO_4^{2-} concentrations in the bottom water, and sedimentation

rates (SRs). At the zone of anaerobic oxidation of methane (AOM), microbes use SO_4^{2-} and oxidize CH_4 according to the net equation:



(e.g., Barnes and Goldberg, 1976; Reeburgh, 1976; Boetius et al., 2000). Under steady state conditions, SO_4^{2-} decreases linearly with depth, while the alkalinity increases towards the zone of AOM, where HCO_3^- and HS^- are liberated. In fact, this correlation is a simplification in several aspects. Linear profiles always show a pore water system being in equilibrium. However, continuous bioirrigation is reflected by non-linear profiles although the system can be described as steady state with respect to the depositional conditions. Additionally, there are practically no steady state systems in nature. For example, very slow (seasonal) changes cannot be resolved by the temporal resolution of sampling.

The depth at which downward diffusing SO_4^{2-} and upward diffusing CH_4 coexist, is referred to as sulfate-methane transition zone (SMTZ). Drastic changes in SRs, CH_4 fluxes, the intensity of bioirrigation, or advective processes, as well as submarine landslides may disrupt the steady state conditions and lead to transient kink-shape, concave-up, concave-down, or s-type SO_4^{2-} profiles (e.g., Aller, 1983; Hensen et al., 2003; Kasten et al., 2003). Non-steady state SO_4^{2-} profiles are therefore sometimes used for geochemical modeling in order to trace back such intensive changes in environmental and/or depositional conditions (Zabel and Schulz, 2001; Hensen et al., 2003; Riedinger et al., 2005).

Here we present an interdisciplinary approach to examine a supposedly young (i.e., sub-recent) MTD at the continental margin off Uruguay. The aim of the study is to overcome the aforementioned problems with respect to the identification and dating of slide blocks by applying a wide range of methods. We exemplarily demonstrate how the link between pore water geochemistry and more conventional submarine landslide investigation methods can be used to detect recent gravitational events.

Possible trigger mechanisms for young failure events can be identified by analyzing the historical record of “extreme” events in the study area that may have been responsible for sediment remobilization. For instance, many studies have shown that the ultimate trigger mechanism for submarine slope failures often relates to earthquakes, even along passive continental margins with very low seismicity (Hampton et al., 1996; Bryn et al., 2005; ten Brink et al., 2009; Stigall and Dugan, 2010). Correlating identified and dated (by means of geochemical analysis) young MTDs with the historical earthquake catalogue may thus

provide the means of reconstructing recent submarine landslide scenarios as well as assessing the geohazard potential and recurrence of similar events in the future.

3.2 Setting

The study area is located off Uruguay, ~300 km east of the Río de la Plata mouth (Fig. 11). Krastel et al. (in press) refer to it as the “northern slide area”. In this area, MTDs were identified during RV *Meteor* cruise M78/3 (May 2009).

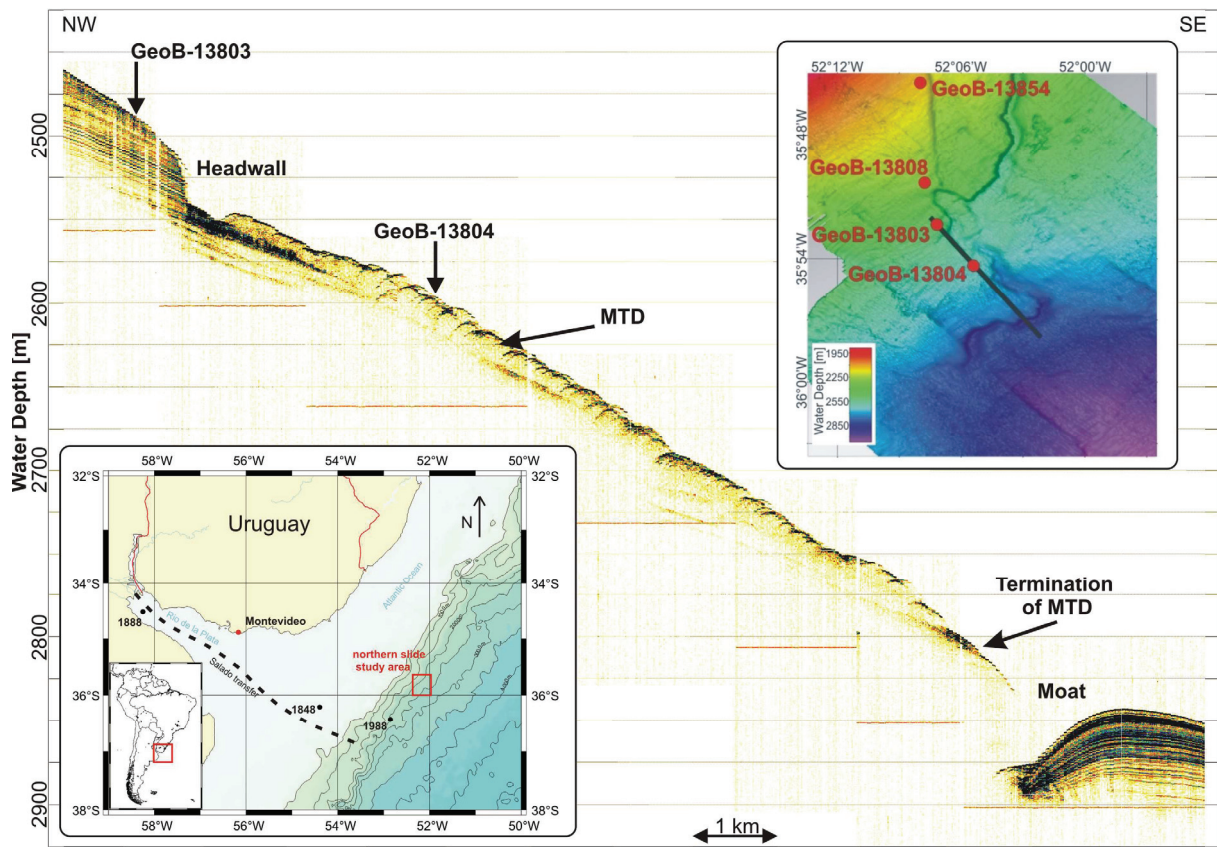


Fig. 11: The map on the lower left side shows the location of the study area offshore Uruguay (red frame) and the epicenter of recent earthquakes (black dots with dates). The dashed line represents the Salado transfer fault. The multibeam bathymetry of the study area including the location of the Parasound profile, the studied core GeoB 13804 and the core locations GeoB 13803, 13808, and 13854 of which the input parameters for the slope stability analysis were deduced, are shown on the right side. The Parasound profile indicates a multi-stage MTD at the position of core GeoB 13804. The Parasound figure was created using the free software SENT developed by H. Keil, University of Bremen.

Post rifting Tertiary tectonic activity is generally considered to be insignificant in the study area (Hinz et al., 1999; Schnabel et al., 2008). However, recent historically documented intraplate seismicity aligned along the Martín García fracture zone or “Salado transfer” (i.e., a inherited extensional tectonic lineament striking NW-SE; Fig. 11) suggests present-day tectonic activity in the area, which likely is in a state of active subsidence (Benavídez Sosa,

1998). Earthquakes producing significant macroseismic intensities in the coastal cities of Buenos Aires and Montevideo recently occurred in the years 1888, 1848, and 1988 A.D. (Benavídez Sosa, 1998; Fig. 11). The epicenter of the latter was located close to our study area and an earthquake magnitude of $\sim 5.2 m_b$ was estimated (Assumpção, 1998). It has not been investigated so far, whether or not recent seismotectonic activity had influence on sediment dynamics along the continental margin off Uruguay and Argentina.

Sedimentation along this margin is strongly influenced by the structure of the water column. Strong contour-parallel currents lead to the formation of depositional and erosional sedimentary features, such as contourite deposits, moats, contouritic channels, and erosional terraces (Hernández-Molina et al., 2009). The oceanographic conditions in the upper water column are strongly determined by the highly energetic Brazil-Malvinas Confluence near $38^\circ S$ (Brennecke, 1921; Deacon, 1937; Gordon and Greengrove, 1986).

There have been several scientific cruises to the South American continental slope and the Argentine Basin during the past decades. Geophysical surveys showed that slope failure is a common characteristic at this continental margin. Most of the research, however, focused on undisturbed hemipelagic sediment successions to reconstruct the paleoclimate and the ocean current history (Bleil et al., 1994; Segl et al., 1994; Bleil et al., 2001a; Bleil et al., 2001b; Schulz et al., 2001; Spiess et al., 2002). Only a few studies on mass wasting in this highly dynamic system are available (Lonardi and Ewing, 1971; Klaus and Ledbetter, 1988; Hensen et al., 2003; Krastel et al., in press).

The seafloor in the study area is characterized by a series of three scarps (Fig. 11) as described in detail by Krastel et al. (in press). The NW-SE orientated Parasound profile (for methods see next section) imaging the location of core GeoB 13804 (Fig. 11) crosses two of these scarps with heights of 25 m and 50 m (NW and SE, respectively). The deposits in the north-western part of the profile appear as distinct, parallel layered facies of moderate amplitude, partly intercalated by thin acoustically transparent layers. The area between both scarps is characterized by an up to 20 m thick acoustically transparent/chaotic body with hummocky surface located on top of a prolonged reflector. This sediment body pinches out upslope of the south-eastern scarp in a water depth of 2800 m. Continuous high-amplitude reflectors showing a convex reflection configuration are imaged downslope of this scarp. The acoustically transparent/chaotic body with hummocky surface was interpreted as a multi-stage MTD by Krastel et al. (in press). Consequently, the north-western scarp on the Parasound profile represents the headwall of the mass-transport complex whereas the section upslope of the headwall shows rather undisturbed sediments, probably of

hemipelagic and turbiditic origin. The convex unit in the south-eastern part of the profile (Fig. 11) is interpreted as contouritic drift deposit, and the adjacent scarp in 2850 m water depth as a contouritic moat, which redirects and intensifies the ocean currents locally. Based on the results of hydro-acoustic subsurface imaging methods, no hemipelagic drape overlying the hummocky surface could be identified. Therefore, a relatively young age of the uppermost MTD was suggested. However, we need to consider that the vertical resolution of the Parasound data is in dm-scale (see section 3.3.1). Therefore, in order to estimate the exact age of the youngest slide deposit, other methods, such as geochemical analyses on sediments needed to be applied.

3.3 Material and methods

3.3.1 Geophysical mapping

Sediment echosounder data were collected with the Parasound system (Atlas Hydrographic GmbH), which utilizes the parametric effect to emit a 4 kHz signal in a cone of 4.5-5° opening angle. This configuration results in a vertical resolution of a few decimeters and a horizontal resolution of 7% of the water depths, which is less than 200 m in the study area. Features of smaller dimensions are thus integrated. Details can be found in Grant and Schreiber (1990). Bathymetric data were collected with the Kongsberg EM120 multibeam system. The data were automatically and manually edited to create a grid of 100 m bin size.

3.3.2 Sampling

A gravity core and a multicorer (MUC) core, 6.07 m and 0.28 m long, were retrieved at site GeoB 13804 (35°54.30' S, 52°05.42' W) from 2593 m water depth (Fig. 11). The sampling took place in May 2009 during cruise M78/3a with the German research vessel *Meteor*. The core handling and geochemical sample processing was performed following the standard procedures after Schulz (2006). After recovery, the gravity core was cut into segments of 1 m length. Syringe samples (3 cm³) for CH₄ analyses were taken directly during cutting at the lower ends of the segments. The sediment was immediately transferred into 20 ml headspace vials, which were pre-filled with 10 ml of a 5 M NaCl solution. The headspace vials were closed, shaken, and stored at 4°C until analysis onshore. Immediately after splitting the core segments into halves, geotechnical sampling for density, moisture, and porosity determinations were performed every 50 cm according to IODP onboard laboratory practices (Blum, 1997). Subsequently, pore water sampling with rhizons (Seeberg-Elverfeldt et al., 2005) was carried out at ~4°C. The redox-potential (E_H) was measured by use of a punch-in electrode. For the determination of the ²¹⁰Pb activity, the MUC core was sliced in 1

to 2 cm intervals. The sediment was transferred into Petri-dishes and stored at 4°C until further processing.

3.3.3 Geotechnical and sedimentological analyses

The undrained shear strength of the sediment was determined onboard using a Wykeham-Farrance cone penetrometer WF 21600 and a Mennerich Geotechnik vane shear device (rotation 90°/min) following the procedures of Boyce (1977) and Blum (1997). Sedimentological investigations involved a detailed visual core description and preparation of radiographies.

3.3.4 Pore water analyses

Sulfate measurements were performed onboard using a Sykam solvent delivery system coupled to a Waters 430 conductivity detector. Daily standard calibrations using seawater provided by the International Association for the Physical Sciences of the Oceans (IAPSO) were performed. Alkalinity was determined by titration of a 1 ml pore water aliquot with 10-100 mM HCl. For calculating the alkalinity, the equation given by Schulz (2006) was used. Sulfide concentrations ($\Sigma\text{H}_2\text{S} = \text{H}_2\text{S} + \text{HS}^- + \text{S}^{2-}$) were analyzed onboard using the methylene blue method of Cline (1969). Phosphate (HPO_4^{2-}) was determined using the photometric method described by Grasshoff et al. (1999). Phosphate samples that contained $\Sigma\text{H}_2\text{S}$ were purged with argon prior to the addition of the reagents. Dissolved Fe^{2+} was determined photometrically at 565 nm after addition of a sample aliquot (1 ml) to 50 μl of Ferrospectral solution to complex the Fe^{2+} . Samples with high concentrations of Fe^{2+} ($>1 \text{ mg l}^{-1}$) were pretreated with 10 μl ascorbic acid and diluted with O_2 -free artificial seawater prior to complexation. Methane was measured with a Hewlett Packard 5890A gas chromatograph (GC) using a splitless injector, a stainless steel Porapak-Q column, and a flame ionization detector. Chromatographic response on the GC instrument was calibrated against three different standards with variable concentrations of CH_4 . The measured concentrations were corrected for sediment porosity.

3.3.5 Dating of sediment

Analyses of ^{210}Pb , ^{226}Ra , and ^{137}Cs were performed at the Max Planck Institute for Marine Microbiology in Bremen. The sediment samples were freeze-dried, ground in an agate mortar and subsequently analyzed by non-destructive gamma spectrometry. Sample analyses ran for a minimum of 24 hours each. Unsupported ^{210}Pb ($^{210}\text{Pb}_{\text{unSUPP}}$; airborne, not produced in the sediment by decay of ^{226}Ra) was calculated for each depth by subtracting the activity of ^{226}Ra

from the activity of ^{210}Pb . Sediment ages were calculated using the C.I.C. (constant initial concentration) and the C.R.S. (constant rate of supply) models of Robbins (1978) and Appleby and Oldfield (1978).

3.3.6 Modeling of sulfate profile development

The re-equilibration of the SO_4^{2-} profile at site GeoB 13804 based on molecular diffusion was simulated with the computer software CoTRem, which is a modular, numerical transport and reaction model based on the operator splitting approach. Adler et al. (2001) and Wenzhöfer et al. (2001) provide detailed descriptions of the software. Similar to our approach, Hensen et al. (2003) and Riedinger et al. (2005) successfully applied CoTRem to simulate the diffusive re-equilibration of the SO_4^{2-} profile after a submarine landslide and the movement of the SMTZ as a consequence of changing SRs and upward CH_4 fluxes, respectively.

Tab. 3: Parameters and boundary conditions for the CoTRem modeling of the sulfate profile at station GeoB 13804.

Basic parameters for CoTRem		
Model length [m]		8
Cell discretisation [cm]		5
Time step [yr]		0.05
Porosity ϕ		0.6
Temperature [$^{\circ}\text{C}$]		3.5
Boundary conditions		
	Before slide	After slide
Sedimentation rate [cm kyr^{-1}]	80	180
Upper boundary		
SO_4^{2-} [mmol l^{-1}]	28	28
CH_4 [mmol l^{-1}]	0	0
Lower boundary		
SO_4^{2-} [mmol l^{-1}]	0	0
CH_4 [mmol l^{-1}]	40	40
Diffusion coefficients^a	D_0	D_{sed}
SO_4^{2-} [$\text{cm}^2 \text{yr}^{-1}$]	179.5	88.79
CH_4 [$\text{cm}^2 \text{yr}^{-1}$]	293.6	145.2

^a Diffusion coefficient in free solution (D_0) calculated for a temperature of 3.5°C and corrected for tortuosity (θ) after Boudreau (1997); $D_{\text{sed}} = D_0/\theta^2$, while $\theta^2 = 1-\ln(\phi^2)$.

A model length of 8 m was chosen and subdivided into cells of 5 cm thickness. A length of 8 m allows displaying potential changes of the SMTZ depth whilst inhibiting excessive computing times. The time-step to fulfill numerical stability was set to 5×10^{-2} yrs. Analogous to Hensen et al. (2003) and Riedinger et al. (2005) we used a constant porosity for the simulation. We applied a value of 0.6 that represents the average porosity, as measured for the upper 6 m of the sediment column - the section, in which the processes most relevant for our approach (AOM according to equation (1) and downward diffusion of SO_4^{2-}) take place. The transport mechanisms generally considered in the model were molecular diffusion (D_s) and bioirrigation for the pore water species and sediment accumulation for solutes and the solid phase. Details can be found in section 3.5.1. The boundary conditions are given in Table 3 and discussed in section 3.5.

3.3.7 Limit Equilibrium slope stability analysis

In order to quantitatively investigate possible trigger scenarios for the observed slope failures we performed a computer-based probabilistic Limit Equilibrium slope stability analysis. This analysis was carried out by using the commercially available software package *Slide* (Rocscience Inc.) that is widely used in geotechnical engineering for slope stability assessments under subaerial conditions, but can be adapted to the sub-aqueous environment by applying full-saturation and effective stress condition in the model scenarios (e.g., Strasser et al., 2007). The program uses equal-width slices and allows for input of a slope profile, sub-bottom geometry of layers and their geotechnical properties, and a predefined failure surface geometry, as reconstructed for pre-failure conditions from the Parasound and multibeam bathymetry data and compiled physical property core data gathered during *Meteor* cruise M78/3. Additionally, a pseudostatic acceleration can be used to model the peak ground acceleration generated by earthquakes and to evaluate the seismic slope stability. This parameter implies that the earthquake acceleration is applied over a significantly long period of time so that the induced stresses can be considered constant (Hampton et al., 1996). Thus, the dynamic response of the sediment is not taken into account. The output factor of safety (FS; i.e., the ratio between the resisting shear strength and the sum of all loading forces (mobilized shear stress)) is calculated using a combined General Limit Equilibrium (GLE)/Morgenstern-Price method (Morgenstern and Price, 1965; Fredlund and Krahn, 1977).

To account for uncertainties in model input parameters (Tab. 4), the analyses were performed in a probabilistic mode. Contrary to a deterministic approach that uses one single constant value for each input parameter, the probabilistic approach considers variability and hence uses a mean and standard deviation value. Here, the input data samples are

randomly generated using the Monte Carlo sampling method simulating the uncertainty and variability of each input parameter. The FS is calculated for 5000 runs and model outputs reveal the mean FS value of the modeled slope and the corresponding probability of failure (i.e., % of all analyses with FS <1).

Tab. 4: Input parameters for geotechnical slope stability model.

Parameter	[]	Mean value	Variability	Absolute minimum	Absolute maximum
Slope angle	°	2.25	0.25	2	2.5
Failure depth	mbsf	75	25	50	100
Unit weight	kN m ⁻³	15.8	1	14.8	16.8
Shear strength at seafloor	kPa	1	7	0	15
Shear strength gradient with depth	kPa m ⁻¹	1.5	0.7	0.4	2.6
General model assumptions:	1-layer, infinite slope model, GLE/Morgenstern-Price method, undrained failure, hydrostatic conditions, additional horizontal forces due to horizontal seismic accelerations				

3.4 Results

Generally, the applied methods refer to data at very different scales. The theoretical vertical resolution of the Parasound data (several decimeters) is reduced by a combination of diffractions, interferences, and side echoes. Pore water data of the gravity core in contrast integrate over a few centimeters, but were gained only in dm-scale, whereas the visual core description as well as pore water and ²¹⁰Pb data of the MUC core are accurate to within 1-2 cm. Therefore, different units and decimal places for the vertical scale are used in the following sections depending on the data referred to.

3.4.1 Geotechnical and sedimentological data

The sedimentological core examination reveals that the upper unit (0.00–2.43 m core depth) consists of soft hemipelagic mud with a succession of several cm thick, undeformed sand layers (Fig. 12). The sharp boundary of this unit coincides with an abrupt downward increase in shear strength from ~10 kPa to >20 kPa at 2.43 m core depth (Figs. 13, 14). The sediments below this boundary are over-consolidated (as inferred from the high ratio between the undrained shear strength and reconstructed hydrostatic overburden stress; e.g.,

Locat and Lee, 2002) and are composed of cohesive mud with sandy layers. Below 3.07 m, the sediments are also fine-grained, contain scattered shell fragments and are internally deformed (Fig. 12). The radiographies indicate that this lowest section towards the bottom of the core resembles internal flow structures of plastically-deformed sediments, as evidenced by distorted mud layers with varying silt content. This unit is interpreted as debrite deposit.

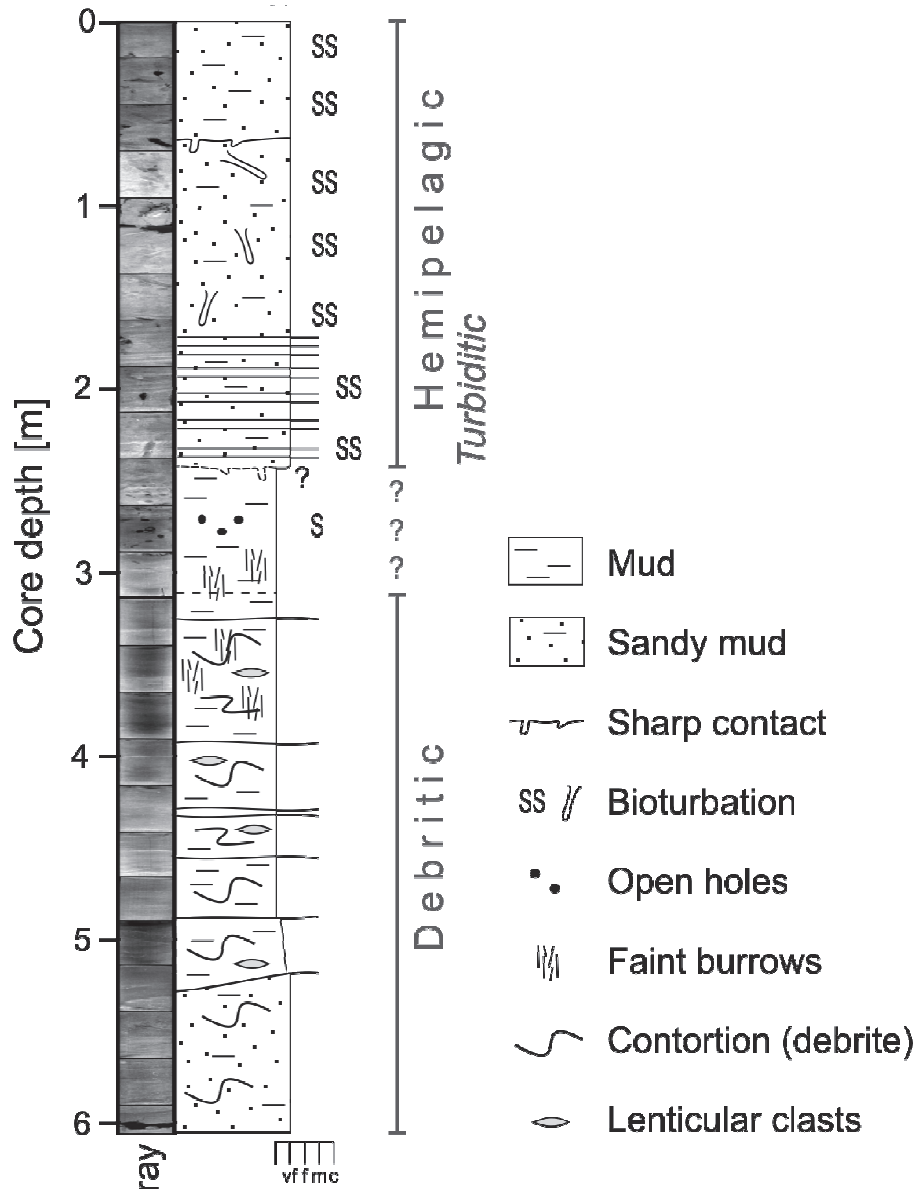


Fig. 12: Radiographies and lithological column of gravity core GeoB 13804.

Bioturbation has overprinted the contact at 2.43 m and diffused the original structures. The upper part of the core (above 2.79 m) shows macro-structures including filled burrows of up to 1.5 cm in diameter and 12 cm in length. Besides these unambiguous bioturbation structures, several open, tube-like holes of similar diameter are present at 2.63 m, 2.65 m, and 2.69-2.72 m (Fig. 12). Below 2.79 m, large macroscopic bioturbation is absent. Only fine

bright burrows of 2-15 cm length and approximately 0.5 mm width sub-vertically penetrate the sediment between 2.79 and 4.37 m.

3.4.2 Geochemical data

At site GeoB 13804, the pore water profiles are characteristic for non-steady state conditions (Fig. 13). The SO_4^{2-} concentrations stay more or less constant within the upper 2.8 m and scatter around the typical seawater value of ~ 28 mM. Below this depth, SO_4^{2-} concentrations strongly decrease. Methane concentrations start to increase at approximately 4.0 m core depth and reach 1.7 mM at the bottom of the core. The SO_4^{2-} and CH_4 profiles overlap producing a broad SMTZ at 4.0-6.0 m core depth, which is characterized by maximum $\Sigma\text{H}_2\text{S}$ concentrations of ~ 2.4 mM at ~ 4.6 m. Alkalinity and HPO_4^{2-} profiles follow an inverse trend to SO_4^{2-} . The uppermost ~ 2.8 m of the sediment show low values similar to seawater concentrations; below 2.8 m the concentrations increase with depth. Dissolved Fe^{2+} is present between 0.03 m and 1.0 m with values of up to $14 \mu\text{M}$. The E_{H} values decrease from 161 mV at 0.1 m to -206 mV at 5.8 m core depth.

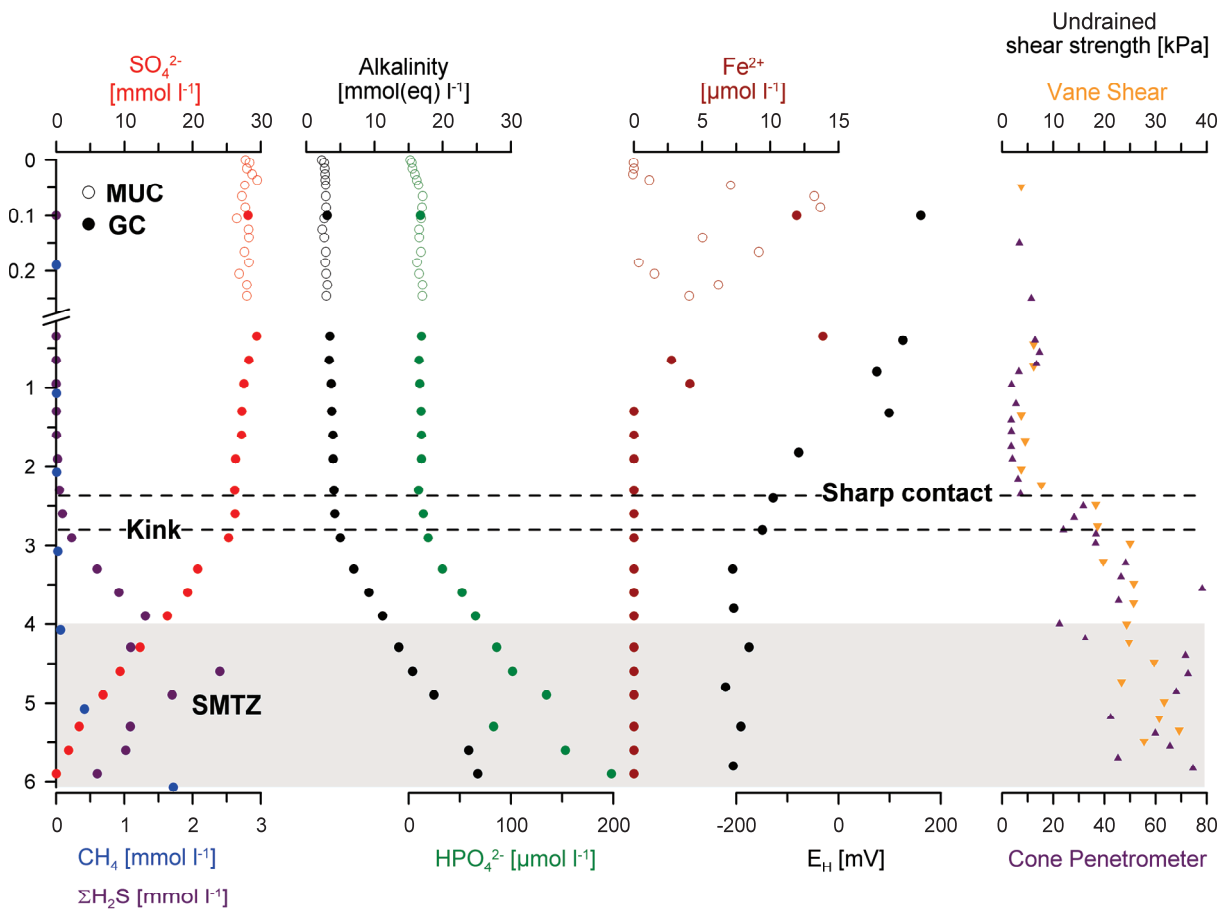


Fig. 13: Geochemical pore water and geotechnical data of gravity core GeoB 13804-1 and MUC core GeoB 13804-2. The gray shaded interval represents the SMTZ. Note that the kink in the pore water profiles is located about 0.35 m deeper than the change from under-consolidated to over-consolidated sediments (see Locat and Lee, 2002 for details to over- and under-consolidation).

The activity of $^{210}\text{Pb}_{\text{unSUPP}}$ shows an exponential decrease with depth but seems to be somehow disturbed between 2 and 4 cm (Fig. 14). At 15 cm, $^{210}\text{Pb}_{\text{unSUPP}}$ is completely depleted. We applied the C.I.C. and the C.R.S. models (see 3.3.5; Fig. 14) in order to determine the sediment age and SRs. The C.R.S. data, which are more accurate than the C.I.C. results since they account for SR changes, indicate a sediment age of 112 yrs at 11.5 cm depth. ^{137}Cs could not be applied as a check for the sediment age, since the activities are extremely low throughout the cored depths. The application of this radioactive element as an age check is generally difficult for regions in the southern hemisphere, where the overall ^{137}Cs inventory is low (e.g., Tsumune et al., 2011). Around 1988, the SR as determined from the C.R.S. ages increased drastically. The average SR between 1988 and 2009 was 0.18 cm yr^{-1} and thus more than twice as high as the average SR of 0.08 cm yr^{-1} prior to 1988 (Fig. 14).

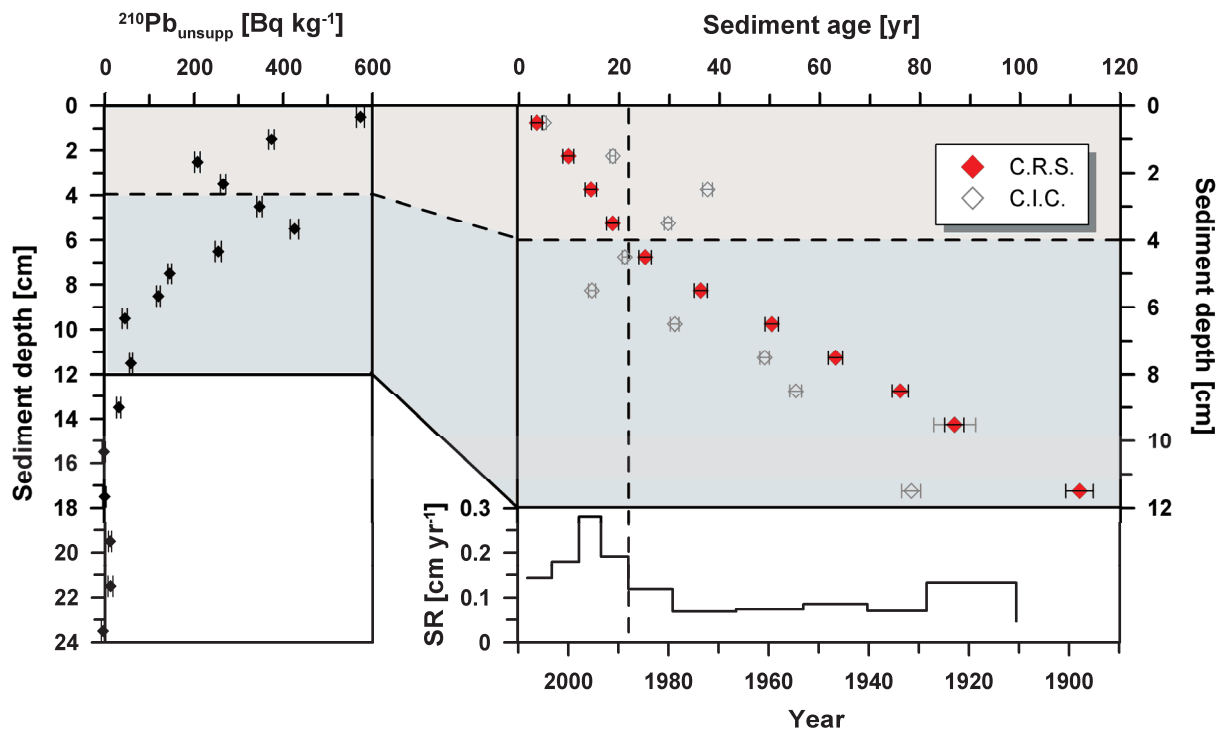


Fig. 14: Unsupported ^{210}Pb activity at site GeoB 13804 and sediment ages calculated from $^{210}\text{Pb}_{\text{unSUPP}}$ using the C.I.C. and the C.R.S. model. The sedimentation rates (SRs) appear not to be constant over time. Therefore, the C.R.S. data is valid. A drastic change in SRs happened at about 1988. The average SR from 1888-1988 was 0.08 cm yr^{-1} , whereas the average SR from 1988-2009 amounted to 0.18 cm yr^{-1} .

3.5 Discussion

3.5.1 Non-steady state pore water conditions at site GeoB 13804

Generally, the reason for non-steady state conditions at a particular study site is difficult to assess, because the processes able to cause disequilibrium are numerous. As mentioned above, they include bioirrigation (e.g., Fossing et al., 2000), fluid seepage or bubble ebullition of CH₄ (e.g., Haeckel et al., 2007), variations in the diffusive upward flux of CH₄ (e.g., Kasten et al., 2003), and mass-transport events (Zabel and Schulz, 2001; Hensen et al., 2003). If some of these processes take place simultaneously, it is practically impossible to reconstruct them based on a single approach.

In the following section, potential scenarios for the development of non-steady state conditions at site GeoB 13804 are discussed and evaluated in consideration of the complementary data. Kasten et al. (2003) and Riedinger et al. (2005) demonstrated that sudden variations in the upward CH₄ flux (possibly in combination with extremely high SRs) cause concave rather than kink-shaped profiles. Thus, the observed SO₄²⁻ profile at site GeoB 13804 cannot be explained by such a process.

Gas seepage or fluid flow

The occurrence of several open tube-like structures in core GeoB 13804 at 2.63 m, 2.65 m, and 2.69-2.79 m (Fig. 12) could be a result of ongoing lateral or vertical advection. Constant upward release of gas (CH₄ or other hydrocarbons) does not seem to be an option since the holes only appear above the SMTZ. Upward fluid seepage can result from hydro-fracturing and sudden drainage of marine sediment as a consequence of transient pore pressure increase due to dynamic loading (e.g., earthquake tremor) or due to fast deposition of low-permeable sediments (Mörz et al., 2007). A vertical advective fluid flow (upward as well as downward) through the entire upper ~2.8 m is, however, in conflict with the observed increase of pore water Fe²⁺ at 0.03 m core depth that indicates an oxygen penetration depth of less than 0.03 m (Fig. 13). A lateral fluid flow through the aforementioned open, tube-like structures with a diffusion-dominated transport of chemical species into the surrounding cohesive mud could produce the observed kink-shaped pore water profiles. Possibly, a lateral flow of SO₄²⁻-rich water would be related with more positive values of E_H at the respective depth compared to the underlying sediment. As shown in Fig. 13, this is not the case for site GeoB 13804. The value at 2.8 m (-149 mV) shows reducing conditions that follow the overall decrease of redox potential towards the bottom of the core. Therefore we

exclude the idea of an advection-controlled process for the formation of the SO_4^{2-} kink at site GeoB 13804.

Mass-transport and bioirrigation

Zabel and Schulz (2001) as well as Hensen et al. (2003) explained kink-shape SO_4^{2-} profiles by overthrusting of sediment by a cohesive sediment slide block that carries its initial pore water characteristics downslope. Given that the SO_4^{2-} gradient in the slide block differs from the gradient in the underlying sediment, the base of the MTD is, according to the authors, characterized by an inflexion point in the SO_4^{2-} profile. Considerable variation in SO_4^{2-} gradients over small distances as well as SO_4^{2-} concentrations scattering around the concentration in bottom water over the whole lengths of m-long gravity cores are known to occur in the study area (e.g., sites GeoB 2803-3 and GeoB 2806-5 shown by Bleil et al., 1994). A similar study dealing with the imprint of a slide event on pore water geochemistry focusing, however, on Cl^- profiles was published by De Lange (1983). The relocation of a coherent sediment package that produces a kink in the pore water profiles is consistent with the sedimentological data of our core. The base of the relocated sediment package appears to be located at 2.43 m core depth where the lithological boundary and the drastic change in shear strength were observed. Macroscopic bioturbation structures down to 2.79 m depth suggest that the paleosurface was exposed for a while and densely populated by macrofauna. The SO_4^{2-} kink being located approximately at the base of the bioturbation structures can consequently be explained by a continuous exchange of pore water with bottom water down to a paleo-depth of ~ 0.35 m before the mass-transport event happened (Fig. 15). Although m deep and cm thick burrows are known to exist in deep-sea sediments (Löwemark and Schäfer, 2003), active bioirrigation within the entire 2.79 m thick sediment package can be excluded as reason for the present-day SO_4^{2-} kink profile due to the Fe^{2+} increase in 0.03 m depth. Active bioirrigation in such an extent would increase the oxygen penetration depth and inhibit the shallow dissolution of iron oxides (Ziebis et al., 1996).

We suggest that the kink-shape pore water profile at site GeoB 13804 is the consequence of a mass-transport event, as proposed by Zabel and Schulz (2001) and Hensen et al. (2003). Given the undisturbed sand layers and the lamination at 1.80-2.00 m core depth, a transport of this unit by any process that includes plastic deformation, such as by a debris flow, can be excluded. Therefore, we propose that the section above 2.43 m core depth represents a coherent package transported downslope by a submarine landslide.

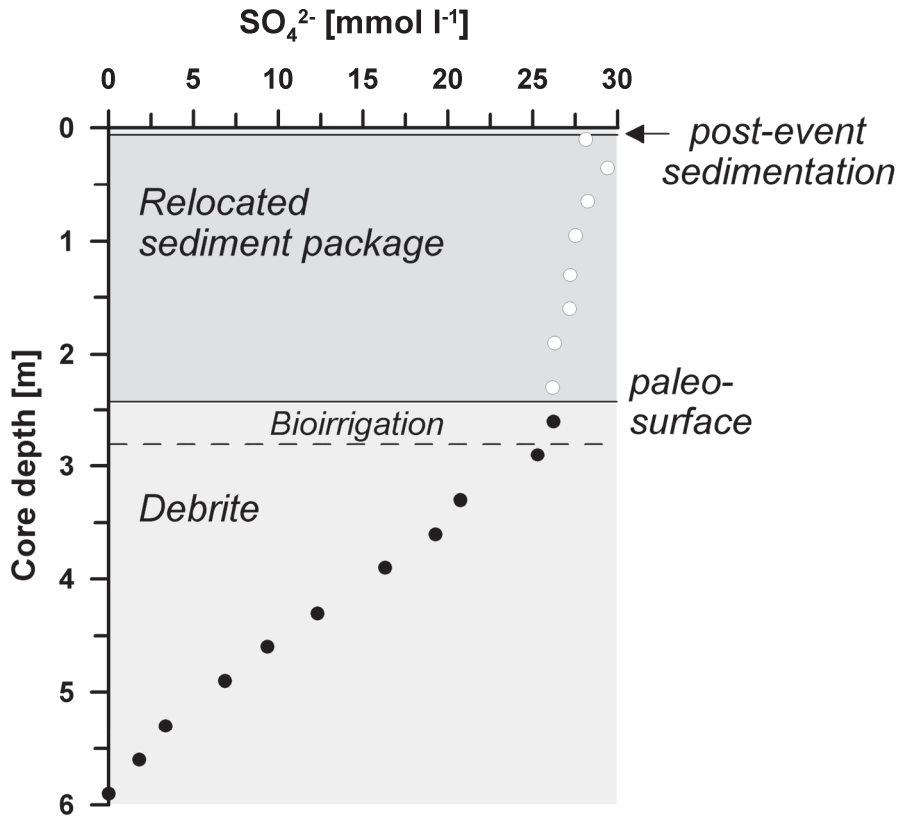


Fig. 15: Hypothesized scenario for CoTReM simulation for site GeoB 13804. The sediment package between 0.04 and 2.43 m is interpreted as a slid block overlying the debrite. The uppermost part of the debrite (~0.35 m) has been affected by bioirrigation before the most recent MTD emplacement.

Since the ^{210}Pb method allows dating sediments as far back in time as about 150 years - a time span that would lead to a considerable smoothing of the pore water profiles - the ^{210}Pb profile should cover the timing or rather the sediment accumulation after (and possibly before) the suspected sliding event. We consider the scattered $^{210}\text{Pb}_{\text{unsupp}}$ values in the thin interval of 2-4 cm to be a result of varying (increasing) sediment accumulation that led to a dilution of $^{210}\text{Pb}_{\text{unsupp}}$ rather than reflecting a sudden deposition of remobilized material (e.g., from a turbidity current). This assumption is supported by the absence of a distinct layer of coarse material indicating redeposition at this depth upon visual MUC core inspection. The $^{210}\text{Pb}_{\text{unsupp}}$ profile suggests continuous sedimentation of the uppermost 11.5 cm (below no $^{210}\text{Pb}_{\text{unsupp}}$ detected), albeit with a drastic change of SRs at about 1988. A laminar flow of this part of the sediment column would be reflected by a strong scatter of ^{210}Pb or (in the case that the eroded material was older than 150 years) overall low or absent $^{210}\text{Pb}_{\text{unsupp}}$ activities (Garcia-Orellana et al., 2006; Huh et al., 2006; e.g., Alexander and Lee, 2009) and can thus be excluded. We hypothesize that the observed drastic change of the SR at about 1988 indicates the timing of the youngest MTD event. The sediment below 4 cm might consequently represent the top of a coherently relocated package from the nearby upper headwall. The sediment above 4 cm depth is interpreted as post-event sedimentation

(Fig. 15). The reasons for the change to extremely high SRs in the late 1980's remain speculative. The increase might be explained by ongoing retrogressive erosion of the headwall that supplies sediment to the area downslope or by changed current velocities at the core location.

Although we obtained a very broad dataset, we can not reconstruct the exact sequence of the depositional events at the study site. A km wide transport of a 2.4 m thick sediment package is likely to lead to plastic deformations. Such disturbances are, however, completely absent in the respective core section and are also not verified by $^{210}\text{Pb}_{\text{unSUPP}}$. Additionally, the over-consolidation of the sediment below 2.43 m core depth indicates that at some point in the past it has been overlain by a much thicker sediment package than at present. With our approaches we are unable to resolve this part of the sedimentary history.

Geochemical modeling

Regardless of its original source, the SO_4^{2-} profile will develop into a concave-up and finally a linear shape over time if the process that caused the kink-shape profile is not active anymore. Zabel and Schulz (2001) and Hensen et al. (2003) used the diffusive re-equilibration of the SO_4^{2-} profile to date young MTDs. We set up a comparable simulation to estimate the maximum age of the kink-shaped SO_4^{2-} profile at the study site.

For determining the CH_4 flux for the start of the simulation (steady state situation), we considered only the part of the SO_4^{2-} profile below 2.43 m and “shifted” this section towards the sediment surface considering bioirrigation within in the uppermost 0.35 m (Fig. 16). In other words, we subtracted or “removed” the youngest part of the sediment column (the suspected MTD and overlying recent sediment drape). The measured CH_4 could not be used for the simulation because conventional sampling techniques like those applied here always lead to considerable degassing amounting to up to 99.8% (Dickens et al., 1997). To determine the CH_4 flux into the SMTZ, we applied the approaches of Borowski et al. (1996) and Niewöhner et al. (1998), which are based on the reaction stoichiometry for the use of SO_4^{2-} and CH_4 during AOM. The CH_4 concentration determined for 8.0 m sediment depth (40 mM) produces an upward flux that corresponds to the measured downward-directed SO_4^{2-} flux. This CH_4 concentration is lower than the concentration in pore water equilibrated with gas hydrate (55 mM), as calculated after Tishchenko et al. (2005) for the *in situ* pressure, salinity, and temperature. For AOM, a maximum reaction rate ($R_{\text{max}} = 0.1 \text{ mol dm}^{-3} \text{ yr}^{-1}$) was defined to produce a broad SMTZ with overlapping CH_4 and SO_4^{2-} profiles. That rate was used as long as the reactants were available in sufficient amounts (0th order

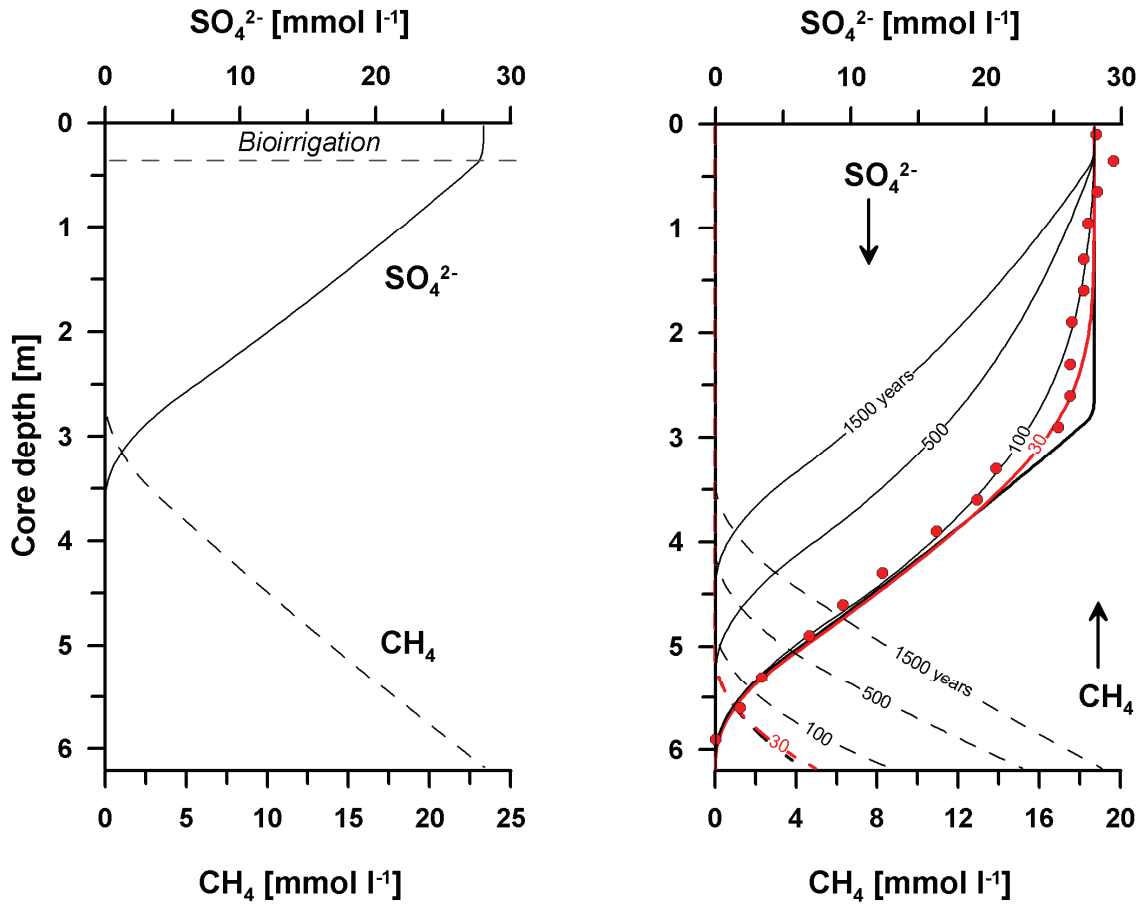


Fig. 16: The graph on the left side shows the starting conditions of the geochemical transport and reaction model, i.e. the situation before deposition of the MTD. A constant CH_4 source at 8 m depth was applied. On the right side, the development of the SO_4^{2-} profile after the inferred deposition of the MTD at site GeoB 13804 is shown. The best fit of between model result and the measured data (red dots) is reached after about 30 yrs. However, after 30 yrs the profile is already reasonably smoothed. Thus, this estimate is regarded as a maximum age of the observed SO_4^{2-} profile.

kinetics). For lower concentrations of the reactants, the AOM rate was determined based on 2nd order kinetics. The reaction-specific change in concentration at a specific sediment depth ($\Delta C_{s,d}$) was calculated as follows:

$$\Delta C_{s,d} = R_{s,d} \times dt_{\text{num}} \times SC_{s,d}$$

Where $R_{s,d}$ [in $\text{mol l}^{-1} \text{yr}^{-1}$] is the reaction rate, dt_{num} is the time step used in the model run, and $SC_{s,d}$ is a stoichiometric factor (for further details see Hensen et al., 2003; Riedinger et al., 2005). Diffusion coefficients were corrected for tortuosity (Boudreau, 1997) using the temperature of the water mass overlying the sediment (North Atlantic Deep Water: 3.5°C). The physical parameters of the water mass were measured during a CTD (conductivity/temperature/depth) sensor deployment at 36°10.28' S and 51°44.10' W during cruise M78/3b in June 2009. Bottom water concentrations of the chemical species derived

from the MUC deployment define the upper boundary conditions. The lower boundary of the model is defined as an open boundary for all solutes except for CH₄, which means that the gradient of the last two cells is extrapolated to allow diffusion across the boundary. For the steady state situation (simulated to determine the CH₄ flux), a SR of 0.08 cm yr⁻¹, as deduced from the ²¹⁰Pb_{unsupp} data, was used. The mass movement event was simulated by shifting the steady state pore water profiles downward by the thickness of the MTD and assigning bottom water SO₄²⁻ concentrations of 28 mM to all cells above 2.4 m (Fig. 16). Subsequently, the simulation was continued using the average post-event SR of 0.18 cm yr⁻¹. A compilation of all input parameters for the simulation runs is given in Table 3.

The simulation of the SO₄²⁻ profile development shows that the best fit between modeled and measured SO₄²⁻ data at the study site is reached after 30 years (Fig. 16). At this time, the profile shows, however, already a concave-up curvature. Therefore we consider 30 years to be the maximum age of the observed SO₄²⁻ profile. In fact, this result is irrespective of the actual cause for the non-steady state SO₄²⁻ profile as long as the process that initiated the formation of the kink is inactive.

3.5.2 Earthquakes as possible trigger for the slope failure?

Although there is no evidence for the origin of the supposed slide block, it is probable that the most recent failure event has reactivated the scarp to the northwest of site GeoB 13804 (Fig. 11). Both, ²¹⁰Pb dating and the results of the geochemical modeling, hint to a possible submarine mass accumulation in the study area max. 30 years ago that might thus have happened in coincidence with one of the largest historically-documented earthquake that stroke this region on June 26, 1988. The earthquake had a magnitude 5.2 m_b, nucleated in about 30 km depth, and its epicenter was located about 70 km to the southwest of site GeoB 13804 (Fig. 11; Assumpção, 1998; Benavidez Sosa, 1998). Seismic ground shaking during this 1988 earthquake would thus be a plausible candidate to have triggered slope failures along the upper scarp and subsequent downslope mass-transport.

In order to test this hypothesis, we use probabilistic Limit Equilibrium slope stability calculations to back-analyze critical seismic ground accelerations needed to initiate slope failures in the study area (see methods). We assume that the undisturbed slope above the prominent scarp represents a realistic pre-failure slope and that submarine landslides were initiated by translational sliding along a 2 to 2.5°-inclined failure plane in 75 (+/-25) m subsurface depth. This assumption is justified by acoustic subsurface images showing evenly-stratified, 2 to 2.5°-inclined reflections representing the general hemipelagic stratigraphic layering. The reflections are truncated by the upper scarp. A parallel reflection

at the base of the scarp is continued at the base of the multi-stage MTD seaward of the scarp and is thus interpreted as the main failure plane (Fig. 11; and also Fig. 4 by Krastel et al., in press, showing a parallel profile to the NE of our studied transect). The sub-seafloor depth of this reflection in “undisturbed” slope segments above the headwall scarp (and thus the inferred failure-plane depth) increases towards NE from ~50 m to ~100 m, as shown by Parasound and multibeam data. We therefore use this depth range as varying input parameter for our stability model. The overall translational geometry of the observed mass-movement justifies the general assumption of the infinite slope model. Sediment cores from upslope of the headwall scarp (GeoB 13803, GeoB 13808, and GeoB 13854; Fig. 11) generally show uniform hemipelagic mud, with constant bulk densities of 1.58 g cm^{-3} ($\pm 0.1 \text{ g cm}^{-3}$) and linearly increasing undrained shear strength values (1.5 kPa m^{-1} ; $\pm 0.7 \text{ kPa m}^{-1}$). This supports the assumption of a uniform slope-model of homogenous fine-grained sediments for which an undrained failure criterion can be applied. Table 4 summarizes all input parameters and their variability, as used for the probabilistic slope stability calculations.

Results from slope-stability calculations reveal a stable slope under static loading condition that may only fail if a lower minimum of additional seismic ground acceleration of 5.5% g (gravitational acceleration) is reached during earthquake shaking (Fig. 17). The probability of failure increases with increasing ground accelerations and the slope should fail with a probability of >50% if the earthquake produces ground accelerations >9.75% g.

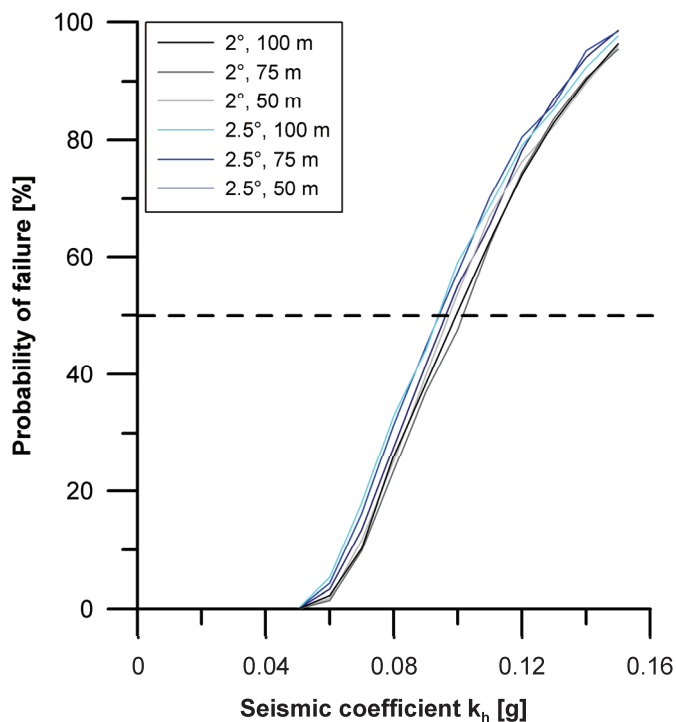


Fig. 17: Probability of slope failure as a function of the simulated seismic coefficient k_h in the study area. The simulation was performed for a uniform slope with slope angles (α) of 2 and 2.5° and a subsurface depth of failure surface of 75 ± 25 m, as inferred from geophysical data (see text). The dashed line indicates a probability for slope failure of 50%.

In order to compare these results with ground motion intensities induced by the 1988 A.D. magnitude 5.2 earthquake, an empirical seismic attenuation relationship by Campbell and Bozorgnia (2008) was applied to estimate the median ground motions of peak ground acceleration at our study site. We use their equation 1 for magnitudes <5.5, non-specified fault mechanism, a factor 2 for shallow site response of marine sediments with low shear velocities, and account for uncertainties in epicentral location and magnitude (Assumpção, 1998 and references therein) in the order of 10 km and 0.1 magnitude units, respectively. Then, horizontal ground motions range between 2% g and 4% g. These estimates are slightly lower than the minimum required seismic ground accelerations needed to trigger the observed slope failure in the study area, as reconstructed from our slope stability model.

The slope stability model does not include pore-pressures and the pre-conditioning is set to normally-consolidated and hydrostatics. This is mainly because there are no data available from cores or drilling in the study area for constraining possible *in situ* overpressures. A recent study by Stigall and Dugan (2010) in the Gulf of Mexico, however, has shown that overpressure can be caused by high sedimentation and lateral fluid flow, reducing significantly slope stability to such low levels that even a magnitude 5 earthquake at epicentral distance of up to 140 km was sufficient to eventually have initiated observed past failures at the study site. We therefore interpret the critical seismic ground accelerations from our slope stability calculations as upper-limit maximal requirement to initiate failure. The observed mass movement event could thus have been initiated at lower seismic ground shaking intensities, given the fact that overpressures are likely to be present, as indicated by the high SRs (see discussion from ^{210}Pb data in section 3.4.2) and the generally low-permeable nature of the fine-grained hemipelagic sediments, which may not drain the sediment sufficiently during fast compaction.

Taking this into account, and given that the discrepancy of estimated ground motions and the calculated minimum acceleration needed to trigger failure is relatively small (i.e., 1.5% g), we conclude that the 1988 earthquake is a plausible trigger for the observed sedimentological and geochemical features associated with the youngest slide event observed at our study site, if likely additional weakening processes, such as excess pore pressure, preconditioned the slope towards failure.

3.6 Conclusions

A young (only a few decades old) MTD was identified at the continental margin off Uruguay based on geophysical mapping, geotechnical shear strength data, and a distinct kink in SO_4^{2-} profile. Although it shows a sharp lithological contact at its base, the 2.4 m thick MTD is inconspicuous with respect to visually observable sedimentological features as it appears undisturbed apart from bioturbation. Geochemical modeling suggests that the timing of this most recent MTD deposition coincided with a drastic change of SRs at the end of the 1980's, as inferred from $^{210}\text{Pb}_{\text{unSUPP}}$ data. This study shows that gravitational processes at the continental margin off Uruguay are young processes that are currently occurring. It further documents that, even if located in a passive margin tectonic setting, weak earthquakes are a potential trigger mechanism for instabilities, if other weakening processes pre-conditioned the slope for failure. The complexity of integrating all results from the individual datasets shows that an approach using just one method is highly risky in order to interpret the structure and evolution of a MTD. A multidisciplinary approach seems to be essential to decipher relevant processes in a comprehensive view. Therefore, more interdisciplinary studies like this one are necessary to reach a holistic understanding of submarine mass movements.

Acknowledgments. We gratefully acknowledge the support of Captain Baschek, the crew of RV *Meteor*, and the scientists on board during cruise M78/3a. Natascha Riedinger is greatly acknowledged for her support during the cruise, for providing sulfide and sulfate data, and for reviewing the manuscript in its early stage. Tim Ferdelmann and Andrea Schipper are thanked for their assistance with the ^{210}Pb samples. We thank Jana Friedrich for help with the interpretation of the ^{210}Pb dataset and Kerstin Nöthen for support with CoTRem. Gert J. de Lange is acknowledged for fruitful discussions during the writing-process. This study was funded by the Deutsche Forschungsgemeinschaft (DFG) in the frame of the International Graduate College "Proxies in Earth History" (EUROPROX) and the Research Center/Cluster of Excellence "The Ocean in the Earth System" (MARUM). We acknowledge further financial support from the Helmholtz Association (AWI Bremerhaven). All data are available on the database Pangaea (<http://www.pangaea.de>).

References

- Adler, M., Hensen, C., Wenzhöfer, F., Pfeifer, K., and Schulz, H.D., 2001, Modeling of calcite dissolution by oxic respiration in supralysoclineal deep-sea sediments: *Marine Geology*, v. 177, p. 167-189.
- Alexander, C.R. and Lee, H.J., 2009, Sediment accumulation on the Southern California Bight continental margin during the twentieth century, *in* Lee, H.J. and Normark, W.R., eds., *Earth science in the urban ocean: the Southern California continental borderland*: GSA Special Papers, The Geological Society of America, p. 69-87.
- Aller, R.C., 1983, The importance of the diffusive permeability of animal burrow linings in determining marine sediment chemistry: *Journal of Marine Research*, v. 41, p. 299-322.
- Appleby, P.G. and Oldfield, F., 1978, The calculation of ^{210}Pb dates assuming a constant rate of supply of unsupported ^{210}Pb to the sediment: *Catena*, v. 5, p. 1-8.
- Assumpção, M., 1998, Seismicity and stresses in the Brazilian passive margin: *Bulletin of the Seismological Society of America*, v. 88, p. 160-169.
- Barnes, R.O. and Goldberg, E.D., 1976, Methane production and consumption in anoxic marine sediments: *Geology*, v. 4, p. 297-300.
- Benavídez Sosa, A., 1998, Sismicidad y sismotectónica en Uruguay: *Física de la Tierra*, p. 167-186.
- Bleil, U., Albrecht, N., Breitzke, M., Brüning, M., Dehning, K., Diekamp, V., Domingues, J.M., Donner, B., Franke, P., Gerdes, A., Klann, M., Krastel, S., Krüger, D., von Lom-Keil, H., Martins Lima, L., Mulitza, S., Quental, S., Rudolf, T., Rühlemann, C., Santiago Grossmann, G., Steinborn, W., Thiele, J., and Truscheit, T., 2001a, Report and preliminary results of *Meteor* Cruise M49/3, Montevideo (Uruguay) - Salvador (Brazil), March 9 - April 1, 2001, *Berichte aus dem Fachbereich Geowissenschaften der Universität Bremen*, Volume 185, p. 99.
- Bleil, U., Alin, A., Bickert, T., Böke, W., Breitzke, M., Drachenberg, S., Eades, E., Frederichs, T., Frenz, M., Heuer, V., Hilgenfeldt, C., Hopfauf, V., de Leon, A., Von Lom-Keil, H., Michels, K., Pfeifer, K., Rosiak, U., Rühlemann, C., Segl, M., Spiess, V., Violante, R., Watanabe, S., Westerhold, T., and Zatloucal, N., 2001b, Report and preliminary results of *Meteor* Cruise M46/3, Montevideo (Uruguay) - Mar del Plata (Argentina), January 4 - February 7, 2000, *Berichte aus dem Fachbereich Geowissenschaften der Universität Bremen*, Volume 172, p. 161.
- Bleil, U., Breitzke, M., Buschhoff, H., von Dobeneck, T., Dürkoop, A., Ehrhardt, I., Engelbrecht, I., Giese, M., Gingele, F., Hacke, S., Haese, R., Hensen, C., Hinrichs, S., Höll, C., Holmes, E., Jahn, B., Janke, A., Kasten, S., Nowald, N., Otto, S.,

- Petermann, H., Raulfs, M., Rosiak, U., Schmidt, A., Scholz, M., and Zabel, M., 1994, Report and preliminary results of *Meteor* Cruise M29/2, Montevideo - Rio de Janeiro, 15.07.1994 - 08.08.1994, Berichte aus dem Fachbereich Geowissenschaften der Universität Bremen, Volume 59, p. 153.
- Blum, P., 1997, Physical Properties Handbook: A guide to the shipboard measurement of physical properties of deep-sea cores: ODP Technical Notes, v. 26.
- Boetius, A., Ravensschlag, K., Schubert, C.J., Rickert, D., Widdel, F., Gieseke, A., Amann, R., Jørgensen, B.B., Witte, U., and Pfannkuche, O., 2000, A marine microbial consortium apparently mediating anaerobic oxidation of methane: *Nature*, v. 407, p. 623-626.
- Borowski, W.S., Paull, C.K., and Ussler, W., 1996, Marine pore-water sulfate profiles indicate in situ methane flux from underlying gas hydrate: *Geology*, v. 24, p. 655-658.
- Boudreau, B.P., 1997, Diagenetic models and their implementation: modeling transport and reactions in aquatic sediments: Berlin, Heidelberg, New York, Springer, 414 p.
- Boyce, R.E., 1977, Deep Sea Drilling Project procedures for shear strength measurement of clayey sediment using modified Wykeham Farrance laboratory vane apparatus, *in* Barker, P.F. and Dalziel, I.W.D., eds., Initial Reports DSDP (U.S. Govt. Printing Office), Volume 36: Washington, p. 1059-1068.
- Brennecke, W., 1921, Die Ozeanographischen Arbeiten der Deutschen Antarktischen Expedition, 1911-1912, Archiv der Deutschen Seewarte, Volume 39: Hamburg, p. 1-214.
- Bryn, P., Berg, K., Forsberg, C.F., Solheim, A., and Kvalstad, T.J., 2005, Explaining the Storegga Slide: *Marine and Petroleum Geology*, v. 22, p. 11-19.
- Campbell, K.W. and Bozorgnia, Y., 2008, NGA ground motion model for the geometric mean horizontal component of PGA, PGV, PGD and 5% damped linear elastic response spectra for periods ranging from 0.01 to 10 s: *Earthquake Spectra*, v. 24, p. 139-171.
- Cline, J.D., 1969, Spectrophotometric determination of hydrogen sulfide in natural waters: *Limnology and Oceanography*, v. 14, p. 454-458.
- De Lange, G.J., 1983, Geochemical evidence of a massive slide in the southern Norwegian Sea: *Nature*, v. 305, p. 420-422.
- Deacon, G.E.R., 1937, The hydrology of the Southern Ocean, *Discovery Reports*, Volume 15, p. 1-124.
- Dickens, G.R., Paull, C.K., and Wallace, P.J., 1997, Direct measurement of in situ methane quantities in a large gas-hydrate reservoir: *Nature*, v. 385, p. 426-428.
- Fossing, H., Ferdelman, T.G., and Berg, P., 2000, Sulfate reduction and methane oxidation in continental margin sediments influenced by irrigation (South-East Atlantic off Namibia): *Geochimica et Cosmochimica Acta*, v. 64, p. 897-910.

- Fredlund, D.G. and Krahn, J., 1977, Comparison of slope stability methods of analysis: Canadian Geotechnical Journal, v. 14, p. 429-439.
- Garcia-Orellana, J., Gràcia, E., Vizcaino, A., Masqué, P., Olid, C., Martínez-Ruiz, F., Piñero, E., Sanchez-Cabeza, J.A., and Dañobeitia, J., 2006, Identifying instrumental and historical earthquake records in the SW Iberian margin using ^{210}Pb turbidite chronology: Geophysical Research Letters, v. 33, L24601.
- Gordon, A.L. and Greengrove, C.L., 1986, Geostrophic circulation of the Brazil-Falkland confluence: Deep Sea Research Part I. Oceanographic Research Papers, v. 33, p. 573-585.
- Grant, J.A. and Schreiber, R., 1990, Modern swathe sounding and subbottom profiling technology for research applications - the Atlas Hydrosweep and Parasound Systems: Marine Geophysical Researches, v. 12, p. 9-19.
- Grasshoff, K., Kremling, K., and Ehrhardt, M., 1999, Methods of seawater analysis: Weinheim, Wiley-VCH, 600 p.
- Haeckel, M., Boudreau, B.P., and Wallmann, K., 2007, Bubble-induced porewater mixing: A 3-D model for deep porewater irrigation: Geochimica et Cosmochimica Acta, v. 71, p. 5135-5154.
- Hampton, M.A., Lee, H.J., and Locat, J., 1996, Submarine landslides: Reviews of Geophysics, v. 34, p. 33-59.
- Hensen, C., Zabel, M., Pfeifer, K., Schwenk, T., Kasten, S., Riedinger, N., Schulz, H.D., and Boetius, A., 2003, Control of sulfate pore-water profiles by sedimentary events and the significance of anaerobic oxidation of methane for the burial of sulfur in marine sediments: Geochimica et Cosmochimica Acta, v. 67, p. 2631-2647.
- Hernández-Molina, F.J., Paterlini, M., Violante, R., Marshall, P., de Isasi, M., and Somoza, L., 2009, Contourite depositional system on the Argentine Slope: An exceptional record of the influence of Antarctic water masses: Geology, v. 37, p. 507-510.
- Hinz, K., Neben, S., Schreckenberger, B., Roeser, H.A., Block, M., Souza, K.G.d., and Meyer, H., 1999, The Argentine continental margin north of 48°S: sedimentary successions, volcanic activity during breakup: Marine and Petroleum Geology, v. 16, p. 1-25.
- Huh, C.A., Su, C.C., Wang, C.H., Lee, S.Y., and Lin, I.T., 2006, Sedimentation in the Southern Okinawa Trough - Rates, turbidites and a sediment budget: Marine Geology, v. 231, p. 129-139.
- Kasten, S., Zabel, M., Heuer, V., and Hensen, C., 2003, Processes and signals of nonsteady-state diagenesis in deep-sea sediments and their pore waters, *in* Wefer, G., Mulitza, S., and Ratmeyer, V., eds., The South Atlantic in the Late Quaternary:

- Reconstruction of Mass Budget and Current Systems: Berlin, Heidelberg, New York, Springer, p. 431-459.
- Klaus, A. and Ledbetter, M.T., 1988, Deep-sea sedimentary processes in the Argentine Basin revealed by high-resolution seismic records (3.5 kHz echograms): Deep Sea Research Part I. Oceanographic Research Papers, v. 35, p. 899-917.
- Krastel, S., Wefer, G., Antobreh, A.A., Freudenthal, T., Hanebuth, T.J.J., Preu, B., Schwenk, T., Strasser, M., Violante, R., Winkelmann, D., and M78/3 shipboard scientific crew, in press, Sediment dynamics and geohazards off Uruguay and the de la Plata River region (Northern-Argentina): Geo-Marine Letters.
- Locat, J. and Lee, H.J., 2002, Submarine landslides: advances and challenges: Canadian Geotechnical Journal, v. 39, p. 193-212.
- Lonardi, A.G. and Ewing, M., 1971, Sediment transport and distribution in the Argentine Basin. 6. Exploration and study of the Argentine basin: Physics and Chemistry of the Earth, v. 8, p. 253-263.
- Löwemark, L. and Schäfer, P., 2003, Ethological implications from a detailed X-ray radiograph and C-14 study of the modern deep-sea Zoophycos: Palaeogeography, Palaeoclimatology, Palaeoecology, v. 192, p. 101-121.
- Morgenstern, N.R. and Price, V.E., 1965, The analysis of the stability of general slip surfaces: Géotechnique, v. 15, p. 79-93.
- Mörz, T., Karlik, E.A., Kreiter, S., and Kopf, A., 2007, An experimental setup for fluid venting in unconsolidated sediments: New insights to fluid mechanics and structures: Sedimentary Geology, v. 196, p. 251-267.
- Niewöhner, C., Hensen, C., Kasten, S., Zabel, M., and Schulz, H.D., 1998, Deep sulfate reduction completely mediated by anaerobic methane oxidation in sediments of the upwelling area off Namibia: Geochimica et Cosmochimica Acta, v. 62, p. 455-464.
- Reeburgh, W.S., 1976, Methane consumption in Cariaco Trench waters and sediments: Earth and Planetary Science Letters, v. 28, p. 337-344.
- Riedinger, N., Pfeifer, K., Kasten, S., Garming, J.F.L., Vogt, C., and Hensen, C., 2005, Diagenetic alteration of magnetic signals by anaerobic oxidation of methane related to a change in sedimentation rate: Geochimica et Cosmochimica Acta, v. 69, p. 4117-4126.
- Robbins, J.A., 1978, Geochemical and geophysical applications of radioactive lead, *in* Nriagu, J.O., ed., Biogeochemistry of lead in the environment: Rotterdam, Elsevier Scientific, p. 285–393.
- Schnabel, M., Franke, D., Engels, M., Hinz, K., Neben, S., Damm, V., Grassmann, S., Pelliza, H., and Dos Santos, P.R., 2008, The structure of the lower crust at the

- Argentine continental margin, South Atlantic at 44°S: *Tectonophysics*, v. 454, p. 14-22.
- Schulz, H.D., 2006, Quantification of early diagenesis: dissolved constituents in pore water and signals in the solid phase, *in* Schulz, H.D., and Zabel, M., eds., *Marine Geochemistry*: Berlin, Springer, p. 73-124.
- Schulz, H.D., Ayres Neto, A., Boetius, A., Enneking, K., Fabian, K., Feseker, T., Funk, J., Gorke, M., Heidersdorf, F., Hensen, C., Heuer, V., Hill, H.G., Hinrichs, S., Kasten, S., Klann, M., Lacerda de Souza, C., Martinez Briao, A., Meyer, S., Mulitza, S., Niebler, H.-S., Ochsenhirt, W.T., Panteleit, B., Pfeifer, K., Schewe, F., Schwenk, T., Señorans, J.L., Siemer, S., Steinmetz, E., and Wenzhöfer, F., 2001, Report and preliminary results of *Meteor* Cruise M46/2, Recife (Brazil) - Montevideo (Uruguay), December 2 - December 29, 1999, *Berichte aus dem Fachbereich Geowissenschaften der Universität Bremen*, Volume 174, p. 107.
- Seeberg-Elverfeldt, J., Schlüter, M., Feseker, T., and Kölling, M., 2005, Rhizon sampling of porewaters near the sediment-water interface of aquatic systems: *Limnology and Oceanography: Methods*, v. 3, p. 361-371.
- Segl, M., Cepek, M., Dehning, K., Diekamp, V., Von Dobeneck, T., Frey, U., Harloff, J., Hinrichs, S., Janke, A., Joppich, C., Kasten, S., Keil, K., Lange, C., Nowald, N., Ochsenhirt, W.T., Rühlemann, C., Schmieder, F., Schüring, J., Siemer, S., Steinmetz, E., di Tomaso, I., Uliana, E., Vetere, F., Wunsch, S., and Zabel, M., 1994, Report and preliminary results of *Meteor*-Cruise M29/1, Buenos-Aires - Montevideo, 17.6.-13.7.94, *Berichte, Fachbereich Geowissenschaften*, Volume 58, p. 94.
- Spieß, V., Albrecht, N., Bickert, T., Breitzke, M., Brüning, M., Dreyzehner, A., Groß, U., Krüger, D., von Lom-Keil, H., Möller, H.-J., Nimrich, M., Ochsenhirt, W.-T., Rudolf, T., Seiter, C., Truscheit, T., Violante, R., and Westerhold, T., 2002, Report and preliminary results of *Meteor* Cruise M49/2, Montevideo (Uruguay) - Montevideo, 13.02.-07.03.2001, *Berichte aus dem Fachbereich Geowissenschaften der Universität Bremen*, Volume 203, p. 70.
- Stigall, J. and Dugan, B., 2010, Overpressure and earthquake initiated slope failure in the Ursa region, northern Gulf of Mexico: *Journal of Geophysical Research-Solid Earth*, v. 115, B04141.
- Strasser, M., Stegmann, S., Bussmann, F., Anselmetti, F.S., Rick, B., and Kopf, A., 2007, Quantifying subaqueous slope stability during seismic shaking: Lake Lucerne as model for ocean margins: *Marine Geology*, v. 240, p. 77-97.
- ten Brink, U.S., Lee, H.J., Geist, E.L., and Twichell, D., 2009, Assessment of tsunami hazard to the US East Coast using relationships between submarine landslides and earthquakes: *Marine Geology*, v. 264, p. 65-73.

- Tishchenko, P., Hensen, C., Wallmann, K., and Wong, C.S., 2005, Calculation of the stability and solubility of methane hydrate in seawater: *Chemical Geology*, v. 219, p. 37-52.
- Tsumune, D., Aoyama, M., Hirose, K., Bryan, F.O., Lindsay, K., and Danabasoglu, G., 2011, Transport of ^{137}Cs in the Southern Hemisphere in an ocean general circulation model: *Progress in Oceanography*.
- Wenzhöfer, F., Adler, M., Kohls, O., Hensen, C., Strotmann, B., Boehme, S., and Schulz, H.D., 2001, Calcite dissolution driven by benthic mineralization in the deep-sea: in situ measurements of Ca^{2+} , pH, pCO_2 and O_2 : *Geochimica et Cosmochimica Acta*, v. 65, p. 2677-2690.
- Zabel, M. and Schulz, H.D., 2001, Importance of submarine landslides for non-steady state conditions in pore water systems - lower Zaire (Congo) deep-sea fan: *Marine Geology*, v. 176, p. 87-99.
- Ziebis, W., Forster, S., Huettel, M., and Jørgensen, B.B., 1996, Complex burrows of the mud shrimp *Callinassa truncata* and their geochemical impact in the sea bed: *Nature*, v. 382, p. 619-622.

Chapter 4: Pore water geochemistry as a tool for identifying and dating recent mass-transport deposits

Susann Henkel¹, Tilmann Schwenk², Till J.J. Hanebuth², Michael Strasser², Natascha Riedinger³, Michael Formolo⁴, Juan Tomasini⁵, Sebastian Krastel⁶, and Sabine Kasten¹

¹Alfred Wegener Institute for Polar and Marine Research (AWI), Am Handelshafen 12, 27570 Bremerhaven, Germany

²Center for Marine Environmental Sciences (MARUM), Leobener Str. and Faculty of Geosciences, University of Bremen, Klagenfurter Str., 28359 Bremen, Germany

³University of California, Riverside, 900 University Avenue, Riverside, CA 92521, USA

⁴The University of Tulsa, 800 South Tucker Drive, Tulsa, OK 74104, USA

⁵Administración Nacional de Combustibles Alcohol y Portland (ANCAP), Paysandú s/n esq. Avenida del Libertador, Montevideo 11100, Uruguay

⁶Leibniz Institute of Marine Sciences (IFM-GEOMAR), Wischhofstr. 1-3, 24148 Kiel, Germany

Revised manuscript submitted for publication in the 4th Edition of the Springer-book
“Submarine Mass-Movements and Their Consequences”

Abstract

Several previous studies have shown that submarine mass movements can profoundly impact the shape of pore water profiles. Therefore, pore water geochemistry and diffusion models were proposed as tools for identifying and dating recent (max. several thousands of years old) mass-transport deposits (MTDs). In particular, sulfate (SO_4^{2-}) profiles evidentially indicate transient pore water conditions generated by submarine landslides. After mass-movements that result in the deposition of sediment packages with distinct pore water signatures, the SO_4^{2-} profiles can be kink-shaped and evolve into the concave and linear shape with time due to molecular diffusion. Here we present data from the M78/3 expedition (M for research vessel *METEOR*) along the continental margin off Uruguay and Argentina. Sulfate profiles of 15 gravity cores are compared with the respective acoustic facies recorded by a sediment echosounder system. Our results show that in this very dynamic depositional setting, non-steady state profiles occur often, but are not exclusively associated with mass

movements. Three sites that show acoustic indications for recent MTDs are presented in detail. Where recent MTDs are identified, a geochemical transport/reaction model is used to estimate the time that has elapsed since the perturbation of the pore water system and, thus, the timing of the MTD emplacement. We conclude that geochemical analyses are a powerful complementary tool in the identification of recent MTDs and provide a simple and accurate way of dating such deposits.

4.1 Introduction

Seismo-acoustic approaches provide the means to estimate dimensions of MTDs, but for absolute dating and identifying small-scale internal structures they need to be complemented by sediment data. However, based on visual core descriptions, MTDs are often hard to distinguish from homogenous hemipelagic sediments, as both might lack clear stratification. Pore water profiles can be used to close this gap as was demonstrated first by De Lange (1983), who identified a “fresh-to-brackish sediment ‘slab’, with preservation of structural and pore water composition” underlying marine sediments in the Norwegian Sea.

With respect to pore water, sediments are classified into steady state and non-steady state systems (Schulz, 2006). Simplified, steady state systems are in equilibrium and show a linear SO_4^{2-} decrease with depth towards the sulfate-methane transition zone (SMTZ) where the process of anaerobic oxidation of methane (AOM; e.g., Barnes and Goldberg, 1976) occurs. Zabel and Schulz (2001) and Hensen et al. (2003) presented non-steady state SO_4^{2-} profiles from the Zaire deep-sea fan and the continental margin off Uruguay and suggested that kink, concave-up, and s-type SO_4^{2-} profiles can be explained by submarine landslides that carry their initial pore water signals downslope. The base of an MTD can, according to the authors, be indicated by a kink of the pore water profile, which evolves into a concave and finally a linear shape due to molecular diffusion. The re-equilibration of the SO_4^{2-} pore water profile was modeled to estimate the timing of the mass movement.

With this review paper, we expand on the previous approaches and give a regional compilation showing the pervasiveness of non-steady state SO_4^{2-} profiles at the continental margin off Uruguay and Argentina and their relation to MTDs, as indicated by sediment echosounder data. The integration of geochemical, sedimentological, and geophysical data allows a better understanding of the dynamic interactions of pore water, sediments, and physical processes and offers a unique approach to date recent MTDs.

4.2 Study area

The study area (Fig. 18) is characterized by dynamic oceanographic conditions including the Brazil-Malvinas Confluence near 38°S and the interaction of Antarctic water masses with the North Atlantic Deep Water at different depths (Piola and Matano, 2001). The sedimentary processes along the margin were described in detail by Krastel et al. (in press). Mass movements occur within canyons and on the lower slope (Krastel et al., in press).

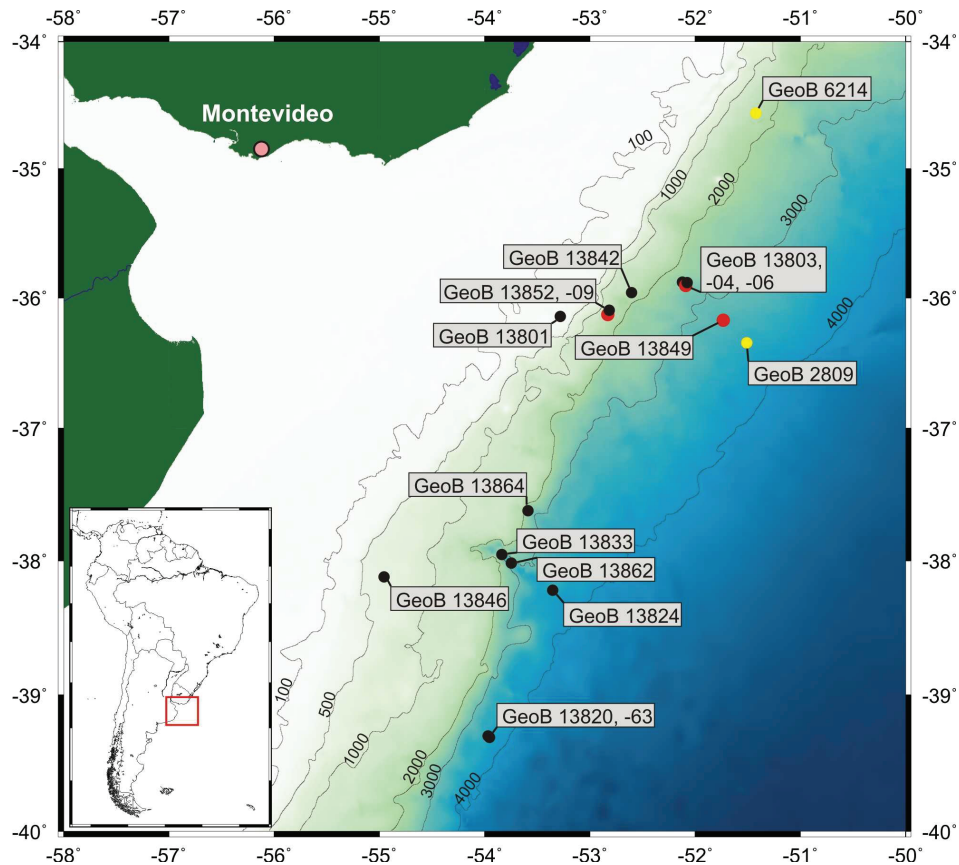


Fig. 18: Study area off Uruguay and Argentina and core locations. The sites marked in red are discussed in this study. The yellow dots mark the sites that are discussed in detail by Hensen et al. (2003).

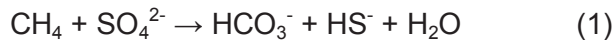
4.3 Material and methods

Sediment echosounder data were obtained with the Atlas Hydrographic Parasound system, which gives a dm-scale vertical resolution and a horizontal resolution of 7% of the water depth. Gravity cores were retrieved from various water depths (Tab. 5). Methane (CH₄) and pore water samples were gained as described by Henkel et al. (subm.).

Tab. 5: M78/3 core locations complemented by the shape of SO_4^{2-} profile and the acoustic facies.

GeoB #	Latitude	Longitude	Depth [mbsf]	SO_4^{2-} profile	Acoustic facies
13801-2	36°08.49' S	53°17.16' W	243	concave-up	Parallel layered; low to high amplitudes
13803-2	35°52.65' S	52°07.19' W	2462	concave-up	Parallel layered; medium to high amplitudes
13804-1	35°54.30' S	52°05.42' W	2593	kink	Chaotic, hummocky
13806-1	35°52.82' S	52°04.61' W	2586	concave-up	Transparent sheet-like layer; parallel layered sediment below
13809-1	36°07.67' S	52°49.90' W	1400	linear	Transparent sheet-like layer; parallel layered sediment below
13820-1	39°18.06' S	53°58.03' W	3613	linear	Parallel layered; low to high amplitudes
13824-1	38°13.14' S	53°21.29' W	3821	linear	Parallel layered; low to high amplitudes
13833-2	37°57.45' S	53°50.21' W	3404	concave-up	No data
13842-1	35°57.57' S	52°36.30' W	1555	kink	Parallel-subparallel layered; low to high amplitudes
13846-2	38°07.19' S	54°57.46' W	637	linear	Parallel layered; low to high amplitudes
13849-1	36°10.41' S	51°43.96' W	3278	concave-up	Lens-shaped transparent unit; parallel layered below
13852-1	36°05.70' S	52°48.98' W	1320	concave-up	Transparent sheet-like layer; parallel layered below
13862-1	38°01.11' S	53°44.70' W	3588	kink	No data
13863-1	39°18.70' S	53°57.16' W	3687	linear	Parallel layered; low to high amplitudes
13864-2	37°37.47' S	53°35.33' W	2757	linear	Parallel layered; medium to high amplitudes

We performed transport/reaction modeling using the software CoTRem (Adler et al., 2001) and following the method of Hensen et al. (2003). We consider AOM (Eq. 1) as the most important process for SO_4^{2-} reduction at depth.



Borowski et al. (1996) proposed that the upward flux of CH_4 can be quantitatively estimated from the downward flux of SO_4^{2-} . Measured CH_4 data were not used for the simulation because of the known inaccuracy related to the sampling (e.g., Dickens et al., 1997). Except for bioirrigation and sedimentation rate (SR) that are considered in the model as advective terms, we simulated exclusively diffusive transport of pore water species. The reaction-specific change in concentration at a specific sediment depth ($\Delta C_{s,d}$) was calculated as follows:

$$\Delta C_{s,d} = R_{s,d} \times dt_{\text{num}} \times SC_{s,d} \quad (2)$$

Where $R_{s,d}$ is the reaction rate, dt_{num} is the time step used in the model run, and $SC_{s,d}$ is a stoichiometric factor (see Hensen et al., 2003). Details to $R_{s,d}$ are given in section 4.4.

4.4 Results and discussion

Identification of submarine landslides by SO_4^{2-} profiles is restricted to MTDs that are only a few meters thick. A thicker MTD that is not completely penetrated by the gravity corer may show a linear SO_4^{2-} profile in the cored interval. In such a case, the change in gradient (the kink) occurs below the cored depth and the MTD could thus not be identified on the basis of the SO_4^{2-} profile. Fifteen of the investigated cores penetrated the SMTZ and therefore provided the required information for an appropriate description of the SO_4^{2-} profile (Tab. 5, Fig. 18). The SO_4^{2-} profiles are classified into the types linear, concave-up, and kink shape (Tab. 5). The acoustic facies with special emphasis on reflection configuration and amplitude are included as well in Tab. 5. Nine of the investigated cores reveal non-linear profiles. Three of these nine cores (GeoB 13801, -03, -42) are not related to MTDs, as indicated by Parasound data (Tab. 5). We therefore consider that the non-linearity of these SO_4^{2-} profiles can be attributed to alternative processes, such as CH_4 gas ebullition (Haeckel et al., 2007) or a sudden increase in the diffusive upward CH_4 flux (Kasten et al., 2003) possibly due to gas hydrate dissociation.

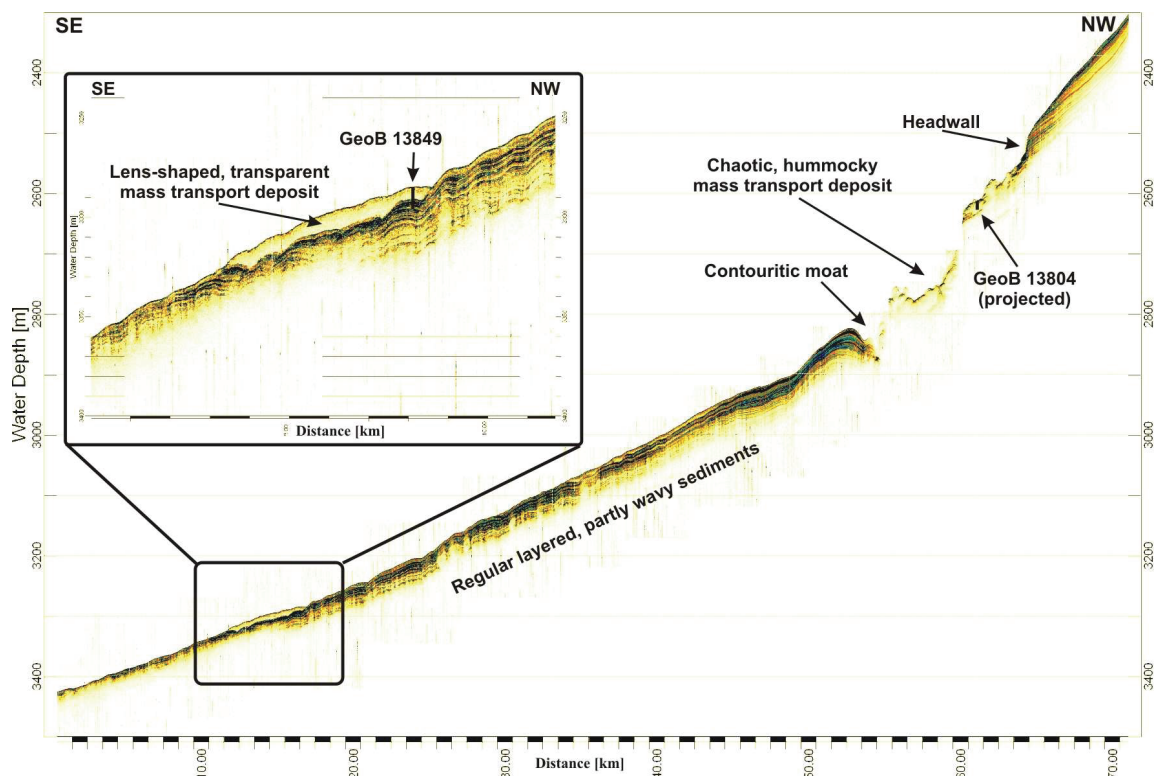


Fig. 19: Parasound profile obtained during *Meteor* Cruise M78/3 crossing the continental slope in SE-NW direction. The profile shows the position of core GeoB 13804 (projected) at a hummocky surface interpreted as mass-transport deposit. Site GeoB 13849 is shown in the close-up at the rim of a lens-shaped transparent unit overlying parallel layered sediments. At the core location, the transparent unit interpreted as a gravity flow deposit is ~6 m thick.

At several sites (GeoB 13806, -09, -49, -52), acoustically transparent deposits overlay parallel layered sediments (Tab. 5, Figs. 20, 21). In general, such transparent units represent either homogeneous or extremely heterogenous sediments with loss of internal bedding (Kuehl et al., 2005). Transparent acoustic facies often represent MTDs, which may also show a hummocky surface and an erosional base (Hampton et al., 1996).

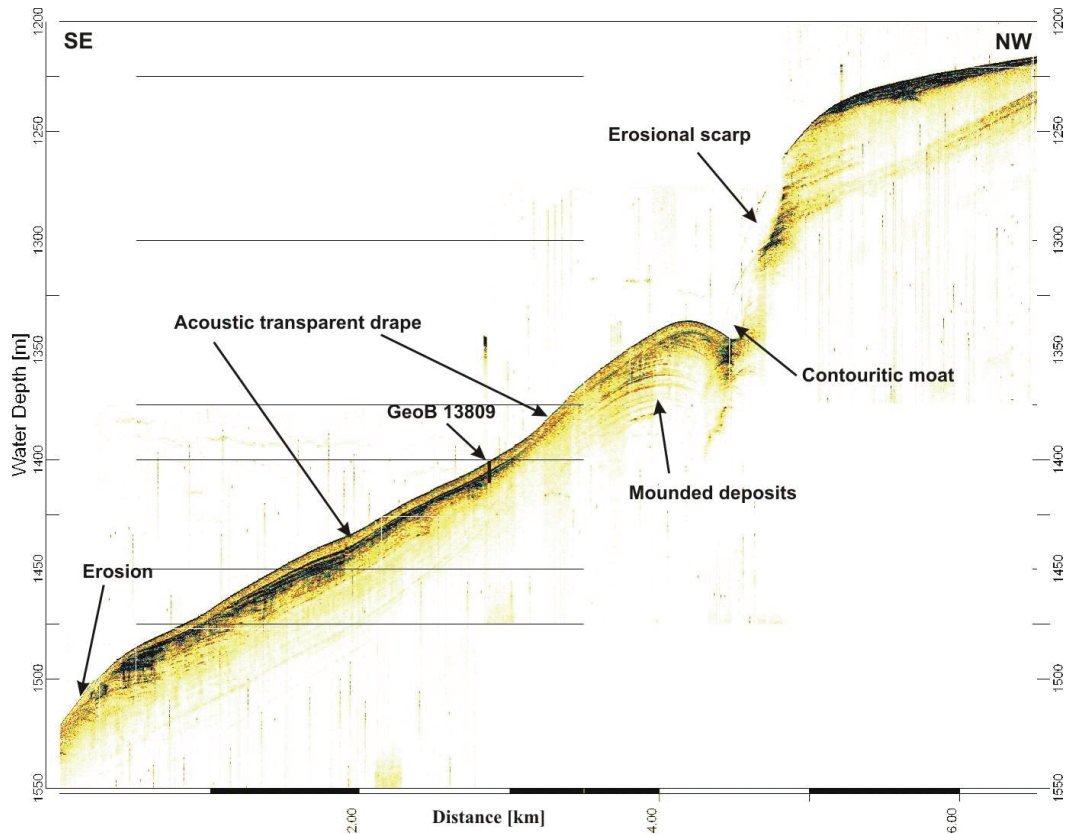


Fig. 20: Parasound profile obtained during Cruise M78/3 crossing the continental slope in SE-NW direction. Station GeoB 13809 is located to the SE of a contouritic moat. The profile at the core location shows parallel layered sediments and a strong reflector in 5-6 m depth that has an erosive character and is overlain by a sheet-like transparent unit.

Three sites (GeoB 13804, -49, and -09) will be discussed, that represent the three different categories of SO_4^{2-} profiles and which have all been recovered from sites that show acoustic indication of potential MTDs (Fig. 21). Core GeoB 13804 was retrieved from an acoustically chaotic facies with a hummocky surface. Core GeoB 13849 was recovered from a lens-shaped transparent unit (Fig. 19) and core GeoB 13809 was taken from an acoustically-transparent, sheet-like deposit downslope of a prominent scar (Krastel et al., in press). This 5-6 m thick sedimentary body is characterized by parallel upper and lower boundaries and shows no termination within the surveyed area (Fig. 20). The interpretation of this feature from Parasound data is therefore not unambiguous. It may result either from downslope

sediment-transport processes or from sheeted-contouritic deposition of homogenous material (see discussion below).

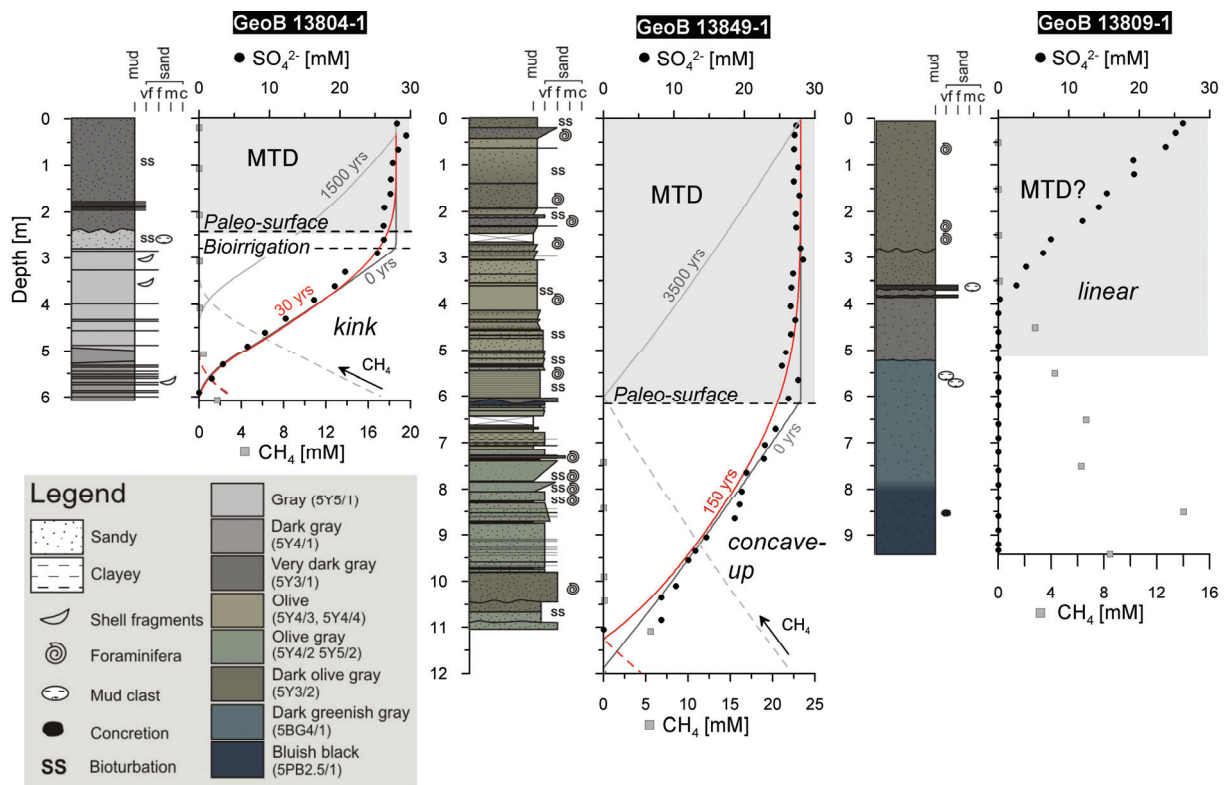


Fig. 21: Lithology, SO_4^{2-} , and CH_4 profiles of gravity cores. The non-steady state SO_4^{2-} profiles at sites GeoB 13804 and GeoB 13849 are related to recent MTDs (gray shaded). The gray lines labeled with “0 yrs” in the graphs of GeoB 13804 and -49 show the starting conditions for the models that were set up to estimate the timing of the mass-transport deposition. Data of site GeoB 13804 including the geochemical simulation are described in detail by Henkel et al. (subm.). The values in brackets (legend) represent the Munsell color code.

Pore water profiles at potential MTD sites

The SO_4^{2-} profile at site GeoB 13804 has a kink shape with a gradient change at ~2.8 m (Fig. 21). A sedimentological boundary between gray and very dark gray mud occurs at 2.43 m, thus ~0.35 m above the gradient change of the SO_4^{2-} profile (Fig. 21). Above this sedimentological contact, which is also reflected by a significant downcore increase in undrained shear strength (Henkel et al., subm.), the core shows a stack of undisturbed sand/silt layers (Fig. 21). Bioturbation structures are present between 0 and 2.79 m depth. Bioirrigation and vertical gas or fluid migration in the whole ~2.8 m thick package can be excluded (Henkel et al., subm.). Therefore, we conclude that the kink shaped SO_4^{2-} profile is the result of the combination of bioirrigation to a paleo-depth of 0.35 m and a ~2.4 m thick slide mass. In accordance with the studies of Zabel and Schulz (2001) and Hensen et al. (2003) at other locations, the most recent mass-transport event at site GeoB 13804 must have happened in the form of a coherent slide mass carrying its initial SO_4^{2-} profile

downward, because the internal structure of this package was not destroyed. It is known from previous expeditions that sites with nearly constant SO_4^{2-} concentrations over the length of a gravity core (as it is expected for the source area of the slide) occur in the study area (Bleil et al., 1994).

Site GeoB 13849 is characterized by a concave-up shaped SO_4^{2-} profile (Fig. 21). Based on Parasound data, the thickness of the surficial MTD unit is estimated to be ~6 m (Fig. 19), which fits well to the SO_4^{2-} profile showing a change in gradient at the same depth. The lithology displays a sharp contact between bluish black fine sand interbedded with olive muddy fine sand below and dark gray muddy fine sand above 6.10 m. Based on the geochemical and Parasound data this boundary is interpreted as the base of the MTD.

The visual description of core GeoB 13809 reveals a sharp, irregular contact at 5.12 m. Since this boundary correlates to the base of the acoustically transparent layer imaged in Parasound data, it possibly represents the base of an MTD (Fig. 21). Core GeoB 13809 displays a linear SO_4^{2-} profile. If a mass-movement affected this site, it definitely took place several hundreds to thousands of years ago, so that the SO_4^{2-} profile could diffusively re-equilibrate into a linear shape.

Geochemical transport/reaction modeling

The diffusive re-equilibration of the SO_4^{2-} profile over time was simulated for sites GeoB 13804 and -49 (parameterization in Tab. 6). A maximum reaction rate $R_{s,d}$ of $0.1 \text{ mol dm}^{-3} \text{ yr}^{-1}$ was defined to produce a broad SMTZ with overlapping CH_4 and SO_4^{2-} profiles at site GeoB 13804 (Fig. 21). That rate was used as long as the reactants were available in sufficient amounts (0^{th} order kinetics). For lower concentrations of the reactants and for site GeoB 13849, where the SMTZ is restricted to a distinct depth, the AOM reaction rate was determined based on 2^{nd} order kinetics. The starting conditions for the model runs are shown as gray lines in Fig. 21: Each sediment package (the MTD and the sediment below) still hosts its initial pore water characteristic. For site GeoB 13804, the model results reveal that the proposed mass movement took place less than 30 years ago (Fig. 21; Henkel et al., *subm.*). The event could therefore have been associated with a weak ($5.2 m_b$) earthquake in 1988 (Henkel et al., *subm.*). The epicenter was ~70 km away from the core location (Assumpção 1998; Benavídez Sosa 1998).

Tab. 6: Parameterization for transport and reaction modeling for sites GeoB 13804 and -49.

Basic parameters GeoB 13804/ -49		Boundary conditions GeoB 13804/ -49	
Model length [m]	8/15	Sedimentation rate [cm kyr ⁻¹]	80-180 ^{b/5} ^c
Cell discretisation [cm]	5	Upper boundary SO ₄ ²⁻ [mmol l ⁻¹]	28 ^d
Time step [yr]	0.05	Upper boundary CH ₄ [mmol l ⁻¹]	0 ^d
Porosity ϕ	0.6/0.7 ^a	Lower boundary SO ₄ ²⁻ [mmol l ⁻¹]	0
Temperature [°C]	3.5	Lower boundary CH ₄ [mmol l ⁻¹]	40/35
Diffusion coefficients ^e		D ₀	D _{sed}
SO ₄ ²⁻ [cm ² yr ⁻¹]		179.5	88.79
CH ₄ [cm ² yr ⁻¹]		293.6	145.2

^a Average porosity, as measured on board. ^b Exceptionally high sedimentation rate derives from unsupported ²¹⁰Pb. For details see Henkel et al. (subm.). ^c According to Ewing et al. (1971) and Hensen et al. (2003). ^d Bottom water concentrations. ^e Diffusion coefficient in free solution (D₀) calculated for a temperature of 3.5°C and corrected for tortuosity (θ) after Boudreau (1997); $D_{sed} = D_0/\theta^2$, while $\theta^2 = 1-\ln(\phi^2)$.

According to the best fit between measured SO₄²⁻ concentrations and the simulation (red line in Fig. 21), the MTD at site GeoB 13849 occurred approximately 150 years ago. The age of the MTD roughly corresponds to an earthquake in 1848 (intensity in Montevideo IV-V based on the Mercalli scale) with an epicenter ~200 km west of the study site (Benavidez Sosa 1998). Complete re-equilibration of the SO₄²⁻ profile is reached after ~3500 years (Fig. 21).

4.5 Conclusions

This study demonstrates that integrating geophysical, sedimentological, and pore water data provides a scientifically valid approach to constrain the ages of recent MTDs. Pore water geochemical analyses are cost-efficient, easily accessible compared to other methods, and can provide information regarding paleosurfaces or erosive contacts that are not apparent from visual core inspection. Applying a comprehensive, multi-disciplinary approach as presented in this study over a larger region could provide a historical record of the frequencies of mass-transport events. Such a record may be compared to documented earthquakes and in this way shed light on the dynamic and complex links between various geological processes.

Acknowledgments. G.L. Arnold and J. Sawicka are acknowledged for analyzing SO₄²⁻. R. Violante and V. Bender are acknowledged for the visual description of the cores. The Parasound figures were created using the free software SENT developed by H. Keil, University of Bremen. The manuscript benefited from the very constructive reviews of C.

Hensen and B. Dugan. This study was funded by the Deutsche Forschungsgemeinschaft (DFG) in the frame of the International Graduate College "Proxies in Earth History" (EUROPROX) and the Research Center/Cluster of Excellence "The Ocean in the Earth System" (MARUM). We appreciate further financial support from the Helmholtz Association (AWI Bremerhaven). All data are available via the database Pangaea (<http://www.pangaea.de>).

References

- Adler, M., Hensen, C., Wenzhöfer, F., Pfeifer, K., and Schulz, H.D., 2001, Modeling of calcite dissolution by oxic respiration in supralysocinal deep-sea sediments: *Marine Geology*, v. 177, p. 167-189.
- Assumpção, M., 1998, Seismicity and stresses in the Brazilian passive margin: *Bulletin of the Seismological Society of America*, v. 88, p. 160-169.
- Barnes, R.O. and Goldberg, E.D., 1976, Methane production and consumption in anoxic marine sediments: *Geology*, v. 4, p. 297-300.
- Benavídez Sosa, A., 1998, Sismicidad y sismotectónica en Uruguay: *Física de la Tierra*, p. 167-186.
- Bleil, U. and cruise participants, 1994, Report and preliminary results of *Meteor* Cruise M29/2, Montevideo - Rio de Janeiro, 15.07.1994 - 08.08.1994 *Berichte aus dem Fachbereich Geowissenschaften der Universität Bremen*, Volume 59, p. 153.
- Borowski, W.S., Paull, C.K., and Ussler, W., 1996, Marine pore-water sulfate profiles indicate in situ methane flux from underlying gas hydrate: *Geology*, v. 24, p. 655-658.
- , 1999, Global and local variations of interstitial sulfate gradients in deep-water, continental margin sediments: Sensitivity to underlying methane and gas hydrates: *Marine Geology*, v. 159, p. 131-154.
- Boudreau, B.P., 1997, Diagenetic models and their implementation: modeling transport and reactions in aquatic sediments: Berlin, Heidelberg, New York, Springer, 414 p.
- De Lange, G.J., 1983, Geochemical evidence of a massive slide in the southern Norwegian Sea: *Nature*, v. 305, p. 420-422.
- Dickens, G.R., Paull, C.K., and Wallace, P.J., 1997, Direct measurement of in situ methane quantities in a large gas-hydrate reservoir: *Nature*, v. 385, p. 426-428.
- Ewing, M., Eittrheim, S.L., Ewing, J.I., and Le Pichon, X., 1971, Sediment transport and distribution in the Argentine Basin. 3. Nepheloid layer and processes of sedimentation: *Physics and Chemistry of the Earth*, v. 8, p. 49-77.

- Haeckel, M., Boudreau, B.P., and Wallmann, K., 2007, Bubble-induced porewater mixing: A 3-D model for deep porewater irrigation: *Geochimica et Cosmochimica Acta*, v. 71, p. 5135-5154.
- Hampton, M.A., Lee, H.J., and Locat, J., 1996, Submarine landslides: *Reviews of Geophysics*, v. 34, p. 33-59.
- Henkel, S., Strasser, M., Schwenk, T., Hanebuth, T.J.J., Hüsener, J., Arnold, G.L., Winkelmann, D., Formolo, M., Tomasini, J., Krastel, S., and Kasten, S., *subm.*, An interdisciplinary investigation of a recent submarine mass-transport deposit at the continental margin off Uruguay.
- Hensen, C., Zabel, M., Pfeifer, K., Schwenk, T., Kasten, S., Riedinger, N., Schulz, H.D., and Boetius, A., 2003, Control of sulfate pore-water profiles by sedimentary events and the significance of anaerobic oxidation of methane for the burial of sulfur in marine sediments: *Geochimica et Cosmochimica Acta*, v. 67, p. 2631-2647.
- Hernández-Molina, F.J., Paterlini, M., Violante, R., Marshall, P., de Isasi, M., and Somoza, L., 2009, Contourite depositional system on the Argentine Slope: An exceptional record of the influence of Antarctic water masses: *Geology*, v. 37, p. 507-510.
- Kasten, S., Zabel, M., Heuer, V., and Hensen, C., 2003, Processes and signals of nonsteady-state diagenesis in deep-sea sediments and their pore waters, *in* Wefer, G., Mulitza, S., and Ratmeyer, V., eds., *The South Atlantic in the Late Quaternary: Reconstruction of Mass Budget and Current Systems*: Berlin, Heidelberg, New York, Springer, p. 431-459.
- Krastel, S., Wefer, G., Antobreh, A.A., Freudenthal, T., Hanebuth, T.J.J., Preu, B., Schwenk, T., Strasser, M., Violante, R., Winkelmann, D., and M78/3 shipboard scientific crew, *in press*, Sediment dynamics and geohazards off Uruguay and the de la Plata River region (Northern-Argentina): *Geo-Marine Letters*.
- Kuehl, S.A., Allison, M.A., Goodbred, S.L., and Kudrass, H.R., 2005, The Ganges-Brahmaputra Delta, *in* Giosan, L., and Bhattacharya, J.P., eds., *River Deltas - Concepts, Models, and Examples*, SEPM Special Publication, p. 413-434.
- Piola, A.R. and Matano, R.P., 2001, Brazil and Falklands (Malvinas) Currents, *in* John, H.S., Karl, K.T., and Steve, A.T., eds., *Encyclopedia of Ocean Sciences*: Oxford, Academic Press, p. 422-430.
- Schulz, H.D., 2006, Quantification of early diagenesis: dissolved constituents in pore water and signals in the solid phase, *in* Schulz, H.D., and Zabel, M., eds., *Marine Geochemistry*: Berlin, Springer, p. 73-124.
- Seeberg-Elverfeldt, J., Schlüter, M., Feseker, T., and Kölling, M., 2005, Rhizon sampling of porewaters near the sediment-water interface of aquatic systems: *Limnology and Oceanography: Methods*, v. 3, p. 361-371.

Zabel, M. and Schulz, H.D., 2001, Importance of submarine landslides for non-steady state conditions in pore water systems - lower Zaire (Congo) deep-sea fan: *Marine Geology*, v. 176, p. 87-99.

Chapter 5: Diagenetic phosphorus cycling in surface and subseafloor sediments at the continental margin off Uruguay and Argentina

Susann Henkel¹, Gert J. de Lange², Natascha Riedinger³, Michael Formolo⁴, Gail L. Arnold⁵, Juan Tomasini⁶, and Sabine Kasten¹

¹Alfred Wegener Institute for Polar and Marine Research, Am Handelshafen 12, 27570, Bremerhaven, Germany

²Department of Earth Sciences - Geochemistry, Utrecht University, Budapestlaan 4, 3584 CA Utrecht, The Netherlands

³University of California, Riverside, 900 University Avenue, Riverside, CA 92521, USA

⁴The University of Tulsa, 800 South Tucker Drive, Tulsa, OK, 74104, USA

⁵Max Planck Institute for Marine Microbiology, Celsiusstr. 1, 28359 Bremen, Germany

⁶Administración Nacional de Combustibles Alcohol y Pórtland (ANCAP), Paysandú s/n esq. Avenida del Libertador, Montevideo, 11100, Uruguay

Manuscript in preparation for submission to *Earth and Planetary Science Letters*

Abstract

Phosphorus (P) cycling in surface and subsurface sediments was studied at three sites at the continental slope off Uruguay and Argentina. The core locations are characterized by different depositional characteristics and sedimentation rates and can be distinguished into steady state and non-steady state systems with respect to pore water geochemistry. As for other continental margin settings, the sediments are rich in iron (Fe) and P cycling is closely coupled to the reduction of Fe (oxyhydr)oxides. However, besides the liberation of phosphate (HPO_4^{2-}) at the front where Fe (oxyhydr)oxides react with dissolved sulfide (HS^-), the fast burial of Fe (oxyhydr)oxides below the sulfidic zone during glacial times led to an additional modern HPO_4^{2-} liberation below the sulfidic zone, which is attributed to ongoing deep Fe (oxyhydr)oxide reduction. The HPO_4^{2-} reaches shallower sediment depths, where it is partly retained by 'fresh' Fe (oxyhydr)oxides. In contrast to previously investigated slope settings,

precipitation of authigenic P-minerals (e.g., vivianite) below the sulfidic zone is not evident from pore water profiles and the biogenic/authigenic P distribution. Sedimentation rates and the extent of the sulfidic zone are the main factors determining the shape of the HPO_4^{2-} profiles and the post-depositional redistribution of P.

5.1 Introduction

Phosphorus is one of the nutrients that control marine primary productivity and thus influence carbon sequestration and climate change (e.g., Van Cappellen and Ingall, 1996; Benitez-Nelson and Buesseler, 1999; Diaz et al., 2008). For this reason, there have been numerous studies focusing on the benthic cycling of P with the aim to determine the flux of P across the sediment/water interface (e.g., Slomp et al., 1996; Hensen et al., 1998; Hensen et al., 2004; Küster-Heins et al., 2010a). Most of the organic matter that is produced in the photic zone is degraded in the water column, which leads to a release of P that is uncoupled from post-depositional processes. However, oxidation of the remaining organic compounds continues at and below the ocean floor and liberates P into the pore water (Ruttenberg, 1993; Ruttenberg and Goñi, 1997). Dissolved P in sea- and pore water is mainly present as phosphate (HPO_4^{2-}) and has a strong affinity to adsorb on Fe (oxyhydr)oxide particles such as ferrihydrite ($\text{Fe}_5\text{O}_3(\text{OH})_9$), lepidocrocite ($\gamma\text{-FeOOH}$), goethite ($\alpha\text{-FeOOH}$), and hematite ($\alpha\text{-Fe}_2\text{O}_3$) (e.g., Froelich, 1988; Sundby et al., 1992). Due to the settling and burial of these oxide minerals, HPO_4^{2-} is removed from the water column. In particular, sediments at continental margins to which high amounts of Fe (oxyhydr)oxides are delivered by rivers (e.g., Poulton and Raiswell, 2002) may act as sinks or depotcenters for P (Ruttenberg, 1993). If subjected to anoxic conditions, the accumulated Fe (oxyhydr)oxides undergo reduction and release HPO_4^{2-} into the pore water. Phosphate may then diffuse upwards where it may be adsorbed again on Fe (oxyhydr)oxide surfaces or (if the retention potential of the Fe (oxyhydr)oxides is exhausted) are liberated back into the water column. Mixing or upwelling processes are then required to transport the nutrient back into the photic zone, where it is available again for biological uptake. This pattern is well-known and has been described for example by Mortimer (1971), Krom and Berner (1981), Froelich et al. (1982), Jensen et al. (1995), and Anschutz et al. (1998).

Comparatively little is known about the “deep” diagenetic overprint of the P record in marine sediments. “Deep” refers here to depths below the sulfate-methane transition zone (SMTZ), where the anaerobic oxidation of methane (AOM) coupled to sulfate (SO_4^{2-}) reduction occurs (e.g., Barnes and Goldberg, 1976; Niewöhner et al., 1998; Hinrichs et al., 1999; Boetius et al., 2000). In continental slope sediments, the SMTZ usually is located at a few to tens of

meters sediment depth, depending on the burial of organic carbon, the upward flux of methane (CH₄), sediment porosity, and sedimentation rate. Understanding the processes that drive the early diagenetic cycling of P is of particular interest, because this will increase the quality of interpretation of fossil sedimentary archives, e.g., Cretaceous black shales that are a major topic of current research (e.g., März et al., 2008b; Mort et al., 2008; März et al., 2009; Tsandev and Slomp, 2009; Kraal et al., 2010b). Most of these studies involve the determination of the P speciation in the solid phase. However, even if the relative proportions of all P fractions are known, it often remains unclear to which extent the primary signal has already been altered (Slomp et al., 2009). Sinks for pore water P are the aforementioned re-adsorption onto Fe (oxyhydr)oxide surfaces and the precipitation of authigenic minerals such as thermodynamically stable carbonate fluorapatite (CFA, Ca₅(PO₄,CO₃)₃F). According to Slomp et al. (2009), the *in situ* conversion of fish bone hydroxyapatite to CFA is especially problematic for paleoenvironmental studies based on P records because this alteration makes the differentiation between biogenic and authigenic Ca-P fractions impossible. Another process that was suggested to lead to a considerable redistribution of P in slope sediments is the precipitation of vivianite (Fe₃(PO₄)₂ × 8H₂O) (Schulz et al., 1994; Burns, 1997; Ruttenberg and Goñi, 1997; März et al., 2008a). Even more challenges arise when sediments are exposed to oxygen, e.g., during sample storage. Kraal et al. (2009) demonstrated that pyrite oxidation leads to an acidification of the pore water, which promotes the dissolution of Ca-P minerals. The released P was then shown to adsorb onto the surfaces of secondary Fe oxides.

Here we investigate sediments from three sites at the passive continental margin off Uruguay and Argentina showing different depositional characteristics and sedimentation rates in order to assess the specific reactions/processes that determine the cycling of P above, at, and below the SMTZ. We delineate similarities and differences to other continental slope settings and aim at deciphering the factors that control the shape of HPO₄²⁻ profiles.

5.2 Study sites

The passive continental margin off Uruguay and Argentina shows very unique, highly dynamic oceanographic and depositional conditions: The southward directed, subtropical Brazil Current interacts with the Malvinas Current that transports Antarctic water masses northward. The Brazil-Malvinas Confluence (BMC) is located near 39°S (Gordon and Greengrove, 1986; Gordon, 1989; Piola and Matano, 2001) and thus near the mouth of the Río de la Plata (Fig. 22). Antarctic Intermediate Water (AIW) is present at depths of 700-1000 m and is underlain by North Atlantic Deep Water (NADW), Upper and Lower

Circumpolar Deep Water (UCDW and LCDW), and Antarctic Bottom Water (AABW) that forms a strong contour current along the margin and transports predominantly fine sediments into the Argentine Basin (Ewing et al., 1971; Piola and Matano, 2001). The interfaces of the water masses roughly coincide with erosive morphological features and contouritic depositional systems, which are evidence of an intense reworking of the sediment (Hernández-Molina et al., 2009). As indicated by surface sediment composition and benthic mineralization rates, huge amounts of sediment are transported from the shelf to the slope and into the Argentine Basin (Romero and Hensen, 2002; Hensen et al., 2004). This lateral transport of sediment (and organic matter) affects the benthic HPO_4^{2-} fluxes from surface sediments into the bottom water. Extremely high HPO_4^{2-} fluxes (up to $11 \text{ mmol m}^{-2} \text{ yr}^{-1}$) were determined for a large region extending to the lower continental slope (Hensen et al., 1998).

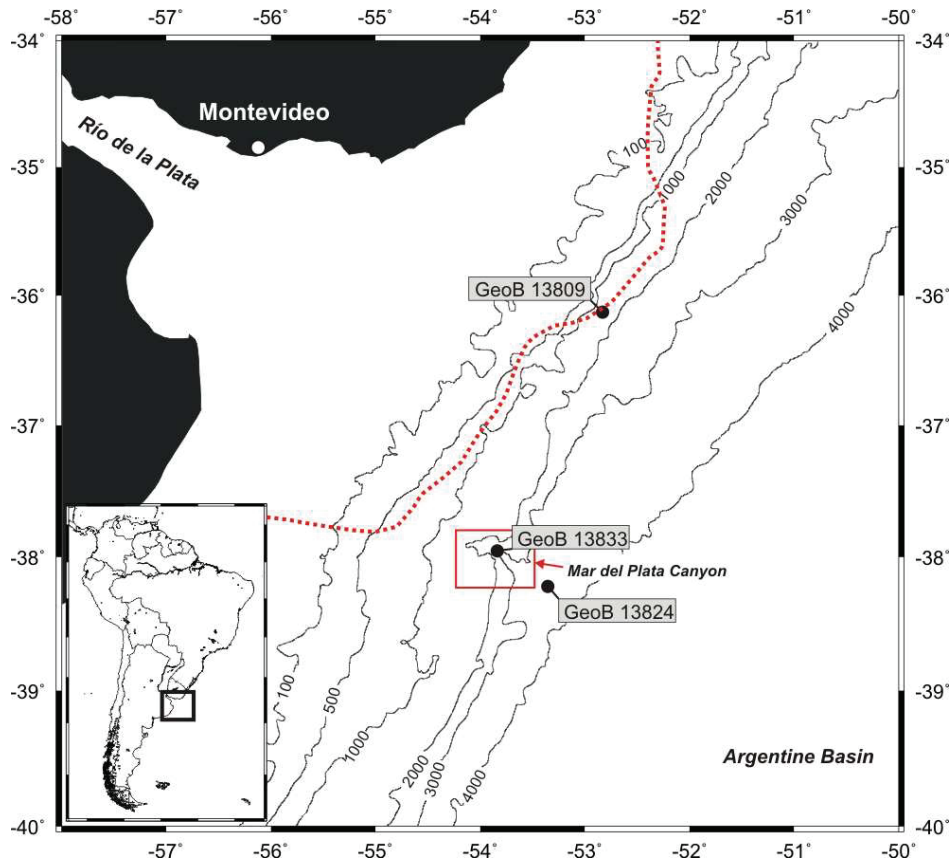


Fig. 22: Position of core locations at the passive continental margin off Uruguay. Modified after Henkel et al. (subm.). The red line after Piola et al. (2008) shows the extent of the Río de la Plata plume in January (southern summer), i.e. the position of the 33.5 isohaline derived from historical hydrographic data.

The three locations investigated in this study (GeoB 13824, GeoB 13809, and GeoB 13833) are located at the continental slope off Uruguay and Argentina in water depths between 1400 and 3821 m (Tab. 7, Fig. 22). Core GeoB 13824 was retrieved west of the Mar del Plata Canyon. The sediment echosounder profile for this site is given in Fig. 23. The sediments are

Tab. 7: Geochemically investigated stations from RV Meteor expedition M78/3. GC = gravity core, MUC = multicorer core, GBC = giant box corer.

Station	Device	Water depth [m]	Latitude	Longitude
GeoB 13809-1	GC	1400	36°07.67' S	52°49.90' W
GeoB 13809-2	MUC	1397	36°07.67' S	52°49.90' W
GeoB 13824-1	GC	3821	38°13.14' S	53°21.29' W
GeoB 13833-1	GBC	3369	37°57.45' S	53°50.21' W
GeoB 13833-2	GC	3404	37°57.45' S	53°50.21' W

parallel layered and show low to high amplitudes (Henkel et al., *subm.*) indicating strong density changes within the cored sediment interval. Core GeoB 13809 penetrated a 5-6 m thick, acoustically transparent sheet-like deposit downslope of a prominent scar (Fig. 24). The formation of this scar might be associated to strong contour currents (Krastel et al., *in press*). It has been suggested by Henkel et al. (*subm.*) that the transparent sediment unit represents a mass-transport deposit. Site GeoB 13833 is located in the Mar del Plata Canyon and is thus possibly affected by turbidites and/or other mass movements, which are common in the study area (e.g., Hensen et al., 2003; Krastel et al., *in press*). Unfortunately, sediment echosounder data for this site is not available.

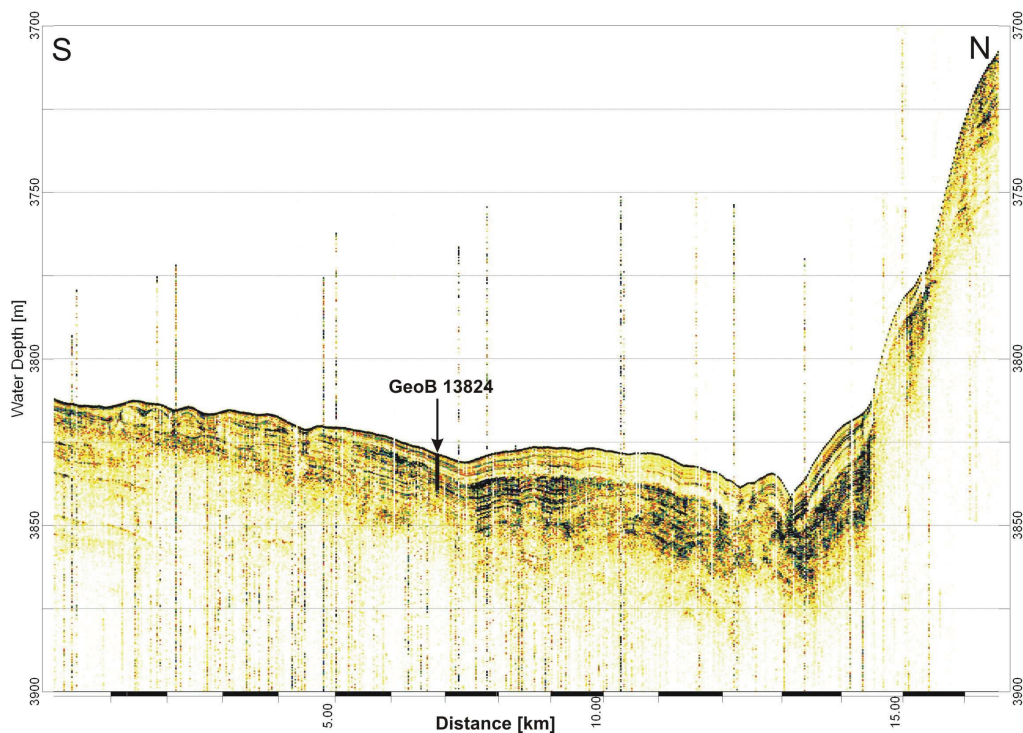


Fig. 23: Sediment echosounder profile showing the position of core GeoB 13824. The profile runs in S-N direction. At the core location, the sediments are parallel layered and show low to high amplitudes.

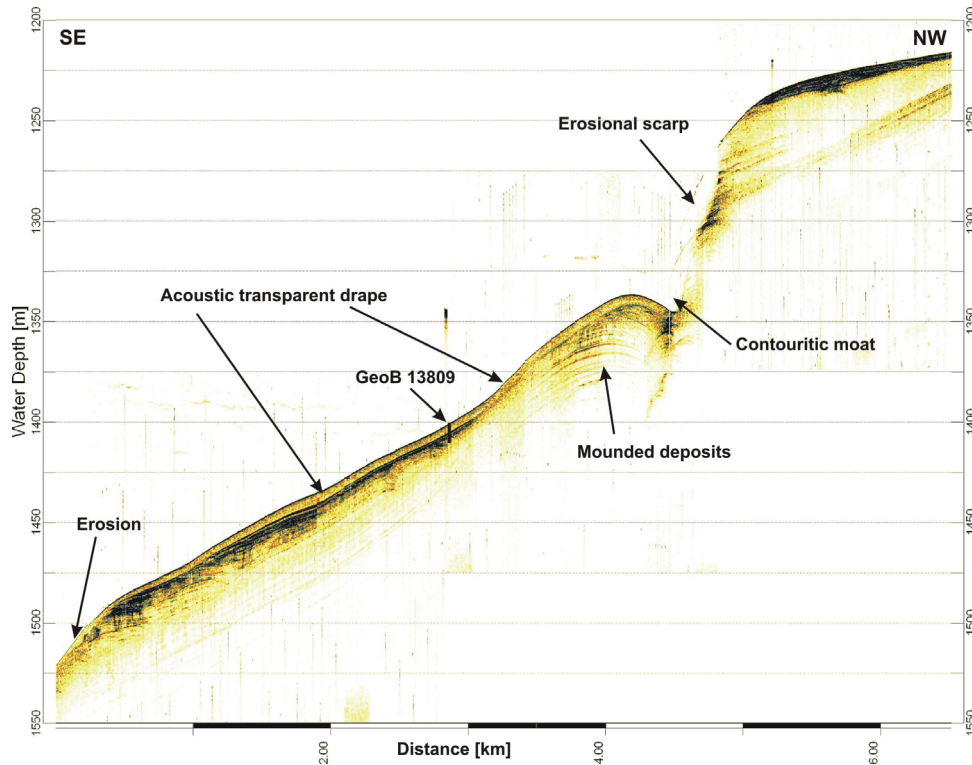


Fig. 24: Sediment echosounder profile showing the position of site GeoB 13809 from Henkel et al. (subm.). The profile crosses the continental slope in SE-NW direction. Station GeoB 13809 is located to the SE of a contouritic moat. The gravity core penetrated parallel layered sediments with a strong reflector in 5-6 m depth, which is overlain by an acoustically transparent sheet-like unit.

All sites are located close (<400 km) to the Río de la Plata mouth. With respect to the discharge of water ($23\,000\text{ m}^3\text{ s}^{-1}$) the Río de la Plata is the fifth largest river on Earth (Campos et al., 2008b). It drains ~20% of South America (Piola et al., 2008) and delivers approximately 92 Gt of terrigenous material into the South Atlantic annually (Milliman and Meade, 1983). Most of the terrigenous clayey sediment is transported to the north and accumulates in a mud belt on the shelf (Martins et al., 2005; Psuty and Mizobe, 2005). Fluvially derived material is also rapidly redistributed eastward by the strong ocean currents and reaches the continental slope and the Argentine Basin (Hensen et al., 2003; Seiter et al., 2004). The terrigenous sediment that accumulates on the shelf between the Río de la Plata mouth and 33°S is comparatively coarse (silt and sand). It consists mainly of quartz, feldspar, and calcite (Campos et al., 2008a). The plume of the river outflow changes seasonally and may extend beyond 1000 km of the estuary (Campos et al., 1999). Associated with the wind pattern, the plume may particularly affect the study area (especially site GeoB 13809) during southern summer (January, February) (Fig. 22). The Río de la Plata also delivers large amounts of organic matter to the continental slope (Mollenhauer et al., 2006). Additionally, due to the confluence of the Brazil and the Malvinas Currents, the primary productivity is

enhanced at the continental margin and reaches up to $1200 \text{ g C m}^{-2} \text{ yr}^{-1}$ (Gordon, 1989; Peterson and Stramma, 1991; Antoine et al., 1996).

5.3 Material and methods

This study involves data of three gravity cores, one multicorer (MUC) core, and a MUC core that was sub-sampled from a giant box corer (GBC). The material was obtained during RV *Meteor* expedition M78/3a in May-June 2009 (Krastel et al., in prep.). Sediment echosounder data were obtained using the Atlas Hydrographic Parasound system, which gives a dm-scale vertical resolution and a horizontal resolution of 7% of the water depth.

5.3.1 Sampling

After recovery, the gravity cores were cut into segments of 1 m length. For CH_4 analyses, syringe samples of 3 cm^3 were taken immediately after cutting of the segments following the procedure described by Schulz (2006). The samples were transferred into 20 ml He-flushed headspace vials filled with 10 ml of a 5 M NaCl solution. After closing and shaking the vials, the samples were stored at 4°C until analysis.

Sampling of pore water was carried out in a cold room at $\sim 4^\circ\text{C}$ within a few hours after core recovery. Rhizons with a pore size of $\sim 0.1 \mu\text{m}$ were used to extract the interstitial water (Seeberg-Elverfeldt et al., 2005; Dickens et al., 2007) at intervals of $\sim 0.30 \text{ m}$ (gravity cores) and 1-2 cm (MUC cores). Aliquots of pore water were taken for SO_4^{2-} , sulfide (furthermore referred to as HS^- although also present as H_2S), alkalinity, HPO_4^{2-} , dissolved iron (Fe^{2+}), and cation (e.g., Ca^{2+}) analyses. Samples for sulfide were preserved by addition of ZnAc. Cation samples were diluted 1:10 with 1 M HNO_3 .

Solid phase sampling for sequential extractions and total acid digestion was performed onboard within a few hours after splitting the cores. Samples were obtained from gravity cores using syringes with cut tips. The syringes were sealed and stored frozen at -20°C to avoid any microbially mediated degradation. A few days after sampling, the syringes were put into impermeable nitrogen-flooded bags and stored frozen until further processing. Sediment of the MUC cores was transferred into Falcon tubes and subsequently put into an argon-flooded glovebox, where pore water sampling was performed. Afterwards, the tubes were closed properly and stored in the same way as the gravity core samples. All sequential extractions and multi-element analyses were performed on these samples. Only for gravity core GeoB 13809 additional sampling for the chemical composition of bulk sediment was performed onshore.

5.3.2 Analyses

Pore water

Sulfate measurements were performed either onboard using the Sykam solvent delivery system coupled to a Waters 430 conductivity detector or onshore by suppressed ion chromatography at a 1:100 dilution with 18M Ω -water on a Metrohm 761 compact IC. Seawater provided by the International Association for the Physical Sciences of the Oceans (IAPSO) was used in each run either for preparation of the calibration standards or as a quality control sample. Sulfide was determined photometrically applying the methylene blue method by Cline (1969). Alkalinity was measured within a few hours after sampling on a 1 ml aliquot of pore water by titration with HCl (10, 50, and 100 mM). Calculations of the alkalinity were done after Schulz (2006). For analysis of Fe²⁺, 1 ml aliquots were transferred into cuvettes pre-filled with a 50 μ l Ferrospectral solution immediately in the cold room. At high Fe²⁺ concentrations (>1 mg l⁻¹), the aliquots were preserved with 10 μ l of 1% ascorbic acid and subsequently diluted with oxygen-free artificial seawater. Pore water phosphate was analyzed within a few hours after sampling applying the photometric method described by Grasshoff (1999). Samples containing sulfide were previously purged with argon. Photometric analyses of Fe²⁺ and HPO₄²⁻ were performed using a CECIL CE2021 photometer at wavelengths of 565 nm and 820 nm. Dissolved Ca²⁺ concentrations in the pore water were measured by inductively coupled plasma optical emission spectrometry (ICP-OES) using a Thermo Scientific IRIS Intrepid instrument. Daily standard calibrations and quality checks were performed using multi-element standards of different concentrations that were prepared from single element stock solutions in 1M HNO₃ and adapted Na-content. The accuracy of all measurements was better than 5%, the relative standard deviation of the three measurements per sample (precision) was usually better than 5% as well. Methane was measured with a Hewlett Packard 5890A gas chromatograph (GC) equipped with a splitless injector, a stainless steel Porapak-Q column, and a flame ionization detector. Chromatographic response on the GC instrument was calibrated against three different standards with variable concentrations of CH₄. The measured concentrations were corrected for sediment porosity.

Solid phase

Total organic carbon, CaCO₃, total element composition

Total carbon (TC) and inorganic carbon (IC) were determined by measuring dried and homogenized bulk samples using an ELTRA carbon sulfur analyzer. Total organic carbon (TOC) contents were calculated subtracting IC concentrations from TC.

Multi-element analyses of the bulk sediment were performed after complete digestion of about 50 mg of freeze-dried and homogenized sediment using a MLS ETHOS 1600 Microwave system and a mixture of 3 ml HNO₃, 2 ml HCl, and 0.5 ml HF. After evaporation of the acids, the residues were re-dissolved in 1 M HNO₃. The standard reference sediment NIST SRM 2702 was processed every 4-5 samples to check the accuracy of the digestion and the analytical procedure. Element concentrations (P, Fe, and Al) were subsequently measured by ICP-OES using a Thermo Scientific IRIS Intrepid instrument. Daily standard calibrations and quality checks were performed using multi-element standards of 5 different concentrations prepared from single element stock solutions in 1 M HNO₃. The recoveries with respect to the NIST SRM 2702 standard material were 99.5 ± 3.1% for P, 98.5 ± 3.0% for Fe, and 100.3 ± 4.9% for Al.

Stable isotope composition of carbonates

Stable isotope analyses ($\delta^{13}\text{C}_{\text{carb}}$ and $\delta^{18}\text{O}_{\text{carb}}$) on bulk carbonate were performed at Utrecht University using a VG Sira 24 instrument. The samples were treated with phosphoric acid at 90°C. The liberated CO₂ was frozen onto a cold finger for approximately 7 minutes and subsequently released into the inlet of a mass spectrometer. Isotope data is given in δ -notation (‰) relative to Vienna PeeDee Belemnite standard (V-PDB).

Phosphorus fractions

The speciation of solid-phase P was determined applying the sequential P extraction method SEDEX developed by Ruttenberg (1992). Several modifications were applied as proposed by Slomp et al. (1996). For example, the MgCl₂ washing steps were reduced to 30 minutes and H₂O rinses were omitted. Details can be found in Table 8. The SEDEX method allows us to distinguish five fractions of solid P: (1) loosely bound/easily exchangeable P, (2) Fe-bound P (the fraction that is adsorbed to Fe (oxyhydr)oxides), (3) biogenic/authigenic P including CFA, biogenic Ca-P, and CaCO₃-bound P, (4) detrital P, and (5) organic P. In contrast to previous protocols (see also März et al., 2008b; Kraal et al., 2010b), we used wet sediment that was stored frozen under anoxic conditions. The transfer of approximately 1-2 g of wet sediment into pre-weighed centrifuge tubes was performed under argon atmosphere. The tubes were then closed tightly and weighed again to determine the sample mass that underwent the sequential dissolution. An argon factor for correction of the mass between oxygen- and argon-filled centrifuge tubes was applied. A split of wet sediment was filled into additional pre-weighed vials for determination of the wet/dry mass ratio that was needed for the conversion of P-concentrations into 'extracted P per g of dry bulk sediment'. The extraction steps were all performed at room temperature (20°C). Extraction steps 1 and 2

(Tab. 8) were carried out in an argon-flooded glove box. An in-house standard and duplicates were processed to assure accuracy and reproducibility of the extraction procedure and measurements. Except for the supernatant of the Na-citrate dithionite buffer (CDB; step 2), all P concentrations were determined photometrically following the method described by Strickland and Parson (1972). Different sulfuric acid concentrations for preparation of the ammoniumheptamolybdate solutions (AHM) were used depending on the type of samples (normal or containing HCl) to be analyzed. The supernatant of step 2 was measured at Utrecht University using a SPECTRO CIROS^{CCD} ICP-OES. The recovery of P in the quality check was 101%. The recoveries for the specific P-fractions of six analyzed standards in comparison with previously determined averaged values were 101% for exchangeable P, 125% for Fe-bound P, 100% for biogenic/authigenic P, 163% for detrital, and 170% for organic P. Although the recoveries were considerably higher than those of previous standard extractions (especially for steps 4 and 5) we are confident that the extraction scheme worked well for our set of samples. Our recoveries showed low variability and are in the range of the maximum values that were determined during previous extractions of the in-house standard.

Tab. 8: Sequential P extraction method after Ruttenberg (1992) and Slomp et al. (1996).

Step	Extracted P fraction	Procedural method
Step 1	Exchangeable/ loosely sorbed P including pore water phosphate	Addition of 10 ml 1 M MgCl ₂ ; shaking for 30 min; filtration of supernatant
Step 2	P associated with Fe (oxyhydr)oxides (Fe-bound P)	Addition of 10 ml CDB (pH ~7.5); shaking for 8 h; filtered supernatant stored at -20°C; washing of residue with 10 ml 1 M MgCl ₂ ; shaking for 30 min; filtration of supernatant
Step 3	Authigenic carbonate fluorapatite (CFA), biogenic apatite, CaCO ₃ -bound P, and possibly smectite-bound P	Addition of 20 ml acetate buffer (pH 4); shaking for 6 h; filtration of supernatant; washing of residue with 10 ml 1 M MgCl ₂ ; shaking for 30 min; filtration of supernatant (repeated twice)
Step 4	Detrital apatite and other inorganic P (e.g., of igneous or metamorphic rocks)	Addition of 10 ml 1 M HCl; shaking for 24 h; filtration of supernatant
Step 5	Organic P	Transfer of residue into ceramic crucible; drying at 50°C (24 h); ashing at 550°C (2 h); transfer of ashed samples in to centrifuge tubes; addition of 10 ml 1 M HCl; shaking for 24 h; filtration of supernatant

Reactive iron fractions

Reactive ferric iron fractions were determined applying a sequential extraction scheme on frozen and anoxically stored sediments according to the protocols by Ferdelman (1988), Raiswell et al. (2010), Lord III (1980), Poulton and Canfield (2005), and Phillips and Lovley

(1987) (Tab. 9). Sequential extractions were carried out under anoxic conditions. All applied solutions were deoxygenated prior to the respective extraction step. In the first step an ascorbic acid solution (50 g l⁻¹ sodium citrate (0.17 M), 50 g l⁻¹ sodium bicarbonate (0.6 M), 20 g l⁻¹ of ascorbic acid (0.11 M)) was added to the samples. For the second step a sodium dithionite solution (50 g l⁻¹ buffered to pH 4.8 with 0.35 M acetic acid/0.2 M sodium citrate) was used followed by a 0.2 M ammonium oxalate/0.17 M oxalic acid solution (pH 3.2) during the third step. The Fe extracted by ascorbate (Fe_{Asc}) represents the fraction of easily reducible, poorly crystalline Fe-(oxyhydr)oxides. Dithionite-soluble Fe (Fe_{Dit}) includes the residual Fe oxides (Haese et al., 2000). Oxalate (Fe_{Oxa}) dissolved mainly magnetite (Phillips and Lovley, 1987).

Tab. 9: Sequential iron extraction method.

Step	Extracted fraction	Procedural method	References
Step 1	(Oxyhydr)oxides (e.g., ferrihydrite)	Addition of 10 ml ascorbic acid solution (pH 7.5); shaking for 24 h	Ferdelman (1988), Raiswell et al. (2010)
Step 2	'Reducible', crystalline oxides (e.g., goethite, hematite)	Addition of 10 ml sodium dithionite solution (pH 4.8); shaking for 2 h	Lord III (1980), Poulton and Canfield (2005)
Step 3	Magnetite	Addition of 10 ml ammonium oxalate solution (pH 3.2); shaking for 6 h	Phillips and Lovley (1987), Poulton and Canfield (2005)

Physical sediment properties

Bulk density and porosity were determined according to IODP practices (Blum, 1997). Wet and dry mass were measured onboard on ~10 cm³-samples of sediment. A seagoing balance equipped with two electronic balances and a computer-averaging system to compensate for the ship motion was used. Dry volume measurements for determination of the porosity were performed at the MARUM using helium-displacement penta-pycnometers. The data were corrected for evaporated seawater.

Magnetic volume susceptibility (κ) analyses were performed on whole core segments (before they were split into halves) using a Bartington MS2C susceptibility meter with a 135 mm diameter loop sensor that was mounted on a aluminum frame with adjusted core liner guidance. Gravity cores GeoB 13824 and GeoB 13833 were measured at 2 cm spacing at high sensitivity (1 x 10⁻⁶ SI). Core GeoB 13809 was measured at 2 cm intervals as well, but at lower intensity resolution (10 x 10⁻⁶ SI). The data were corrected for the temperature drift of the sensor. The susceptibility signal represents a weighted mean over an interval (in

direction of the core length) of about ± 8 cm. Changes in the sediment susceptibility are thus smoothed in the κ log.

5.4 Results

The uppermost decimeters of the sediment are usually lost during gravity coring or the core retrieval. Based on comparison of pore water profiles of the MUC and the gravity cores, the extent of the sediment loss could not be determined quantitatively for sites GeoB 13809 and GeoB 13833. At site GeoB 13833, a quantification of the sediment loss by comparing the pore water profiles would hardly be possible anyway, because there is no considerable change in the pore water concentrations of dissolved species in the uppermost ~ 1.3 m of the sediment column (Fig. 25c). To preclude possible impreciseness we refer to the core depths instead of the exact sediment depths in the following sections.

5.4.1 Pore water geochemistry

GeoB 13824

The pore water parameters for site GeoB 13824 are given in Fig. 25a. Dissolved iron concentrations of $21 \mu\text{M}$ at 0.10 m indicate anoxic conditions in the shallow subsurface sediments. Sulfate decreases linearly with depth. Methane concentrations are very low at and above the SMTZ and increase downcore to 6.1 mM at 10.66 m (end of core). The sulfidic zone extends from ~ 4.20 to 6.70 m. At the SMTZ (in ~ 5.45 m depth), HS^- concentrations reach a maximum of 0.7 mM . Interstitial Fe^{2+} is depleted within the sulfidic zone, but increases further below to a maximum concentration of $60 \mu\text{M}$ at 10.15 m. Phosphate concentrations increase with depth and reach a maximum of $\sim 202 \mu\text{M}$ at the lower boundary of the sulfide-bearing zone. Further downcore, the values decrease to $160 \mu\text{M}$ at 10.45 m. The upward flux of HPO_4^{2-} calculated for the interval above the SMTZ is $1.2 \times 10^{-8} \text{ mol cm}^{-2} \text{ yr}^{-1}$. The uppermost value at 0.10 m of the gravity core is $19 \mu\text{M}$. Due to the lack of a MUC core we were not able to determine if HPO_4^{2-} is released into the bottom water. Alkalinity concentrations steadily increase with depth from $3.8 \text{ mmol}(\text{eq}) \text{ l}^{-1}$ at 0.10 m to $44.8 \text{ mmol}(\text{eq}) \text{ l}^{-1}$ at 10.45 m. Calcium concentrations decrease linearly from 10.8 mM at the core top towards a minimum of 3.6 mM at the SMTZ. Below this zone, Ca^{2+} concentrations slightly increase with depth. The diffusive fluxes into the SMTZ are $7.1 \times 10^{-7} \text{ mol cm}^{-2} \text{ yr}^{-1}$ and $2.6 \times 10^{-7} \text{ mol cm}^{-2} \text{ yr}^{-1}$, respectively (Fig. 25a).

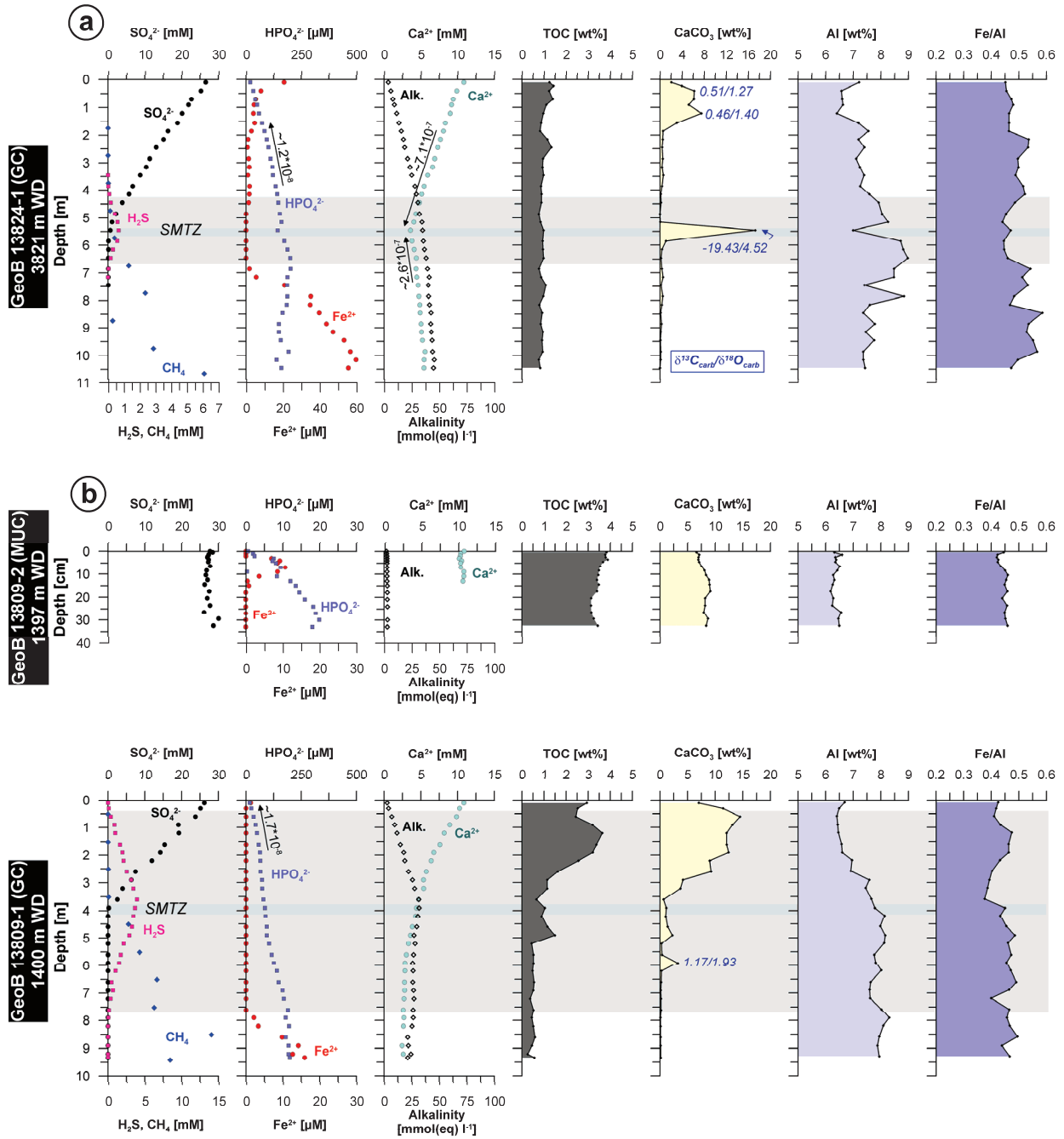
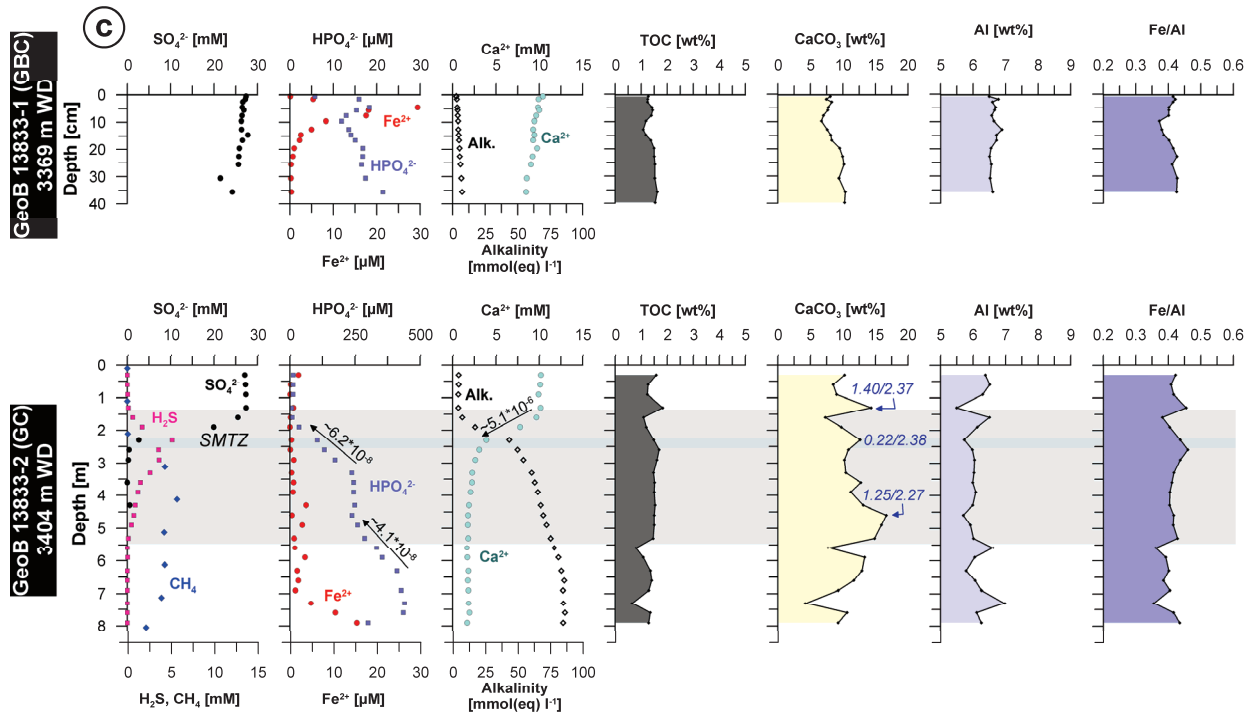


Fig. 25 (continued on the next page): Pore water data and sedimentary TOC and CaCO₃ concentrations of sites GeoB 13824, 13809, and 13833. Fluxes of HPO₄²⁻ and Ca²⁺ are given in mol cm⁻² yr⁻¹. Note that the scales HPO₄²⁻ and Fe²⁺ are different between MUC and gravity cores and that the scale for H₂S and CH₄ at location GeoB 13824 differs from the one at the other stations. The gray bar indicates the depth of the SMTZ. The light gray bar shows the extent of the sulfide-bearing zone. The $\delta^{13}\text{C}_{\text{carb}}$ and $\delta^{18}\text{O}_{\text{carb}}$ data (blue numbers next to the CaCO₃ plot) are given in ‰ V-PDB.



GeoB 13809

Figure 25b shows the pore water profiles of site GeoB 13809 of which the SO_4^{2-} profile was discussed earlier by Henkel et al. (subm.). Similar to site GeoB 13824, the SO_4^{2-} profile shows a linear shape. At 4.51 m 2.78 mM CH_4 were detected. The CH_4 concentrations increase downcore to a maximum concentration of 14.0 mM at 8.51 m. The SMTZ is located at ~3.8 m and sulfide concentrations are comparably high with a maximum of 3.9 mM at 3.60 m. Accordingly, the sulfidic zone is much broader than at site GeoB 13824 extending from 0.30 m to 7.60 m depth. In the MUC core, Fe^{2+} was detected between 0.02 and 0.15 m. The Fe^{2+} concentration in this upper zone of iron reduction was below 11 μM . Dissolved Fe^{2+} was not detected in most of the sampled sediment intervals. Only below the sulfidic zone, Fe^{2+} concentrations increase again and reach 16 μM at 9.33 m. The concentrations of HPO_4^{2-} at site GeoB 13809 increase with depth from 0.6 μM in the bottom water to 198 μM at 9.33 m and show a local maximum at 7.60 m, at the lower boundary of the sulfidic zone. The upward flux of HPO_4^{2-} above the SMTZ is comparable to site GeoB 13824 ($1.7 \times 10^{-8} \text{ mol cm}^{-2} \text{ yr}^{-1}$). The alkalinity shows a maximum value of 31.8 $\text{mmol}(\text{eq}) \text{ l}^{-1}$ at the depth of the SMTZ. The Ca^{2+} concentrations at site GeoB 13809 decrease with depth from ~10.8 mM at the sediment surface to 2.6 mM at 9.20 m.

GeoB 13833

Sulfate concentrations in the upper ~1.30 m at site GeoB 13833 scatter around 27 mM. The SO_4^{2-} profile has a kink to concave shape according to the classification by Borowski et al. (1999), Kasten et al. (2003), and Hensen et al. (2003). The CH_4 concentrations increase from 4.3 mM at 3.11 m to a maximum of 5.7 mM at 4.12 m. Between 5.12 and 7.12 m, the concentrations scatter around 4.2 mM. Towards the bottom of the core (8.05 m), CH_4 decreases to a concentration of 2.2 mM. The SMTZ is located at 2.30-2.40 m. The maximum concentration of HS^- (5.2 mM) was measured at 2.30 m. The sulfidic zone extends from ~1.30 to 5.50 m. Dissolved iron concentrations between 1 and 29 μM were detected in the MUC core between 0.01 and 0.23 m depth. In the gravity core, Fe^{2+} concentrations within the sulfidic zone scatter between 0 and 3 μM . Further downcore, the concentrations increase and reach 16 μM in the lowermost pore water sample (7.90 m). Phosphate contents at site GeoB 13833 scatter between 6 and 21 μM from 0.00-1.60 m depth. The concentrations increase further downcore to 245 μM at 3.60 m. Between 3.60 and 4.60 m, the concentrations are rather constant, whereas from 4.60 to 7.60 m depth, an increase of HPO_4^{2-} with a maximum of 441 μM was detected. The upward fluxes of HPO_4^{2-} between 6.30 and 4.60 m and 3.30 and 1.90 m are $4.1 \times 10^{-8} \text{ mol cm}^{-2} \text{ yr}^{-1}$ and $6.2 \times 10^{-8} \text{ mol cm}^{-2} \text{ yr}^{-1}$. Similar to SO_4^{2-} , the alkalinity and Ca^{2+} stay fairly constant between 0.00 and 1.30 m. Below 1.30 m, alkalinity shows a steep increase and reaches concentrations of $\sim 49 \text{ mmol}(\text{eq}) \text{ l}^{-1}$ at the depth of the SMTZ. Further below, the concentrations still increase, although with a lower gradient. The Ca^{2+} profile shows again an opposite trend, i.e. a strong decrease below 1.30 m towards the SMTZ, a slight decrease between 2.60 and 4.30 m and constant concentrations of $\sim 1.8 \text{ mM}$ below 4.30 m. The flux of Ca^{2+} into the zone of AOM is $\sim 5.1 \times 10^{-6} \text{ mol cm}^{-2} \text{ yr}^{-1}$ and thus an order of magnitude higher than at station GeoB 13824.

5.4.2 Sediment composition

Total organic carbon, carbonate

Site GeoB 13824 shows homogeneous TOC concentrations of $\sim 1 \text{ wt}\%$ (Fig. 25a). The CaCO_3 concentrations in core GeoB 13824 are very low ($< 0.6 \text{ wt}\%$) except for the interval 0.00-1.80 m (3.0-7.5 wt%) and the depth of the SMTZ (5.45 m), where a prominent CaCO_3 peak of 17.2 wt% was detected (Fig. 25c). At site GeoB 13809, TOC concentrations in the uppermost part of the sediment column (0.00-2.00 m) are comparatively high. They scatter around 3-4 wt% (Fig. 25b). The concentrations decrease between 2.00 and 3.50 m. The lower core section, except for a local maximum at $\sim 5.00 \text{ m}$, shows overall low TOC values of $\sim 0.5 \text{ wt}\%$ (Fig. 25b). Carbonate concentrations increase from $\sim 6.6 \text{ wt}\%$ in the surface

sediment to ~14.5 wt% at 0.6 m depth. The carbonate concentrations remain high (>12 wt%) until 1.90 m. Further downcore, the concentrations decrease to ~3.0 wt% and less below a depth of 3.50 m. Site GeoB 13833 is characterized by TOC concentrations that scatter around 1.5 wt% without showing a clear trend over the core length (Fig. 25c). At this site, CaCO₃ concentrations are high compared to sites GeoB 13824 and 13809. Over the whole core length, CaCO₃ contents range between 4.2 and 16.7 wt% (AVG 10.1 wt%; Fig. 25c).

Compared to the rest of the analyzed samples, which scatter between 0.24 and 1.39‰ the stable carbon isotopic composition of carbonate shows the lightest value of -19.49‰ at 5.45 m depth at site GeoB 13824 (Fig. 25a, Tab. 10). The δ¹⁸O_{carb} value at the SMTZ at site GeoB 13824 is 4.52‰ and thus much heavier than in the rest of the carbonate samples that range between 1.27 and 2.33‰ (Fig. 25, Tab. 10).

GeoB #	Depth [m]	δ ¹³ C [‰]	δ ¹⁸ O [‰]
13824-1	0.40	0.51	1.27
	1.20	0.46	1.40
	5.45	-19.43	4.52
13809-1	5.80	1.17	1.93
13833-2	1.30	1.40	2.37
	2.30	0.22	2.38
	4.60	1.25	2.27

Tab. 10: Results of isotope analyses of carbonates at selected depths. Strong depletion of ¹³C, which is evident for the diagenetic origin of the carbonate, has been determined for the depth of the SMTZ at site GeoB 13824.

Phosphorus

At site GeoB 13824, a distinct maximum in total sedimentary P (1197 ppm) was determined at the current depth of the SMTZ (5.45 m, Fig. 26a) while total P concentrations fluctuate around 612 ± 34 ppm in the rest of the sampled sediment interval. The peak in total P coincides with the peak in CaCO₃ (Fig. 25a) and is reflected by maximum values of all P species except for organic P. The major part of P in the sediment is of biogenic/authigenic (258 ± 49 ppm) and detrital (213 ± 45 ppm) origin. The maximum value of organic P was measured at 0.10 m depth (126 ppm). Further downcore, the values scatter around 75 ppm. The fraction of Fe-bound P shows homogeneous concentrations of ~50 ppm in the section above the SMTZ. At 5.45 m, the concentration is 8-times higher (407 ppm). Thus, the fraction collected by dissolution step 2 (Tab. 8) accounts for at least 60% of the total P maximum at the SMTZ. Although of minor importance for total sedimentary P, exchangeable P shows an overall trend to higher concentrations from the top of the core (4 ppm) towards 5.45 m depth

(18 ppm). Further downcore, the concentrations of exchangeable P decrease to a level lower than in the uppermost core section (0.00-3.85 m).

At site GeoB 13809, the concentrations of total P indicate a trend to lower concentrations with depth (1057 ppm in surface sediment, 661 ppm at 9.28 m; Fig. 26b). A peak of total P at the SMTZ as observed at site GeoB 13824 was not detected. The decrease of organic P concentrations with depth is more pronounced than in core GeoB 13824: 323 ppm of organic P were measured in the surface sediment and the concentrations decrease to ~90 ppm at

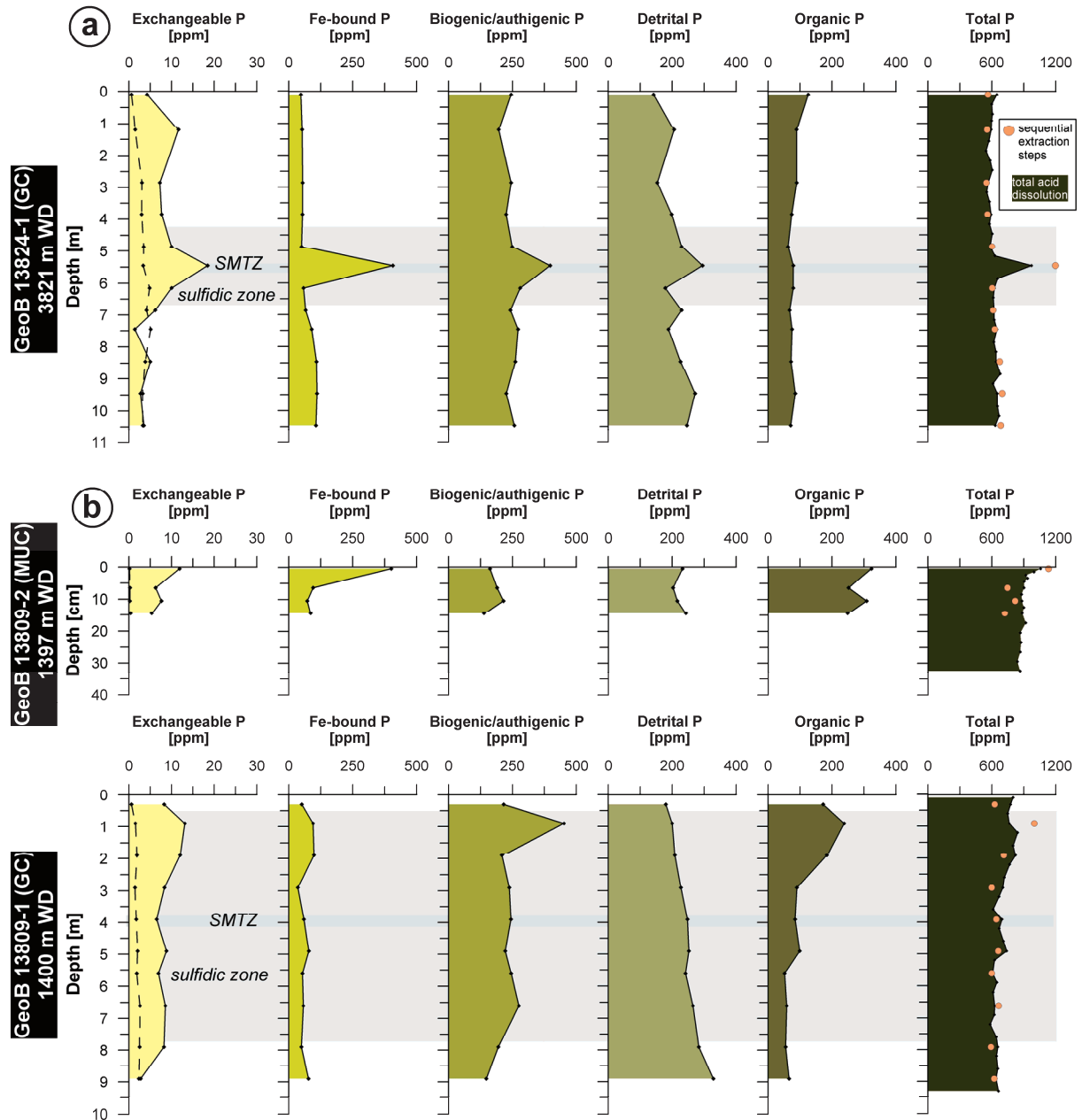
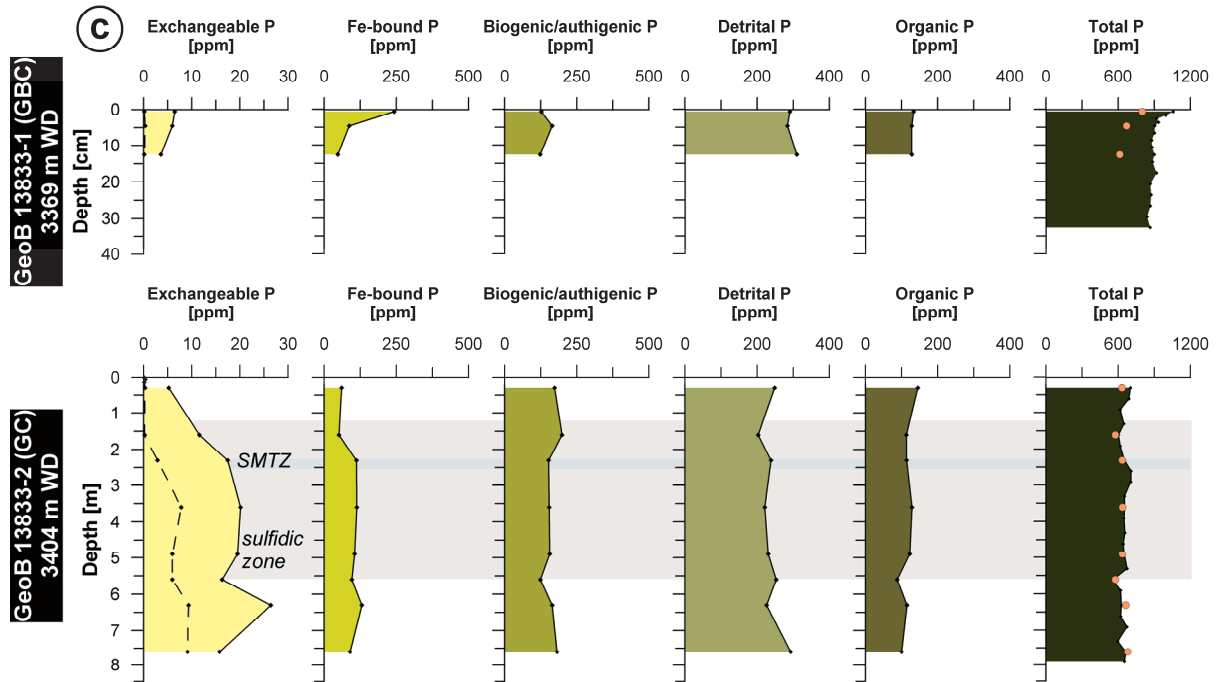


Fig. 26 (continued on the next page): Sedimentary P-fractions as determined from the sequential extractions and total acid dissolution. Overall, the sum of the P-fractions recovered from sequential dissolution (orange dots in right plot) is $98 \pm 10\%$ of the total P as determined by ICP-OES analysis of dissolved bulk sediment. The dashed line in the exchangeable P fraction indicates the amount of P that might be associated with pore water phosphate.



2.90 m and ~ 60 ppm below 5.60 m. Detrital P shows an opposite trend towards higher values in the lowermost core section. Overall, the concentrations of detrital P range between 180 and 329 ppm and are, thus, slightly higher compared to site GeoB 13824. A biogenic/authigenic P peak (452 ppm) is present at 0.90 m. In the rest of the core the concentrations of biogenic/authigenic P are 207 ± 40 ppm with a trend to lower concentrations from 6.60 to 8.90 m. The highest concentration of Fe-bound P was measured in the surface sediment (401 ppm). Already at 0.06 m depth, the sediment is depleted in Fe-bound P as indicated by comparatively low concentrations of 96 ppm. Below the surface sediment, there are no distinctly elevated contents of this P fraction over the recovered sediment depth. Exchangeable P is present in low concentrations (8 ± 3 ppm) with a maximum at 0.90 m depth.

Total P at site GeoB 13833 shows fairly constant concentrations of 659 ± 41 ppm over the whole core length (Fig. 26c). Organic P concentrations scatter around 120 ppm. In contrast to site GeoB 13809, organic P does not show higher values towards the sediment surface. With concentrations of 254 ± 35 ppm and 156 ± 24 ppm, detrital and biogenic/authigenic P represent the major P fractions at site GeoB 13833. Iron-bound P is comparably high in the surface sediment (243 ppm), but the concentrations decrease drastically to ~ 50 ppm between 0.12 and 1.60 m. At and below 2.30 m, the concentrations increase by a factor of 2. Exchangeable P concentrations are higher than at stations GeoB 13824 and GeoB 13809, especially at and below the depth of the SMTZ, where they range between 16 and 26 ppm.

Magnetic susceptibility and iron speciation

Aluminum-normalized Fe and total Fe concentrations of the bulk sediment (Fig. 25, 27) are highest at site GeoB 13824 ($Fe/Al \sim 0.45$, $Fe_{tot} 3.7 \pm 0.4$ wt%). At site GeoB 13809, Fe_{tot} concentrations are 3.2 ± 0.4 wt%. Site GeoB 13833 displays slightly lower and rather constant Fe_{tot} concentrations (2.6 ± 0.1 wt%). In core GeoB 13833, highly reactive ferric Fe ($Fe_{HR} = Fe_{Asc} + Fe_{Dit}$) is almost absent in the sulfidic zone and below. At site GeoB 13809 this fraction accounts for <2% of Fe_{tot} in the sulfidic zone. In contrast to site GeoB 13833, the concentrations of Fe_{HR} increase further downcore to 6% of Fe_{tot} . At site GeoB 13824, Fe_{HR} is present throughout the core, but shows lowest values within the sulfidic zone. Especially the concentrations of Fe_{Dit} are high compared to sites GeoB 13809 and 13833. As for site GeoB 13809, the relative amount of Fe_{HR} increases below the sulfidic zone to up to 12% of Fe_{tot} . At sites GeoB 13824 and 13809, the increases of Fe_{HR} in the deep sediments correlate with increases of Fe^{2+} in the pore water. The distribution of reactive Fe phases at these two sites is nicely reflected by the susceptibility profiles indicating relatively low amounts of magnetic minerals (i.e. Fe oxides) within the sulfidic zones (Fig. 27a,b). In contrast, at site GeoB 13833, the magnetic susceptibility remains on a low level below the sulfide-bearing zone (Fig. 27c). Magnetite (Fe_{Oxa} fraction, Fig. 27), which is less reactive towards HS^- is enriched below the sulfidic zone at site GeoB 13824 and GeoB 13809 and in the surface sediments above the sulfidic zone at site GeoB 13833.

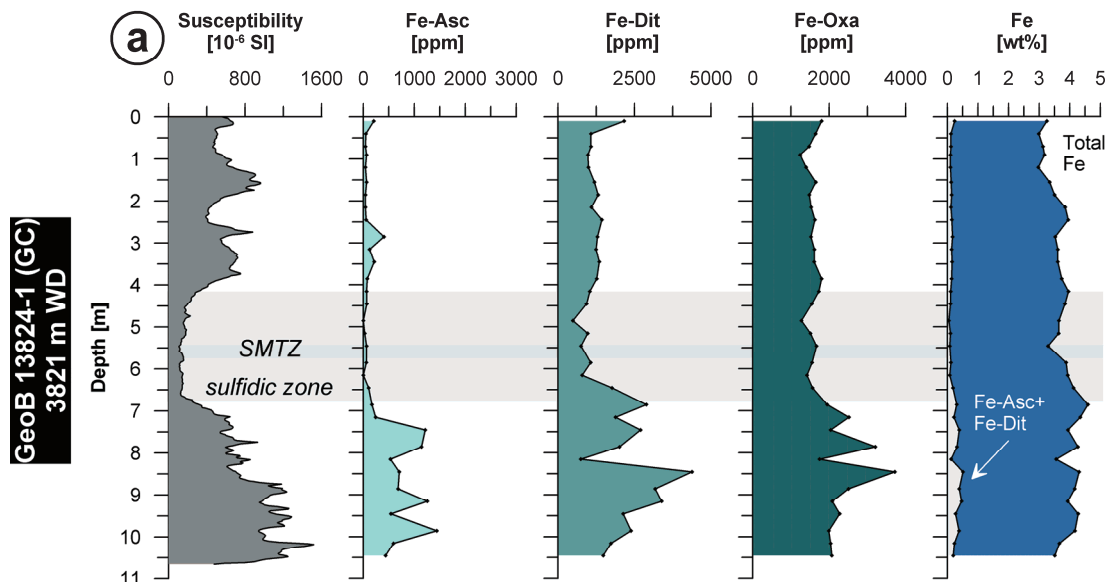
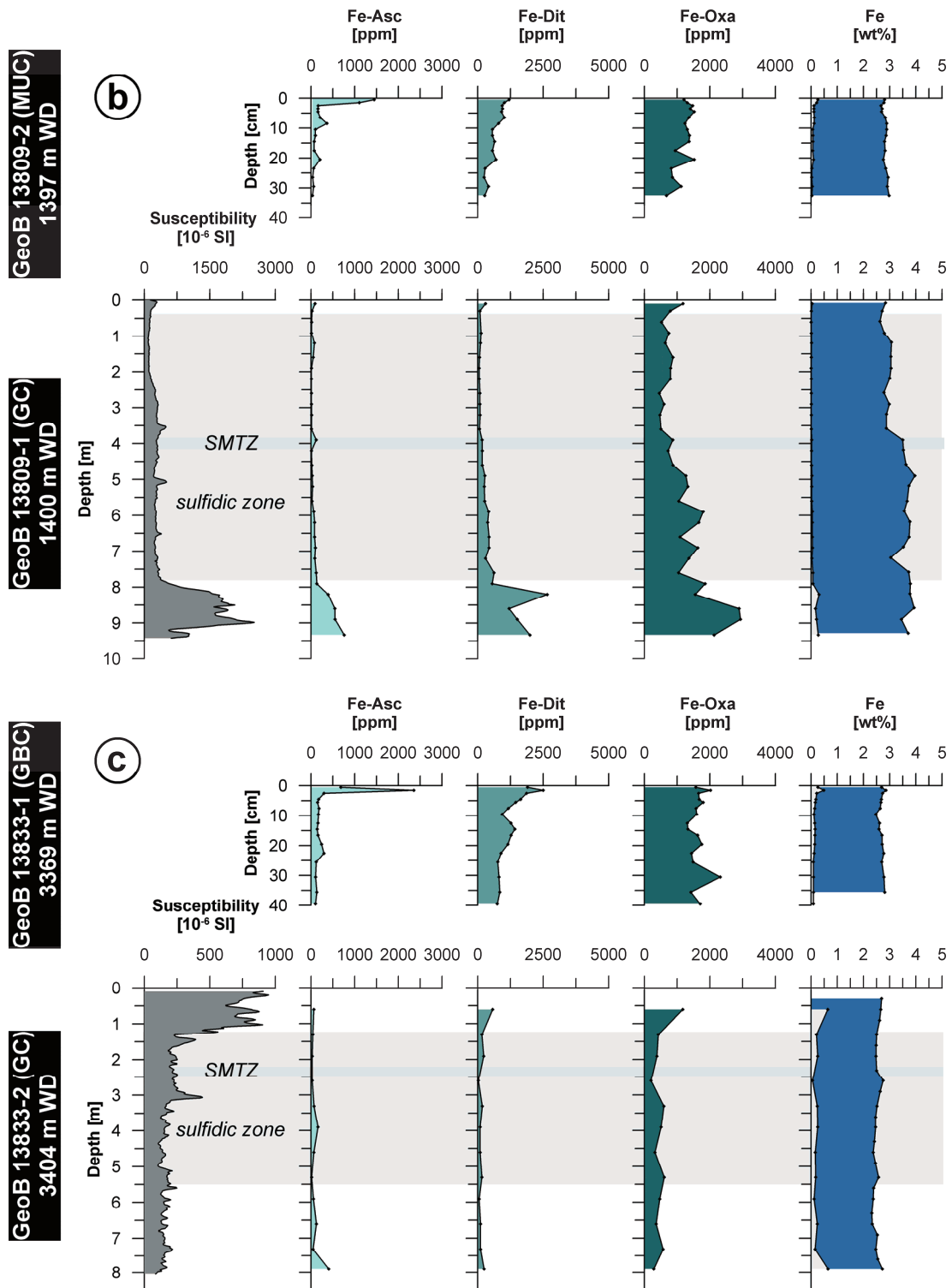


Fig. 27 (continued on the next page): Magnetic susceptibility, sedimentary reactive Fe fractions as determined by sequential extraction, and total Fe concentrations of bulk sediment at the locations GeoB 13824, 13809, and 13833. Note that the scale of the x-axes of susceptibility is not the same for all locations.



5.5 Discussion

5.5.1 Bulk sediment and sulfate-methane transition zone

The gravity cores at sites GeoB 13824 and 13809 reflect distinct upward changes from low to high CaCO_3 concentrations at 1.80 and 3.50 m depth (Fig. 25a,b). Similar transitions were observed in sediments from the Amazon Fan (Kasten et al., 1998) and two sites from the

continental margin off Uruguay and Argentina (GeoB 6308-4 and GeoB 6229-6; Riedinger et al., 2005). In these previous studies, the upward transition to carbonate-rich sediments was interpreted to mark the Pleistocene/Holocene boundary. According to this, the average Holocene sedimentation rates at sites GeoB 13824 and 13809 are in the range of 15 to 30 cm kyr⁻¹. Taking into account that mass movements (turbidites etc.) could have affected site GeoB 13809, the Holocene background sedimentation rate can be considerably lower than 30 cm kyr⁻¹. Core GeoB 13833 shows overall high carbonate concentrations. Therefore, the transition to the Pleistocene might not have been penetrated, which would suggest overall high Holocene sedimentation rates. This assumption is well in agreement with sedimentation rates determined for this site by comparison of Ca/Fe ratios of XRF scans with those of adjacent cores for which ¹⁴C ages are available. These preliminary data suggest maximum sedimentation rates of up to 110 cm kyr⁻¹ at site GeoB 13833 (I. Voigt, personal communication).

In a previous study by Henkel et al. (subm.), the SO₄²⁻ profile at site GeoB 13809 was interpreted to show a pore water system in steady state. This site was possibly affected by a mass movement as indicated by sediment echosounder data (Fig. 24). However, the linear shape of the SO₄²⁻ profile demonstrates that sufficient time (several thousands of years) has passed since the supposed mass movement event to achieve diffusive re-equilibration (Henkel et al., subm.). Similarly, steady state pore water conditions can be inferred for site GeoB 13824 based on the constant gradient of the SO₄²⁻ decrease with depth. The steady state condition of the pore water system at these two sites is also reflected by a distinct loss of the magnetic susceptibility within the current sulfidic zones (Fig. 25a,b; 27a,b), which is due to the reaction of HS⁻ with ferromagnetic Fe (oxyhydr)oxides. Riedinger et al. (2005) have shown for the same study area that distinct gaps in magnetic susceptibility are the result of an extreme decrease in sedimentation from rates in the order of 100 cm kyr⁻¹ in the Pleistocene to ~5 cm kyr⁻¹ in the Holocene. The sedimentation rates during the glacial must have been high enough to quickly bury highly reactive Fe (oxyhydr)oxides below the SMTZ without considerable alteration by hydrogen sulfide. Subsequently, when sedimentation rates are reduced, the SMTZ is fixed at a particular depth and the Fe (oxyhydr)oxides are subject to reduction for a longer time span and in this way pronounced minima in the magnetic susceptibility profile are produced (Riedinger et al., 2005). Exactly this pattern occurs at sites GeoB 13824 and 13809. A complete loss of the magnetic susceptibility signals in distinct sediment intervals can occur over time scales of several thousands of years. The extent of the sulfidic zone and thus the width/thickness of the interval that has undergone a reduction the magnetic susceptibility is an indicator for the time that the SMTZ has been fixed at a distinct depth. Sulfide is produced at the SMTZ by AOM and subsequently diffuses up- and

downwards and react with buried Fe (oxyhydr)oxides to form Fe sulfides. The Fe (oxyhydr)oxides will thus be depleted first at the depth of the SMTZ. If the SMTZ stays fixed at a particular depth, the sulfidic zone will widen with time and in this way also enlarge the sediment interval affected by Fe (oxyhydr)oxide reduction and thus the loss in magnetic susceptibility. From these considerations it can be concluded that the SMTZ at site GeoB 13809 has been stable or fixed at a particular horizon for a longer time compared to site GeoB 13824.

At site GeoB 13824, there is a CaCO_3 peak at the depth of the SMTZ (Fig. 25a). The anaerobic oxidation of methane produces HCO_3^- , which promotes diagenetic carbonate precipitation. The diagenetic origin of the CaCO_3 peak is indicated by the strong depletion in $^{13}\text{C}_{\text{carb}}$ (-19.4‰; Tab. 10; Fig. 25a) that is thought to be a consequence of the preferential oxidation of light CH_4 during AOM (e.g., Pape et al., 2005; Aquilina et al., 2010). However, a contribution of dissolved inorganic carbon from organic matter oxidation can not be excluded (Irwin et al., 1977; Coleman and Raiswell, 1981; Okita et al., 1988). The diagenetic formation of the carbonate peak at 5.45 m depth is also suggested by a heavy $\delta^{18}\text{O}_{\text{carb}}$ value (4.5‰). In the shallower, presumably Holocene sediments, a $\delta^{18}\text{O}_{\text{carb}}$ value of ~1.4‰ (Tab. 10; Fig. 25a) suggests biogenic carbonate precipitation to have taken place in surface water at a temperature of ~11°C (equation by Shackleton, 1974), which is in good agreement with surface water temperatures measured during the expedition M78/3b in June-July 2009 Krastel et al. (in prep.). If interpreted as primary (biogenic carbonate) signal, the shift of ~3‰ to a $\delta^{18}\text{O}_{\text{carb}}$ value of 4.5‰ would suggest an unreliable low sea surface temperature of ~1°C. The depth of the SMTZ must have been stable for a period of time that was sufficient for the build-up of this authigenic carbonate enrichment. Calculations based on the supply of Ca^{2+} (current fluxes into the SMTZ based on measured Ca^{2+} profile, Fig. 25a) and physical property data result in a time span of 750-800 years that is needed for the formation of the Ca enrichment of 6.9 wt% (1.69 mol kg^{-1} dry sediment) at the SMTZ, as determined from IC measurements, assuming that IC is mainly present as CaCO_3 . Since the enrichment calculation is based on the assumption that Ca^{2+} fluxes into the zone of carbonate precipitation have been constant over time, this approach certainly only gives a rough estimate of the time since when diagenetic carbonate formation at site GeoB 13824 takes place. A sink of Ca^{2+} at the depth of AOM is also displayed by the pore water profile at site GeoB 13809, although the zone of carbonate precipitation is less distinct (Fig. 25b). The profile of Ca^{2+} at site GeoB 13833 displays carbonate precipitation at the depth of AOM. However, the carbonate formation is hard to quantify due to the high background CaCO_3 concentrations (Fig. 25c).

Station GeoB 13833, located in the Mar de Plata Canyon, is characterized by non-steady state pore water conditions as indicated by a kink- to concave-shaped SO_4^{2-} profile and the distinct gradient changes in alkalinity (Fig. 25c). The magnetic susceptibility, Fe_{HR} and magnetite (Fe_{Oxa}) concentrations below the sulfidic zone are lower than at the other two sites. Therefore, we conclude that this site was either not affected by extreme changes of sedimentation rates and experienced overall rather low sedimentation rates, which assured the reduction of Fe (oxyhydr)oxides during exposure to sulfidic conditions or that the SMTZ has currently shifted upwards, suggesting that the reactive Fe phases in the lower core section were previously altered by reaction with HS^- . Given the kink- to concave-up shape of the SO_4^{2-} profile, the asymmetry of the sulfide zone above and below the current SMTZ, the aforementioned indication for overall high sedimentation rates, and the increase of Fe^{2+} in the lower core section that suggests reduction of deeply buried Fe (oxyhydr)oxides, the upward movement of the SMTZ (e.g., caused by an increase of the CH_4 flux or induced by a mass wasting event) seems to be more reasonable. Preliminary assessment of the SO_4^{2-} profile suggests that either attributed to a mass movement or to an increase in the CH_4 flux, the perturbation of the pore water system must have happened at most a few hundred years ago.

5.5.2 Phosphate fluxes into the bottom water

Flux calculations considering the uppermost sample of the MUC cores at stations GeoB 13809 and 13833 and the respective bottom water concentrations suggest that the release of HPO_4^{2-} into the water column might be as high as $1.2 \times 10^{-3} \text{ mol m}^{-2} \text{ yr}^{-1}$ and $4.4 \times 10^{-3} \text{ mol m}^{-2} \text{ yr}^{-1}$ at the study sites. These estimates represent minimum values, because bioirrigation, which was not specifically examined, could lead to an additional transfer of HPO_4^{2-} into the bottom water. The values determined here are slightly lower compared to estimates by Hensen et al. (1998), who suggested that HPO_4^{2-} fluxes off Argentina and Uruguay can be extraordinarily high and partly exceed $11 \times 10^{-3} \text{ mol m}^{-2} \text{ yr}^{-1}$. Hensen et al. (2000) demonstrated that HPO_4^{2-} release from the surface sediments adjacent to the Río de la Plata mouth is highest in water depths of 1500-3500 m. Core GeoB 13809-2 was retrieved from a slightly shallower area, but the 100 m difference in depth does certainly not account for a difference in the HPO_4^{2-} flux of one order of magnitude. However, the area off Uruguay has been shown to be extremely dynamic and inhomogeneous with respect to depositional conditions. Therefore, we consider the HPO_4^{2-} release into the bottom water to show considerable lateral and seasonal variability as well. The P speciation (Fig. 26) with strong decreases of Fe-bound P (Fig. 26b,c) and organic P (Fig. 26b) in the uppermost decimeter of the sediment reveals that these fractions are the most dynamic P pools in the uppermost part of the sediment column.

The key role of the surface sediment with respect to the removal of Fe-bound P from the pore water can be deduced from Fig. 28, which shows the concentrations of Fe_{HR} vs. the concentration of Fe-bound P. These P concentrations are particularly high in the uppermost centimeter of the sediment. The surface sediments do, however, not contain the highest concentrations of reactive Fe. There is no clear correlation between Fe_{HR} and Fe-bound P, which suggests that in most of the sampled depths, the retention capacity of reactive Fe phases with respect to HPO_4^{2-} is not reached.

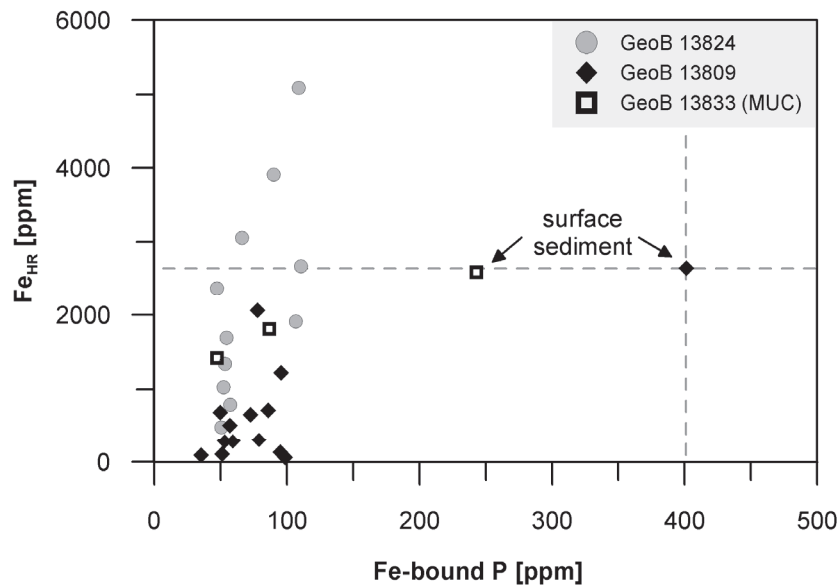


Fig. 28: Fe_{HR} vs. Fe-bound P for all investigated sites. Data of the gravity core GeoB 13833 is not displayed, because Fe and P extractions were not performed for the same depths. Fe-bound P concentrations are high in the surface sediment, although this depth (0.5 cm) does not show maximum concentrations of Fe_{HR} . The dashed lines show that Fe_{HR} concentrations of ~2600 ppm can account for the retention of at least 400 ppm of P. The absence of a distinct correlation between Fe_{HR} and Fe-bound P indicates that the retention potential of Fe oxides with respect to phosphate is not reached in most parts of the samples intervals. The depth 5.45 m at site GeoB 13824 was omitted in the plot, because the results (the text) indicate that authigenic carbonate was subject to dissolution during the dithionite extraction step.

5.5.3 Organic phosphorus

At site GeoB 13809, a significant decrease of organic P with sediment depth occurs between ~1.00 and 2.50 m (Fig. 26b). This trend correlates with a decrease in TOC and CaCO_3 concentrations (Fig. 25b). Thus, the shift to lower organic P concentrations in this interval is considered to display a change in primary productivity and/or sedimentation rates at the Holocene/Pleistocene transition rather than an *in situ* degradation of organic matter. In principal, there is a high positive correlation between TOC and organic P ($r^2 = 0.92$, Fig. 29). However, the molar TOC:organic P ratios at the investigated sites show considerable

scattering (Fig. 30). Whereas at site GeoB 13824 and 13833 the ratios increase with depth, possibly revealing a preferential loss of P during organic matter degradation as proposed by Krom and Berner (1981), Ingall et al. (1993), and Ingall and Jahnke (1994; 1997), a reverse trend is apparent at site GeoB 13809. Certainly, the extent of the preferential P loss depends not only on *in situ* processes, but also (or mainly) on processes that took place during the settling of particles through the water column. These might be controlled by the sinking velocity (particle size of organic matter, current velocities), the initial composition of organic matter, and reworking and transport of refractory organic compounds. It has been shown by Bishop et al. (1977) that organic matter C:P ratios are a function of particle size and water depth. According to Redfield et al. (1963), fresh organic matter produced in the photic zone shows molar C:P ratios of 106:1. Molar TOC:organic P ratios exceeding 250-300 occur already in the surface sediment (Fig. 30), which indicates that the preferential loss of P takes place before deposition. Similar and even higher ratios in surface sediment have been found by Küster-Heins et al. (2010a; 2010b) off West Africa. However, variations in molar C:P ratios might also be indicative for changes in the source of organic matter. An upward trend to higher C:P as it is observed at site GeoB 13809 possibly reflects an increasing contribution of terrestrial organic matter that shows higher C:P ratios of up to or exceeding 800 (Likens et al., 1981; Ruttenberg and Gofñi, 1997). As stated by Mollenhauer et al. (2006), the study area is affected by sediment (and organic matter) winnowing and focusing. Changing contributions of organic matter sources dependent on the current pattern can thus not be ruled out, particularly at site GeoB 13809, which is seasonally affected by the Río de la Plata plume (Fig. 22).

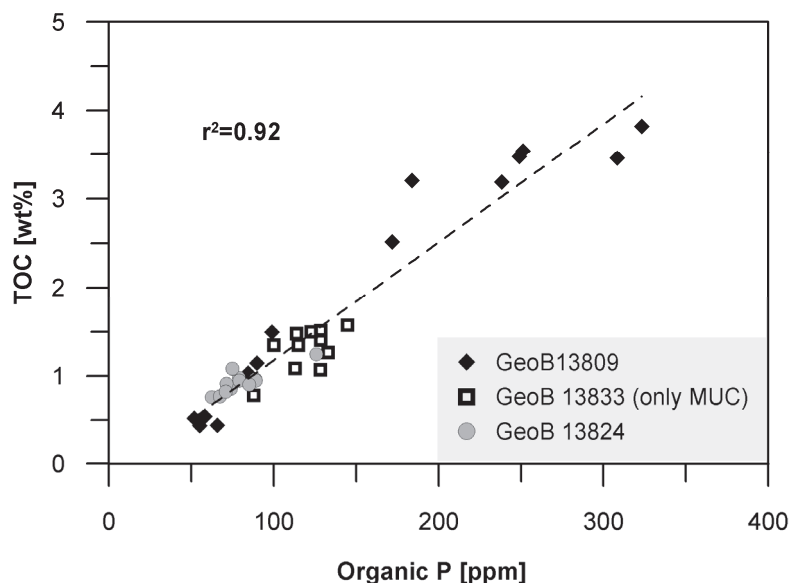


Fig. 29: Organic P vs. TOC. There is a good correlation between the two parameters. Data of gravity core GeoB 13833 is not displayed, because TOC measurements and P extractions were performed at different depths.

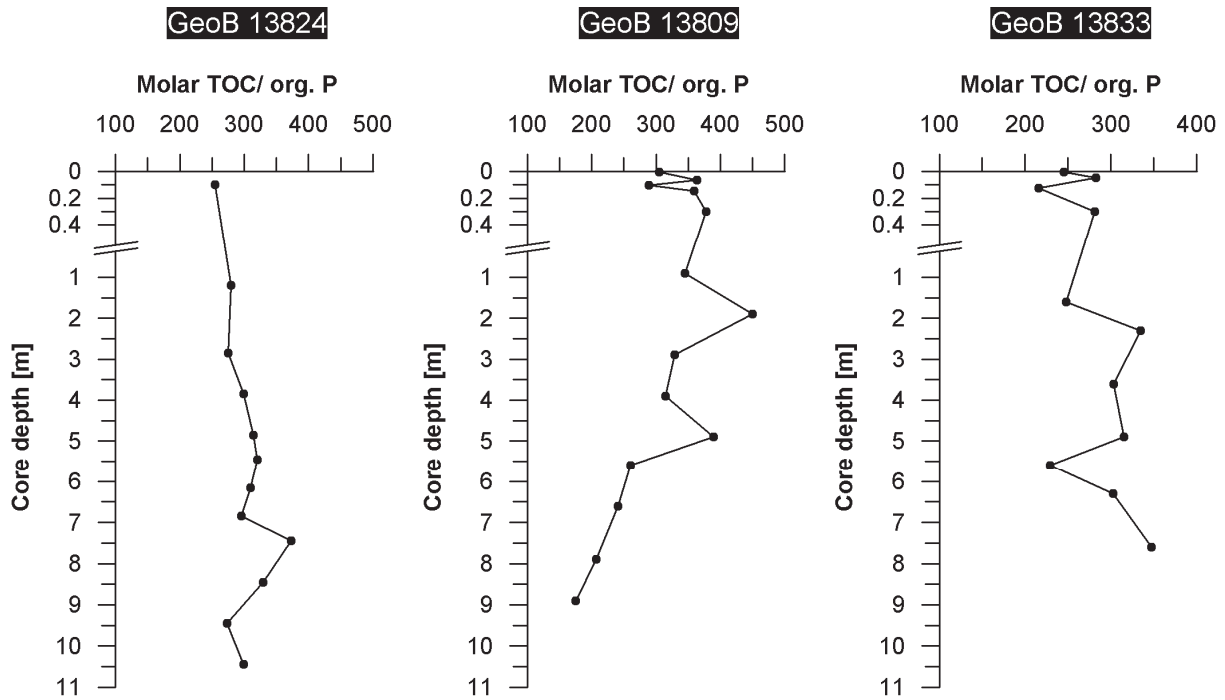


Fig. 30: Molar TOC/organic P ratios for all investigated sites.

5.5.4 Inorganic phosphorus

Exchangeable P represents only a minor portion of total P. A significant portion of the exchangeable P fraction, especially in the lower parts of cores GeoB 13809 and 13833, can be attributed to pore water HPO_4^{2-} (dashed line in Fig. 26). The overall shape of the HPO_4^{2-} profile at site GeoB 13833 (Fig. 25c) shows drastic changes in the gradient, which is in accordance with the non-steady state condition of the pore water system as deduced from the SO_4^{2-} profile shape and the asymmetry of the sulfidic zone. The HPO_4^{2-} profile clearly indicates a sink for pore water P at a depth of ~1.50 m, approximately coinciding with the current upper boundary of the sulfidic zone. Above the sulfide-bearing zone, Fe_{Asc} and Fe_{Dit} concentrations are lower than at site GeoB 13824. Nevertheless, more HPO_4^{2-} than at site GeoB 13824 seems to be trapped by adsorption onto Fe (oxyhydr)oxide surfaces (see fluxes, Fig. 25a,c). The comparison of these two sites is in accordance with the findings of Lijklema (1980), Froelich (1988), and Sundby et al. (1992), who showed that the removal of P from pore water by adsorption processes is not only a function of the amount of Fe (oxyhydr)oxides present, but also depends on the surface properties and retention capacity of these Fe particles. High sedimentation rates at site GeoB 13833 (or even a mass movement, which might have caused the non-steady state of the pore water system) deliver fresh Fe (oxyhydr)oxides more rapidly than at site GeoB 13824, which entails the more efficient removal of phosphate from the interstitial water in the uppermost part of the sediment column (surface sediment to ~1.50 m) by adsorption (compare to Fig. 11 by

Sundby et al. 1992). However, the HPO_4^{2-} flux from deep sediments into the sulfidic zone is much higher at site GeoB 13833 compared to sites GeoB 13824 and GeoB 13809. This can possibly be attributed to high carbonate contents in the sampled sediment interval. Carbonate dilutes the relative amount Fe-minerals. Additionally, reactive Fe phases have been diminished to a large extent in depths below ~1.50 m (Fig. 27c) resulting in a lower retention potential for HPO_4^{2-} in the sulfidic zone and below.

Generally, the dissolved HPO_4^{2-} concentrations of 150-440 μM determined in deep sediments at the stations off Uruguay and Argentina are much higher than in the benthic zone and they are in the range of previously reported data for other continental margin settings. März et al. (2008a) measured lower values of up to 80 μM in sediments of the Zambezi deep-sea fan. Dissolved phosphate concentrations in sediments of the Amazonas Fan reach values of up to 400 μM (Schulz et al., 1994; Burns, 1997; Ruttenberg and Goñi, 1997). All of these studies have shown a liberation of HPO_4^{2-} right at the SMTZ, which was explained by the remineralization of organic matter (Ruttenberg and Goñi, 1997) or by the reaction of HS^- with Fe (oxyhydr)oxides (März et al., 2008a). However, in contrast to these studies, the pore water profiles investigated in this study do not show a distinct maximum at the SMTZ or a drawdown of HPO_4^{2-} concentrations below the SMTZ. Vivianite formation below the SMTZ as proposed by Schulz et al. (1994), Burns (1997), Ruttenberg and Goñi (1997), and März et al. (2008a) to account for the removal of HPO_4^{2-} from pore water below the SMTZ is indicated neither by HPO_4^{2-} nor by the Fe^{2+} profiles at the locations off the Río de la Plata. On the contrary, HPO_4^{2-} is released from the sediments below the SMTZ. Phosphorus liberation occurs 1) directly at the lower boundaries of the sulfide-bearing zones (at 6.70 m at site GeoB 13824 and at 7.60 m at site GeoB 13809, Fig. 25a,b) and 2) further below in correlation with increasing Fe^{2+} concentrations (towards the bottom of gravity core GeoB 13833, Fig. 25c). In accordance with the study of März et al. (2008a), we attribute the HPO_4^{2-} release at the lower boundary of the sulfidic zone to the reaction of HS^- with Fe (oxyhydr)oxides. The liberation of HPO_4^{2-} in deeper sediments, especially at site GeoB 13833 seems to be coupled to deep iron reduction. The deep Fe^{2+} increase is due to the reduction of previously buried Fe (oxyhydr)oxides (Riedinger et al., 2005). Although the exact process of this deep Fe_{HR} reduction is not yet known, we conclude that pore water P is set free from the sediments below the sulfidic zone due to the ongoing dissolution of its carrier phase (Fe_{HR}). Therefore the amount of Fe (oxyhydr)oxides that reached the depths below the sulfide-bearing zone should ultimately determine the amount of HPO_4^{2-} , which is liberated into the pore water. Unfortunately, the lengths or the gravity cores were not sufficient to allow a quantitative assessment of the relationship between the amounts of Fe_{HR} buried and HPO_4^{2-} released from deep sediments at the study sites. The Fe^{2+} concentrations are highest

at site GeoB 13824, where the sulfidic zone is comparatively narrow. The respective HPO_4^{2-} concentrations are in the same range as at site GeoB 13809 but much lower than at site GeoB 13833. However, the maxima of Fe^{2+} concentrations are most likely located below the cored depths, so the zone of maximum Fe (oxyhydr)oxide dissolution and HPO_4^{2-} liberation is not reached at any of the investigated sites. There is a two-fold increase in Fe^{2+} concentrations below the sulfidic zone at site GeoB 13824 compared to the interval above the sulfidic zone (Fig. 26a), which is consistent with the magnetic susceptibility profile (Fig. 27a) and our interpretation of P being released from surfaces of deeply buried Fe (oxyhydr)oxides. However, a distinct decrease of Fe-bound P within the sulfidic zones, where the magnetic susceptibility and Fe-extractions indicate a depletion of Fe_{HR} , can not be observed at any of the sites (Fig. 25, 27). We assume that HPO_4^{2-} is retained by the magnetite fraction that is less reactive than Fe_{Asc} and Fe_{Dit} and not yet completely depleted within the sulfidic zones (Fig. 27).

In contrast to sites GeoB 13809 and 13833, site GeoB 13824 shows a distinct enrichment of P at the depth of the SMTZ. The P peak is displayed by all of the extracted P fractions except of organic P. However, an increase of Fe-bound P (and detrital P) at the SMTZ is not what is to be expected because as Fe (oxyhydr)oxides will first be depleted at the depth of AOM. We believe that part of the diagenetically formed carbonate, which likely contained P, was dissolved during the CDB step of the extraction protocol (Tab. 8).

In general, organic and Fe-bound P are proposed to represent major sources for authigenic CFA precipitation (Ruttenberg and Berner, 1993; Lucotte et al., 1994; Filippelli and Delaney, 1996; Slomp et al., 1996). Current sinks of HPO_4^{2-} are indicated at ~1.50 m and 4.50 m depth at site GeoB 13833 (Fig. 25c). As mentioned before, we attribute the sink at 1.50 m depth to the retention by Fe (oxyhydr)oxides. The drawdown of HPO_4^{2-} at 4.50 might indicate precipitation of authigenic P-minerals, which is, however, not reflected by enriched authigenic P concentrations (Fig. 26c). Except of these depths, zones of current diagenetic P-mineral formation could not be detected based on the HPO_4^{2-} profiles. However, precipitation of CFA has been suggested to occur in continental margin settings that receive a lot of terrestrial material (Ruttenberg and Berner, 1993) and thus likely plays a role at in sediments off Uruguay and Argentina. Since during step 3 of the SEDEX method both, authigenic and biogenic compounds are recovered, we were not able to distinguish between these two fractions. Thus, for example the peak of authigenic/biogenic P at 0.90 m at site GeoB 13809 (Fig. 26b) could either be attributed to *in situ* formation of CFA or to focusing/enhanced burial of fish bone particles (hydroxyapatite). To bypass the combined recovery of authigenic and biogenic apatite in future studies, we recommend the application of a combination of the

extraction schemes by Schenau and De Lange (2000) and Ruttenberg (1992) as it was described by Slomp et al. (2002) and Kraal et al. (2010a).

The behavior of vivianite as one of the main authigenic P-minerals was not determined for the common extraction protocols after Ruttenberg et al. (1992), De Lange (1992), and Schenau and De Lange (2000). It has been suggested by März et al. (2008a) that secondarily oxidized vivianite (kertschenite or santabarbarite) is dissolved during the second extraction step with CDB. However, we assume that for the most part, oxidation during sample storage and treatment was prevented and that vivianite would be recovered during steps 3 or 4 (biogenic/authigenic or detrital P). Similar to CFA, peaks in these P-fractions can therefore not clearly be attributed to vivianite. Since a drawdown of HPO_4^{2-} below the SMTZ, as it commonly is attributed to vivianite precipitation, was not observed at the investigated sites, we assume that vivianite precipitation does not contribute significantly to the diagenetic redistribution of P in the analyzed sediment intervals.

5.6 Summary and Conclusions

In marine sediments at the continental slope off Uruguay and Argentina, inorganic P recycling dominates the liberation of P into the pore water. In the surface sediments as well as in the deep sediment below the SMTZ, the redistribution of P is closely coupled to the dissolution of Fe (oxyhydr)oxides. However, HPO_4^{2-} concentrations in the deep sediment are considerably higher than in the benthic zone and reach up to 440 μM . Phosphate is released into the pore water at depths where HS^- reacts with Fe (oxyhydr)oxides. Furthermore, reduction of Fe (oxyhydr)oxides that were buried below the sulfidic zone during the last glacial period attributes to the liberation of adsorbed P from deep sediments. The key parameters that determine the shape of the HPO_4^{2-} profiles off Uruguay and Argentina are 1) high sedimentation rates in the Pleistocene that led to a fast burial of reactive Fe (oxyhydr)oxides below the SMTZ and 2) current sedimentation rates (and methane fluxes) that control the fixation/migration of the SMTZ and influence the retention potential of the sediment with respect to phosphate. The core from the canyon site that is characterized by extremely high Holocene sedimentation rates shows the highest HPO_4^{2-} flux from deep sediments into the sulfidic zone, which we attribute to a low retention potential due to comparably high CaCO_3 contents and an almost complete post-depositional reduction of Fe (oxyhydr)oxides between 1.50 m depth and the end of the core. The HPO_4^{2-} profiles determined in this study differ considerably from those shown previously for the Amazon Fan and the Zambezi deep-sea fan. We demonstrated that early diagenesis even far below the SMTZ might lead to a delayed geochemical lock-in, which needs to be considered especially

when older sediments (e.g., OAE sequences), for which pore water data are not available, are investigated.

Acknowledgments. We thank captain Walter Baschek and the crew and scientific party of cruise M78/3a for the successful collaboration onboard. The group Marine Technologies/Environmental Research at the University of Bremen provided the sediment echosounder data. The respective figures were created using the free software SENT developed by Hanno Keil, University of Bremen. The Marine Geophysics group at the University of Bremen, especially Hendrik Müller, Christian Hilgenfeldt, and Sebastian Razik, are thanked for providing the susceptibility data. The dissolution of bulk sediment and the major element composition analyses were performed by Olaf Kreft, Eva Kirschenmann, and Ingrid Stimac - we highly acknowledge this support. Jewgenij Derr is thanked for the ICP-OES measurements of pore water samples. Ilse Stölting is acknowledged for support with the ICP-OES at the Alfred Wegener Institute. Sediment porosity and density data were provided by Michael Strasser (MARUM). The help of Tom Jilbert, Peter Kraal, and Helen de Waard with sequential P extractions at Utrecht University is highly appreciated. Arnold van Dijk is thanked for isotope measurements on carbonates. This study was funded by the Deutsche Forschungsgemeinschaft (DFG) in the framework of the International Graduate College "Proxies in Earth History" (EUROPROX) and the Research Center/Cluster of Excellence MARUM "The Ocean in the Earth System" as well as by the Helmholtz Association (AWI Bremerhaven). All geochemical data are available via the database Pangaea (<http://www.pangaea.de>).

References

- Anschutz, P., Zhong, S., Sundby, B., Mucci, A., and Gobeil, C., 1998, Burial efficiency of phosphorus and the geochemistry of iron in continental margin sediments: *Limnology and Oceanography*, v. 43, p. 53-64.
- Antoine, D., Andre, J.M., and Morel, A., 1996, Oceanic primary production: 2. Estimation at global scale from satellite (coastal zone color scanner) chlorophyll: *Global Biogeochemical Cycles*, v. 10, p. 57-69.
- Aquilina, A., Knab, N.J., Knittel, K., Kaur, G., Geissler, A., Kelly, S.P., Fossing, H., Boot, C.S., Parkes, R.J., Mills, R.A., Boetius, A., Lloyd, J.R., and Pancost, R.D., 2010, Biomarker indicators for anaerobic oxidizers of methane in brackish-marine sediments with diffusive methane fluxes: *Organic Geochemistry*, v. 41, p. 414-426.
- Barnes, R.O. and Goldberg, E.D., 1976, Methane production and consumption in anoxic marine sediments: *Geology*, v. 4, p. 297-300.

- Benitez-Nelson, C.R. and Buesseler, K.O., 1999, Variability of inorganic and organic phosphorus turnover rates in the coastal ocean: *Nature*, v. 398, p. 502-505.
- Bishop, J.K.B., Edmond, J.M., Ketten, D.R., Bacon, M.P., and Silker, W.B., 1977, The chemistry, biology, and vertical flux of particulate matter from upper 400 m of equatorial Atlantic Ocean: *Deep-Sea Research*, v. 24, p. 511-548.
- Blum, P., 1997, *Physical Properties Handbook: A guide to the shipboard measurement of physical properties of deep-sea cores*: ODP Technical Notes, v. 26.
- Boetius, A., Ravenschlag, K., Schubert, C.J., Rickert, D., Widdel, F., Gieseke, A., Amann, R., Jørgensen, B.B., Witte, U., and Pfannkuche, O., 2000, A marine microbial consortium apparently mediating anaerobic oxidation of methane: *Nature*, v. 407, p. 623-626.
- Borowski, W.S., Paull, C.K., and Ussler, W., 1999, Global and local variations of interstitial sulfate gradients in deep-water, continental margin sediments: Sensitivity to underlying methane and gas hydrates: *Marine Geology*, v. 159, p. 131-154.
- Burns, S.J., 1997, Early diagenesis in Amazon Fan sediments, *in* Flood, R.D., Piper, D.J.W., Klaus, A., and Peterson, L.C., eds., *Proceedings of the Ocean Drilling program, Scientific Results, Volume 155*: College Station, TX.
- Campos, E.J.D., Lentini, C.A.D., Miller, J.L., and Piola, A.R., 1999, Interannual variability of the sea surface temperature in the South Brazil Bight: *Geophysical Research Letters*, v. 26, p. 2061-2064.
- Campos, E.J.D., Mulkherjee, S., Piola, A.R., and de Carvalho, F.M.S., 2008a, A note on a mineralogical analysis of the sediments associated with the Plata River and Patos Lagoon outflows: *Continental Shelf Research*, v. 28, p. 1687-1691.
- Campos, E.J.D., Piola, A.R., Matano, R.P., and Miller, J.L., 2008b, PLATA: A synoptic characterization of the southwest Atlantic shelf under influence of the Plata River and Patos Lagoon outflows: *Continental Shelf Research*, v. 28, p. 1551-1555.
- Cline, J.D., 1969, Spectrophotometric determination of hydrogen sulfide in natural waters: *Limnology and Oceanography*, v. 14, p. 454-458.
- Coleman, M.L. and Raiswell, R., 1981, Carbon, oxygen and sulfur isotope variations in concretions from the Upper Lias of NE England: *Geochimica et Cosmochimica Acta*, v. 45, p. 329-340.
- De Lange, G.J., 1992, Distribution of various extracted phosphorus-compounds in the interbedded turbiditic pelagic sediments of the Madeira abyssal-plain, eastern North-Atlantic: *Marine Geology*, v. 109, p. 115-139.
- Diaz, J., Ingall, E., Benitez-Nelson, C., Paterson, D., de Jonge, M.D., McNulty, I., and Brandes, J.A., 2008, Marine polyphosphate: A key player in geologic phosphorus sequestration: *Science*, v. 320, p. 652-655.

- Dickens, G.R., Kölling, M., Smith, D.C., and Schnieders, L., 2007, Rhizon sampling of pore waters on scientific drilling expeditions: An example from the IODP Expedition 302, Arctic Coring Expedition (ACEX): *Scientific Drilling*, v. 4, p. 22-25.
- Ewing, M., Eittreim, S.L., Ewing, J.I., and Le Pichon, X., 1971, Sediment transport and distribution in the Argentine Basin. 3. Nepheloid layer and processes of sedimentation: *Physics and Chemistry of the Earth*, v. 8, p. 49-77.
- Ferdelman, T.G., 1988, The distribution of sulphur, iron, manganese, copper and uranium in a salt marsh sediment core as determined by a sequential extraction method [Master's thesis], University of Delaware.
- Filippelli, G.M. and Delaney, M.L., 1996, Phosphorus geochemistry of equatorial Pacific sediments: *Geochimica et Cosmochimica Acta*, v. 60, p. 1479-1495.
- Froelich, P.N., 1988, Kinetic control of dissolved phosphate in natural rivers and estuaries - a primer on the phosphate buffer mechanism: *Limnology and Oceanography*, v. 33, p. 649-668.
- Froelich, P.N., Bender, M.L., Luedtke, N.A., Heath, G.R., and Devries, T., 1982, The marine phosphorus cycle: *American Journal of Science*, v. 282, p. 474-511.
- Gordon, A.L., 1989, Brazil-Malvinas Confluence-1984: Deep Sea Research Part I. *Oceanographic Research Papers*, v. 36, p. 359-361, 363-384.
- Gordon, A.L. and Greengrove, C.L., 1986, Geostrophic circulation of the Brazil-Falkland confluence: Deep Sea Research Part I. *Oceanographic Research Papers*, v. 33, p. 573-585.
- Grasshoff, K., Kremling, K., and Ehrhardt, M., 1999, *Methods of seawater analysis*: Weinheim, Wiley-VCH, 600 p.
- Haese, R.R., Schramm, J., Rutgers van der Loeff, M., and Schulz, H.D., 2000, A comparative study of iron and manganese diagenesis in continental slope and deep sea basin sediments off Uruguay (SW Atlantic): *International Journal of Earth Sciences*, v. 88, p. 619-629.
- Henkel, S., Schwenk, T., Hanebuth, T., Strasser, M., Riedinger, N., Formolo, M., Tomasini, J., Krastel, S., and Kasten, S., *subm.*, Pore water geochemistry as a tool for identifying and dating recent mass-transport deposits, *in* Yamada, Y., Kawamura, K., Ikehara, K., Ogawa, Y., Urgeles, R., Mosher, D., Chaytor, J., and Strasser, M., eds., *Advances in Natural and Technological Hazards Series, Volume 4*: Kyoto, Springer.
- Hensen, C., Landenberger, H., Zabel, M., and Schulz, H.D., 1998, Quantification of diffusive benthic fluxes of nitrate, phosphate and silicate in the southern Atlantic Ocean: *Global Biogeochemical Cycles*, v. 12, p. 193-210.
- Hensen, C., Pfeifer, K., Wenzhöfer, F., Volbers, A., Schulz, H.D., Holstein, J., Romero, O., and Seiter, K., 2004, Fluxes at the benthic boundary layer - A global view from the

- South Atlantic, in Wefer, G., Mulitza, S., and Ratmeyer, V., eds., *The South Atlantic in the Late Quaternary: Reconstruction of Material Budgets and Current Systems*: Berlin, Heidelberg, New York, Springer-Verlag, p. 401-430.
- Hensen, C., Zabel, M., Pfeifer, K., Schwenk, T., Kasten, S., Riedinger, N., Schulz, H.D., and Boetius, A., 2003, Control of sulfate pore-water profiles by sedimentary events and the significance of anaerobic oxidation of methane for the burial of sulfur in marine sediments: *Geochimica et Cosmochimica Acta*, v. 67, p. 2631-2647.
- Hensen, C., Zabel, M., and Schulz, H.D., 2000, A comparison of benthic nutrient fluxes from deep-sea sediments off Namibia and Argentina: *Deep Sea Research Part II: Topical Studies in Oceanography*, v. 47, p. 2029-2050.
- Hernández-Molina, F.J., Paterlini, M., Violante, R., Marshall, P., de Isasi, M., and Somoza, L., 2009, Contourite depositional system on the Argentine Slope: An exceptional record of the influence of Antarctic water masses: *Geology*, v. 37, p. 507-510.
- Hinrichs, K.-U., Hayes, J.M., Sylva, S.P., Brewer, P.G., and DeLong, E.F., 1999, Methane-consuming archaeobacteria in marine sediments: *Nature*, v. 398, p. 802-805.
- Ingall, E. and Jahnke, R., 1994, Evidence for enhanced phosphorus regeneration from marine sediments overlain by oxygen depleted waters: *Geochimica et Cosmochimica Acta*, v. 58, p. 2571-2575.
- , 1997, Influence of water-column anoxia on the elemental fractionation of carbon and phosphorus during sediment diagenesis: *Marine Geology*, v. 139, p. 219-229.
- Ingall, E.D., Bustin, R.M., and Van Cappellen, P., 1993, Influence of water column anoxia on the burial and preservation of carbon and phosphorus in marine shales: *Geochimica et Cosmochimica Acta*, v. 57, p. 303-316.
- Irwin, H., Curtis, C., and Coleman, M., 1977, Isotopic evidence for source of diagenetic carbonates formed during burial of organic-rich sediments: *Nature*, v. 269, p. 209-213.
- Jensen, H.S., Mortensen, P.B., Andersen, F.O., Rasmussen, E., and Jensen, A., 1995, Phosphorus cycling in a coastal marine sediment, Aarhus Bay, Denmark: *Limnology and Oceanography*, v. 40, p. 908-917.
- Kasten, S., Freudenthal, T., Gingele, F.X., and Schulz, H.D., 1998, Simultaneous formation of iron-rich layers at different redox boundaries in sediments of the Amazon deep-sea fan: *Geochimica et Cosmochimica Acta*, v. 62, p. 2253-2264.
- Kasten, S., Zabel, M., Heuer, V., and Hensen, C., 2003, Processes and signals of nonsteady-state diagenesis in deep-sea sediments and their pore waters, in Wefer, G., Mulitza, S., and Ratmeyer, V., eds., *The South Atlantic in the Late Quaternary: Reconstruction of Mass Budget and Current Systems*: Berlin, Heidelberg, New York, Springer, p. 431-459.

- Kraal, P., Slomp, C.P., and de Lange, G.J., 2010a, Sedimentary organic carbon to phosphorus ratios as a redox proxy in Quaternary records from the Mediterranean: *Chemical Geology*, v. 277, p. 167-177.
- Kraal, P., Slomp, C.P., Forster, A., and Kuypers, M.M.M., 2010b, Phosphorus cycling from the margin to abyssal depths in the proto-Atlantic during oceanic anoxic event 2: *Palaeogeography, Palaeoclimatology, Palaeoecology*, v. 295, p. 42-54.
- Kraal, P., Slomp, C.P., Forster, A., Kuypers, M.M.M., and Sluijs, A., 2009, Pyrite oxidation during sample storage determines phosphorus fractionation in carbonate-poor anoxic sediments: *Geochimica et Cosmochimica Acta*, v. 73, p. 3277-3290.
- Krastel, S., Wefer, G., Antobreh, A.A., Freudenthal, T., Hanebuth, T.J.J., Preu, B., Schwenk, T., Strasser, M., Violante, R., Winkelmann, D., and M78/3 shipboard scientific crew, in press, Sediment dynamics and geohazards off Uruguay and the de la Plata River region (Northern-Argentina): *Geo-Marine Letters*.
- Krastel, S., Wefer, G., and M78/3 shipboard scientific party, in prep., Report and preliminary results of RV *METEOR*-Cruise M78/3. Montevideo - Montevideo, 19.05. - 06.07.2009 *Berichte aus dem Fachbereich Geowissenschaften der Universität Bremen: Bremen, Universität Bremen*.
- Krom, M.D. and Berner, R.A., 1981, The diagenesis of phosphorus in a nearshore marine sediment: *Geochimica et Cosmochimica Acta*, v. 45, p. 207-216.
- Küster-Heins, K., de Lange, G.J., and Zabel, M., 2010a, Benthic phosphorus and iron budgets for three NW African slope sediments: a balance approach: *Biogeosciences*, v. 7, p. 469-480.
- Küster-Heins, K., Steinmetz, E., De Lange, G.J., and Zabel, M., 2010b, Phosphorus cycling in marine sediments from the continental margin off Namibia: *Marine Geology*, v. In Press, Accepted Manuscript.
- Lijklema, L., 1980, Interaction of orthophosphate with iron(III) and aluminum hydroxides: *Environmental Science & Technology*, v. 14, p. 537-541.
- Likens, G.E., Bormann, F.H., and Johnson, N.M., 1981, Interaction between major biogeochemical cycles in terrestrial ecosystems, *in* Likens, G.E., ed., *Some Perspectives of the Major Biogeochemical Cycles-SCOPE*, Volume 17: New York Wiley, p. 93-112.
- Lord III, C.J., 1980, The chemistry and cycling of iron, manganese and sulfur in salt marsh sediment [Dissertation thesis], University of Delaware.
- Lucotte, M., Mucci, A., Hillairemarcel, C., and Tran, S., 1994, Early diagenetic processes in deep Labrador Sea sediments - Reactive and nonreactive iron and phosphorus: *Canadian Journal of Earth Sciences*, v. 31, p. 14-27.

- Martins, L.R., Martins, I.R., and Martins, R.R., 2005, Utilização de Testemunhador Livre na Região dos Poços de Lama: Gravel, v. 3, p. 1-8.
- März, C., Beckmann, B., Franke, C., Vogt, C., Wagner, T., and Kasten, S., 2009, Geochemical environment of the Coniacian-Santonian western tropical Atlantic at Demerara Rise: *Palaeogeography, Palaeoclimatology, Palaeoecology*, v. 273-301, p. 286.
- März, C., Hoffmann, J., Bleil, U., de Lange, G.J., and Kasten, S., 2008a, Diagenetic changes of magnetic and geochemical signals by anaerobic methane oxidation in sediments of the Zambezi deep-sea fan (SW Indian Ocean): *Marine Geology*, v. 255, p. 118-130.
- März, C., Poulton, S.W., Beckmann, B., Küster, K., Wagner, T., and Kasten, S., 2008b, Redox sensitivity of P cycling during marine black shale formation: Dynamics of sulfidic and anoxic, non-sulfidic bottom waters: *Geochimica et Cosmochimica Acta*, v. 72, p. 3703-3717.
- Milliman, J.D. and Meade, R.H., 1983, World-wide delivery of river sediment to the oceans: *Journal of Geology*, v. 91, p. 1-21.
- Mollenhauer, G., McManus, J.F., Benthien, A., Müller, P.J., and Eglinton, T.I., 2006, Rapid lateral particle transport in the Argentine Basin: Molecular C-14 and Th-230(xs) evidence: *Deep-Sea Research Part I-Oceanographic Research Papers*, v. 53, p. 1224-1243.
- Mort, H.P., Adatte, T., Keller, G., Bartels, D., Follmi, K.B., Steinmann, P., Berner, Z., and Chellai, E.H., 2008, Organic carbon deposition and phosphorus accumulation during Oceanic Anoxic Event 2 in Tarfaya, Morocco: *Cretaceous Research*, v. 29, p. 1008-1023.
- Mortimer, C.H., 1971, Chemical exchanges between sediments and water in Great Lakes - Speculations on probable regulatory mechanisms: *Limnology and Oceanography*, v. 16, p. 387-404.
- Niewöhner, C., Hensen, C., Kasten, S., Zabel, M., and Schulz, H.D., 1998, Deep sulfate reduction completely mediated by anaerobic methane oxidation in sediments of the upwelling area off Namibia: *Geochimica et Cosmochimica Acta*, v. 62, p. 455-464.
- Okita, P.M., Maynard, J.B., Spiker, E.C., and Force, E.R., 1988, Isotopic evidence for organic-matter oxidation by manganese reduction in the formation of stratiform manganese carbonate ore: *Geochimica et Cosmochimica Acta*, v. 52, p. 2679-2685.
- Pape, T., Blumenberg, M., Seifert, R., Egorov, V.N., Gulin, S.B., and Michaelis, W., 2005, Lipid geochemistry of methane-seep-related Black Sea carbonates: *Palaeogeography, Palaeoclimatology, Palaeoecology*, v. 227, p. 31-47.
- Peterson, R.G. and Stramma, L., 1991, Upper-level circulation in the South Atlantic Ocean: *Progress in Oceanography*, v. 26, p. 1-73.

- Phillips, E.J.P. and Lovley, D.R., 1987, Determination of Fe(III) and Fe(II) in oxalate extracts of sediment: *Soil Science Society of America Journal*, v. 51, p. 938-941.
- Piola, A.R. and Matano, R.P., 2001, Brazil and Falklands (Malvinas) Currents, *in* John, H.S., Karl, K.T., and Steve, A.T., eds., *Encyclopedia of Ocean Sciences*: Oxford, Academic Press, p. 422-430.
- Piola, A.R., Romero, S.I., and Zajaczkovski, U., 2008, Space-time variability of the Plata plume inferred from ocean color: *Continental Shelf Research*, v. 28, p. 1556-1567.
- Poulton, S.W. and Canfield, D.E., 2005, Development of a sequential extraction procedure for iron: implications for iron partitioning in continentally derived particulates: *Chemical Geology*, v. 214, p. 209-221.
- Poulton, S.W. and Raiswell, R., 2002, The low-temperature geochemical cycle of iron: From continental fluxes to marine sediment deposition: *American Journal of Science*, v. 302, p. 774-805.
- Psuty, N.P. and Mizobe, C., 2005, South America, Coastal Geomorphology, *in* Schwartz, M.L., ed., *Encyclopedia of coastal science*: Dordrecht, Springer, p. 905-909.
- Raiswell, R., Vu, H.P., Brinza, L., and Benning, L.G., 2010, The determination of labile Fe in ferrihydrite by ascorbic acid extraction: Methodology, dissolution kinetics and loss of solubility with age and de-watering: *Chemical Geology*, v. 278, p. 70-79.
- Redfield, A.C., Ketchum, B.H., and Richards, F.A., 1963, The influence of organisms in the composition of sea-water, *in* Hill, M.N., ed., *The composition of seawater. Comparative and descriptive oceanography*: New York, Interscience, p. 26-77.
- Riedinger, N., Pfeifer, K., Kasten, S., Garming, J.F.L., Vogt, C., and Hensen, C., 2005, Diagenetic alteration of magnetic signals by anaerobic oxidation of methane related to a change in sedimentation rate: *Geochimica et Cosmochimica Acta*, v. 69, p. 4117-4126.
- Romero, O. and Hensen, C., 2002, Oceanographic control of biogenic opal and diatoms in surface sediments of the Southwestern Atlantic: *Marine Geology*, v. 186, p. 263-280.
- Ruttenberg, K.C., 1992, Development of a sequential extraction method for different forms of phosphorus in marine sediments: *Limnology and Oceanography*, v. 37, p. 1460-1482.
- , 1993, Reassessment of the oceanic residence time of phosphorus: *Chemical Geology*, v. 107, p. 405-409.
- Ruttenberg, K.C. and Berner, R.A., 1993, Authigenic apatite formation and burial in sediments from non-upwelling, continental-margin environments: *Geochimica et Cosmochimica Acta*, v. 57, p. 991-1007.
- Ruttenberg, K.C. and Goñi, M.A., 1997, Depth trends in phosphorus distribution and C:N:P ratios of organic matter in Amazon Fan sediments: Indices of organic matter source and burial history, *in* Flood, R.D., Piper, D.J.W., Klaus, A., and Peterson, L.C., eds.,

- Proceedings of the Ocean Drilling Program, Scientific Results, Volume 155: College Station, TX.
- Schenau, S.J. and De Lange, G.J., 2000, A novel chemical method to quantify fish debris in marine sediments: *Limnology and Oceanography*, v. 45, p. 963-971.
- Schulz, H.D., 2006, Quantification of early diagenesis: dissolved constituents in pore water and signals in the solid phase, *in* Schulz, H.D., and Zabel, M., eds., *Marine Geochemistry*: Berlin, Springer, p. 73-124.
- Schulz, H.D., Dahmke, A., Schinzel, U., Wallmann, K., and Zabel, M., 1994, Early diagenetic processes, fluxes, and reaction rates in sediments of the South Atlantic: *Geochimica et Cosmochimica Acta*, v. 58, p. 2041-2060.
- Seeberg-Elverfeldt, J., Schlüter, M., Feseker, T., and Kölling, M., 2005, Rhizon sampling of porewaters near the sediment-water interface of aquatic systems: *Limnology and Oceanography: Methods*, v. 3, p. 361-371.
- Seiter, K., Hensen, C., Schroter, E., and Zabel, M., 2004, Organic carbon content in surface sediments - defining regional provinces: *Deep-Sea Research Part I-Oceanographic Research Papers*, v. 51, p. 2001-2026.
- Shackleton, N.J., 1974, Attainment of isotopic equilibrium between ocean water and benthonic foraminifera genus *Uvigerina*: Isotopic changes in the ocean during the last glacial: *Colloq. Int. C.N.R.S.*, v. 219, p. 203-209.
- Slomp, C.P., Epping, E.H.C., Helder, W., and Van Raaphorst, W., 1996, A key role for iron-bound phosphorus in authigenic apatite formation in North Atlantic continental platform sediments: *Journal of Marine Research*, v. 54, p. 1179-1205.
- Slomp, C.P., Kraal, P., Reed, D.C., and Tsandev, I., 2009, Reconstructing phosphorus and carbon cycling during Cretaceous oceanic anoxic events: Why we need modern analogues: *Geochimica et Cosmochimica Acta*, v. 73, p. A1237-A1237.
- Slomp, C.P., Thomson, J., and de Lange, G.J., 2002, Enhanced regeneration of phosphorus during formation of the most recent eastern Mediterranean sapropel (S1): *Geochimica et Cosmochimica Acta*, v. 66, p. 1171-1184.
- Strickland, J.D.H. and Parsons, T.R., 1972, *A Practical Handbook of Seawater Analysis*: Ottawa, Fisheries Research Board of Canada, 310 p.
- Sundby, B., Gobeil, C., Silverberg, N., and Mucci, A., 1992, The phosphorus cycle in coastal marine sediments: *Limnology and Oceanography*, v. 37, p. 1129-1145.
- Tsandev, I. and Slomp, C.P., 2009, Modeling phosphorus cycling and carbon burial during Cretaceous Oceanic Anoxic Events: *Earth and Planetary Science Letters*, v. 286, p. 71-79.
- Van Cappellen, P. and Ingall, E.D., 1996, Redox stabilization of the atmosphere and oceans by phosphorus-limited marine productivity: *Science*, v. 271, p. 493-496.

Chapter 6: Perturbations of the sulfur, iron, and phosphorus cycles during Cretaceous oceanic anoxic events (Abstract)

Simon W. Poulton¹, Susann Henkel², Hannah Urquhart¹, Sabine Kasten², Stefan Schouten³,
and Thomas Wagner¹

¹School of Civil Engineering and Geosciences, Newcastle University, Drummond Building,
Newcastle upon Tyne, NE1 7RU, UK

²Alfred Wegener Institute for Polar and Marine Research, Am Handelshafen 12, 27570
Bremerhaven, Germany

³Royal Netherlands Institute for Sea Research (NIOZ), P.O. Box 59, NL-1790 AB Den Burg
(Texel), The Netherlands

Manuscript in preparation for submission to *Nature Geoscience*

The Cretaceous period (~145-65 million years ago) was characterized by several intervals of enhanced organic carbon burial associated with increased primary production and global ocean anoxia (Kuypers et al., 2002; Mort et al., 2007; Jenkyns, 2010). These ocean anoxic events (OAEs) lasted up to one million years (Jenkyns, 2010), but the potential for short-term (orbital and shorter) variability in ocean redox conditions and connections between the shallow and deep ocean remains to be explored. Here, we present a high-resolution reconstruction of ocean redox conditions, as recorded in subtropical shelf sediments from Tarfaya, Morocco, spanning the onset of OAE2. Iron-sulphur systematics demonstrate that deeper shelf waters were dominantly anoxic and sulphidic, with biomarker evidence suggesting encroachment of sulfide into the lower photic zone. These conditions were, however, punctuated by distinct cyclic episodes of anoxic, ferruginous (Fe-rich) conditions. Bulk geochemical data and sulfur isotope analyses suggest that ferruginous conditions were not a consequence of nutrient or sulfate limitation, but instead may have been driven by fluctuations of the hydrological cycle on orbital time scales. During ferruginous intervals, phosphorus was effectively remobilized from the shelf sediments. This contrasts with strikingly similar intervals of ferruginous conditions observed in the tropical deep ocean (März et al., 2008), suggesting that resupply of nutrients from the shelf to the deep ocean during ferruginous intervals may have been instrumental for maintaining the perturbed state of the ocean during OAEs.

References

- Jenkyns, H.C., 2010, Geochemistry of oceanic anoxic events: *Geochemistry, Geophysics, Geosystems*, v. 11.
- Kuypers, M.M.M., Pancost, R.D., Nijenhuis, I.A., and Sinninghe Damsté, J.S., 2002, Enhanced productivity led to increased organic carbon burial in the euxinic North Atlantic basin during the late Cenomanian oceanic anoxic event: *Paleoceanography*, v. 17, 1051.
- März, C., Poulton, S.W., Beckmann, B., Küster, K., Wagner, T., and Kasten, S., 2008, Redox sensitivity of P cycling during marine black shale formation: Dynamics of sulfidic and anoxic, non-sulfidic bottom waters. *Geochimica et Cosmochimica Acta*, v. 72, p. 3703-3717.
- Mort, H.P., Adatte, T., Föllmi, K.B., Keller, G., Steinmann, P., Matera, V., Berner, Z., and Stuben, D., 2007, Phosphorus and the roles of productivity and nutrient recycling during oceanic anoxic event 2: *Geology*, v. 35, p. 483-486.

Chapter 7: Conclusions and outlook

Element redistributions coupled to the SMTZ are not yet well understood, although they have important implications for the interpretation of paleo-records. In Chapters 2-5, different aspects of early diagenetic processes mainly related to the depth of the SMTZ were addressed. The studies included the assessment of the redistribution of barium in Black Sea sediments, the cycling of phosphorus in sediments of the continental margin off Uruguay and Argentina, and the use of authigenic minerals, pore water profile shapes, and transport/reaction modeling for reconstructing (paleo-)environmental and depositional conditions.

The study presented in Chapter 2 reveals that sediments underlying an anoxic water column show a strong overprint of the sedimentary Ba record due to dissolution and diagenetic precipitation of barite at the shallow SMTZ. High sedimentation rates in the Black Sea bury the sediments rapidly into the sulfate-depleted zone. Thus, the initial Ba signal is erased a couple of thousand years after deposition. For three reasons, the results of this study demonstrate that using Ba as a productivity indicator is highly risky when the respective sediment interval accumulated under conditions similar to those in the Black Sea: 1) Anoxia in the water column leads to a high preservation of organic matter and ultimately favors the generation of methane in the sediment. Consequently, there is an increase in the upward flux of methane, which leads to a condensed redox zonation and a shallow depth of the SMTZ. Diagenetic overprinting of the Ba signal thus occurs already in 1-2 m depth. 2) Two types of barite crystals (ellipsoidal and irregular) were present in the surface sediment. Whereas the ellipsoidal grains represent the biogenic barite, the origin/formation process of the irregular barite particles remains unclear. Furthermore, diagenetic and biogenic barite crystals can not be distinguished by their size. Thus, in Black Sea sediments neither the morphology of the barite crystals nor their size can be used to reveal the origin of barite enrichments. 3) The causal relation between organic matter decay and biogenic barite precipitation in anoxic waters likely is affected by the enhanced preservation of organic compounds. The coupling between barite formation and organic carbon preservation in anoxic water columns is not well-studied and requires further examination. We conclude that with respect to productivity-reconstructions based on Ba in fossil sediments, caution is advised when distinct barium enrichments occur above sediment intervals that show consistently low Ba concentrations. Especially in OAE successions, the chance that the barite enrichments were produced post-depositionally is high.

Increasing salinities in response to the Holocene flooding of the Black Sea with Mediterranean seawater led to a downward migration of the SMTZ. Simulating the evolution of this downward movement by use of a transport and reaction model showed that the

horizons of authigenic Ba enrichments that potentially formed during this shift of the SMTZ are currently located in the sulfate-depleted zone. Thus, Ba enrichments found in the sediments at the two study sites do not trace the migration of the SMTZ in response to the salinity increase.

In Chapters 3 and 4 we used an interdisciplinary approach to improve the identification and dating of recent mass-transport deposits and complemented sediment echosounder and sedimentological investigations by pore water geochemical analyses and transport/reaction modeling. In Chapter 3 we examined a site at the continental margin off Uruguay where a recent slide deposit was indicated by a kink-shaped sulfate profile, a sudden increase of the shear strength at the base of the mass-transport deposit, and a sharp lithological contact at the respective depth. We modeled the diffusive re-equilibration of the sulfate profile. Fitting of the model results to the measured sulfate data revealed an age of the mass-transport deposit of less than 30 years. The mass movement could have been related to a weak earthquake that occurred in 1988 near to the study site. Slope stability analyses suggest that the earthquake in 1988 was a likely trigger for mass movement in the study area if additional factors (e.g., excess pore pressure) preconditioned the slope for failure. Chapter 4 also shows that on a regional scale, estimating the ages of recent landslides by transport and reaction modeling might allow relating the detected mass movements to historically documented earthquakes. However, possible reasons for non-steady state conditions are numerous and geophysical and sedimentological data is always required to minimize the risk of misinterpretation. In Chapter 4 it is emphasized that concave and kink-shape sulfate profiles are not consistently coupled to acoustically transparent sediment layers/mass-transport deposits. The exact reasons for non-linear sulfate profiles at the sites that are unaffected by mass movements remain speculative and should be examined in further studies.

In Chapter 5 we addressed the diagenetic cycling of P in sediments of the continental margin off Uruguay and Argentina. The main outcome of this study is that P liberation into pore water in the deep sediments (within the methanic zone) is driven by the reduction of iron (oxyhydr)oxides. The iron (oxyhydr)oxides were buried below the SMTZ rapidly enough to not being subject to significant alteration within the sulfidic zone. The exact process of the deep iron (oxyhydr)oxide reduction is not yet known and part of ongoing research. Compared to the benthic zone, dissolved phosphate concentrations in deep sediments were significantly high. Vivianite precipitation as it has been proposed as a deep P sink at continental margin settings does not play a major role at our study sites. Nevertheless, a considerable part of the released P does not reach the sediment/water interface, because it is retained by

'fresh(er)' iron (oxyhydr)oxides in the overlying sediment intervals. Unfortunately, the procedural method we used for the sequential P extraction did not allow a discrimination of biogenic apatite and CFA at the sites investigated. The cycling of P at the study sites, however, likely includes the formation of CFA. Mineralogical/microscopic approaches that allow a differentiation between authigenic and biogenic apatite could be applied to complement the dataset.

The critical parameter that controls the burial and the deep liberation of P into the pore water at the investigated sites is the sedimentation rate. The sediment accumulation effects the time for which iron (oxyhydr)oxides are subject to reduction within the sulfidic zone, the burial of 'fresh' iron (oxyhydr)oxides, and the dilution by carbonate that decreases the relative amount of iron (oxyhydr)oxide and thus diminishes the retention potential of the sediment with respect to phosphate. In addition to that, the stability of the SMTZ and the extent of the sulfidic zone determine the amount of iron(III) minerals that may reach the methanic zone. Broad sulfidic zones combined with low sedimentation rates lengthen the time the iron (oxyhydr)oxides react with sulfide and thus diminish the chance of iron (oxyhydr)oxides to reach the underlying sediments. In a wider context, this study showed that in marine sediments, P liberation into pore is not restricted to the benthic and the sulfidic zone. An early diagenetic overprint of fossil sediments related to the SMTZ should be taken into consideration especially if the geomagnetic investigations reveal distinct and broad sediment intervals of low magnetic susceptibility as they are produced upon the reaction of iron (oxyhydr)oxides with sulfide. For records that reveal high sedimentation rates, a post-depositional liberation of P into the pore water due to the reduction of iron (oxyhydr)oxides in deep sediments (the methanic zone) needs to be taken into account.

In summary, this thesis gave a broad overview of geochemical methods as they are used for the determination of early diagenetic element redistributions. Mineral dissolution and precipitation at and around the SMTZ were highlighted to improve our understanding of these processes and to evaluate the consequences of early diagenesis for the application of specific proxies. Furthermore, we demonstrated that investigations on recent mass movements can benefit considerably from the integration of geochemical pore water data and transport/reaction modeling. Pore water profile analyses are helpful tools especially for investigating recent slide deposits that are usually hard to identify by sedimentological approaches.

Danksagung

Mein herzlicher und ganz besonderer Dank für das mir entgegengebrachte Vertrauen und die Vergabe und Betreuung dieser Arbeit gilt meiner Doktormutter PD Dr. Sabine Kasten, die mich in jeglichen Situationen motiviert, unterstützt und gefördert hat. Sie hat mir stets den nötigen Freiraum für die Umsetzung eigener Ideen gelassen und mir so ermöglicht, mein eigenes Potential zu erkennen und auszuschöpfen. Mit Ihrer begeisternden und motivierenden Art hat sie mich die Entscheidung für diese Doktorarbeit nie bereuen lassen.

Ebenfalls von ganzem Herzen danken möchte ich Prof. Gert J. de Lange, der diese Arbeit von Anfang an intensiv mitbetreut und sich zur Übernahme des Zweitgutachtens bereit erklärt hat. Die einzelnen Manuskripte profitierten stark vom regen Informationsaustausch mit ihm sowie von mehreren Gastaufenthalten in seiner Arbeitsgruppe in Utrecht.

Den Kollegen vom Fachbereich Geowissenschaften in Bremen sowie diversen anderen Instituten in und außerhalb Deutschlands danke ich für ihr Interesse an dieser Arbeit und ihre Bereitschaft zur Diskussion. Insbesondere möchte ich hier Dr. Michael Strasser, Dr. Natascha Riedinger, Dr. Tilmann Schwenk, Dr. Gail L. Arnold, Dr. Michael Formolo, Dr. Till Hanebuth, Dr. Sebastian Krastel, Dr. Daniel Winkelmann, Dr. Thomas Pape, Dr. Michael Blumenberg, Dr. André Bahr, Dr. Christine Franke, Dr. Eric Robin und Dr. Bärbel Sinha erwähnen. Für die Hilfestellungen während der Aufenthalte in Utrecht seien besonders Dr. Caroline P. Slomp, Dr. Tom Jilbert, Dr. Peter Kraal sowie den technischen Angestellten der Fakultät Geowissenschaften an der Universität Utrecht Helen de Waard, Dineke van de Meent und Tilly Bouten gedankt. Dr. Jaap Sinninghe Damsté, Dr. Stefan Schouten und Marianne Baas danke ich für ihre Unterstützung bei Laborarbeiten am NIOZ (Texel).

Den Sprechern, Post-Docs und Doktoranden des Graduiertenkollegs EUROPROX danke ich für die Unterstützung in Form von Organisationen von Workshops, Kursen und wissenschaftlichen Diskussionen.

Ich bedanke mich bei den Mitgliedern der AG Marine Geochemie am AWI für die nette Zusammenarbeit in den letzten Jahren. Dr. Kerstin Nöthen, Prof. Michael Schlüter und Dr. Michiel van der Loeff danke ich für viele anregende Diskussionen. Besonders zu erwähnen sind auch Ingrid Stimac und Ludmila Baumann, die mir eine große Hilfe bei den Laborarbeiten waren. Auch Jewgenij Derr, Olaf Kreft, und Eva Kirschenmann haben mit ihrem Fleiß im Labor zu dieser Arbeit beigetragen. Ein herzliches Dankeschön geht an Dr. Jana Friedrich für Ihren moralischen Beistand und viele Lacher im gemeinsamen Büro.

Torben Gentz und Roi Martínez danke ich dafür, dass sie v.a. in der Endphase des Schreibens dieser Arbeit mit Kaffee, Shakira und St. Pauli immer für gute Stimmung gesorgt haben und mit Rat und Tat zur Seite standen, wenn es mal wieder irgendwo „brannte“.

Ebenso danke ich Harald Poigner, den ich immer mit Manner-Waffeln, Sachertorte, und Schokocroissants in Verbindung bringen werde. Unser Büro sah zwar chaotisch aus, hatte aber definitiv Wohlfühlatmosphäre. Und gehungert haben wir nie!

Meinen Eltern Kristine und Christian sowie meinen Brüdern André und Marc und meiner Großtante Herta Peschke gilt mein großer Dank für die Unterstützung bei der Berufswahl, während des Studiums und meiner Doktorandenzeit.

Mein innigstes Dankeschön gilt Daniel, der immer fest hinter mir stand, mir für den Abschluss dieser Arbeit den Rücken gestärkt und mich mit einer Selbstverständlichkeit unterstützt hat, wo immer es ging.

**Erklärung gemäß § 6 Abs. 5 der Promotionsordnung der Universität
Bremen für die mathematischen, natur- und ingenieurwissenschaft-
lichen Fachbereiche**

Hiermit versichere ich, dass ich

1. die vorliegende Arbeit ohne unerlaubte fremde Hilfe angefertigt habe,
2. keine anderen als die von mir angegebenen Quellen und Hilfsmittel benutzt habe
und
3. die den benutzten Werken wörtlich oder inhaltlich entnommenen Stellen als solche
kenntlich gemacht habe.

Bremen, den 21.04.2011

Susann Henkel